

**A novel use for oil-contaminated drill cuttings in the manufacture of  
lightweight aggregate**

**Bamdad Ayati**

A thesis submitted in partial fulfilment of the requirements of the University of East  
London for the degree of Doctor of Philosophy

September 2018

## **Abstract**

Contaminated waste drill cuttings produced from drilling activities in the North Sea is currently transported onshore and landfilled at high costs, as there is no existing option for alternative and viable recycling. The aim of this research was therefore to investigate the technical feasibility of transforming this waste into an inert, porous, ceramic material to potentially be utilised as lightweight aggregate (LWA). In this project, three samples of waste drill cuttings were obtained and characterised for chemical compositions, mineralogy, thermal behaviour and contaminant leaching. To manufacture LWA, the raw materials were dried, ball milled, formed into pellets and fired above their initial sintering temperature. The effect of firing temperature on particle density, water absorption, compressive strength and microstructure was studied and compared with those of standard commercial products such as LECA and Lytag. The mineralogy before and after firing and its effect on leaching behaviour was also investigated. Washing pre-treatments were employed to mitigate the leaching of chlorides in the manufactured LWA and the potential of milled waste glass incorporated into LWA as a matrix forming material was evaluated. Finally, the research proposed a novel approach for calculating carbon dioxide emissions for the production of drill cuttings LWA.

The results of this research showed that drill cuttings contained variable amounts of minerals with poor sintering capabilities. This limited their viability to be readily used as a raw material in LWA production – due to the unfavourable physical properties and environmental compatibility of the final products. In samples with high concentrations of chloride salts, a two-step washing pre-treatment using deionised water at an L/S ratio of 10 l/kg was necessary for leaching to comply with the End of Waste criteria. In samples with high concentrations of barium sulphate and carbonate minerals, the addition of 40 wt.% waste glass in the mix and firing at 1150 °C, produced LWA with physical properties comparable to commercially available products. However, mitigating the leaching of sulphates remained a challenge in samples with high initial concentrations of drilling fluids. Carbon dioxide emissions as low as 236.0 kg per 1.0 tonne of drill cuttings LWA were estimated and compared favourably with those for current management scenarios and other waste derived LWA. Overall, the research showed that LWA manufacturing represents a beneficial reuse of drill cuttings that diverts waste from landfill.

## Declaration of originality

I hereby declare that the work presented in this PhD thesis is my own original work, and information derived from other research works have been appropriately cited.

Bamdad Ayati

September 2018

# Table of Contents

1	Chapter 1 Aim and objectives .....	1
1.1	Background .....	1
1.2	Aim and objectives .....	5
1.3	Summary of novelty and innovation .....	6
1.4	Experimental approach .....	6
2	Chapter 2 Waste drill cuttings and LWA potential .....	8
2.1	Oil and gas drilling technology .....	8
2.2	Drilling wastes .....	18
2.3	Drill cuttings mineralogy and the geology of the North Sea .....	22
2.4	Current disposal, treatment and management options .....	26
2.5	Lightweight aggregate .....	33
2.6	Summary .....	50
3	Chapter 3 Materials and methods .....	51
3.1	Materials .....	51
3.2	Methods .....	52
4	Chapter 4: Characterization of drill cuttings .....	78
4.1	Chemical compositions .....	78
4.2	Riley diagram .....	81
4.3	Mineralogy of drill cuttings .....	82
4.4	Particle Morphology .....	87
4.5	Thermal analysis .....	89
4.6	Total Petroleum Hydrocarbon (TPH) .....	96
4.7	Total heavy metal content .....	97
4.8	Leaching analysis .....	98
4.9	Discussions .....	102
5	Chapter 5 Properties of drill cuttings LWA .....	105
5.1	Structural characteristics of LWA .....	105
5.2	Physical properties of LWA .....	108
5.3	Microstructure of LWA .....	115
5.4	Mineralogy of LWA .....	118
5.5	Leaching analysis of LWA .....	123
5.6	Discussion .....	127

6	Chapter 6: Effect of washing pre-treatments on properties of LWA .....	129
6.1	Potential treatments for mitigation of Cl – .....	129
6.2	Designing the washing pre-parameters .....	132
6.3	Effect of washing on structural characteristics.....	134
6.4	Effect of washing on physical properties .....	136
6.5	Effect of washing on microstructure .....	139
6.6	Effect of washing on mineralogy .....	143
6.7	Effect of washing on contaminant leaching from LWA .....	148
6.8	Discussions .....	151
7	Chapter 7: Effect of glass addition on properties of LWA .....	153
7.1	Potential secondary material for incorporation in LWA .....	153
7.2	Incorporation of glass in LWA.....	158
7.3	Effect of glass addition on structural characteristics .....	160
7.4	Effect of glass addition on physical properties.....	162
7.5	Effect of glass addition on microstructure.....	168
7.6	Effect of glass addition on mineralogy.....	174
7.7	Effect of glass addition on leaching characteristics .....	178
7.8	Discussions .....	182
8	Chapter 8 Estimation of energy and CO <sub>2</sub> emissions.....	185
8.1	Energy and CO <sub>2</sub> emissions.....	185
8.2	Results and discussions .....	189
9	Chapter 9 Conclusions and future works .....	192
9.1	Conclusions .....	192
9.2	Contribution to knowledge .....	195
9.3	Production process framework .....	195
9.4	Recommendations for future work.....	198
	References .....	199
	Appendix I (SEM images of drill cuttings samples).....	230
	Appendix II .....	234

## List of figures

Figure 1.1 Total hazardous waste (including major mineral wastes) generated in the UK based on the classification of economic activities .....	2
Figure 1.2 Total hazardous waste (including major mineral wastes) treatment .....	3
Figure 1.3 Map of the UK offshore oil and gas discoveries .....	4
Figure 2.1 Oil and gas drilling operation. Modified from (CAPP, 2001).....	9
Figure 2.2 Classification of solids in drilling muds based on the particle size, mo.....	15
Figure 2.3 Drill cuttings separation techniques: (a) adjustable linear shale shaker, (b) hydrocyclones and (c) decanting centrifuge .....	17
Figure 2.4 Decision Tree for Inorganic Hazardous Waste that can be used for managing oil-contaminated drill cuttings waste. ....	21
Figure 2.5 Evaporation sequence in seawater .....	25
Figure 2.6 Thermal desorption unit.....	28
Figure 2.7 Lightweight aggregate manufacturing process .....	34
Figure 2.8 (a) LWA manufacturing rotary kiln with different heating zones.....	35
Figure 2.9 Ideal pore structure shown for an individual clay LWA pellet .....	40
Figure 2.10 Relationships between raw material characteristics, production parameters and physical properties, showing the pore structure as an intermediate variable. ...	42
Figure 3.1 Synthetic-based mud (SBM) drill cuttings: a) as received and b) air-dried..	51
Figure 3.2 Demonstration of Bragg's law (Rachwal, 2010).....	54
Figure 3.3 Signals resulting from electron beam and sample surface interaction .....	59
Figure 3.4 End-to-end rotary tumbler used for leaching test. ....	65
Figure 3.5 Ion chromatography (IC) system flow diagram.....	68
Figure 3.6 Flowchart of pre-processing, pre-treatments and LWA manufacturing .....	71

Figure 3.7 Heating regimes applied in muffle furnace during the LWA manufacture. .	73
Figure 3.8 Relations investigated between properties of LWA.....	77
Figure 4.1 The location of bulk chemical composition for samples of drill cuttings in Riley diagram. ....	81
Figure 4.2 X-ray diffraction patterns with some important peak markers for crystalline phase identification in SDC, CDC and EDC samples. ....	85
Figure 4.3 SEM micrographs of (a) SDC, (b) CDC and (c) EDC samples showing irregular morphology of drill cutting particles.....	88
Figure 4.4 Outline area % change as a function of temperature .....	92
Figure 4.5 DTA data of (a) SDC, (b) CDC and (c) EDC.....	95
Figure 5.1 Appearance of drill cuttings LWA pellets surface and internal structure. (a) SDC-LWA, (b) CDC-LWA, and (c) EDC-LWA. ....	107
Figure 5.2 Effects of firing temperature on physical properties of SDC-LWA: (a) particle density, (b) water absorption and (c) compressive strength.....	110
Figure 5.3 Effects of firing temperature on physical properties of CDC-LWA: (a) particle density, (b) water absorption, and (c) compressive strengths.....	112
Figure 5.4 Effects of firing temperature on physical properties of EDC-LWA: (a) particle density, (b) water absorption, and (c) compressive strengths .....	114
Figure 5.5 SEM micrographs of EDC-LWA: (a) outer surface fired at 1180 °C, (b) core (fracture surface) fired at 1180 °C, .....	117
Figure 5.6 X-ray diffraction patterns with some important peak markers for crystalline phase identification .....	121
Figure 6.1 Schematic representation of electro-kinetic cell modified from.....	131
Figure 6.2 Appearance of the surface and internal structure for fired pellets manufactured from EDC subjected to W1 and W5 pre-treatments. ....	135

Figure 6.3 Effects of firing temperature on physical properties of W1EDC-LWA and W5EDC-LWA: .....	138
Figure 6.4 SEM micrographs of W1EDC-LWA: (a) core (fracture surface) at 1160 °C, (b) core (fracture surface) at 1190 °C .....	141
Figure 6.5 SEM micrographs of W5EDC-LWA: (a) outer surface fired at 1160 °C, (b) outer surface at 1190 °C .....	142
Figure 6.6 X-ray diffraction patterns with some important peak markers for crystalline phase identification in W1EDC and W5EDC .....	145
Figure 6.7 X-ray diffraction patterns with some important peak markers for crystalline phase identification in W1EDC-LWA and W5EDC-LWA .....	146
Figure 7.1 Compositional location of drill cuttings after addition of glass .....	159
Figure 7.2 Appearance of the surface and internal structure of (a) SDC-LWA, (b) CDC-LWA and (c) EDC-LWA with 40 wt.% added glass .....	161
Figure 7.3 Effects of firing temperature on particle density of (a) SDC-LWA, (b) CDC-LWA and (c) EDC-LWA with 20 wt.% .....	163
Figure 7.4 Effects of firing temperature on water absorption of (a) SDC-LWA, (b) CDC-LWA and (c) EDC-LWA with 20 wt.% and 40 wt.% glass .....	165
Figure 7.5 Effects of firing temperature on compressive strength of (a) SDC-LWA, (b) CDC-LWA and (c) EDC-LWA with 20 wt.% and 40 wt.% glass .....	167
Figure 7.6 SEM micrographs of SDC-LWA fired at 1150 °C with: a) 20 wt.% glass (core fracture surface), b) 20 wt.% glass (outer surface). .....	169
Figure 7.7 SEM micrographs of CDC-LWA fired at 1150 °C with: a) 20 wt.% glass (core fracture surface), b) 20 wt.% glass (outer surface) .....	171
Figure 7.8 SEM micrographs of EDC-LWA fired at 1180 °C with: a) 20 wt.% glass (core fracture surface), b) 20 wt.% glass (outer surface). .....	173
Figure 7.9 X-ray diffraction patterns with some important peak markers .....	176
Figure 9.1 Production process framework for manufacturing .....	197

## List of tables

Table 1.1 Experimental approach for each objective of the research.....	7
Table 2.1 Continuous phase categories in synthetic-based drilling fluids and their chemical structure and chain length range.....	12
Table 2.2 Concentration and function of components for drilling muds.....	14
Table 2.3 Concentration and composition of salts formed in seawater.....	24
Table 2.4 Summary of available bioremediation techniques.....	30
Table 2.5 Studies using solidification and stabilization (S/S).....	31
Table 2.6 Range of physical properties for commercial LWA.....	37
Table 2.8 Summary of LWAs and characteristics, process conditions and physical properties from existing publications.....	38
Table 2.9 Conditions necessary for LWA bloating.....	41
Table 2.10 XRD analysis for manufactured LWAs from mineral waste.....	48
Table 3.1 Limits for assessing the hazardous properties of waste.....	57
Table 3.2 EoW criteria based on WAC for inert as expressed in (2003/33/EC). .....	64
Table 4.1 Chemical compositions including major oxides and LOI.....	79
Table 4.2 Chemical compositions including minor and trace element concentrations of drill cuttings determined by XRF analysis. ....	80
Table 4.3 Rietveld quantitative analysis of minerals.....	86
Table 4.4 TPH of drill cuttings. ....	96
Table 4.5 Total metal content measured by acid digestion.....	97
Table 4.6 Results of leaching test (BS EN 12457-2) on SDC, CDC and EDC.....	101
Table 5.1 Measured physical properties of Lytag and LECA.....	108
Table 5.2 Results of Rietveld quantification analysis for SDC-LWA fired at 1190 °C, CDC-LWA fired at 1230 °C and EDC-LWA fired at 1180 °C.....	122
Table 5.3 Results of leaching test (BS EN 12457-2) on SDC-LWA fired at 1190 °C, CDC-LWA fired at 1230 °C and EDC-LWA fired at 1180 °C. ....	126
Table 6.1 Washing parameters determined for the pre-treatment of EDC. ....	133

Table 6.2 Results of XRD Rietveld quantification analysis for EDC after washing pre-treatments and LWA fired at 1190 °C. ....	147
Table 6.3 Results of leaching test (BS EN 12457-2, 2002) on W1EDC-LWA and W5EDC-LWA fired at 1190 °C. ....	150
Table 7.1 Typical oxide compositions of matrix forming secondary materials reviewed for incorporation in LWA. ....	157
Table 7.2 Oxide compositions measured by XRF analysis for waste glass sample used for incorporation in LWA. ....	159
Table 7.3 Results of Rietveld quantification analysis for SDC-LWA, CDC-LWA and EDC-LWA with 40 wt.% glass. ....	177
Table 7.4 Results of batch leaching test (BS EN 12457-2) on SDC-LWA, CDC-LWA and EDC-LWA with 40 wt.% added glass. ....	181
Table 8.1 Specific heat capacities used for mass and energy balance. ....	187
Table 8.2 Estimation of energy required and total CO <sub>2</sub> for the manufacture of 1.0 tonne drill cuttings LWA. ....	191

## List of abbreviations (sort alphabetically)

AAS	Atomic Absorption Spectroscopy
APCr	Air Pollution Control residues
BOE	Barrel of Oil Equivalent
BSE	Backscatter Electrons
DECC	Department of Energy and Climate Change
DEFRA	Department of Environment, Food and Rural Affairs
DOC	Dissolved Organic Carbon
DTA	Differential Thermal Analysis
EfW	Energy from Waste
EoW	End of Waste
FA	Fly Ash
FPT	Flash Point Temperature
GC-FID	Gas Chromatographer with Flame Ionisation Detector
HM	Heating Microscope
HP	Hazardous Properties
IBA	Incinerator Bottom Ash
IC	Ion Chromatography
ICP-OES	Inductively Coupled Plasma Optical Emission Spectroscopy
ICDD	International Centre for Diffraction Data
IO	Internal Olefins
LAO	Linear Alpha Olefins
LECA	Lightweight Expanded Clay Aggregate
LOI	Loss on Ignition
LSA	Life Cycle Assessment
L/S	Liquid-to-Solid
LWA	Lightweight Aggregate
MIP	Mercury Intrusion Porosimetry
MSW	Municipal Solid Waste
NABFs	Non-aqueous Based Fluids
NDIR	Nondispersive Infrared
OBM	Oil Based Mud
OGA	Oil and Gas Authority
PAH	Polycyclic Aromatic Hydrocarbon

PAO	Poly Alpha Olefin
PDF	Powder Diffraction Data
PFA	Pulverised Fuel Ash
SBM	Synthetic Based Mud
SBF	Synthetic Based Fluid
SCM	Supplementary Cementitious Materials
SE	Secondary electrons
SEM	Scanning Electron Microscope
SHC	Specific Heat Capacity
SFE	Supercritical Fluid Extraction
S/S	Solidification/Stabilization
SSA	Sewage Sludge Ash
TCLP	Toxicity Characteristic Leaching Procedure
TEC	Thermal Expansion Coefficient
TGA	Thermogravimetric Analysis
TOC	Total Organic Carbon
TPH	Total Petroleum Hydrocarbons
UKCS	United Kingdom Continental Shelf
WAC	Waste Acceptance Criteria
WBF	Water-Based Fluid
WBM	Water Based Mud
XRD	X-ray Diffraction
XRF	X-ray Fluorescence

## Acknowledgements

First of all, I would like to sincerely thank my supervisor Prof Darryl Newport, for his invaluable support during the whole project. The completion of this thesis would not have been possible without his ongoing guidance and encouragement. I also wish to say thank you to my other supervisors, Dr Chloe Molineux, who proofread this thesis and provided me with constructive comments and suggestions, and Dr Mihaela Anca Ciupala. I would also like to thank Prof Chris Cheeseman from Imperial College London for his kind collaboration from the beginning of the project.

The studentship from UEL and SRI is gratefully acknowledged. The biggest thanks go to my colleagues in SRI for their warm company and motivations. It has been a wonderful experience working with you.

I would like to thank Lauren Hill from Augean PLC for providing samples of drill cuttings and facilitating a number of site visits, and Chris Franklin and Sean Houghton for their analytical equipment skills. I would also like to acknowledge Dr Dave Alderton for his expertise and discussions on the XRD analyses. Thanks to Andrei Shishkin for his assistance on conducting the heating microscope and DTA tests. Thankfulness also goes to the UEL concrete testing lab technicians, Neil Goodin, Christopher Donovan and Trevor Rhoden.

And finally, thanks to my wife, Benedetta, for her love and being the source of inspiration throughout my study. This work is dedicated to her.

# 1 Chapter 1 Aim and objectives

## 1.1 Background

Waste drill cuttings consist of a fine mix of rock particles produced by drilling for oil and gas either during exploration or production. They are contaminated with drilling fluids which are often synthetic oils containing several additives to enhance the drilling operation. Waste drill cuttings are classified as hazardous in the EU Waste Catalogue (01 05 05\*), mainly because of high concentrations of total petroleum hydrocarbons (TPH) and soluble salts. Contaminated drill cuttings pose a serious risk to the marine environment and must be shipped onshore for treatment and disposal (Jorissen et al., 2009). In the UK, contaminated drill cuttings are another significant hazardous waste stream, adding further burden to the UK already over-used landfill facilities (Dhir et al., 2010).

### 1.1.1 UK hazardous waste generation overview

The implementation of the EU Council Directive (1999/31/EC) on the landfill of waste and the revised EU Waste Framework Directive (2008/98/EC) on waste has provided a general waste management framework and set target limits for the Member States with regards to the amount of waste landfilled. In 2015, the European Commission published a monitoring report of the EU sustainable development strategy, evaluating the changes in resources productivity, consumption and waste generation (European Commission, 2015). The report highlighted the production of hazardous waste has continued to increase. The generation of hazardous waste including major minerals waste in the EU in 2014 was reported to be 95.6 million tonnes and for that year, for most of the Member States, the ratio of hazardous waste to total waste was at approximately 10% (Eurostat).

Figure 1.1 shows the hazardous waste, including major mineral waste generated in the UK between 2004 and 2014. In 2014, the total generated hazardous waste decreased to nearly 5.7 million tonnes showing more than 25% decrease compared to 2012 (Eurostat). The chart shows the classification of economic activities in the European Community (NACE). The total mineral and solidified waste arising in the UK was 1.4 million tonnes in 2014 which was more than double the amount produced in 2004. It should be noted that waste drill cuttings generated from the petroleum industry both from exploration and production activities) is in this category.

The amount of drill cuttings transferred onshore for disposal varied between approximately 30,000 to 70,000 tonnes per year (Oil and Gas UK, 2016b, Oil and Gas UK, 2017). Waste drill cuttings contributes to 2 – 5% of the total mineral and solidified waste arising in the UK (Eurostat).

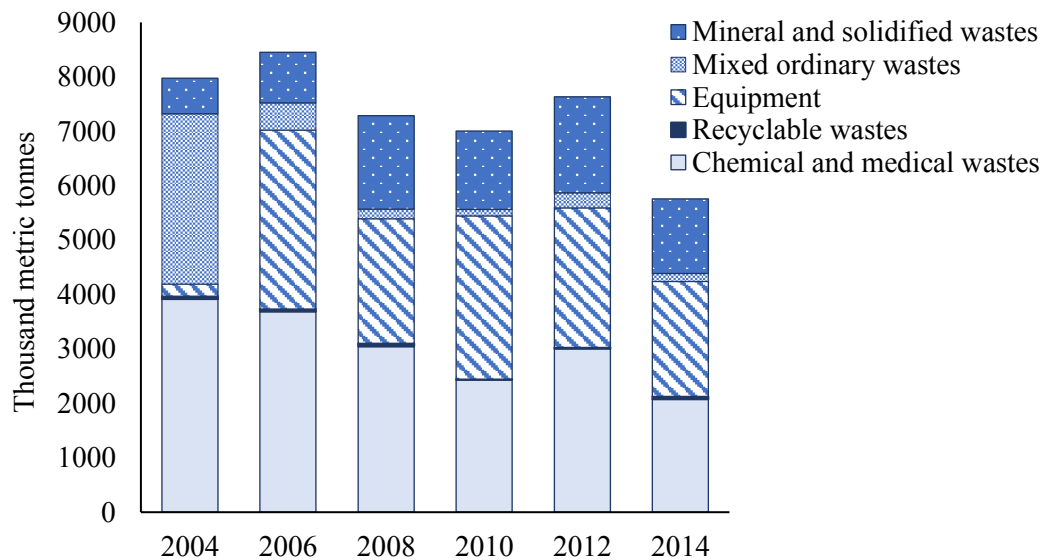


Figure 1.1 Total hazardous waste (including major mineral wastes) generated in the UK based on the classification of economic activities in the European Community (NACE). Source: (Eurostat).

Figure 1.2 shows the status of hazardous waste treatment in the UK. In 2014, approximately 2.8 million tonnes of hazardous waste was treated, comprising almost half of the total amount; with the other half being landfilled (Eurostat). Of this, more than 30% of the total treated hazardous waste was disposed into or onto land or through land treatment and released into water bodies, approximately 9% was incinerated without energy recovery and up to 4% with energy recovery, and the remaining 57% were either recycled or used for backfilling. It is important to note that the share of recycling significantly increased between 2010 and 2014. This shows that the UK is aiming to expand recycling and material reuse as the two main objectives of the Waste Framework Directive. However, comparing the recycled share of the total generated hazardous waste (nearly 26%), it is evident that there is still an enormous challenge which confronts the

UK in employing strategies to develop suitable infrastructures to expand its recycling capacity and thus, minimise its landfill dependency.

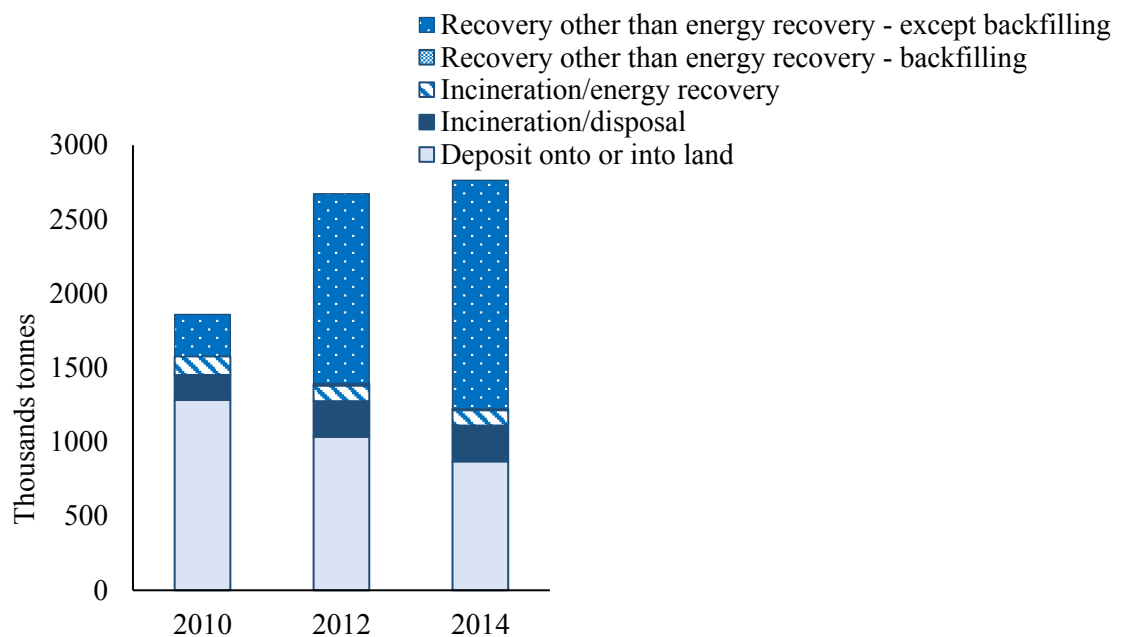
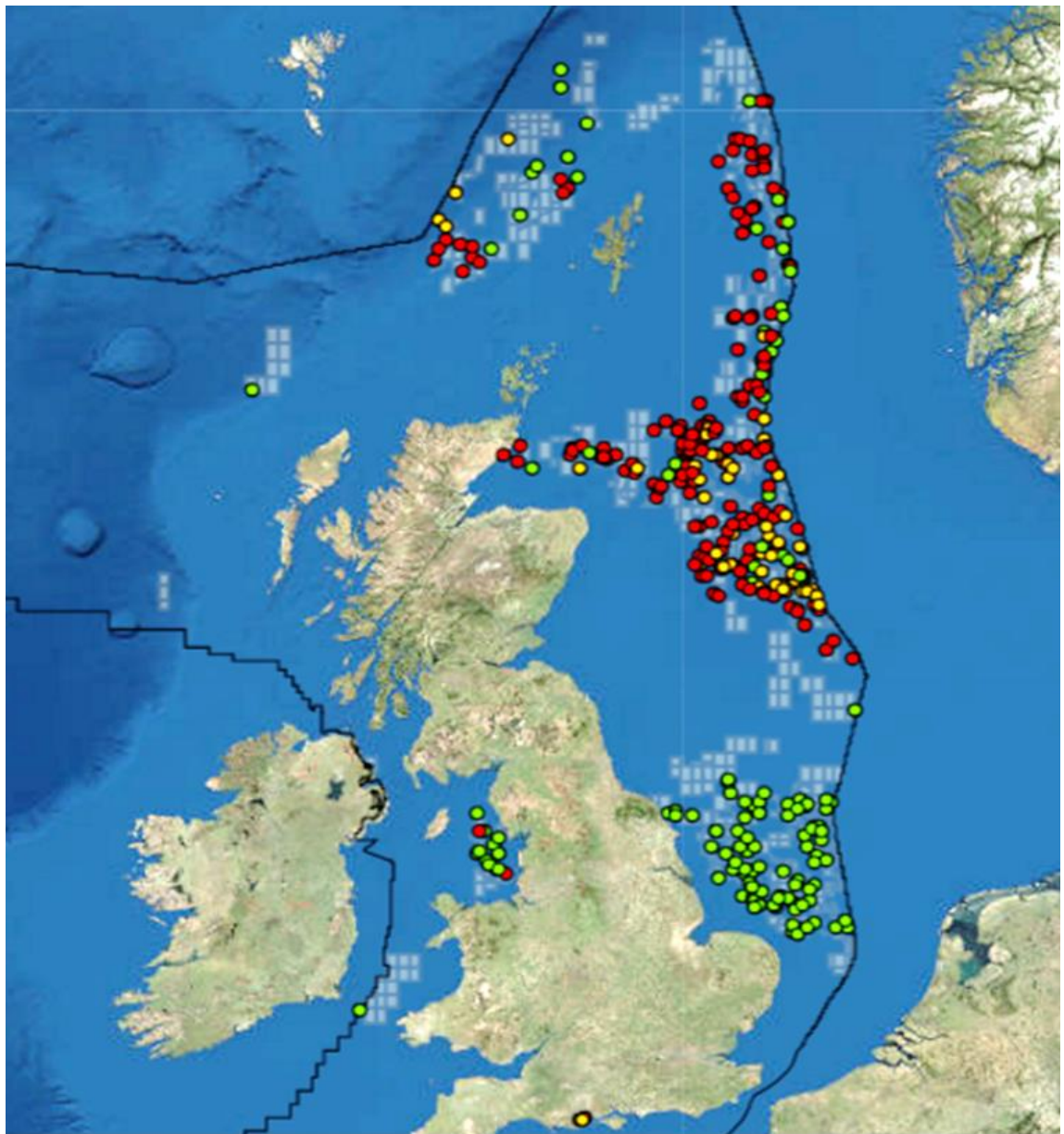


Figure 1.2 Total hazardous waste (including major mineral wastes) treatment in the UK (Eurostat).

### 1.1.2 UK drilling activity

To date, up to 43 billion barrels of oil equivalent (BOE) have been extracted from the UK Continental Shelf (UKCS) and up to 20 billion BOE are predicted to be preserved (Oil and Gas UK, 2016a). In 2016, the UK Oil and Gas Authority (OGA) announced that more than 3 billion BOE are available for utilization in approximately 350 unsanctioned discoveries across the UKCS (Oil and Gas Authority, 2016). The positions of these discoveries are marked in Figure 1.3. The OGA also pointed out that the majority of these discoveries are in reaching distance of existing infrastructure, indicating the vast potential for development in the UK drilling activities. At the same time, due to the consumption of easily accessible hydrocarbon reservoirs in the past, deeper and more complex drilling operations which produce increased amounts of drill cuttings are becoming more prevalent (Pereira, 2013).



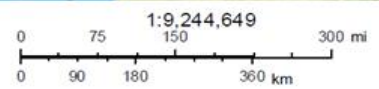
December 20, 2016

**OGA\_Unsanctioned\_Discoveries**

- Condensate
- Gas
- Oil

DECC - Median Line

OGA\_Licensed\_Blocks\_WGS84



Source: Esri, DigitalGlobe, GeoEye, Earthstar Geographics, CNES/Airbus DS, USDA, USGS, AeroGRID, IGN, and the GIS User Community

Figure 1.3 Map of the UK offshore oil and gas discoveries (<https://ogauthority.maps.arcgis.com> [Accessed on 20/12/2016]).

## 1.2 Aim and objectives

There have been only limited investigations into ways to transform waste drill cuttings into products of value and as a result, there is a lack of commercially viable recycling options for this waste. The aim of this research is to investigate an innovative and resource-efficient re-use application for waste drill cuttings that is currently landfilled in the UK. The research investigates the use of waste drill cuttings as a raw material for the manufacture of lightweight aggregates (LWA) and evaluates the effect of production parameters on physical and environmental properties of the end-products.

The following objectives will be delivered:

### Objective 1: Raw material characterization

Drill cuttings will be characterized for chemical compositions, mineralogy, microstructure, thermal behaviour and contaminant leaching. The characteristics of raw materials will provide information on the bloating capability of materials, which is necessary for producing low-density LWA. In addition, the information will be used to optimize the properties of the end products.

### Objective 2: Assessing the effect of production parameters and the production of LWA

To identify effective production parameters, a literature review will be conducted. This involves the determination of pre-processing parameters such as drying, milling and pelletisation condition. For the production, the materials sintering temperature range for use in the kiln firing stage together with the heating/cooling rate and dwell time at the maximum temperature will be established.

### Objective 3: Assessing the properties of the manufactured LWA

To assess the performance of the manufactured LWA, physical properties of the final products such particle density, water absorption capacity (after 24 hours immersion) and compressive strength of the individual pellets will be determined and compared to those of commercially available products. The microstructure, developed during the firing stage and mineralogical phase changes, will be analysed in order to understand the physical properties and leaching behaviour of the manufactured LWA.

#### Objective 4: Developing a process framework to produce LWA complying with technical and environmental requirements

Due to the hazardous nature of the waste drill cuttings, development of effective treatments to mitigate the contaminant leaching will be investigated. To optimize the physical properties of LWA, the use of additional materials in the mix will also be explored. The design of suitable treatments and selection of potential additional material will be based on an extensive literature review. Finally, the amount of carbon dioxide emissions for productions of 1.0 tonne of LWA will be estimated.

#### 1.3 Summary of novelty and innovation

This thesis will provide a novel contribution to the field of sustainable construction materials by: -

- 1) Developing a beneficial reuse application for waste drill cuttings in the manufacture of LWA.
- 2) Characterizing the North Sea waste drill cuttings for which limited compositional and mineralogical data is currently available.
- 3) Developing innovative methods for the mitigation of contaminant leaching and improving the physical properties of the manufactured LWA.
- 4) Proposing a new approach for calculating the carbon dioxide emissions for production of drill cuttings LWA.

#### 1.4 Experimental approach

To achieve the identified objectives a series of laboratory work, material characterization, analytical experiments and statistical calculation will be employed. Table 1.1, shows the experimental approach for each objective.

Table 1.1 Experimental approach for each objective of the research.

Objective 1: Raw materials characterization	Objective 2: Determine production parameters for LWA manufacturing	Objective 3: LWA properties	Objective 4: Development of a production process framework
Oxide compositions	Pre-processing	Particle density	Design suitable pre-treatments
Mineralogy	Sintering range	Water absorption	Use additional materials in the LWA body/matrix
Heavy metal content	Heating and cooling rate	Compressive strength	Estimation of CO <sub>2</sub> emissions for LWA production
Total petroleum hydrocarbons	Firing temperature	Microstructure	
Particle morphology	Dwell time	Mineralogy	
Thermal Analysis		Leaching test	
Leaching test			
Loss on Ignition			

## 2 Chapter 2 Waste drill cuttings and LWA potential

### 2.1 Oil and gas drilling technology

Drilling operations are employed in two major phases of oil and gas extraction: exploration and development. The presence of hydrocarbons is assessed by exploratory drilling and once they are discovered in sufficient quantities for commercial production, development wells are drilled (CAPP, 2001).

#### 2.1.1 Drilling process

The process of oil and gas well drilling consists of rotary drills and drilling fluids, such as water, to transport the drilling fragments (cuttings) that need to be removed. In this setting, as shown in Figure 2.1, the drill bit at the lower end of drill pipe (drill string) cuts through the formation rock to produce the drill cuttings. The drill bit has a larger diameter than the drill pipe to provide a space between the pipe and wellbore wall (annulus). Drilling mud enters the drilling pipe on the surface and exits the drilling bit at high velocities to flush away the drill cuttings to the surface through the annulus. The high viscosity of drilling mud suspends the chipped off cuttings that were produced from the rotation of the drill bit and eases their transportation to the surface where the cuttings are removed, and the drilling mud is recycled for re-injection back into the drill pipe. Cuttings are produced during all stages of the drilling process. However, higher quantities of cuttings are removed at the early stages where the borehole diameter is at the largest (Melton et al., 2004). The drill pipe rotation is provided by a rotary table at the surface to generate a sufficient torque for the drill bit. As drilling continues and the well deepens, steel casings with lower diameters are placed inside the wellbore. The space between the wellbore wall and casings is filled with cement to fix the casing. This process is continued until the final depth is reached and the wellbore is ready for tubing to be installed for oil and gas production.

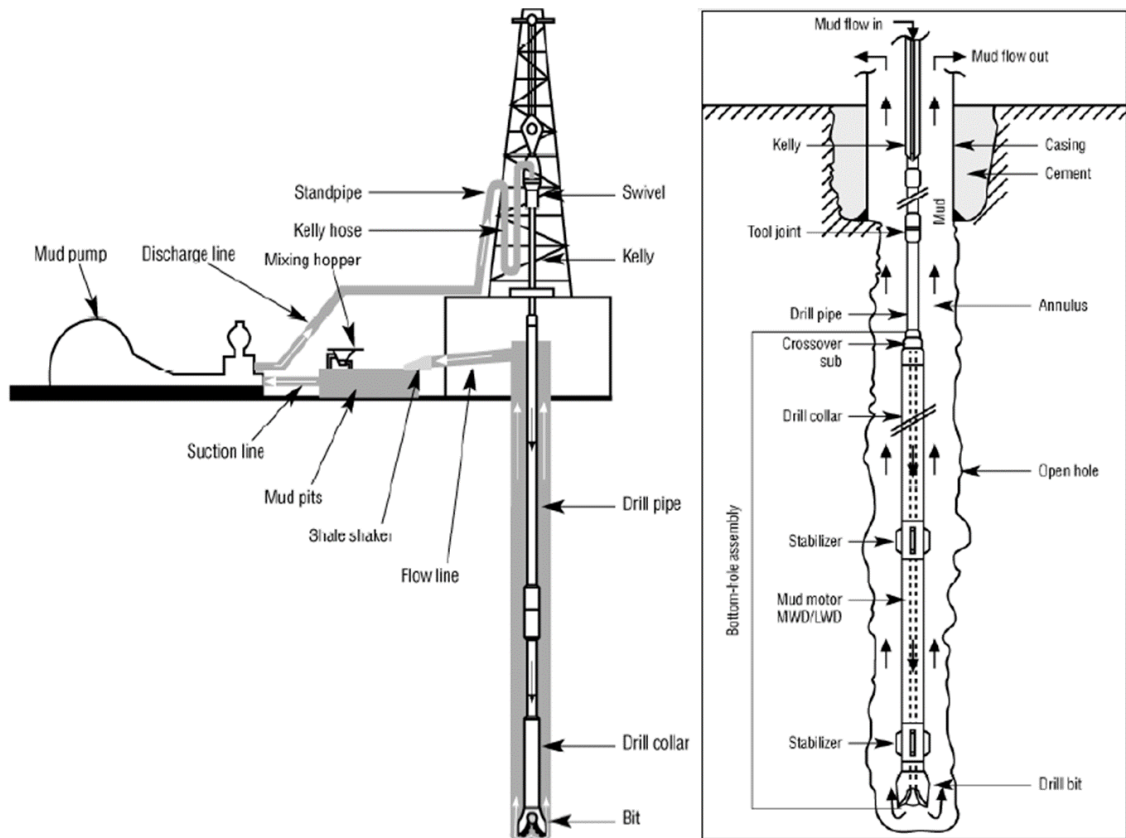


Figure 2.1 Oil and gas drilling operation. Modified from (CAPP, 2001).

### 2.1.2 Drilling mud

Drilling muds are used during drilling operations for (Melton et al., 2004, Neff, 2005):

- a) Maintaining pressure: drilling mud in the wellbore together with the drill pipe provide a hydrostatic load over the formation being drilled. This also prevents the accumulation of formation fluid and ensures a safe drilling operation.
- b) Removing cuttings from the wellbore: the stream of drilling mud coming out of the drill bit carries the cuttings away, preventing it from clogging. It also transports the cuttings from the bottom of the hole to the surface, through the annulus. For this function, sufficient viscosities are vital to suspend the cuttings when drilling stops, particularly for drilling horizontal wells.
- c) Cooling and lubrication: drilling muds cool and lubricate the drill bit and the drill pipe which heat up due to friction at the contact point with the formation.
- d) Protecting, stabilizing and supporting the wellbore wall: formation minerals such as shale can swell in the presence of water during the drilling operation and cast

off the sidewall into the well. Drilling muds contain additives to minimize this effect.

- e) Preventing mud transfer to the formation.

#### 2.1.2.1 Continuous phase in drill muds

The type of drilling muds is based on characterises of the drilled rock formation These formulations can be classified into two major groups (Neff et al., 2000):

- a) Water-based muds (WBM): The continuous phase in WBM is freshwater, seawater or concentrated brine. Historically, most of the drilling operation in the North Sea used water-based muds, however drilling certain formations composed of swelling rocks was problematic due to the wellbore instability (Davies et al., 1984). During drilling operations with WBMs, cuttings are usually discharged into the sea.
- b) Non-aqueous-based muds (NABMs): The continuous phase in NABM is replaced either by a mineral or synthetic oil. NABMs are often used in technically challenging sections of the drilled well, or when wells with non-vertical angles are being drilled (Oil and Gas UK, 2016b). The fluid part in is an invert emulsion with fine water droplets in a water-to-oil ratio of between 1:6 and 1:1. This provides a number of advantages over WBM including better lubrication and stability. In the 1980's and 1990's mineral oil-based muds (OBMs) were developed as a replacement for WBM and for a decade they were extensively employed in the North Sea (Neff, 2005). Used OBMs were commonly sent onshore for disposal whilst cuttings containing absorbed OBM were discharged to the ocean. This experience in the North Sea proved to have a permanent environmental impact and therefore, the discharge of OBM was ultimately banned in 1994 (Bloys et al., 1994, Olsgard and Gray, 1995). The environmental concerns over the use of OBMs forced the oil industry to develop a new group of drilling fluids based on synthetic oils (SBMs) (Candler et al., 1993). Synthetic based muds (SBMs): In SBMs, the continuous phase is composed of synthetic oil and, as opposed to OBMs, neither the fluid nor the additives are of petroleum origin (Neff et al., 2000). SBMs were formulated to be more environmentally compatible i.e. to degrade faster than OBMs if discharged, and contain minimal volatile

compounds such as polycyclic aromatic hydrocarbons (PAHs) - while showing similar functionality to OBMs (Friedheim and Conn, 1996).

Table 2.1 shows the continuous phase in SBMs. Four typical formulations for synthetic oil are available (Neff et al., 2000):

- a) Synthetic hydrocarbons: polymerized olefins such as linear alpha olefins (LAOs), poly alpha olefins (PAOs) and internal olefins (IOs) are the most commonly-used synthetic hydrocarbons (Friedheim and Conn, 1996). Ethylene ( $C_2H_4$ ) is the building block of these polymers with each group containing a mixture of polymers, with different chain lengths, to achieve optimal physical and chemical properties that are important during drilling operations.
- b) Ethers: are saturated hydrocarbons with a wide variety of chain lengths that can provide high hydraulic stability and low toxicity (Candler et al., 1993). Despite these advantages, they have a very low biodegradability and their use in the North Sea has been abandoned.
- c) Esters: are produced from a reaction between a fatty acid (carboxylic acid derived from vegetable or fish oil) and alcohol (most commonly 2-Ethylhexanol). In SBM systems, sometimes a mixture of fatty acid esters is used. They can also be mixed with other polymerized olefins to enhance the drilling performance. Esters are popular in the North Sea.
- d) Acetals: similar to ethers, they are stable in neutral and basic conditions. They have been used in the North Sea in the past but are no longer used today.

Table 2.1 Continuous phase categories in synthetic-based drilling fluids and their chemical structure and chain length range (Neff et al., 2000).

SBM continuous phase	Chemical structure	Chain length
Synthetic hydrocarbons:		
Linear Alpha Olefin (LAO)	$\text{CH}_3 - (\text{CH}_2)_n - \text{CH} = \text{CH}_2$	$\text{C}_{14} - \text{C}_{16}$
Poly Alpha Olefin (PAO)	$\begin{array}{c} \text{CH}_3 - (\text{CH}_2)_n - \text{C} = \text{CH} - (\text{CH}_2)_m - \text{CH}_3 \\   \\ (\text{CH}_2)_p - \text{CH}_3 \end{array}$	$\text{C}_8 - \text{C}_{40}$
Internal Olefin (IO)	$\text{CH}_3 - (\text{CH}_2)_m - \text{CH} = \text{CH} - (\text{CH}_2)_n - \text{CH}_3$	$\text{C}_{16} - \text{C}_{18}$
Ether	$\text{CH}_3 - (\text{CH}_2)_n - \text{O} - (\text{CH}_2)_n - \text{CH}_3$	-
Ester	$\begin{array}{c} \text{CH}_3 - (\text{CH}_2)_n - \text{C} = \text{O} \\   \\ \text{O} - (\text{CH}_2)_m - \text{CH}_3 \end{array}$	$\text{C}_{26}$
Acetal	$\begin{array}{c} \text{CH}_3 - (\text{CH}_2)_n - \text{O} \quad \text{O} - (\text{CH}_2)_n - \text{CH}_3 \\ \backslash / \\ \text{CH} - (\text{CH}_2)_m - \text{CH}_3 \end{array}$	$\text{C}_{20}$

#### 2.1.2.2 Drilling mud additives

During the drilling process, cuttings are constantly separated from the drilling muds, however, there always remains a portion of this mud, which contaminates the cuttings with hydrocarbons (Wheaton and Manu, 2012). Drilling muds contain a number of additives to enhance drilling operations, therefore for any re-use application of drill cuttings, information about the composition of the absorbed mud is crucial. Table 2.2 shows the functions and examples of additives found in drilling muds. These additives are classified as (Neff, 2005):

- a) Weighting materials: the main weighting material that is often used for all types of drilling mud is barite ( $\text{BaSO}_4$ : a natural mineral with density of  $4.1 - 4.5 \text{ g/cm}^3$ ). This material may contain impurities such as  $\text{SiO}_2$ ,  $\text{Fe}_2\text{O}_3$ ,  $\text{CaCO}_3$ ,  $\text{CaMgCO}_3$  and several metal sulphides. The amount of  $\text{BaSO}_4$  in drilling mud ranges from 6.3

kg/m<sup>3</sup> (for drilling near the surface) to 2000 kg/m<sup>3</sup> (for deep wells). The use of large amounts of BaSO<sub>4</sub> can be problematic due to high concentrations of metals. Therefore, hematite (Fe<sub>2</sub>O<sub>3</sub> with a density of 5.3 g/cm<sup>3</sup>) or ilmenite (FeTiO<sub>3</sub> with a density of 4.5 – 5.0 g/cm<sup>3</sup>) can be used as a replacement for BaSO<sub>4</sub> to produce high-density drilling muds, with a lower environmental risk if disposed of offshore (Chénard, 1984, Commission, 2004).

- b) Viscosifiers: these are the second most abundant additives in the composition of drilling muds. Bentonite (sodium montmorillonite) or palygorskite clay are often added to drilling muds to provide gel-like properties with sufficient viscosity capable of suspending the drill cuttings. Cellulose polymers and starch can be used as a replacement for clay to provide a better viscosity while preventing fluid loss to permeable formations (Hudgins, 1991).
- c) Thinners and dispersants: The addition of weighting materials and viscosifiers increases the energy required for pumping. Thinners and dispersants can be added to balance the viscosity by forming complexes with the charged clay particles, preventing them from flocculation (particles clumping together). Several deflocculants such as chrome and ferrochrome lignosulfonates have been used for offshore bentonite-based WBMs. However, oil industries in the North Sea have replaced these materials with calcium and iron lignosulfonates and other deflocculants such as lignite, due to the high toxicity of Cr compounds (Conklin et al., 1983, Hudgins, 1991).
- d) Other additives: a number of other additive are available in drilling fluids at lower amounts (Husein et al., 2010): asphalt (to reduce fluid loss to permeable formations); diesel fuels, vegetable or mineral oils as lubricants (to reduce torque); water-soluble emulsifiers (to disperse the oils in the water phase); and, Fe<sub>2</sub>O<sub>3</sub> and ZnO as sulphide scavengers (to deal with the H<sub>2</sub>S that may seep into the wellbore from the formation).

Table 2.2 Concentration and function of components for drilling muds, modified from (Rushing et al., 1991).

Additives	Function	Example
CaCl <sub>2</sub>	Reduce water activity and promote dehydration of shale.	-
Emulsifier	Promote forming and maintaining an inverted emulsion (water in SBF).	Metal soap of fatty acids
Rheological Modifier	Promote suspending drill cutting in the mud.	Organophilic montmorillonite
Lime (CaO)	Enhance the emulsification of water.	-
Wetting agent	To ensure that the formation solids (cuttings) are wet.	Polyamines, fatty acids, and oxidized tall oils
BaSO <sub>4</sub>	Increase the weight of the drilling mud and control the well pressure.	-

### 2.1.3 Separation of drilling fluids from drill cuttings

The drilling fluid must be constantly separated from drill cuttings before re-entering into the wellbore. For an effective separation and control over solids, the knowledge of suspended solid particle sizes in the drilling mud (both cuttings and solid additives) is necessary. A portion of solids, such as bentonite, that are dispersed in the mud system to increase the viscosity has a particle size range below 2  $\mu\text{m}$  (colloidal size). In addition, some of the cuttings as they move up the wellbore may undergo size degradations. This increases the available surface area of the solids and thus, more liquid is needed to keep the newly generated surface wet. The lack of free liquid increases the viscosity above the desirable levels, therefore, it is very important to separate the cuttings before they break down. Figure 2.2 shows the classification of solids in drilling muds based on particle size.

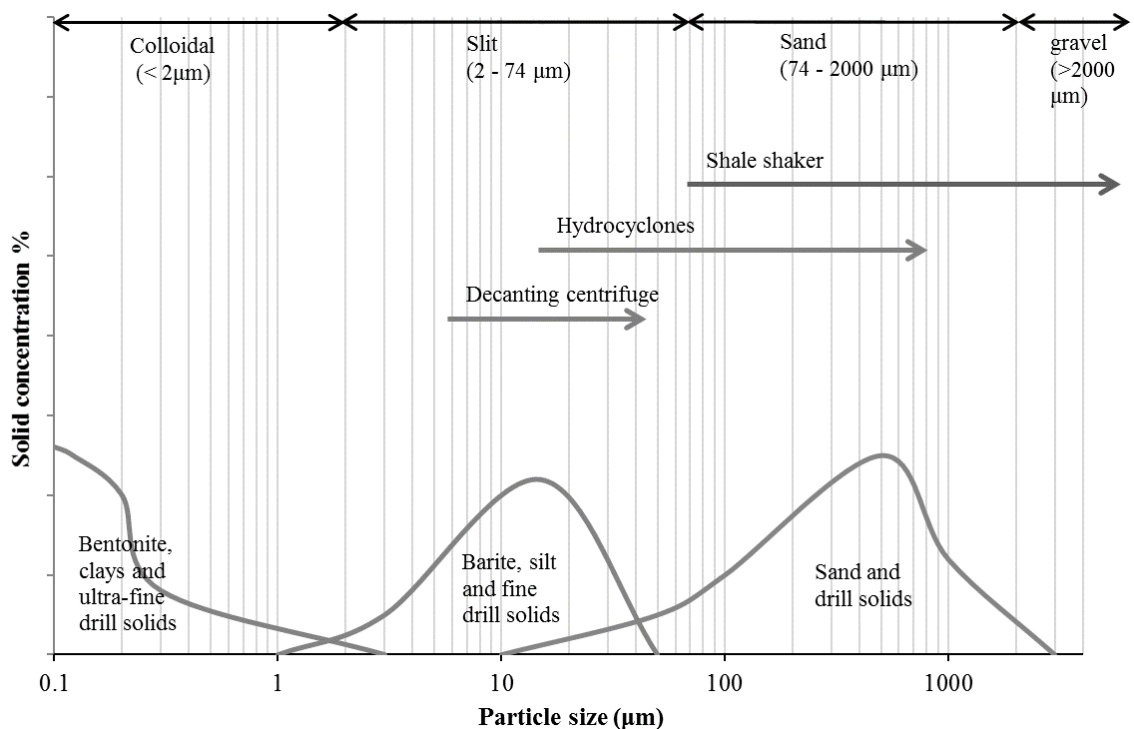


Figure 2.2 Classification of solids in drilling muds based on the particle size, modified from (IOGP, 2016).

Common separation techniques for each particle size range involves (CAPP, 2001):

- a) Shale shaker: the machine basically operates by vibrating screen separators as shown in Figure 2.3a. Shale shakers are used as the first step in the drilling mud solid control process. 100% of the drilling mud with cuttings that are transported

to the surface flows into a shale shaker and fragments that are larger than the mesh size are separated. For a typical shale shaker 5 – 15% of drilling mud remains on the cuttings. Recent technical advances have reduced this portion to 3 – 8% by using a vacuum-assisted technology (IOGP, 2016).

- b) Hydrocyclones: particles with a lower particle size can be separated by hydrocyclones. They use centrifugal force from the pressure produced by a pump to separate the suspended solids from the drilling mud, as shown in Figure 2.3b. De-sanders hydrocyclones are usually used for drilling muds containing high volumes of cuttings produced from the fast drilling of large-diameter top holes (IOGP, 2016). De-silting hydrocyclones are used to separate smaller particles (cuttings in range of 12 – 40  $\mu\text{m}$  and  $\text{BaSO}_4$  in range of 8 – 25  $\mu\text{m}$ ) (IOGP, 2016). They work with the same mechanism as de-sanders but with cones smaller in diameters.
- c) Decanting centrifuges: these are usually used for weighted drilling muds to separate  $\text{BaSO}_4$  which is to be returned to the active mud system. The drilling mud is passed through a high-speed rotating bowl as the centrifugal forces transfer the heavier particles to the bowl wall where they are scraped by a rotating screw (conveyor) and ultimately discharged, as shown in Figure 2.3c (IOGP, 2016).

The discharged materials from each of the above-mentioned separation techniques form the main constituents of waste drill cuttings. Shale shakers produced drill cuttings with the highest amount of absorbed drilling mud. This increases the hazardous properties of the discharged waste and causes a problem for the potential reuse of drill cuttings.

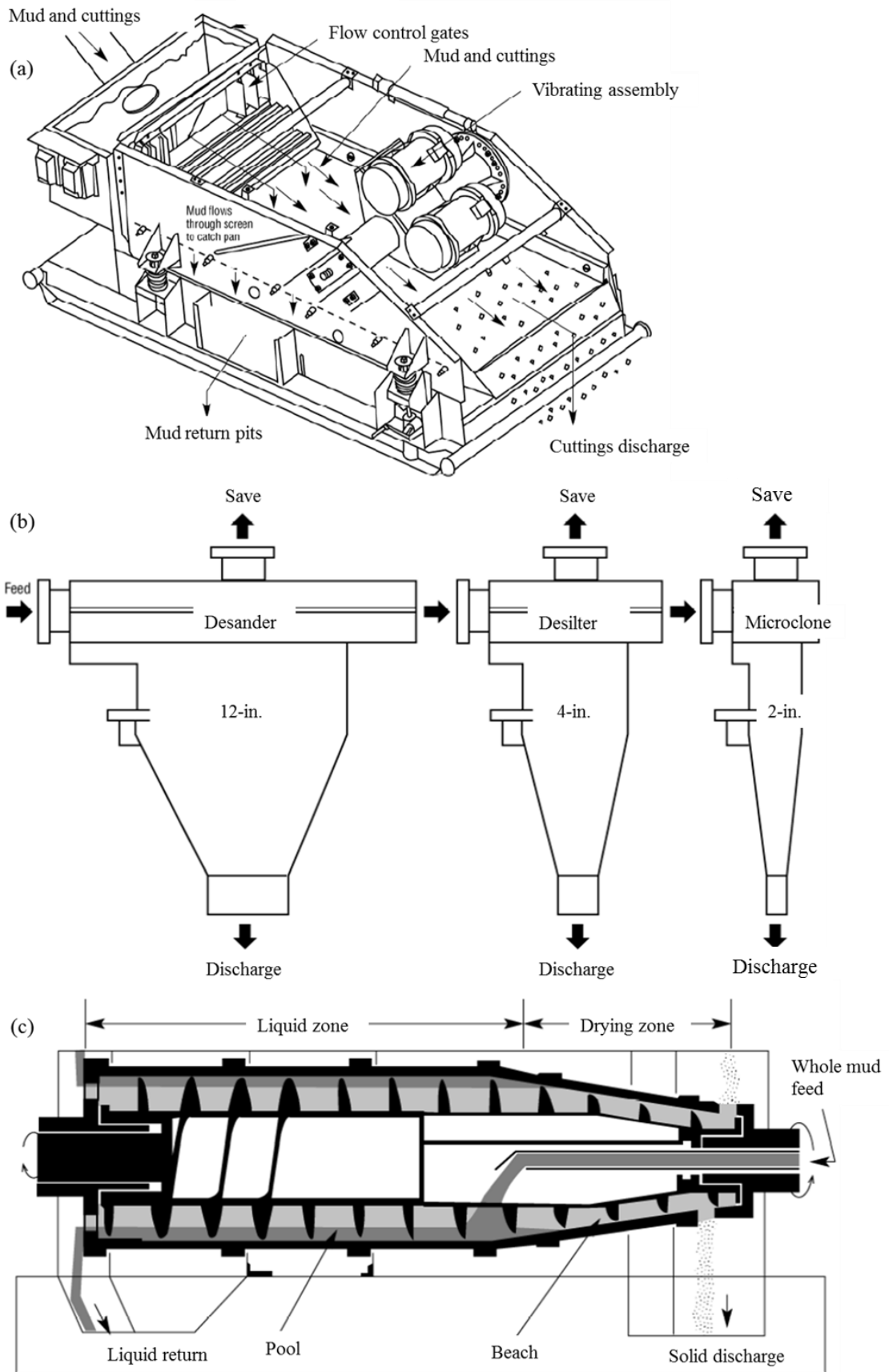


Figure 2.3 Drill cuttings separation techniques: (a) adjustable linear shale shaker, (b) hydrocyclones and (c) decanting centrifuge, modified from (CAPP, 2001).

## 2.2 Drilling wastes

Waste is produced at each stage of the oil and gas production life cycle - including exploration, development, drilling operation and decommissioning. Drilling operations generate two main types of waste, namely; produced formation water and drill cuttings (Oil and Gas UK, 2016b):

### 2.2.1 Produced formation water

Produced water is comprised of petroleum (associated with the naturally occurring reservoir products) and the water that is injected into the formation to maintain the well pressure (Holdway, 2002). According to Oil and Gas UK, 165 million m<sup>3</sup> produced water was discharged into the sea in 2015. This was 37% lower than in 2000, where 263 million m<sup>3</sup> was discharged (Oil and Gas UK, 2016b). The report also highlights that the decrease in the discharged volume was mainly due to a decrease in the UK overall oil and gas production over that time.

### 2.2.2 Waste drill cuttings

During the 1960s and 1970s piles of drill cuttings were formed underneath and around approximately 250 oil platforms in the North sea (Marsh, 2003). In 2004, the drill cuttings volume in the North Sea was estimated to be 12 million m<sup>3</sup> (Breuer et al., 2004). The issue with drill cutting waste piles surrounding platforms in the North Sea is complex with some reports claiming that these waste piles can contain radioactive materials (Ducrotoy et al., 2000). The debate is on whether to leave or to move the piles onshore. It is argued that they are stable due to sediment covering and more importantly, causing any disturbance such as transportation could result in the release of pollutants (Turner, 2002). However, these piles of material have already been redistributed, due to tidal flows, and contaminated the seabed (Breuer et al., 2008). The evidence suggests that the effect of the existing discharge on the seabed and sediment contamination is local and the risk of widespread impact is not significant (Breuer et al., 2004). However, there is very little published information on the effect of drilling waste accumulation on marine populations or communities to know if the effect is actually significant or not (Bakke et al., 2013).

In 1995, the first wells using SBMs were drilled in the North Sea and the cuttings were mainly discharged since the environmental impact of SBM were thought to be lower than

other mud systems (Neff et al., 2000). However, by 2001, all SBM drill cutting discharges were banned by government regulations (Breuer et al., 2004). The growing concerns over marine environmental pollution have been enough to produce change, with obliging the drilling operators to transfer their SBM drill cuttings onshore for treatment or disposal (Marsh, 2003). The Oslo-Paris convention for the protection of the North Sea (OSPAR) was put in force to prohibit the discharge of non-aqueous based cuttings that contain more than 1% fluid (Neff, 2008). The uncertainty over the effect of hydrocarbons on the marine environment has driven the legislator to further limit the offshore operational discharges and promote onshore treatment solutions. Currently, the EU and domestic offshore regulations require the operators to publish extensive details of every proposed exploratory drilling and provide an environmental statement for most developments (Strachan, 2010).

### 2.2.3 Radioactivity of waste drill cuttings

Despite some reports about the radioactivity of drill cutting waste piles (Ducrotoy et al., 2000), relatively low levels of naturally occurring radioactive materials (NORM) may exist in the organic-rich fractions of sediments (Breuer et al., 2004). These radioactive properties are usually measured based on the calculation of the exposure rates by means of activity concentration of naturally radioactive isotopes ( $Ra_{226}$ ,  $Th_{232}$ ,  $K_{40}$ ). For shale drill cutting samples, the levels of radioactivity were actually found to be negligible (Piszcz-Karaś et al., 2016). Currently, NORM testing is not required for drill cuttings waste management companies in the UK.

### 2.2.4 Relevant legislation

The management of any drilling waste must be in accordance with the EU Waste Framework Directive (2008/98/EC) which requires some form of treatment prior to disposal in landfills. In 2010, Department of Environment, Food and Rural Affairs (DEFRA) published a strategy with the aim to establish the practical application of the EU Waste Framework Directive (2008/98/EC). The document set out a methodology for the environmentally sound management of hazardous waste, including six principles (DEFRA, 2010, Lampris, 2013):

1. The waste hierarchy: a hazardous waste should be managed in accordance with the EU waste hierarchy which prioritizes the available management options as prevention, reuse, recycling, recovery and disposal.

2. Infrastructure provision: hazardous waste infrastructure should be developed to ensure the UK's self-sufficiency in terms of hazardous waste disposal and recovery.
3. Reduce reliance on landfill: landfilling practices should only be used when no better option is available.
4. No mixing or dilution: hazardous waste should not be mixed with other categories of hazardous waste or non-hazardous waste, unless under the terms of an environmental permit, and the mixing operation conforms to best available techniques.
5. Treatment of hazardous organic waste: when no reuse, recycling or recovery option is available, hazardous organic waste should be destroyed using best available techniques and should not be landfilled.
6. End reliance on the use of Landfill Directive waste acceptance criteria (WAC) derogations ( $3 \times$  WAC) that enables the hazardous waste landfilling practice to continue.

The strategy also includes decision trees to support the implementation of these principles and assess the best available management option in accordance with the waste hierarchy. Figure 2.4 shows the relevant steps from the Waste Decision Tree for Inorganic Hazardous Waste that can be used for managing oil-contaminated drill cuttings waste. It must be noted that this decision tree is advised when no further separation of oil from drill cuttings is possible and there is no potential for energy recovery from waste. Contaminated drilling waste cannot be directly reused as a raw material or recycled without pre-treatment. A guidance note published by the UK government on the application of decision trees has specified that the use of pre-treatments can be regarded as an interim step towards 'other recovery' but only where the waste is strictly intended to be used as a raw material replacement in a recovery process (Defra, 2011). The guidance gives an example of 'other recovery' for a gypsum-based waste resulting from the washing of air pollution control residues (APCr); suggesting that the waste can be used on its own or mixed with other calcium sulphate-based waste in an authorised construction activity under a permit and dependant on the remaining contaminant. Such recovery routes have been taken for drill cuttings waste in land application and bioremediation which will be discussed in section 2.4.5.

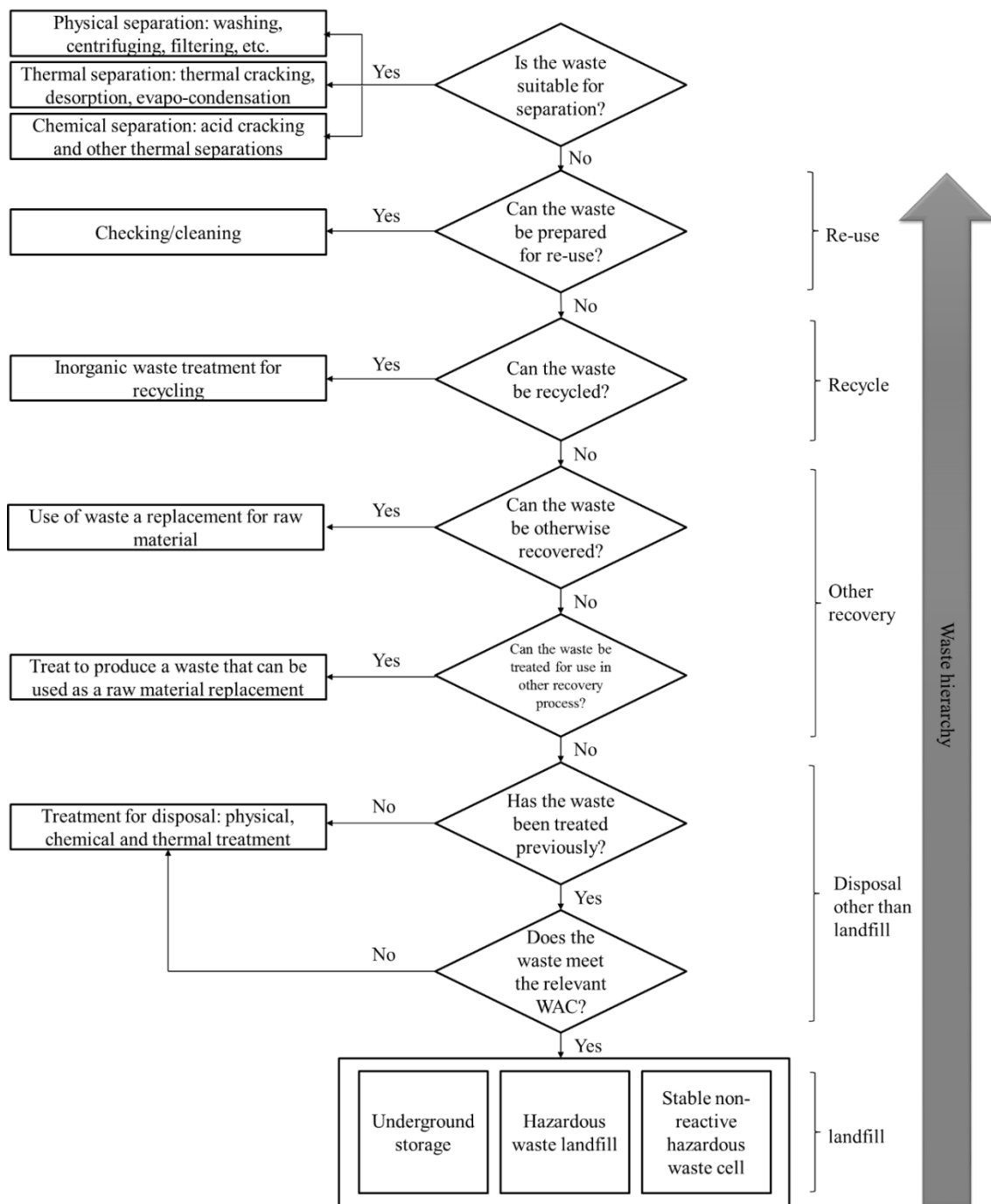


Figure 2.4 Decision Tree for Inorganic Hazardous Waste that can be used for managing oil-contaminated drill cuttings waste on which no further separation and energy recovery can be applied (DEFRA, 2010).

## 2.3 Drill cuttings mineralogy and the geology of the North Sea

In the UKCS, the exploratory and development drilling activities are permitted in specific areas (shown as rectangular blocks in Figure 1.3). Central and northern North Sea have the highest share of oil production in the UK over the last decade and, most of the recent discoveries are also located within these regions. For any management practice of drilling cuttings waste, obtaining knowledge on the history of underlying geological formations and thus, on the petroleum geology of the North Sea is essential.

The North Sea is located between Norway and the UK with an area of approximately 600,000 square kilometres. It has an eventful geological history which has been discovered with extensive drilling activities in recent years. The major reservoir rocks are sandstone and limestone formed during the Middle and Late Jurassic successions (British Geological Survey, 2001). For instance, one of the most important hydrocarbon reservoirs with varying thickness of sedimentary rocks is located by the East Shetland Basin (Brent Group) and belongs to the Middle Jurassic (Johnson et al., 2005). Another important example is the Fladen Group which includes four formations comprising all coal-bearing and overlying transgressive sandstone units (Richards, 1993). The Late Jurassic succession is also significant since the primary source rocks including Kimmeridge Clay (comprising sandstone with high potential for hydrocarbons) were deposited during this period. Therefore, it is believed that a vast portion of the remaining hydrocarbons lies in similar reservoirs (Johnson et al., 2005). Those types of sedimentary rocks, that are important for the accumulation of hydrocarbons, are most likely to be found in drill cuttings and involve (Bjørlykke, 2015):

### 2.3.1 Sandstones

Jurassic sandstones are one of the most important oil reservoirs in the North Sea. Sandstones have high porosity and permeability which is essential for petroleum production. They mainly consist of sand grains up to 2 mm in diameter and various amounts of silt and clay. Sand grains contain quartz (85 – 90%), feldspars and microcrystalline rock fragments (Bjørlykke, 2015). Major clay minerals such as kaolin, illite, smectite, chlorite, and mix layers such as illite-smectite have been co-deposited with sand grains and deformed by mechanical compaction to form into sandstone (Bjørlykke, 1992).

### 2.3.2 Carbonates

Carbonate reservoir rocks contain more than 40% of the petroleum in the world (Bjørlykke, 2015). Pure chalk limestones with clay-rich intervals can be found in the North Sea reservoirs (as in Plenus Marl). Such reservoirs are different to sandstone reservoirs in terms of sediment particles being produced through chemical precipitation<sup>1</sup> or biological processes<sup>2</sup>, mineralogy and texture, solubility in water and porosity. Geochemically, carbonates are characterized by an anionic structure consisting of  $\text{CO}_3^{2-}$  and one or more cations. Rock-forming calcium carbonate ( $\text{CaCO}_3$ ) can be found as calcite (rhombohedral) or aragonite (orthorhombic) based on their crystal habit. Dolomite ( $\text{CaMgCO}_3$ ) is also a common rock-forming mineral found in carbonate reservoirs. In dolomite, layers of  $\text{CaCO}_3$  are alternated with layers of  $\text{MgCO}_3 \cdot \text{Fe}^{+2}$ .

### 2.3.3 Shale and mudrock

A vast majority of sedimentary basins consist of shale and mudrock. These sedimentary rocks have high porosity and can therefore be a suitable source rock for hydrocarbons (the environment where organic materials are initially deposited and are subsequently migrated to reservoir rocks). However, shale may have very low permeability and thus, serve as a caprock (generating trapping mechanism to store hydrocarbons). Shale and mudrock are formed by the consolidation of varying amounts of fine-grained rocks, including a high content of clay-sized particles and other non-clay minerals (Halliburton, 2001). The clay minerals have similar origins to those in sandstones including weathering of non-sedimentary rocks, erosion of older shales, and diagenesis on the seafloor and during burial.

### 2.3.4 Evaporite

Evaporites are impermeable sedimentary rocks that make very effective traps for oil and gas. The presence of evaporite is often associated with hydrocarbons in oil and gas explorations. These traps are found in the form of salt domes especially in the southern North Sea (Bjørlykke, 2015).

---

<sup>1</sup> The chemical process involves dissolution of atmospheric  $\text{CO}_2$  in seawater generating carbonic acid which can react with calcium or magnesium ions and precipitate as calcium carbonate or magnesium carbonate.

<sup>2</sup> The biological process involves calcareous organisms and thus, the mineralogy of such sediments is related to carbonate skeleton.

Evaporites are simply the salt minerals that have formed in normal marine or continental environments by evaporation of water. The percentage composition of dissolved salts in seawater, together with the produced salt minerals, are listed in Table 2.3. Figure 2.5 also shows the sequence of evaporite precipitation as calcite ( $\text{CaCO}_3$ ), gypsum and anhydrite<sup>3</sup> ( $\text{CaSO}_4 \cdot 2\text{H}_2\text{O}$  and  $\text{CaSO}_4$ ), halite ( $\text{NaCl}$ ), sylvite ( $\text{KCl}$ ) and bromide salts (Halliburton, 2001).

Table 2.3 Concentration and composition of salts formed in seawater after evaporation.

Constituents	(%) in seawater	Salts	(wt.%) of produced salts after evaporation
Na	30.64	NaCl	77.76
Mg	3.76	MgCl <sub>2</sub>	10.86
Ca	1.20	MgSO <sub>4</sub>	4.74
K	1.09	CaSO <sub>4</sub>	3.60
Cl	55.21	K <sub>2</sub> SO <sub>4</sub>	2.47
S	7.70	MgBr <sub>2</sub>	0.22
C	0.21	CaCO <sub>3</sub>	0.35
Br	0.19		
Total	100		100

<sup>3</sup> Calcium sulphate may precipitate as a hydrated form  $\text{CaSO}_4 \cdot 2\text{H}_2\text{O}$  (gypsum) with a monolithic crystal system and, as a non-hydrated form  $\text{CaSO}_4$  (anhydrite) with an orthorhombic crystal system (Bollen, 1954).

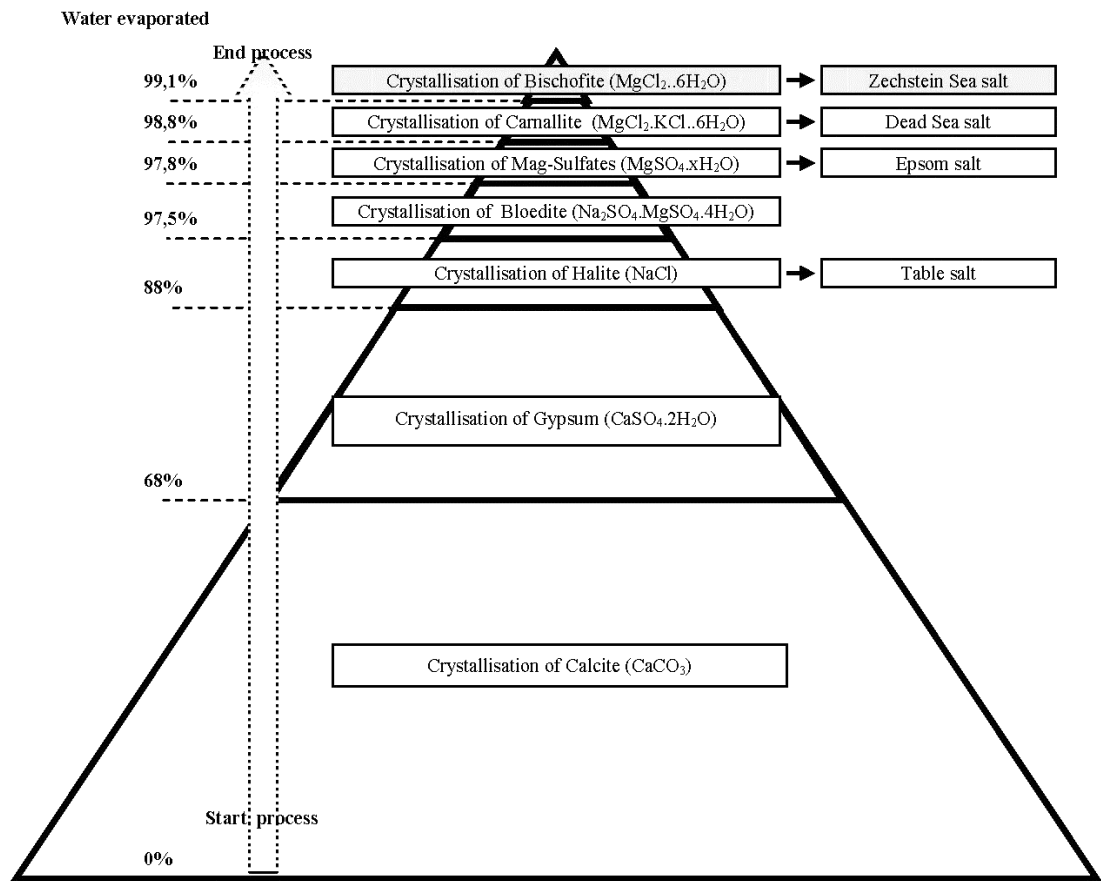


Figure 2.5 Evaporation sequence in seawater (www.ancientminerals.eu [Accessed on 16/10/2016]).

A limited number of studies have investigated the mineralogy of drill cuttings produced in the North Sea. Abbe et al. (2009) examined samples of oil-based drill cuttings from the central North Sea and reported  $\text{SiO}_2$ ,  $\text{CaCO}_3$ ,  $\text{CaMgCO}_3$ ,  $\text{BaSO}_4$ ,  $\text{KAl}_2(\text{Si}_3\text{AlO}_{10})(\text{OH})_2$  (muscovite), kaolinite,  $\text{NaCl}$  and feldspars. Dhir et al. (2010) conducted XRD analyses of drill cuttings originating from four different locations in the North Sea and showed similar major phases with the absence of  $\text{NaCl}$  and clay minerals. However, this notwithstanding, there is no other information available on the mineral composition of drill cuttings to date. The degree of variability reported in these studies would greatly affect the proposed reuse application and thus a great deal work was allocated to characterize the mineral composition of waste drill cuttings in this research.

## 2.4 Current disposal, treatment and management options

Managing the drilling waste contributes significantly to the overall costs of drilling operations (Ikonnikova et al., 2015). Both offshore and onshore-based management options have been tested for contaminated drill cuttings. In the following sections, offshore options including re-injection, direct discharge into the sea and discharge after thermal treatments; and onshore options including landfill, bioremediation, solvent extraction and solidification/stabilization, are discussed.

### 2.4.1 Re-injection

Re-injection is a common offshore practice in which the cuttings are milled and mixed with seawater and pump down the well casing. This method, despite being associated with “zero discharge”, has been strongly criticized due to the risk for the return of cuttings to the surface, significant energy required for pumping, lack of studies on environmental risks and most importantly, the fact that the contaminated cuttings are discharged back into the environment without treatment (Gerrard et al., 1999).

### 2.4.2 Discharge

The direct discharge of drill cuttings into the sea has been banned, as discussed in section 2.2.2. Discharging drill cuttings after reducing the absorbed mud to less than 1% by thermal treatment has been commonly employed in the North Sea; however, due to the environmental risks associated with this practice, governments are now implementing zero discharge policies (Bakke et al., 2013).

### 2.4.3 Thermal treatments

To reduce the discharge impact, a number of thermal treatments can be applied prior to any offshore (re-injection and direct discharge) or onshore (landfill and land applications) scenarios. Thermal treatments can be applied in either standing or portable installations and, based on recovery of the contaminants, are generally classified as incineration or thermal desorption (Ball et al., 2012). Thermal treatments are largely preferred over discharge and re-injection solutions for two main reasons: firstly, due to the removal of contaminants and their associated hazards and secondly, due to the possibility of treatment facilities to be retrofitted onto current platforms (Pereira, 2013). Three available thermal treatment practices used for contaminated drill cuttings are:

#### 2.4.3.1 Incineration

Incineration is a high-temperature thermal oxidation process in which the waste is heated at temperatures between 900 °C and 1500 °C to destroy the organic fraction of the material, reduce the volume of waste and generate less hazardous residues (Oppelt, 1987, Morillon et al., 2002). Hazardous wastes are often a good candidate for incineration as they usually contain toxic and flammable organic materials that are resistant to biodegradation. Incineration of drilling wastes can be done in a rotary kiln, a commercially available technology that has been used for many types of waste. Rotary kilns produce an efficient heat transfer due to the turbulence generated from the tumbling motion of waste and that enhances the contact with hot burner gases (Islam and Khan, 2013). Incineration is not very common for treating drilling waste however, incineration at source (offshore incineration) has been shown to be technically feasible. Overall though, incineration is not considered environmentally acceptable and cost-effective due to the need for added fuel to sustain the process (Turner, 2002).

#### 2.4.3.2 Thermal desorption

Thermal desorption has been mainly used for treating contaminated soil. It involves heating the materials at temperatures up to 600 °C at which organic compounds are volatilized (not oxidized) and subsequently removed from the generated gas phase by means of rapid condensation, scrubbing, filtration or destruction at higher temperatures (Hester and Harrison, 2001). The process has also been broadly used for treating oil-based drill cuttings due to the nature of the base oil for which lower temperature ranges (200 °C – 400 °C) are applied. The technique can recover more than 99% of the absorbed oil with no significant degradation or fractionation (Khodja et al., 2007). Two common designs for thermal desorption are available, namely: rotary dryer and thermal screw (Ball et al., 2012). The rotary dryer design involves a slightly angled horizontal cylinder that is directly or indirectly heated and can treat drill cuttings with a total organic content of lower than 2%. In thermal screw designs, screw conveyors transport materials through hollow augers that are indirectly heated by hot oil or steam, as shown in Figure 2.6. The thermal screw design is cable of treating drill cuttings with more 50% organic content. In such settings, both water and oil are recovered separately due to the difference in boiling point and are usually re-used back into the system (Seaton et al., 2006).

Thermal desorption is a relatively new practice for processing hazardous waste in the UK (Environment Agency, 2012). A number of companies have established a range of low

-temperature thermal desorption facilities to treat oil-based and synthetic-based mud drill cuttings shipped to shore in the UK (Wait and Thomas, 2003). However, over the past few years, the traditional desorption technologies have shown serious drawbacks in terms of efficiency (Pereira, 2013), mainly due to the granular nature of drilling cuttings that makes heat transfer extremely inefficient. Elevating the temperature within the depth of such materials using conventional heating methods requires long dwell times, which creates a significant CO<sub>2</sub> footprint (Robinson et al., 2008). The high energy consumption and equipment cost has driven the waste management companies to invest in potential alternative technologies, such as microwaves capable of dissipating the heat more efficiently and chemical cleaning (Ye et al., 2017).

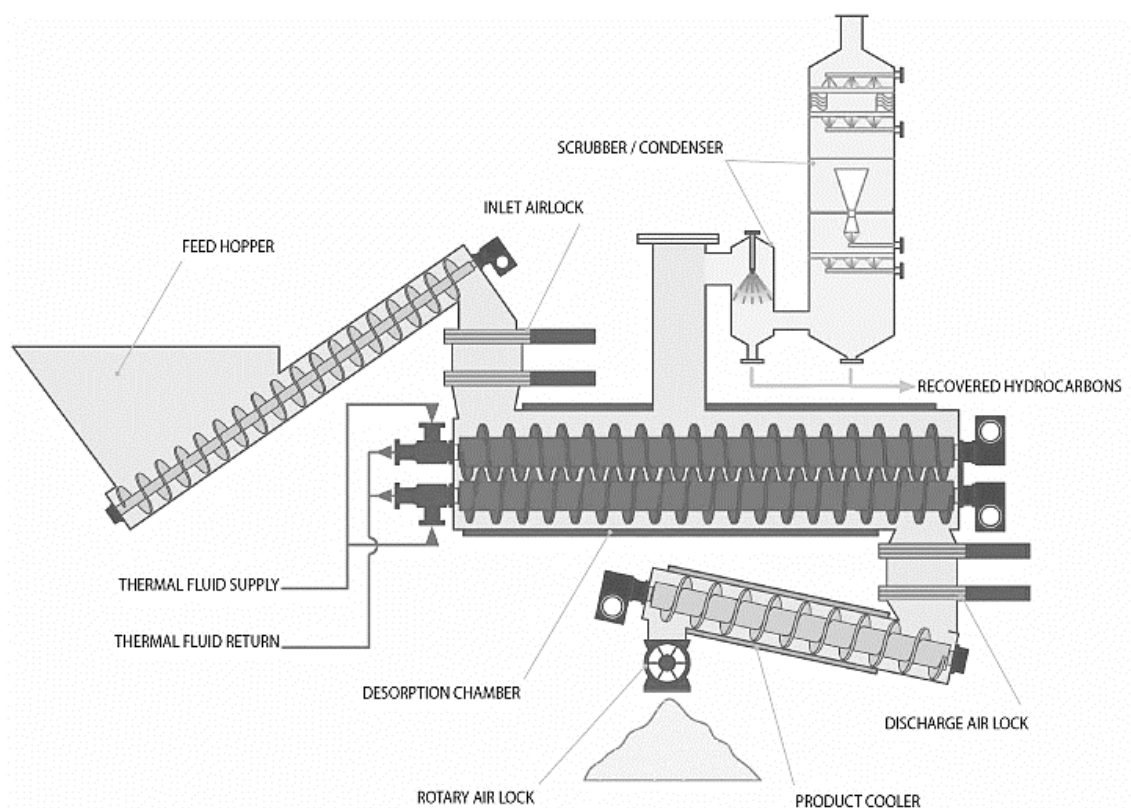


Figure 2.6 Thermal desorption unit with a thermal screw design (thermaldesorption.wordpress.com [Accessed on 17/10/2016]).

#### 2.4.3.3 Microwave

In microwave heating, the energy is directly transferred to depths of materials through molecular interactions with an alternating electromagnetic field (Robinson et al., 2008). This can significantly reduce the heating time (up to three orders) and thus, increase the overall efficiency of the treatment process (Robinson et al., 2008). Microwave heating

techniques have been successfully used for thermal desorption processes for contaminated soil remediation (Jones et al., 2002). This process has been recently tested at a pilot scale and shown to be effective on bringing the portion of hydrocarbons to below 1% in drill cuttings contaminated with synthetic-based fluid (Pereira et al., 2014, Petri Junior et al., 2015).

However, despite the high efficiency of microwave-assisted thermal desorption in reducing the hydrocarbon portion of drill cuttings, and thus the hazardous properties of the waste, such management options still contribute to waste generation – as the final treated solid waste is still required to be landfilled. In addition, other sources of contamination in drill cuttings, including soluble salts and drilling additives, remain unchanged over the temperature ranges used for such methods, and thus this limits the beneficial reuse of thermally treated drill cuttings.

#### 2.4.4 Supercritical fluid extraction (SFE)

In this method, fluids above their critical pressure and temperature are used as a solvent to extract compounds such as hydrocarbons from the solid matrix. Supercritical fluids have a gas-like diffusivity and viscosity, liquid-like density and almost no surface tension allowing their penetration deep into granular materials (Street and Guigard, 2009). This allows an efficient mass transfer of contaminants (hydrocarbons in case of drill cuttings) to the supercritical fluid phase. The method has been used for the treatment of OBM drill cuttings using supercritical carbon dioxide at a pressure range of 16 MPa to 22 MPa and a temperature range of 55 °C to 79.5 °C (Goodarznia and Esmaeilzadeh, 2006). In a more recent study, 89.2% efficiency for total organic carbon (TOC) removal was reported when supercritical water, at pressure of 35 MPa and temperature of 475 °C was used (Chen et al., 2017).

#### 2.4.5 Bioremediation

As the name suggests, it is a biological process that uses microorganisms such as bacteria and fungi to degrade the contaminants into non-toxic residues. It is simple, cost effective and generally, has a high public acceptance. However, its main drawbacks are the relatively long time scales, transportation cost involved and the fact that the process is not effective on the full range of contaminants present (Vidali, 2001). There are a number of bioremediation techniques available for treating contaminated drill cuttings, as listed in Table 2.4. Land applications including land farming and land treatments are less

exploitable in places like the UK where there is limited land availability. Bioreactors, on the other hand, are enclosed vessels in which various parameters can be controlled. Despite being complex, they can achieve rapid and satisfactory results and may represent a viable solution yet, in the UK, bioreactors have only been tested academically and further work to access commercial viability is still required (Turner, 2002).

Table 2.4 Summary of available bioremediation techniques for treating contaminated drill cuttings (Vidali, 2001, Turner, 2002, Ball et al., 2012).

Techniques	Area requirement	Time-scale	Advantages	Disadvantages
Composting/ bio-piling	Low (10 m <sup>2</sup> /tonne)	1 – 2 months	Rapid degradation of contaminants. Low risk of leaching.	Release of hydrocarbon into the environment. Fire risk.
Land application	Medium to very large (500 – 2000 m <sup>2</sup> /tonne)	2 – 3 years	Near complete degradation of contaminants. Low-cost.	Extended treatment time. Contamination build-up on repeated use of land. Bioavailability limitations.
Vermiculture	Low (20 m <sup>2</sup> /tonne)	1 – 2 months	Rapid degradation of contaminants. Useful by-product produced.	Effective for a limited range of contaminants.
Bioreactor	Very low	10 – 30 days	Rapid and complete degradation of contaminants. Short process duration.	Large cost of equipment. Requires skilled operation and maintenance.

#### 2.4.6 Solidification/stabilization (S/S)

This method is a chemical process in which binders such as Portland cement are mixed with certain amounts of waste to reduce the leaching characteristics of materials (Lampris et al., 2011). The method is often used for hazardous waste like energy-from-waste (EfW) residues with high concentrations of heavy metals and soluble salts, to comply with landfills of waste acceptance criteria (Quina et al., 2008). There are also successful examples of using this method for contaminated drill cuttings, as listed in Table 2.5.

Table 2.5 Studies using solidification and stabilization (S/S) for treating petroleum drill cuttings.

Reference	Waste	Binder	Comments
(Al-Ansary and Al-Tabbaa, 2004)	SBM drill cuttings from the North Sea	Portland cement	Significant reduction in leaching of both hydrocarbons and $Cl^-$ ions.
(Leonard and Stegemann, 2010)	Petroleum drill cuttings from an unidentified drilling operator	Portland cement	Enhanced immobilization capability for hydrocarbons and $Cl^-$ ions, with the addition of high carbon fly ash.
(Mostavi et al., 2015)	Petroleum drill cuttings from an unidentified drilling operator	Portland cement, coal fly ash and silica fume	Enhanced strength of concrete sample by adding up to 5 wt.% silica-fume.
(Aboutabikh et al., 2016)	Treated oil sand drill cuttings	Portland cement	Up to 20 wt.% drill cuttings in the mix provided enhanced solidification and reducing heavy metal leaching.
(Kogbara et al., 2016)	Petroleum drill cuttings from Niger Delta	Portland cement	Incorporating activated carbon resulted in up to 99% TPH reduction.

#### 2.4.7 Drill cuttings as a resource

Most of the treatment methods for contaminated drill cuttings are aimed at making the waste compatible with non-hazardous landfill requirements. There is still a lack of commercially viable recycling options for non-aqueous-based drill cuttings and a limited number of studies have investigated options for producing secondary products of value. Sintered glass ceramics with low porosity were produced from the North Sea SBM drill cuttings (Abbe et al., 2009). This was shown to reduce leaching of contaminants through physical encapsulation of salts and heavy metals within a glass matrix - however, such solutions have not reached a large-scale manufacturing level.

Geological materials and mineral wastes with compositions similar to those of drill cuttings have been extensively used in the production of building materials and especially sintered porous ceramic products known as lightweight aggregate (LWA). This indicates a significant potential for drill cuttings to be used as a resource, which will reduce landfill dependency. In addition, the presence of hydrocarbons can also be beneficial because during LWA production process, as organic matter is normally added to the mix to provide some part of the energy required for sintering.

In the UK, the market of LWA is growing due to a large demand for lightweight concrete products. At the same time, the use of naturally occurring materials is becoming limited due to environmental concerns about the overconsumption of natural resources. This generates a significant potential for the reuse of recycled materials (with a suitable composition) in the manufacturing of LWAs. Furthermore, this would allow part of the production costs to be offset against the avoided cost of waste disposal and contribute to the development of a circular economy, in which waste materials remain part of the economic cycle (Cheeseman and Viridi, 2005).

The following sections review the available research on using geological and mineral waste in LWA production, defining the properties of ideal LWA and typical production methods and conditions.

## 2.5 Lightweight aggregate<sup>4</sup>

The British standard (BS EN 13055-1) for lightweight aggregates for concrete, mortar and grout, define LWA as a granular material with a loose bulk density not exceeding 1.2 g/cm<sup>3</sup> or with a particle density not exceeding 2.0 g/cm<sup>3</sup>. An ideal LWA for use in concrete products should have low water absorption capacity, since water absorption can adversely affect the properties of hardened concrete (Molineux et al., 2016). In addition, LWA should be nearly spherical (4 – 14 mm in diameter to be in the range of normal coarse aggregate), strong and have an impermeable rough surface to enhance the cement-aggregate bond (Cheeseman and Viridi, 2005). LWA improves thermal insulation properties of concrete, reduces permeability and reduces structural dead load, allowing the construction of larger buildings with the same foundation size. The use of LWA to replace normal weight aggregate in precast concrete products is associated with additional CO<sub>2</sub> savings gained with more efficient transportation due to lighter loads (Velis et al., 2014).

LWAs can be classified in two groups: natural and synthetic. Natural LWAs consist of particles derived from natural rocks, mainly those of volcanic origin such as pumice, scoria and tuff (Cheeseman and Viridi, 2005). Synthetic LWAs are produced from materials such as shale and expansive clay at high temperature, traditionally in a rotary furnace (González-Corrochano et al., 2009b). These materials contain common clays and some amounts of non-clay minerals such as quartz and feldspars. These minerals produce sufficient viscosities that are capable of entrapping the released gaseous phases at high temperatures and bloat (expand).

### 2.5.1 LWA Manufacturing process

Figure 2.7 shows a typical LWAs manufacturing process and the end products when clay is used as the raw material. The two main stages of lightweight aggregate production are pelletisation and sintering (Anagnostopoulos and Stivanakis, 2009). Before pelletisation, raw materials such as clay and organic matter are finely ground and mixed together in specific proportions. Pelletisation can be achieved either by plastic extrusion or agglomeration of particles with suitable moisture content. Depending on the pelletisation method, water is either added at the beginning or gradually throughout the pellet formation process. ‘Green’ or ‘fresh’ pellets are obtained from this process.

---

<sup>4</sup> A revised version of this section has been published (Ayati et al., 2018).

The physical properties of the ‘green’ pellets are important for handling and stockpiling during the manufacturing process. They are mainly dependant on pelletisation parameters i.e. engineering properties of the raw material, such as particle size distribution, wettability, moisture content and the angle and rotational speed of the pelletisation drum or disc (Baykal and Döven, 2000). The strength of ‘green’ pellets is determined by the quantity of cohesive force acting on the particles and the interlocking effects. In addition, the magnitude of these two factors is a function of void ratio and the surface texture of particles, respectively. The void ratio of the particles is important in affecting the sintering kinetics and therefore, the strength of ‘green’ pellets can correlate to the degree of sintering. Statistical analysis of multifactor pelletisation experiments has shown that the strength of ‘green’ pellets is most significantly influenced by the speed followed by the angle of the drum, while the major parameter affecting the size of pellets is the moisture content (Harikrishnan and Ramamurthy, 2006). It must be appreciated that the way these parameters influence the properties of the ‘green’ pellets has not been fully investigated and a comprehensive model that predicts the pelletisation behaviour is still required.

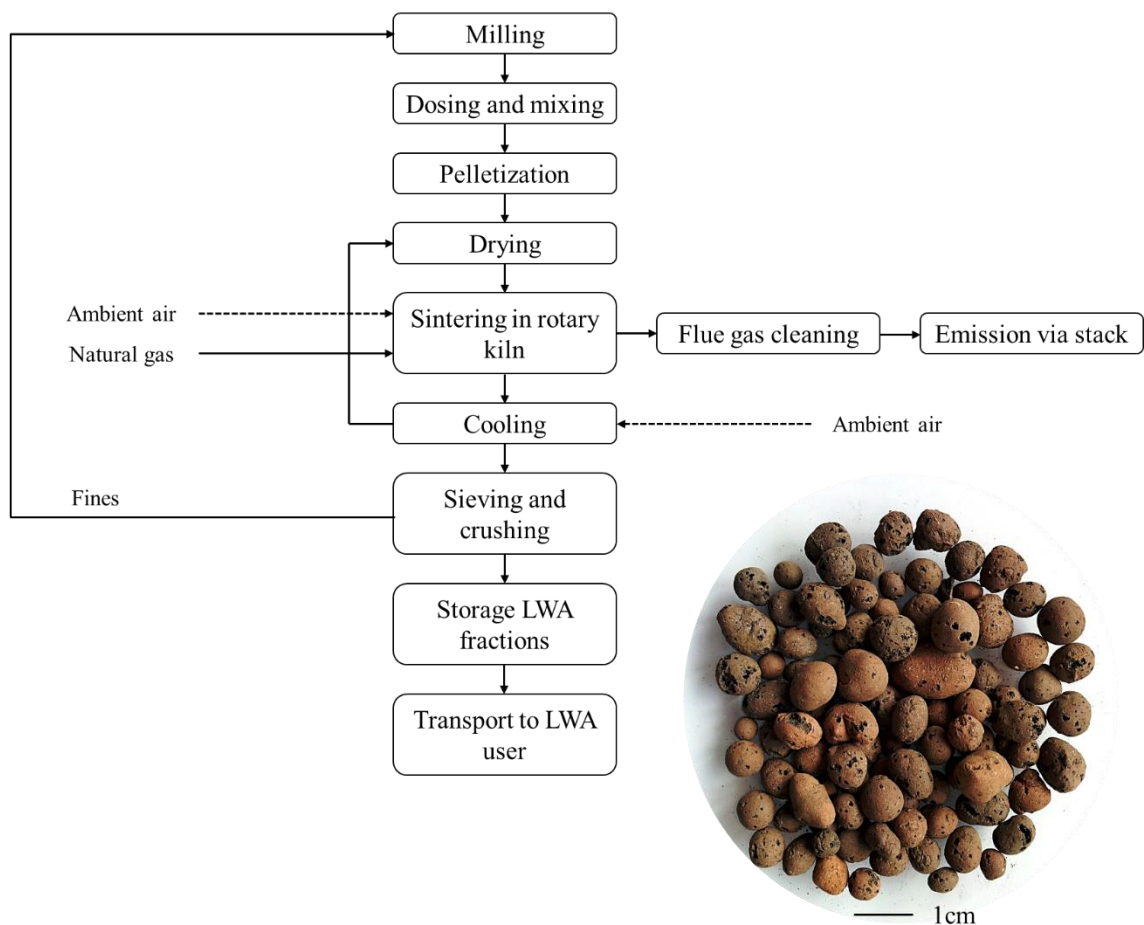


Figure 2.7 Lightweight aggregate manufacturing process (Sarabèr et al., 2012).

Pellets are dried to discard any excess water before sintering. They are then transferred to a kiln and fired at temperatures in the range of 1050 °C to 1250 °C. The time that pellets are fired at the maximum temperature is known as ‘dwell time’ or ‘sintering period’ and this can vary between 3 and 20 minutes depending on the characteristics of raw materials. Sintering is a process in which the particles of a powdered material consolidate by the use of thermal energy and/or pressure (Guo et al., 2017). This involves the fusion of particles at a mutual contact point at a temperature that is up to 80% of the material’s melting point (Rahaman, 2007).

Sintering is the most energy-intensive stage in the LWA manufacturing process. LWA manufacture is reported to emit ~0.3 tonne of CO<sub>2</sub> per tonne of aggregate (Bremner et al., 2005). Energy for LWA production can be provided from biomass combustion given the relatively low sintering temperature required. In addition, a number of studies have used organic matter such as sewage sludge in the mix as an energy source (Xu et al., 2013, Molineux et al., 2016, Liu et al., 2017).

The industrial process for LWA production is usually carried out in a rotary tube kiln with three different zones (Figure 2.8a): 1) drying/pre-heating zone which operates in the range of 100 – 600 °C with up to 40 m lengths and a slow rotation providing two hours of residence time; 2) sintering zone where firing takes place at around 1200 °C with up to 20 m lengths and a fast rotation providing 8 – 10 min dwell time; 3) cooling zone to reduce the pellets temperature to below 100 °C with up to 20 m length and two hours of residence time (Quina et al., 2014b).

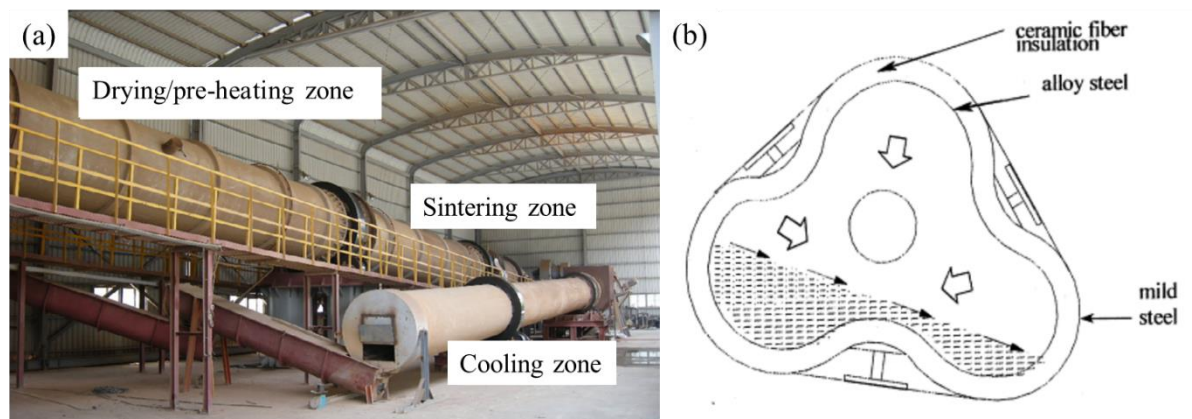


Figure 2.8 (a) LWA manufacturing rotary kiln with different heating zones (Huang and Wang, 2013) and (b) Trefoil design of the kiln inner tube (Laursen et al., 2006).

There are other types of sintering equipment namely: sinter strand, fluidized bed reactors and shaft. Rotary kilns provide a fast heating, required for materials bloating. To improve the thermal efficiency with a faster heat-up and cool-down period, a trefoil design for the kiln inner tube (Figure 2.8b) has been used (Wainwright and Cresswell, 2001). This provides a better control over the sintering process and produces consistent pellet shapes (Sarabèr et al., 2012).

### 2.5.2 Commercial LWA

The UK market for LWA was originated in the 1950's based on clay, shale wastes from mining, and slate. In the 1960's and 1970's other LWA manufacturing facilities were developed to meet the national demand. As an example, the commercial LWA Lytag was first manufactured in 1958 from pulverized fuel ash (PFA), widely available at the time. The production process was also different from traditional 'kiln bloating' by firing. Instead, the aggregates were manufactured in a reducing environment on a coking sinter strand (Boarder et al., 2016). Lytag is still commercially available and has been one of the most commonly used LWA in manufacturing structural lightweight concrete (LWC) (Bai et al., 2004). Another contemporary manufactured LWA in the UK is lightweight expanded clay aggregate (LECA) that is extensively used in the building industry, road construction, gardening etc. It is produced by firing expanding clay in a rotary kiln at 1100 to 1200 °C (Latosińska and Żygadło, 2009). Table 2.6 shows the important properties of some commercial LWA commonly used in the production of lightweight concrete.

A report on LWA demand in the UK construction industry estimated that approximately 1.0 million tonnes of LWA per year are consumed, which is a small portion in comparison with the total supply of normal weight aggregate (270 million tonnes per year) (Cresswell, 2007). The report highlighted that Lytag and LECA form up to 30% of this market whilst the remaining portion of the LWA supply is mainly imported.

Table 2.6 Range of physical properties for commercial LWA and lightweight concrete (Neville, 1995).

	LWA		Typical concrete		
	Particle density (g/cm <sup>3</sup> )	24-hour water absorption (%)	Density (kg/m <sup>3</sup> )	Compressive strength (MPa)	Strength range
LECA	0.3 – 0.9	5 – 30	1000 – 1700	20 – 60	Structural
Lytag	0.6 – 1.1	~20	1500 – 1600	30 – 60	Structural
Pumice	0.5 – 1.6	50	1200 – 1600	5.0 – 15	Moderate
Perlite	0.1 – 0.4	-	400 – 500	1.2 – 3.0	Insulating
Vermiculite	0.1 – 0.4	-	300 – 700	0.2 – 3.0	Insulating

### 2.5.3 Published research on manufactured LWA

A variety of mineral wastes can be utilized as raw materials for LWA production. Table 2.7 provides a summary of LWA production from existing literature sources – using geological materials such as clays and other natural aluminosilicate minerals as the major raw material. For each study,  $\text{SiO}_2/\Sigma$  flux ( $\text{SiO}_2/\Sigma (\text{Fe}_2\text{O}_3 + \text{Na}_2\text{O} + \text{K}_2\text{O} + \text{CaO} + \text{MgO})$ ) and  $\text{SiO}_2/\text{Al}_2\text{O}_3$  were calculated as an indication for chemical composition that controls the viscosity at high temperatures and thus the bloating mechanism. Two main production parameters including firing temperature range and dwell time were reported for each study. Other production parameters such as pre-processing conditions and heating rate were not available for all of the studies. Three main physical properties such as particle density, water absorption after 24 hours and compressive strength were also reported.

The information extracted from the studies in Table 2.7 is used to construct the literature review on effects of production parameters on LWA properties and will be the basis for determining the range of these production parameters for LWA manufacturing methods in this work over the following chapters.

Table 2.7 Summary of LWAs and characteristics, process conditions and physical properties from existing publications, including: Si/ $\Sigma$ F: SiO<sub>2</sub> to total flux ratio; Si/Al: SiO<sub>2</sub> to Al<sub>2</sub>O<sub>3</sub> ratio; T: sintering temperature; t: dwell time;  $\rho_{dr}$ : particle density; WA<sub>24</sub>: water absorption after 24 hours; S: compressive strength; FA: coal fly ash; ISSA: incinerator sewage sludge ash; MSWIFA: municipal solid waste incineration fly ash; APCr: air pollution control residues.

	Minerals	Waste	Si/ $\Sigma$ F	Si/Al	T (°C)	t (min)	$\rho_{dr}$ (g/cm <sup>3</sup> )	WA <sub>24</sub> (%)	S (MPa)
(de' Gennaro et al., 2004)	Zeolite	-	2.4 – 8.3	2.9 – 6.2	1350 – 1500	4	0.51 – 1.68 <sup>lbd</sup>	-	-
(Fragoulis et al., 2004)	Diatomite rock	-	2.9	3.34	1100	15	0.53 – 0.93 <sup>bd</sup>	-	0.41 – 2.01*
(de Gennaro et al., 2005)	Zeolite	-	3.4	3.2	1390	4	0.96 – 1.09	3.6 – 3.6	1.65
(Laursen et al., 2006)	Clay	CaF <sub>2</sub> sludge	1.5	4.5	1200	2	0.31 <sup>lbd</sup>	24.1	-
(de Gennaro et al., 2007)	Zeolite	-	3.2 – 4.8	3.6 – 3.9	1260 – 1380	40	0.46 – 1.85	1.4 – 5.7	0.6 – 2.9*
(Fakhfakh et al., 2007)	Smectite clay	-	2.7 – 3.6	2.3 – 3.1	1060 – 1180	5	0.37 – 0.89 <sup>lb</sup>	3 – 48 <sub>72h</sub>	0.08 – 0.45*
(Huang et al., 2007)	Shale	MSWIFA	1.6	3.6	1050 - 1250	15	0.50 – 1.6	-	4.3 – 7.5*
(Mun, 2007)	Clay	ISSA	2.9 – 4.8	2.6 – 3.6	1100	15	0.65 – 0.91	7.0 – 11.0	-
(Mueller et al., 2008)	Zeolite	-	1.8	5.1	850	-	0.42 – 0.48 <sup>bd</sup>	3.0 – 5.5	0.1 – 0.25*
(González-Corrochano et al., 2009a)	Washing aggregates	FA	2.1 – 2.4	1.4 – 5.1	1150 - 1225	10	1.31 – 1.51	14.5 – 16.0	4 – 8.29
(González-Corrochano et al., 2009b)	Clay sediments	-	2.4 – 2.8	2.7 – 3.5	1150 – 1225	10	1 – 1.88	2.0 – 56.0	1 – 12.55
(Chen et al., 2010)	Reservoir sediment	MSWIFA	1.9 – 3.8	2.5 -2.6	1150 – 1200	15	0.94 – 1.55	2.1 – 10.1	-

(Wei et al., 2011)	Reservoir sediment	Glass	4.7	4.4	1000 – 1150	18	0.79 – 2.35	2.7 – 17.5	-
(Liao and Huang, 2011)	Reservoir sediment	-	2.9	2.7	1170 – 1230	15	1.13 – 2.32	0.4 – 3.8	4.08
(Tang et al., 2011)	Reservoir sediment	-	5.9	3.0	1200	12	1.01 – 1.41	10.4 – 12.3	7.2 – 13.4*
(Hwang et al., 2012)	Reservoir sediment	MSWIFA	6.1	2.4	1070 – 1150	20	0.88 - 1.69	7.6 – 29	5.3 – 13.4*
(Huang and Wang, 2013)	Reservoir sediment	-	2.8 – 5.4	2.4 – 2.8	1150 – 1275	10	0.65 – 1.97	2.7 – 15	-
(González-Corrochano et al., 2014)	Clay	FA	2.0	2.5	1150	3	0.98	6.68	1.53
(Bernhardt et al., 2014a)	Clay	-	3.4	2.3	1100	8	0.31 – 0.57	-	0.54 – 1.58
(Bernhardt et al., 2014a)	Clay	-	3.4	3.3	1120	8	0.41 – 0.48	-	0.76 – 2.39
(Volland et al., 2014)	Sand sludge	-	2.5	9.7	900 – 975	-	0.77 – 1.05	0.1 – 2.17	0.18 – 0.36*
(Quina et al., 2014a)	Clay	APCr	3.0	3.0	1070 – 1100	8	0.5 – 0.60	-	0.19 – 0.46
(Lo et al., 2015)	Clay	FA	3.9	1.7	1150		1.70		6.30*
(Zhang et al., 2015)	Clay	FeCr sludge	1.9	2.2	1000 – 1210	20	0.82 – 2.5 <sup>bd</sup>	-	0.76 -18.27
(Volland and Brötz, 2015)	Sand and zeolites	-	1.8 – 1.9	7.0 – 8.1	850 – 900	-	0.71 – 1.52	0.3 – 2.9	0.7 – 12.9
(Soltan et al., 2016)	Clay	Granite	4.2	3.4 – 5.5	1200	15	0.65 – 1.86 <sup>bd</sup>	-	-
(Molineux et al., 2016)	Clay	Bauxite	0.7 – 1.1	1.8 – 2.1	1200	25	1.63 – 1.71	5.1 – 6.2	-

\* Fracture force (kN): obtained from crushing resistance test.

<sup>bd</sup> Bulk density (apparent density); <sup>lbd</sup> Loose bulk density.

#### 2.5.4 Physical properties of manufactured LWA

As mentioned previously, LWA for use in lightweight concrete products should be strong and have low particle density and water absorption. These properties are mainly affected by the chemical composition of the raw materials as well as their production parameters. However, the pore structure of LWA is an intermediate variable that relates the raw material characteristics and production parameters to the properties of manufactured LWA.

The pore structure of LWA can be defined by the total porosity (total void ratio), pore size distribution, and pore connectivity (pore closeness). An ideal pore structure for a bloated LWA is shown in Figure 2.9. It is comprised of small uniform cellular pores in the matrix, pores decreasing in size adjacent to the surface and indeed, a non-porous surface. The black core indicates the presence of a reducing condition.



Figure 2.9 Ideal pore structure shown for an individual clay LWA pellet (Ayati et al., 2018).

The development of a pore structure is the result of the bloating phenomenon during the firing stage of LWA production. The bloating mechanism has been debated extensively in the literature. However, there is a general agreement that bloating requires sufficient

liquid phase at high temperature to convert the body/matrix to a viscous (pyro-plastic) state. In addition, the occurrence of pyro-plasticity should match the gas release for bubbles to grow and cause expansion (Dondi et al., 2016). Table 2.8 shows the necessity of a suitable viscosity range and gas release for an effective bloating. Materials with a low pyro-plastic viscosity are simply not capable of entrapping the released gas, whilst high pyro-plastic viscosities will cause the materials to melt (flow) and lose their structural integrity completely.

Table 2.8 Conditions necessary for LWA bloating modified from (Dondi et al., 2016).

		Increasing temperature →		
		Viscosity		
		Too low	Suitable	Too high
Gas release	Yes	Bloating and collapse	Bloating	No bloating
	No	Melting with no bloating	Softening with no bloating	No bloating

The pore structure of LWA as an intermediate variable and its dependency on the viscosity of the liquid phase at high temperatures allows a causal pathway to be constructed, as shown in Figure 2.10. The influence of chemical composition and production parameters on viscosity and pore structure are marked as (i) and (ii), respectively. The effect of pore structure on physical properties is marked as (iii). These relations are explained as follows:

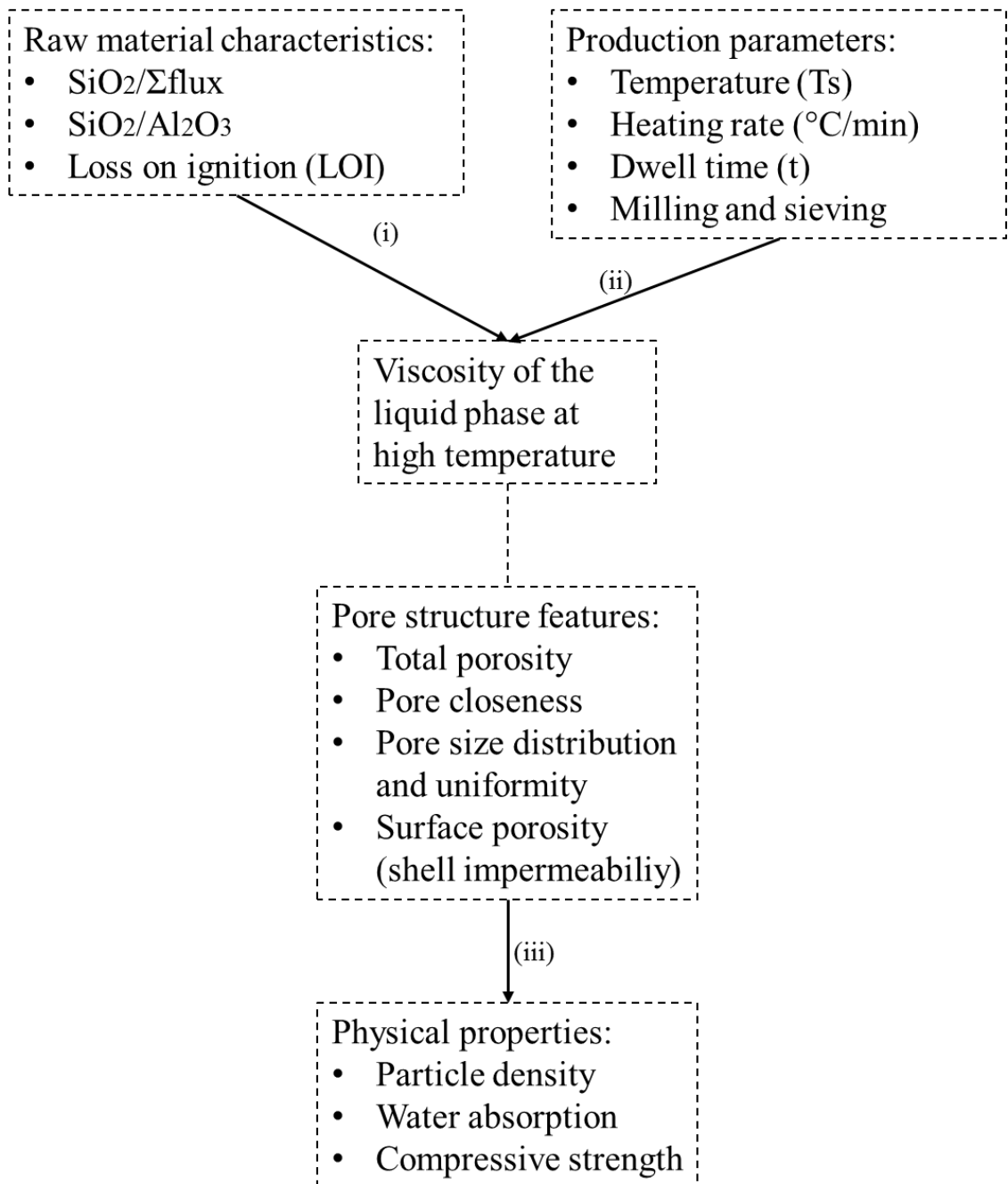


Figure 2.10 Relationships between raw material characteristics, production parameters and physical properties, showing the pore structure as an intermediate variable.

i. Effect of chemical compositions on pore structure

As discussed previously, the bulk chemical composition (oxide composition) of the raw materials affects the pyro-plastic viscosity during the LWA bloating which results in the development of the pore structure. However, it is difficult to pin down the exact measures in bulk chemical compositions that control the viscosity of clay materials at pyro-plastic states. Two important mineralogical features were introduced by Riley (1951) as SiO<sub>2</sub>/Σ

flux ( $\text{Fe}_2\text{O}_3 + \text{Na}_2\text{O} + \text{K}_2\text{O} + \text{CaO} + \text{MgO}$ ) and  $\text{SiO}_2/\text{Al}_2\text{O}_3$  ratios. It has been argued that at a pyro-plastic state, the flux content ( $\text{Fe}_2\text{O}_3 + \text{Na}_2\text{O} + \text{K}_2\text{O} + \text{CaO} + \text{MgO}$ ) controls the softening point of materials and, factors such as the  $\text{SiO}_2$  and  $\text{Al}_2\text{O}_3$  content control the viscosity (Fisher and Garner, 1967). This is because  $\text{SiO}_2$  and  $\text{Al}_2\text{O}_3$  are network formers and thus increase the viscosity (Bernhardt et al., 2014a). In addition, minerals with high  $\text{SiO}_2$  and  $\text{Al}_2\text{O}_3$  contents tend to have very high softening points. However, the presence of fluxing oxides (mainly alkali, alkali earth and ferric oxides) can disrupt the networks and reduce the softening point and pyroclastic viscosity. These oxides can also be added to the raw material prior to firing to adjust the viscosity and therefore improve the bloating behaviour. However, their excessive use can reduce the viscosity and produce a liquid phase causing densification of LWA (Tsai et al., 2006, Liao et al., 2013). The addition of 20 wt.% glass (containing flux i.e.  $\text{Na}_2\text{O}$  and  $\text{CaO}$ ) was shown to be sufficient in decreasing the sintering temperature and improve the pore structure by reducing the amount of open porosity (Kourti and Cheeseman, 2010).

$\text{SiO}_2/\Sigma$  flux and  $\text{SiO}_2/\text{Al}_2\text{O}_3$  ratios have been widely used to determine the bloating capability of various minerals.  $\text{SiO}_2/\Sigma$  flux ratios greater than 2 have been specified as a requirement for bloating behaviour (de' Gennaro et al., 2004, Chiou et al., 2006, González-Corrochano et al., 2009a). However, Dondi et al. (2016) suggested  $\text{SiO}_2/\Sigma$  flux and  $\text{SiO}_2/\text{Al}_2\text{O}_3$  ratios should be in the range of 4 – 7.5 and 4 – 5.6 respectively. Some of the studies in Table 2.7 found a relation between these ratios and the total porosity of manufactured LWAs. For example, in LWAs of de' Gennaro et al. (2004) from zeolitic rocks samples with higher  $\text{SiO}_2/\Sigma$  flux and  $\text{SiO}_2/\text{Al}_2\text{O}_3$  ratios, it was demonstrated that a higher viscosity retained more gas bubbles, resulting in an increase in the total porosity.

The bloating effect also requires sufficient amounts of gas-releasing compounds to be present within the raw materials. The main sources of the gaseous phase in clay materials at high temperatures are understood to be: the dissociation or reduction of ferric oxides, combustion of organic matter, interlayer water molecules and thermal decomposition of carbonates (Quina et al., 2014a).

#### ii. Effect of production parameters on pore structure

Achieving the right combination of microstructural features (high total porosity, pore size uniformity and pore closeness) is the main challenge for LWA production as these

features are sensitive to changes in production parameters. The main controlling production parameters identified from the literature review are:

- Temperature: Firing temperature (the maximum temperature at which LWA is kept in the kiln) is one of the most important production parameters because of its effect on the pyro-plastic viscosity, as shown in Table 2.8. It is very important to note that increasing the firing temperature above the range of pyro-plasticity would result in the formation of a viscous flow, reducing the pore size and consequently increasing the particle density of aggregates (Lin, 2006).
- Heating/cooling rate: Heating rate and the kiln inlet temperature (feeding temperature) have shown to influence the pore structure and resulting quality of LWA. A suitable heating rate can ensure simultaneous gas release and material softening, which are necessary for bloating. Low heating rates ( $<5$  °C/min) causes both the matrix and the surface of the pellets to undergo an identical temperature rise. This would cause the surface to become incompletely vitrified while the gas is generated, making it possible for the gas to escape. High heating rates ( $>10$  °C/min) can also be disadvantageous for bloating (de Gennaro et al., 2007). In fast heating, materials do not have sufficient time for softening before the firing program ends. The use of feeding temperature has also been observed by Huang et al. (2007) to have a positive effect on bloating. When shale and incinerator fly ash pellets were fed at 850 °C into a tunnel kiln, a rapidly-vitrified surface enveloped the released gases and increased the matrix total porosity while kept the surface pores at a minimum. When LWA exits the kiln after the completion of the firing stage, it is transferred to a cooler and the pellets temperature drops as it is exposed to the ambient air. However, in industrial settings, sometimes air is blown onto hot LWA to harvest the available heat, which is then forwarded for use in the pellet drying stage. Fast cooling rates may have a direct negative effect on the strength of LWAs, due to the formation of micro-cracks. This is because, above the glass transition temperature ( $T_g$ ), the core incorporates iron in the reduced form and acts as a viscous body with a higher thermal expansion coefficient (TEC). Meanwhile, the surface is oxidized and contracts differently during the cooling. This would result in the shell and the core experiencing different thermal contractions due to their different TECs, which would induce compressive stress in the shell, producing micro-cracks and consequently reducing the strength of the granules. This effect was

avoided in LWAs of Bernhardt et al. (2014a) where a double post-treatment at 800 °C in the air together with a subsequent slow cooling regime (0.7 °C/min) resulted in 114% increase in strength. In a more recent study by Zhang et al. (2015) on the influence of cooling methods on the strength of LWA, a relation between the pore structure and cooling rate was observed. The authors reported that the total porosity and average pore size were high for fast-cooled LWAs compared to LWAs subjected a slow cooling regime. The smaller average pore size would have also allowed the slow-cooled pellets to form a continuous framework structure and obtain a higher compressive strength as opposed to fast-cooled pellets where the cracks were developed from the boundary of the largest pores (the weakest region in the structure).

- Dwell time: The majority of studies in Table 2.7 used dwell time between 4 and 20 minutes. Determining an optimal duration to keep LWA at maximum temperature is important because low dwell times may cause an insufficient sintering and therefore an open porosity. High dwell times are not economically viable due to the amount of fuel needed to keep the kiln contents at the maximum temperature. In addition, dwell time has been shown to be the factor that most strongly affects the connectivity of pores. A study by Korat et al. (2013) used X-ray micro-tomography and mercury intrusion porosimetry (MIP) to characterise the pore-forming process in LWAs based on silica sludge. This study showed that, by increasing the dwell time up to 60 minutes, the number of pores decreases while the total porosity increases. This change in the pore structure features indicates an increase in the connectivity of the pores. Hence, a definite dwell time is desirable to obtain a low degree of connectivity within the pore structure, and therefore low water absorptions.
- Milling and sieving: Pre-processing of raw materials to achieve a fine particle size distribution can affect the bloating and pore structure of LWA (Chindaprasirt et al., 2009). Some levels of uniformity in pore size can be achieved through homogenization of raw materials with techniques such as milling and sieving. However, the effect of pre-processing parameters such as milling time and size distribution of raw material particles on the pore structure has not been fully studied.

### iii. Effect of pore structure on physical properties

The physical properties of LWA may be affected only by one of the pore structure features. For example, the particle density is mainly influenced by the total porosity

produced from the materials bloating, and less dominantly by the other features. The porosity of LWA surface is one of the main parameters which determine the water absorption capacity of LWAs (Hwang et al., 2012). In addition to an impermeable surface, LWA matrix pore structure with a low degree of connectivity is desirable. Insufficient sintering is the main cause for an open porosity and results in LWAs with high water absorption capacity (Kourti and Cheeseman, 2010).

High total porosity and the presence of large pores have been related to the lower compressive strength of the manufactured LWAs (González-Corrochano et al., 2014). The uniformity of pore size can also be influential in enhancing the compressive strength as it promotes a homogeneous distribution of stress throughout the inner structure. In addition, small pore size and strong matrix material can be attributed to the strength of LWAs (Cheeseman and Viridi, 2005, Bernhardt et al., 2014b). However, no satisfactory evidence has yet been reported in the literature on the effect of pore structure on the strength of LWAs.

#### 2.5.5 Mineralogical changes during firing

The XRD analysis for some of the LWAs in Table 2.7 including the initial phases and final phases after firing treatment were extracted from the literature, as shown in Table 2.9. The mineral wastes used in the manufacture of LWA, contained common clay minerals such as smectite, kaolinite, chlorite and illite. Additionally, considerable amounts of non-clay minerals such as quartz, feldspar and  $\text{CaCO}_3$  were present in the raw materials. In general, some clay minerals found in shale and expansive clay including illite, montmorillonite, vermiculite and chlorite, and some rock-forming minerals such as quartz and feldspar - have been associated with the bloating capability (Tang et al., 2011, Huang and Wang, 2013). Carbonates can also play a role in the bloating mechanism however this depends on the nature of clay mineral present in the mix. For example, it has been shown that illitic clays were more effective in entrapping the released  $\text{CO}_2$  than kaolinitic clays and, in a zeolitic mix,  $\text{CaCO}_3$  mainly acted as a fluxing agent and caused no expansion (Dondi et al., 2016).

The neo-formed minerals in Table 2.9 show that most of the initial phases transformed as the result of heat treatment. The reported amorphous phases could have different origins. For example, diatomite used by (Fragoulis et al., 2004), was found to be mainly composed

of opal, which has an amorphous nature. LWAs of de Gennaro et al. (2007) manufactured from a mixture of zeolitic rock and polishing mud (mainly consisting of glass with 24% quartz) also contained a significant amount of glass. The increase in the glass fraction of LWAs with increases in temperature has also been reported in studies using water reservoir sediments and clay-bearing sand sludge as a raw material (Liao and Huang, 2011, Volland et al., 2014, Volland and Brötz, 2015).

The three main endmembers of the feldspars series including potassium feldspar ( $\text{KAlSi}_3\text{O}_8$  sanidine), calcium feldspar ( $\text{CaAl}_2\text{Si}_2\text{O}_8$  anorthite) and sodium feldspar ( $\text{NaAlSi}_3\text{O}_8$  albite) have been reported in the manufactured LWAs. These minerals can be either relics of primary detrital phases or neo-formed. For example, the formation of the  $\text{CaAl}_2\text{Si}_2\text{O}_8$  phase can be attributed to high contents of CaO that is likely to remain from the decomposition of carbonates.  $\text{Ca}^{2+}$  ions are capable of substitution into the aluminosilicate matrix and facilitate the formation of  $\text{CaAl}_2\text{Si}_2\text{O}_8$  (Erol et al., 2008).  $\text{NaAlSi}_3\text{O}_8$  is the sodium endmember of plagioclase division and is capable of forming a continuous solid solution with potassium feldspars at high temperatures (above 700 °C) (Deer et al., 2001). The formation of  $\text{NaAlSi}_3\text{O}_8$  has been reported in LWAs of Liao et al. (2013) manufactured from reservoir sediment as a result of the addition of sodium hydroxide.

Nevertheless, apart from the above-mentioned examples, studying the effect of neo-formed phases on physical properties of LWA has received little attention; representing a subject area that needs to be addressed by future research.

Table 2.9 XRD analysis for manufactured LWAs from mineral waste. “m” indicates minor phase detected.

Materials	Initial phase in raw materials											Final phase in LWA														
	Quartz	Kaolinite	Smectite	Illite	Vermiculite	Muscovite	Chlorite	Feldspars	Amphibole	Magnetite	Opal	Wusite	Hematite	Corundum	Calcite	Glass	Quartz	Feldspars	Mullite	Hematite	Albite	Anorthite	Hercynite	Sillimanite	Spinel	Forsterite
(Fragoulis et al., 2004)	m		×	m	m		m	m			×					×	×	m	m				m			
(Ducman and Mirtič, 2009)	×			×		×		×									×							×		
(Liao and Huang, 2011)	×					×	×										×			×		×				
(Wei et al., 2011)	×							m				×		×												
(Liao et al., 2013)	×					×	×	×									×			×	×		×			
(Bernhardt et al., 2014a)	×			×		×	×	×	×				×			×	×		×			×				
(Quina et al., 2014a)	×	m	m	×				m					m	m												
(Soltan et al., 2016)	×					×								m		×								×	×	×
(Zhang et al., 2015)	×	×	×					×		m						×	m	m								
(González-Corrochano et al., 2016)	×	×		×												×	×		×							

### 2.5.6 Use of secondary materials in LWA

One of the most important economic aspects of LWA production is the potential for incorporating industrial secondary materials, often waste, as a partial replacement for geological materials. The basic idea in this application is that heavy metals and other leachable constituents such as  $\text{Cl}^-$  present in 'waste', would be encapsulated in a silicate-based matrix or substitute other ions in the crystal structure when the materials are sintered at high temperature making them non-leachable (Chang et al., 2007). This method has been presented as a recycling option for industrial by-products such as sewage sludge and waste glass among others and in some cases for hazardous waste such as air pollution control residue (APCr) from EfW plants. Thermal treatments can cause heavy metals to be integrated into both an amorphous matrix and a crystalline phase, which reduces their availability. A study on leaching behaviour of LWA with incorporation of coal fly ash has found that heavy metals such as Cr, Ni, Mn and Zn can become a part of neo-formed spinel groups and feldspar crystalline structures; while Pb and Cd can react with  $\text{SiO}_2$  (in phyllosilicates) and enter the amorphous phases (González-Corrochano et al., 2012b). The study reported that divalent and trivalent ions such as Mn and Cr can partially replace  $\text{Mg}^{+2}$  and  $\text{Al}^{+3}$  and/or  $\text{Fe}^{+3}$  of the spinel and/or magnetite series. In a similar study on stabilization of heavy metals in LWA incorporating sewage sludge and river sediments (Xu et al., 2013), it was explained that in an oxidative condition,  $\text{Al}^{+3}$  can replace tetrahedral  $\text{Si}^{+4}$ , producing an additional negative charge in the system which therefore can be balanced with any present heavy metal cations (Cd, Cr and Cu). The study also associated the LWAs' leaching behaviour with the degree of sintering. The authors also reported that higher  $\text{Fe}_2\text{O}_3$  content could be beneficial for solidification of Cd, Cu and Pb, as  $\text{Fe}_2\text{O}_3$  can reduce the eutectic point of LWA components. This promotes the formation of a liquid phase sintering which would eventually result in LWAs with a stable structure.

## 2.6 Summary

New discoveries of oil reservoirs in the North Sea and the need for more complex drilling operations will produce large amounts of drilling waste in the future. This will be a burden on the UK landfill facilities and thus, a viable recycling option for drilling wastes and particularly contaminated cuttings is crucial. Currently, most of the management practices aimed at reducing the portion of hydrocarbons to below 1 wt.% making the waste compatible with the requirement for non-hazardous waste criteria.

The literature review highlighted the possibility of turning the contaminated drilling waste into lightweight aggregate for use in concrete products. Major areas in the field of LWA production from mineral wastes were explored. Studies have shown that various geological materials can be used for the manufacture of LWA, but the main challenge for producing high-quality LWA is to control the bloating mechanism to obtain an ideal pore structure. Reviewing previous research identified the key factors that influence the bloating and development of pore structure during the firing stage. These were classified into two groups. The first group involves the chemical composition (proportion of major oxides) of the raw materials, which determines the pyro-plastic viscosity and the presence of gas releasing compounds (measured through mineralogical and thermal analysis) to facilitate the bloating mechanism. The second group involves the production parameters such as the firing temperature, heating/cooling rate, dwell time and pre-processing techniques including milling and sieving. In addition, the review discussed the influence of pore structure on the physical properties of LWA including particle density, water absorption and compressive strength. The information provided in this chapter will be the basis for the experimental design and development of the manufacturing process in the subsequent chapters.

### 3 Chapter 3 Materials and methods

#### 3.1 Materials

Three samples with a minimum of 20 kg oil-contaminated drill cuttings were supplied by Augean PLC, Peterborough, UK, a specialized waste management company that is responsible for managing the majority of the UK drill cuttings produced in the North Sea.

The samples appeared to be varied in the oil content. For those with high oil content, the chunks of cuttings were broken down in the oil using a hand blender until a semi-dried homogeneous powder was achieved. It was observed that the material became drier as the blending progressed due to the absorption of oil on the generated surface area of the cuttings particles. The semi-dried materials were then air-dried over 7 days to minimize the hydrocarbons evaporating from the cuttings. Air-dried drill cuttings were ball milled (milling conditions are described in section 3.2.2) and homogenised in a mixer for 10 min prior to characterization. The samples were named as SDC, CDC and EDC. A picture of the as-received sample of oil-contaminated drill cutting and an air-dried portion of material is shown in Figure 3.1.

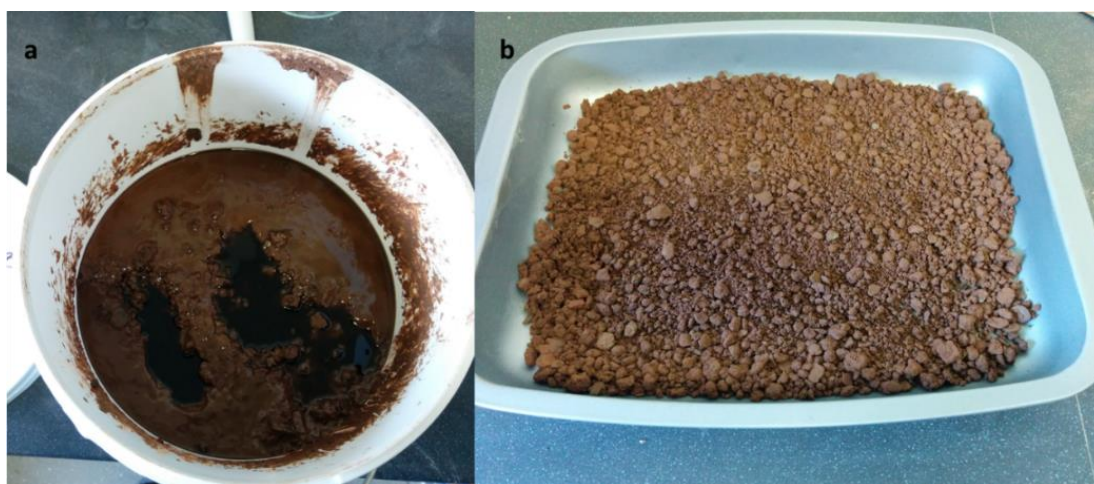


Figure 3.1 Synthetic-based mud (SBM) drill cuttings: a) as received and b) air-dried.

## 3.2 Methods

### 3.2.1 Material characterization

This section provides a description of the selected analytical methods used for characterization of waste samples. As discussed in Chapter 2, to evaluate the bloating capability of the materials, information on chemical composition (major oxides) of drill cuttings is important. For this purpose, X-Ray Fluorescence (XRF) analysis was used. The presence and nature of gas releasing compounds were analysed by X-Ray Diffraction (XRD). Total Petroleum Hydrocarbon (TPH) due to the remaining drilling fluids in cuttings was measured by Gas Chromatography (GC) and used in the calculation of CO<sub>2</sub> emissions for the production of LWA. To determine the firing temperature range and the initial sintering temperature, drill cuttings were analysed by heating microscopy. Differential Thermal Analysis (DTA) was also used to provide complementary data to XRD analysis. Since SBM drill cuttings are waste materials, the release of contaminants including heavy metals and soluble salts were measured for samples of drill cuttings and compared with those for manufactured LWA. The concentration of acid-soluble and water-soluble heavy metals in the drill cuttings were determined by acid digestion and standard leaching analysis, respectively.

#### 3.2.1.1 Chemical composition

XRF spectroscopy is an accurate, fast and non-destructive analytical method for measuring the chemical compositions of a wide range of materials. In this method, the sample is irradiated by x-rays causing the material to produce characteristic x-ray, also known as x-ray fluorescence (Beckhoff et al., 2007). Each atom has specific energy levels that produce characteristic x-rays with a unique set of energies. This can be used as an elemental fingerprint to identify the chemical composition of materials.

The measured intensities of the emitted x-rays are then used for determining the concentration of each element present in the sample (Brouwer, 2006). The sum of measured x-ray photon counts per unit of time is considered as a measure of intensity. Therefore, a calibration curve can be constructed using samples with known concentrations. This curve is used to predict the concentration (wt.%) of elements (often expressed as major oxides for geological materials) for samples of unknown concentration (Pessanha et al., 2018).

In this study, XRF analysis was performed to determine the chemical composition of drill cuttings. The analysis was conducted on  $10 \pm 0.01$  g of homogenised material using a 2010 PANalytical Axios sequential XRF spectrometer with 4kW Rh-anode x-ray tube.

#### 3.2.1.2 Mineralogy

XRD analysis is the most commonly used method for the identification and analysis of clay-sized minerals. It provides information on the bulk properties of materials that is averaged over  $10^{11} - 10^{12}$  unit cells or billions of crystals. The mechanism for x-ray generation, diffraction phenomena and challenges on identification and analysis of minerals are briefly summarized from (Moore and Reynolds, 1989):

Continuous x-rays are produced when fast-moving particles such as electrons are slowed down as they pass through a strong electrical field. Characteristic x-rays are produced when a beam of accelerated electrons strike and knock out an electron from the inner orbital close to the nucleus of a target material such as Cu. The generated vacancy is then filled with another electron from outer orbits and a photon is released as the result of this event. The photon energy is equal to the energy difference between the orbitals, therefore for materials with a higher atomic number, photons with a higher energy and lower wavelength are emitted. If the vacancy is in the K shell and an electron from the closest location in L shell fills it up, the radiation is called  $K\alpha$ . Similarly, the radiation generated by an electron from M shell is called  $K\beta$ .

A beam of x-ray is produced by passing the radiations through a small hole in a metallic plate (usually Pb). The beam then strikes the crystalline phase and produces a diffraction pattern. For an electromagnetic wave of any wavelength, the distance between the diffracting centres must be equal to the wavelength of the incident beam in order to have diffraction phenomena. A measurable diffracted beam must also be composed of a large number of constructive interfering waves that mutually reinforce each other. When a beam of x-ray strikes planes of atoms in a crystal structure, rays can reflect with an equal angle from different atomic planes. Figure 3.2 shows two beams of x-ray that are in the same phase striking the material. As the first ray is reflected from the atom in the top layer, the second ray reflecting from the atom in the second layer has to travel an extra distance ( $2l$ ). For the second ray to remain in the same phase and thus, produce a detectable constructive interference, its extra

travelled distance must be equal to natural multiplications of the incident beam wavelength ( $n\lambda$ ). It can also be seen that the extra distance is equal to  $2d\sin(\theta)$  where  $d$  is the distance between atomic planes and  $\theta$  is the incident angle. The Bragg's law or Bragg's equation uses this relationship to calculate the distances between the diffraction centres in a crystalline material as follows:

$$d = \frac{n\lambda}{2\sin(\theta)} \quad 3.1$$

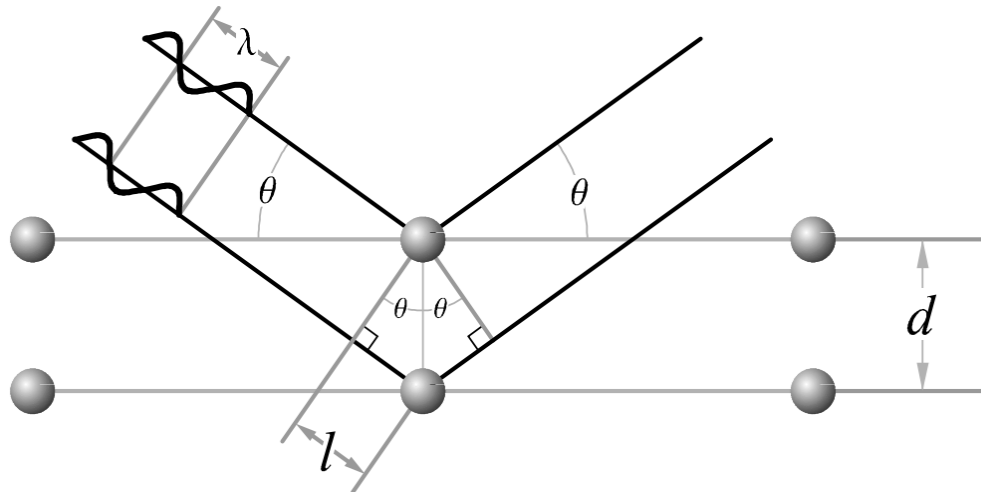


Figure 3.2 Demonstration of Bragg's law (Rachwal, 2010).

The reflected part of the incident beam is also passed through an aperture slit before it goes to the detector. The aperture slit controls the peak sharpness and resolution. This is important for analysing clay minerals as they have inherently broad peaks in comparison to other crystalline materials and thus, the use of fine slits would reduce the intensity of reflections and make them indistinguishable from the background peaks.

Clay minerals are best identified from the pattern of oriented aggregates in the direction of  $(001)^5$  crystal plane; since in X and Y directions, the structures are similar, and it is the Z direction at which the atomic patterns differ. The analysis of bulk rock can be more difficult due to the presence of non-clay (non-platy) minerals that can produce numerous interferences. However, this is not always the case, for example, quartz is normally present in most clay-size fractions of sedimentary rocks and since it does not tolerate any

<sup>5</sup> Miller indices are a notion system for describing the orientation of crystal lattice planes by using their intercepts with xyz axes ([https://www.doitpoms.ac.uk/tlplib/miller\\_indices/index.php](https://www.doitpoms.ac.uk/tlplib/miller_indices/index.php) [Accessed on 29/01/18]).

significant atomic substitution, it shows a distinctive diffraction pattern (strongest peak at  $26.65^\circ 2\theta$  and second strongest at  $20.85^\circ 2\theta$ ).

The above-mentioned difference in the identification process of clay/non-clay also exists in their quantitative analyses by XRD methods. For the majority of non-clay minerals, a simple peak height can be used as the measure for an integrated intensity that can be related to the abundance of that mineral in the mixture. This is because these minerals contain large scattering domains (hundreds of unit cells) that can produce narrow peaks with identical widths. However, the application of such methods for mineral phase quantification is very limited for multi-component mixture such as drill cuttings samples with a high possibility of overlapping peaks. Other factors such as inherent variability of some crystal structures, preferred orientation and the absorption of x-rays by other present phases in the mixture, can also limit the application of traditional peak heights in quantification (Ward and French, 2005). To address these issues, in 1969 Hugo Rietveld proposed a refinement method for crystal structure diffraction data. In his method, the observed diffraction pattern is fitted with a calculated diffraction profile corresponding to the sum of theoretical patterns for each identified phase; and the difference between the two is minimized through a refinement process (Hillier, 2000). At the best fit, the two profiles are related by a scale factor, allowing the relative quantification of each mineral phase (Alves and Omotoso, 2009).

The refinement involves fitting the observed (measured) diffraction pattern with a crystallographic calculated profile (Bish and Howard, 1988). The theoretical diffraction pattern is used as the starting theoretical model and this is adjusted by least-squares to fit the observed pattern (Stinton, 2006). The model contains a number of profile parameters such as unit cell information and  $2\theta$  corrections (deviations in  $2\theta$  caused by displacement of the sample), peak shape functions (for both the sample including the domain size, stress/strain defects, etc. and, the instrument including the radiation source, geometry, slit size, etc.) and a function to model the background (McCusker et al., 1999):

In Rietveld refinement, the function  $\Delta$  is minimised:

$$\Delta = \sum_i w_i \{y_i(\text{obs}) - y_i(\text{calc})\}^2 \quad 3.2$$

where  $y_i(\text{obs})$  is the observed intensity at step  $i$ ,  $y_i(\text{calc})$  is the calculated intensity and  $w_i$  is a weighting factor which is defined as:

$$w_i = \frac{1}{y_i(\text{obs})} \quad 3.3$$

The fit of the calculated pattern to the observed data (the process of convergence) is done in terms of agreement indices or R-factors. The quality of the fit is represented through lower R-factors. The most common is the weighted-profile R-factor which is defined as:

$$R_{\text{wp}} = \left\{ \frac{\sum_i w_i \{y_i(\text{obs}) - y_i(\text{calc})\}^2}{\sum_i w_i \{y_i(\text{obs})\}^2} \right\}^{1/2} \times 100\% \quad 3.4$$

Another R-factor which represents the statistically expected quality of the fit is defined as  $R_{\text{exp}}$ . This is a measure of data quality and  $R_{\text{wp}}$  should approach  $R_{\text{exp}}$ .

$$R_{\text{exp}} = \left\{ (N - P) / \sum_i^N w_i \{y_i(\text{obs})\}^2 \right\}^{1/2} \times 100\% \quad 3.5$$

where N is the total number of observations and P is the number of parameters refined. An example of output model for quantitative analysis of drill cuttings was given in Appendix II.

In this study, XRD analysis was conducted on  $10 \pm 0.01$  g of homogenised material using a Philips x-ray diffractometer system with generator (1830) and the goniometer (3020). Cu K-alpha radiation, a step size of  $0.05^\circ$  and a time for each step of 1.0 second. For peak identification, the programme 'Traces' was used in conjunction with the International Centre for Diffraction Data (ICDD) and Powder Diffraction File (PDF). For quantification, the commercial Rietveld-based software 'Siroquant' was used.

### 3.2.1.3 Total Petroleum Hydrocarbon (TPH)

To measure the concentration of the remaining (absorbed) portion of drilling fluids on cuttings, TPH content of the raw materials was determined. This information was also used to estimate the embodied CO<sub>2</sub> of LWA, discussed in detail in Chapter 8. TPH was extracted from a  $5 \pm 0.01$  g weighted sample of drill cuttings using sodium sulphate and n-heptane digestion according to the British standard method (BS EN ISO 16703) and measured using gas chromatography with flame ionisation detector (CG-FID), Agilent 6890 Network Gas Chromatograph. TPH limits for Hazardous Properties (HP) including Carcinogenic (HP 7), Ecotoxic (HP 14), Toxic for Reproduction (HP 10) and Specific Target Organ Toxicity/Aspiration Toxicity (HP 5) as expressed in the UK's waste catalogue (WM3, 2015) are listed in Table 3.1.

Table 3.1 Limits for assessing the hazardous properties of waste as expressed in the UK's waste catalogue (WM3, 2015).

Total petroleum hydrocarbons (TPH) concentration		Hazardous properties (HP) assessment
≥ 10.0%	100,000 mg/kg	Specific Target Organ Toxicity/Aspiration Toxicity (HP 5)
≥ 3.0%	30,000 mg/kg	Toxic for reproduction (HP 10)
≥ 2.5%	25,000 mg/kg	Ecotoxic (HP 14)
≥ 0.1%	1000 mg/kg	Carcinogenic (HP 7)

#### 3.2.1.4 Microstructural analysis

In the study of materials, the pore structure is an intermediate variable that relates the chemical composition of raw materials and production parameters to physical properties including particle density, water absorption and compressive strength. The pore structure of LWA is developed due to bloating. The occurrence and the degree of bloating can be analysed by microscopy. Scanning electron microscope (SEM) is a powerful imaging instrument which can be used for microstructural analysis of LWA. SEM uses an electron beam for producing images with as low as 10 nm spatial resolution. This provides an opportunity to characterise the main features of pore structure including total porosity, pore connectivity and size distribution and, investigate their effects on LWA physical properties. The surface porosity of LWA can be characterized by SEM and used for investigating the water absorption.

SEM operates by the bombardment of the sample's surface with an electron beam. This results in an activated volume close to the surface (Figure 3.3) where various electron/nuclei interactions take place. These interactions result in emissions of electrons with different energies and x-rays, each of which are collected with a special detector and able to provide information about properties of materials at specific depths (Reed, 2005): Backscatter electrons (BSE) are produced when the incident electrons are elastically scattered in the specimen and leave the surface at highly deflected angles. Secondary electrons (SE) are produced when the inelastically-scattered fraction of the incident electron beam hits and ejects the loosely bound electrons of the specimen. Due to the inelastic interactions, the secondary electrons have lower energies and thus, only those electrons

that are produced at a few nanometres depth can escape. For this reason, SEs are used for conventional SEM imaging when topographical surface details are of interest.

SEM has applications in different fields of geology including sedimentology and mineralogy, as it can produce high-resolution images of sediment grains and inter-growth and so can be very useful in studying the minerals morphology (Reed, 2005). In this study, raw materials in powder form were analysed for particle morphology. The analysis provides insight into the effect of milling on drill cuttings particle size reduction and agglomeration. To analyse drill cuttings particle morphology, small amounts of milled samples were carefully placed on a layer of double-sided carbon tape attached to the specimen stub.

The microstructures of the manufactured LWA were analysed to understand the transformation and degree of sintering for drill cutting particles and, establish relations between the bloating phenomenon and physical properties. For the manufactured LWA, the outer surface and fracture surface produced after compressive strength testing were used for SEM imaging. All samples were coated with gold/platinum in a Polaronprep 2000 (Quorum Technologies) sputter coater to prevent any surface charging effect. A JOEL JSM 6460LV SEM was used for microstructural analysis.

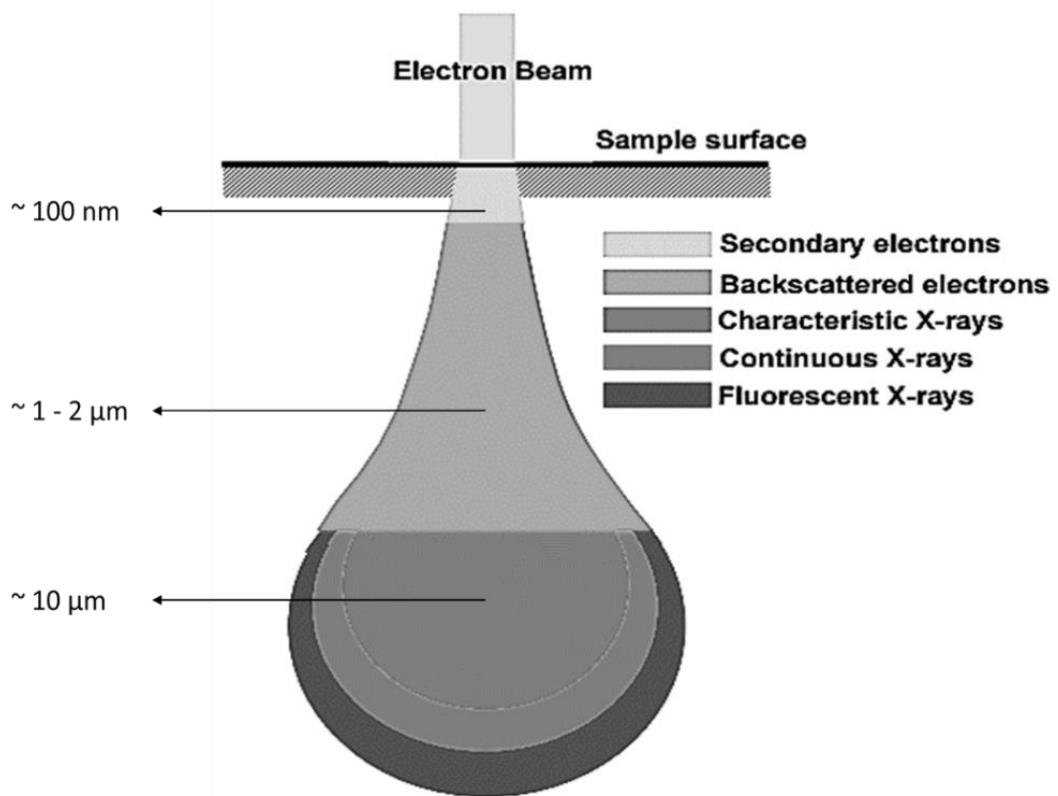


Figure 3.3 Signals resulting from electron beam and sample surface interaction (Fens, 2000).

### 3.2.1.5 Thermal behaviour of drill cuttings

Thermal analysis methods are widely used for characterization of geological materials. In thermal analyses, a sample of material is heated and changes in physical properties are used to provide information on the material chemistry and its behaviour at high temperatures. In this study, heating microscopy (HM) and differential thermal analysis (DTA) were used to investigate the materials high-temperature behaviour. In addition, this study aimed to use HM in combination with DTA to monitor the bloating behaviour and the role that decomposition reactions may play in the bloating mechanism.

- Heating microscopy

Heating microscopy is a method for studying the materials high-temperature events such as shrinkage, sintering, bloating, softening and melting. The method has been widely adopted in the ceramic and glass industry. Heating microscopes work by taking images of a specimen outline during a heating period (starting at the room temperature and finishing above the materials melting point) to define a number of characteristic temperatures corresponding to particular shapes of the outline (Montanari et al., 2014).

The variations in the sample dimensions are measured through an image analysis software during the heating process.

Important characteristic temperatures can be identified based on the matrix viscosity at a pyro-plastic state: as the material heats up and passes the softening point, the viscosity of the matrix decreases and the surface tension of the liquid phase tends to minimize the sample outer surface (Raask, 1979). This phenomenon blunts the sharp edges of the sample outline and if the size of the sample is sufficiently small, the sample transforms into a nearly spherical shape, known as 'sphere' or 'ball' point (Pascual and Pascual, 2001). Above this, as the surface tension of the melted phase reduces by temperature, the sample partially flows and reach a hemispherical shape, known as 'hemisphere' point. As the temperature increases further, the material reaches the melting point.

In this study, a high-temperature optical dilatometer (microscope), EM201/HT163, Hesse Instruments (Germany) with the maximum operating temperature of  $1400\text{ }^{\circ}\text{C} \pm 3\text{ }^{\circ}\text{C}$  was used to examine drill cutting cubic samples ( $3 \times 3 \times 3\text{ mm}$ ). The analysis was conducted at  $10\text{ }^{\circ}\text{C}/\text{min}$  to simulate the heating rate used in the muffle furnace during the LWA firing stage.

- Differential thermal analysis (DTA)

In DTA, a sample of material and an inert reference material are heated and let to cool simultaneously in the same chamber and the temperature difference between them is recorded (Vold, 1949). If the material undergoes a phase transformation, the resulted released or absorbed heat would increase the measured temperature difference and a peak is generated in the DTA curve (thermogram). Conventionally, an exothermic reaction peaks upward and an endothermic reaction peaks downward (towards the abscissa). In this study, a Bahr-Thermoanalyse GmbH (Germany) differential thermal analyser with a heating rate of  $10\text{ }^{\circ}\text{C}/\text{min}$  and using aluminium oxide as the reference material was used.

#### 3.2.1.6 Heavy metal concentration in drill cuttings

The total metals in drill cuttings were extracted through acid digestion with Aqua Regia to produce a liquid digestate compatible with inductively coupled plasma optical emission spectroscopy (ICP-OES). Particular attention was given to elements of the waste acceptance criteria (WAC), including As, Ba, Cd, Cr, Cu, Hg, Mo, Ni, Pb, Sb, Se and Zn.

The acid digestion with Aqua Regia is proposed by the Environment Agency for

extracting total metals to be determined using an appropriate end-detection technique, such as ICP-OES (Environment Agency, 2006). A sample of 1.0 g air-dried drill cuttings was digested on a hot block for 3 hours at 110 °C with 20 ml Aqua Regia (consisting a mixture of concentrated HNO<sub>3</sub> and concentrated HCl at a volumetric ratio of 1:3). Once cooled, the digestate was diluted with 100 ml deionised water and then filtered and analysed using an ICP-OES for the desired metals. The extract concentrations are converted from mg/l to mg/kg as follows:

$$C_s = (C_e \times V_e) / (M_{sd} \times 1000) \quad 3.6$$

where  $C_s$  is the concentration of the metal in the sample in mg/kg;  $C_e$  is the concentration of the metal in the sample extract solution in mg/l;  $V_e$  is the volume of extract (elute) in ml; and  $M_{sd}$  is the mass of dry sample in kg.

### 3.2.1.7 Leaching analysis of drill cuttings and manufactured LWA

Leaching is defined as the release of soluble constituents from a solid phase (waste) to a liquid phase (water) over the course of long periods of time (Saveyn et al., 2014). It is a complex phenomenon that is affected by a series of factors - such as element chemistry, pH, redox potential, complexation, liquid-to-solid (L/S) ratio and contact time with solvent (van der Sloot et al., 1996). The major element compositions are very important as they determine the chemistry of pore water which in turn controls the leaching of trace and minor elements. The pH also plays a vital role in regulating the solubility of the constituents. In addition, inorganic complexing agents such as Cl<sup>-</sup> can increase the leaching behaviour of specific heavy metals. The liquid to solid (L/S) ratio simulates the actual time-scale through which the infiltration occurs (van der Sloot et al., 1996).

Currently, the potential release of contaminants from granular solids is measured according to two major classes of leaching tests (Kosson et al., 1996). First, single batch extraction tests that simulate the release under specific environmental conditions, examples include ‘Compliance test for leaching of granular waste materials’ (BS EN 12457-2, 2002) and, ‘Toxicity Characteristic Leaching Procedure’ (TCLP, United States). Second, sequential chemical extraction tests that evaluate the release under a series of increasingly more aggressive solvents, such as ‘Characterization of waste. Leaching behaviour test. Influence of pH on leaching with initial acid/base addition’ (BS EN 14429, 2005) and, ‘Leaching characteristics of solid earthy and stony building and waste

materials' (NEN, 1995). In each class of tests, a fundamental leaching parameter, either availability or solubility, is set to control the release mechanism as discussed below (Kosson et al., 1996):

- Availability controlled condition: is used often to estimate the potential release in batch tests with high L/S ratios (>10 l/kg) and near neutral pH. When the leachate concentration is below the saturation for a specific constituent, its release is under availability-controlled condition. Availability for most of the heavy metals like Pb is significantly lower than their total content. For such constituents, the availability is an estimate of release in more than 1000 years. However, for highly soluble salts such as NaCl, the availability can be almost equal to its total content and thus, it can be reached over the course of just a few years under different disposal or utilization scenarios.
- Solubility controlled condition: occurs when the solvent is in saturation with respect to a specific constituent. The condition is likely to happen at low L/S ratio in the fields where water contact with the solid is through percolation. For a saturated solution, the solubility of dissolved constituents can be affected by pH. In the case of heavy metal cations, such as Pb and Zn the solubility is very sensitive to pH and the presence of complexing agents. Therefore, the condition is often reproduced in pH-dependence leaching tests to estimate the solubility of a constituent of interest and is given as a function of pH.

In this research, the manufactured LWA are aimed to perform in construction scenarios where the material own/natural pH governs the release of the constituents (the leachate pH is determined by the released/water-soluble constituents). Therefore, drill cuttings and manufactured LWA were subjected to the leaching test without acid or base addition as described by British standard method (BS EN 12457-2) and the results were compared with designated End of Waste (EoW) criteria.

#### 3.2.1.8 End of Waste (EoW) criteria

EoW criteria determine when a waste gains the status of a product. The EU Waste Framework Directive (2008/98/EC) introduces provisions to define EoW criteria that provide a high level of environmental protection and economic benefits. This provides an opportunity to encourage recycling and use of waste as a resource,

whilst aiming to inhibit over-consumption of natural resources and creates landfill diversion. For aggregate manufacturers in the UK, EoW criteria for the production and use of aggregates from inert waste are outlined in the Aggregate Quality Protocol (Environment Agency, 2013), in which no specific leaching criteria is provided.

Most European countries, except the UK, have founded the EoW criteria on the leaching properties of materials. However, each country uses a specific leaching test and thus establishing leaching limit would be irrelevant without referring to the test condition (Velzeboer and Zomeren, 2017). For the research on the use of hazardous waste in the production of construction materials, studies have often based the criteria on batch leaching test (BS EN 12457) and the EU inert landfill Waste Acceptance Criteria (WAC) as expressed in (2003/33/EC). Therefore, the EoW criteria based on WAC limit values for inert waste were used in this study as listed in Table 3.2.

Table 3.2 EoW criteria based on WAC for inert landfill as expressed in (2003/33/EC).

Constituents	WAC
Arsenic (As)	0.5
Barium (Ba)	20.0
Cadmium (Cd)	0.04
Chromium (Cr)	0.5
Copper (Cu)	2.0
Mercury (Hg)	0.01
Molybdenum (Mo)	0.5
Nickle (Ni)	0.4
Lead (Pb)	0.5
Antimony (Sb)	0.06
Selenium (Se)	0.1
Zinc (Zn)	4.0
Chloride (Cl <sup>-</sup> )	800
Fluoride (F <sup>-</sup> )	10
Sulphate (SO <sub>4</sub> <sup>-2</sup> )	6000*
DOC	500

\* 6000 mg/kg at L/S = 10 l/kg is complying with the inert limit if the leaching is caused only by SO<sub>4</sub><sup>-2</sup> and Cl<sup>-</sup>

### 3.2.1.9 Leaching test procedure:

Since drill cuttings are classified as a hazardous waste, leaching behaviour of the final products was of concern. Leaching tests were conducted according to the European standard (BS EN 12457-2): 0.090 ± 0.005 kg of dry sample was ground (to a particle size of 4 mm or less) and added into a 2-litre high-density polyethylene bottle containing deionised water at a liquid to solid ratio (L/S) of 10 l/kg. The volume of deionised water was determined according to the following equation:

$$V_e = \left( x - \left( \frac{m_c}{100} \right) \right) \times M_{sd} \times 1000 \quad 3.7$$

where:  $V_e$  = Volume of deionised water (elute) in ml;  $x$  = Liquid to solid ratio in l/kg (10 l/kg for this experiment);  $m_c$  = Moisture content in %;  $M_{sd}$  = Dry mass in kg.

The moisture content was calculated as:

$$m_c = 100 \times (M_w - M_{sd})/M_{sd} \quad 3.8$$

where  $M_w$  = The mass of wet sample in kg.

The bottle was placed under constant rotation in an end-over-end tumbler (5 rpm - 10 rpm) for 24 hours (see Figure 3.4), and then allowed to rest for 15 min to settle the solid particles. The resulted leachate was then vacuum filtered through a 0.45  $\mu$ m membrane. The concentrations of dissolved constituents were measured by inductively coupled plasma optical emission spectroscopy (ICP-OES) and ion chromatography (IC).



Figure 3.4 End-to-end rotary tumbler used for leaching test.

#### 3.2.1.10 Analysis of metals by ICP-OES:

ICP-OES is an analytical technique for determining trace (<100 ppm) and minor (100 – 1000 ppm) elements with a wide range of applications from geological materials to water and fluid extracts (leachates) (Lichte et al., 1987). For the analysis of solutions, the sample

is transformed into an aerosol (1 -10  $\mu\text{m}$ ) and is passed through the plasma. The plasma is an electrically neutral, highly ionised gas that operates with pure helium or argon to avoid combustion. The ICP induces the plasma using an induction coil to produce a magnetic field (Manning and Grow, 1997). This process excites the outer shell electrons of atoms for which electromagnetic radiation (photon of light) is emitted as electrons are relaxed from the excited state to the ground state. The radiations are emitted at specific energies (characteristics of atomic energy level transition) and are therefore characteristics of each element in the sample. These photons are simultaneously detected by photomultiplier tubes (PMTs) within the detection system (Lichte et al., 1987, Manning and Grow, 1997); having the advantage of directly proportioning an emission of a specific element (at a given wavelength) to its concentration (Beer's Law).

In this study, a Perkin Elmer ICP-OES Optima 8300 was used. The concentration of dissolved metals in leachates from the leaching test was directly analysed by ICP-OES according to the British standard for water quality (BS EN ISO 11885, 2009). The ICP-OES instrument was calibrated running a three-point calibration curve at 0.1 mg/kg, 1 mg/kg and 10 mg/kg for the 12 waste acceptance criteria (WAC) elements including As, Ba, Cd, Cr, Cu, Hg, Mo, Ni, Pb, Sb, Se and Zn, using certified reference solutions.

The instrument detection limits were calculated as three times the standard deviation for the noise of 10 blank runs (baseline noise value). The detection limits for each element was measured as three times the standard deviation of spiked samples, which are prepared for each element at concentrations of three times the instrument limit of detection. Accordingly, the limit of quantification in (mg/kg) was calculated by multiplying the resulted detection limit for each element by 10. It must be noted that as the signal to noise ratio varies for all elements, some have higher detection limit values than others.

#### 3.2.1.11 Analysis of anions with ion chromatography (IC)

Ion chromatography (IC) is a powerful analytical method for measuring the concentration of ionic species in solutions. IC offers a higher sensitivity, speed and simultaneous selectivity for analysis of anions compare to other methods - including ICP and atomic absorption spectroscopy (AAS) (Weiss, 2016). The method is comprised of pumping a liquid mobile phase (eluent) through a solid stationary phase (usually uniform particles, 5  $\mu\text{m}$  in diameters and packed in a 5 – 30 cm long cylindrical column) and then through a flow-through detector (Haddad and Jackson, 1990). The sample is injected into the eluent and enters the separator column as shown in Figure 3.5. The ions travel at different

speeds through the column as they interact differently with the stationary phase and thus, reach the detector at different times. A conductivity suppression unit is used to reduce the background conductivity of the eluent ( $\text{Na}_2\text{CO}_3$  and  $\text{NaHCO}_3$ ) by converting it into a less conductive acid form and to increase the conductivity of anions by protonating them into a highly conductive (up to 3 - 5 times) conjugate acid (Wang, 2010, Mohamed, 2012). The detector simultaneously measures the time it takes for an anion to emerge from the column, versus the conductivity to generate a peak. The concentration is determined by comparing the peak area to standard solutions with known concentrations.

In this study, samples were leached in deionised water according to the single stage leaching process at a L/S ratio of 10 l/kg (BS EN 12457-2, 2002). The leachate was filtered and run through a Dionex Ion Chromatograph for measuring relevant anions i.e.  $\text{Cl}^-$ ,  $\text{F}^-$  and  $\text{SO}_4^{2-}$  according to (BS EN 6068-2.46, 1995). 0.5 M sodium carbonate was used as the eluent. The prepared multi-element calibration standards included:

- a)  $\text{Cl}^- = 2500 \text{ mg/l}$ ,  $\text{F}^- = 1000 \text{ mg/l}$  and  $\text{SO}_4^{2-} = 1000 \text{ mg/l}$
- b)  $\text{Cl}^- = 500 \text{ mg/l}$ ,  $\text{F}^- = 200 \text{ mg/l}$  and  $\text{SO}_4^{2-} = 200 \text{ mg/l}$
- c)  $\text{Cl}^- = 50 \text{ mg/l}$ ,  $\text{F}^- = 20 \text{ mg/l}$  and  $\text{SO}_4^{2-} = 20 \text{ mg/l}$
- d)  $\text{Cl}^- = 5 \text{ mg/l}$ ,  $\text{F}^- = 2 \text{ mg/l}$  and  $\text{SO}_4^{2-} = 2 \text{ mg/l}$

Where the sample chromatogram exceeded the calibration peak, the test was repeated with a higher dilution factor. The measured concentrations were reported as mg/kg.

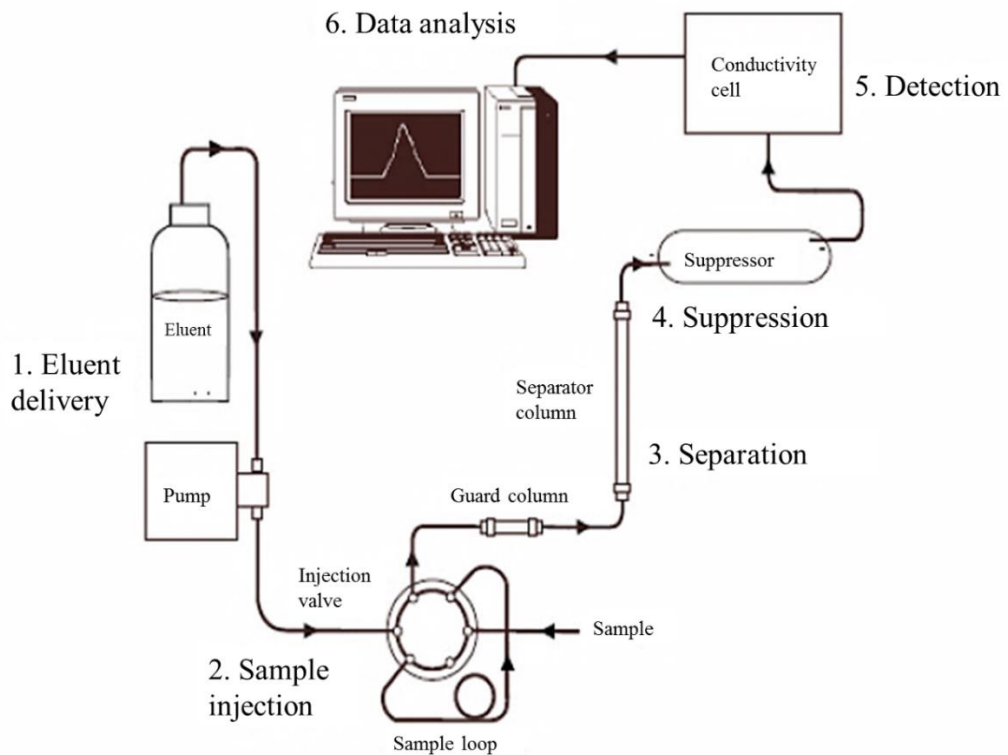


Figure 3.5 Ion chromatography (IC) system flow diagram adapted from (Wang, 2010).

### pH and conductivity

The leachate pH was measured using a Thermo Orion Star - A211 pH meter. The conductivity of the leachate was measured in  $\mu\text{S}/\text{cm}$  using an Orion Star A212 conductivity meter with temperature compensation. These values are required to be reported alongside the leaching concentration measured according to the British standard method (BS EN 12457-2, 2002).

### 3.2.1.12 Dissolved organic carbon (DOC)

DOC was measured by filtering the leachate through a  $0.45\ \mu\text{m}$  membrane and oxidation of organic carbon in water to  $\text{CO}_2$  by supercritical water oxidation (using persulphate as the oxidising agent) according to the British standard method (BS EN 1484, 1997). The gas was then separated and run through a NDIR (Nondispersive infrared) module.

### 3.2.1.13 Loss on ignition (LOI)

LOI is a simple gravimetric test method for measuring the mass loss of a sample of material when it is heated up to high temperatures in presence of air or oxygen. The heating temperature range varies for different research fields and for estimating the presence of different components. For example, in soil science, a sample is heated between 300 °C and 800 °C for 2 – 12 hours to measure the organic and inorganic carbon content; in geological science, the applied temperature range is usually between 550 °C and 950 °C for approximately two hours to measure various volatile salts, structural water and inorganic carbon content including carbonates as in  $\text{CaCO}_3$  and  $\text{CaMgCO}_3$  (Mu et al., 2017).

In this study, the LOI was determined on  $20 \pm 0.01\text{g}$  of dried sample following the (BS EN 12879, 2000). The sample was first dried in a drying oven at 105 °C overnight and allowed to cool down in a desiccator for at least 30 min before the test. The dried sample is then weighed out into a crucible before being heated at 550 °C for four hours. The sample was left to cool before reweighing. The difference in the initial mass and the final mass is the LOI.

### 3.2.2 Manufacturing method

This section provides information on the manufacturing method used for LWA including pelletisation and firing stages. The production parameters selection procedure is described. Tests used for determining the physical properties of LWA including particle density (fired pellets density), water absorption after 24 hours immersion and compressive strength of individual pellets are outlined.

In Figure 2.10, the main production parameters that affect the pore structure and physical properties of LWA were shown. These include pre-processing such as milling and sieving, heating/cooling rate, firing temperature and dwell time. In this study, LWA was manufactured according to the flowchart shown in Figure 3.6. The production parameters and their range of variability used in each step were determined based on the literature (provided in Chapter 2) and material characterization data. In addition, the manufacturing process and the range of parameters were aimed to closely resemble those commonly used in large-scale LWA manufacturing. However, due to the large number of production parameters and the limited time available for a PhD project, investigating the full range of variability for each parameter was not possible and therefore, some parameters were set on an optimal range extracted from the literature. The manufacturing process involved:

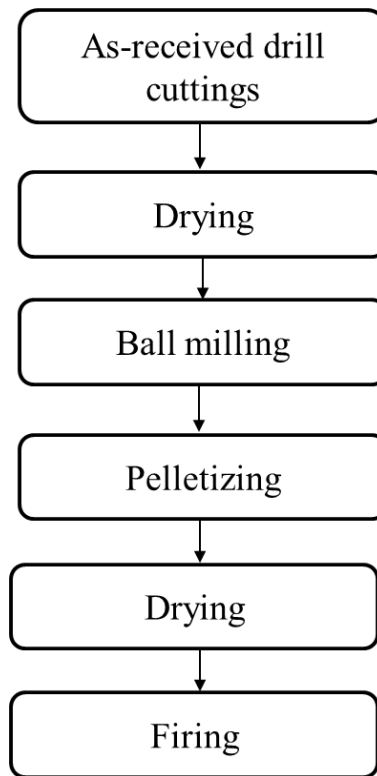


Figure 3.6 Flowchart of pre-processing, pre-treatments and LWA manufacturing in this study.

### 3.2.2.1 Pre-processing

In the large-scale manufacturing of ceramics and mineral processing, both wet and dry milling are commonly used (Kotake et al., 2011). The nature of drill cuttings, containing considerable amounts of soluble salts, necessitated a dry condition employed during the milling stage.

Particle size reduction can serve in favour of bloating through higher sintering efficiencies and better gas entrapments, however a coarser particle size distribution is also needed for sufficient workability of material for pelletisation (Dondi et al., 2016). In this study, the maximum particle size of 250  $\mu\text{m}$  was used, as suggested by the work of Cougny (1990), to ensure both bloating and technological behaviour of LWA. This was the rationale for determining the speed and duration of the milling process. A number of preliminary experiments were carried out to find an optimal milling condition that provided a size reduction to  $<250 \mu\text{m}$ , for the ball mill that was available for this study. Milling was conducted in a dry condition using a 6-litre planetary ball mill (DECO-PBM) at 300 rpm for 6 hours. Milled samples were sieved using a mesh size of 250  $\mu\text{m}$ .

### 3.2.2.2 Pelletisation

To pelletise the samples prior to firing, the amount of water required to facilitate sufficient workability (plastic behaviour) without causing the material to flow was determined through a series of preliminary experiments. The samples were pelletised by adding approximately  $22.5 \pm 2.5$  wt.% water to the ball milled drill cuttings. Roughly spherical pellets with 7 – 12 mm in diameter (to be in the size range of normal-weight course aggregate) were formed by hand rolling. The hand rolling method was selected to provide consistency in the shape and size of ‘green’ pellets for testing.

The remaining moisture after pelletisation can cause the pellets to burst during the firing stage and therefore must be removed by drying. However, the conventional drying temperatures used for LWA manufacturing (100 – 200 °C) could not be used here due to the resultant loss of hydrocarbons from drill cuttings. Therefore, drying was carried out in a cabinet dryer at 65 °C for 24 hours.

### 3.2.2.3 Firing

The ‘green’ pellets were fired in a laboratory-scale programmable muffle furnace (SNOL 6,7/1300). The firing conditions were adjusted to simulate those used in large-scale LWA manufacturing, as described in Chapter 2:

- Heating/cooling rate

In the drying/pre-heating zone of rotary tube kilns, the ‘green’ pellets temperature can reach up to 600 °C before entering the sintering zone and being exposed to firing temperatures of approximately 1200 °C. Such a sudden increase in the temperature is not achievable in a laboratory-scale muffle furnace. Since it normally takes 2 hours for pellets to experience a temperature rise (from ambient to maximum sintering temperature) a mean heating rate of 10 °C/min can be applied during the firing stage in the muffle furnace to resemble the heating regime in the industrial rotary tube kilns. Therefore, the heating rate was set at 10 °C/min throughout this study. Figure 3.7 shows the heating regimes to which LWA pellets were subjected.

The cooling rate was designed to mimic the fate of LWA in cooler units at large-scale commercial manufacture where ambient air is blown on pellets. This could be achieved

by opening the muffle furnace door at the end of the firing stage to expose the pellets to the ambient air. Since this would damage the heating elements, a two-step cooling regime was applied for all samples comprising of a slow cooling regime, at 10 °C/min until 800 °C, followed by rapid cooling in ambient air, at ~40 °C/min, until room temperature is reached.

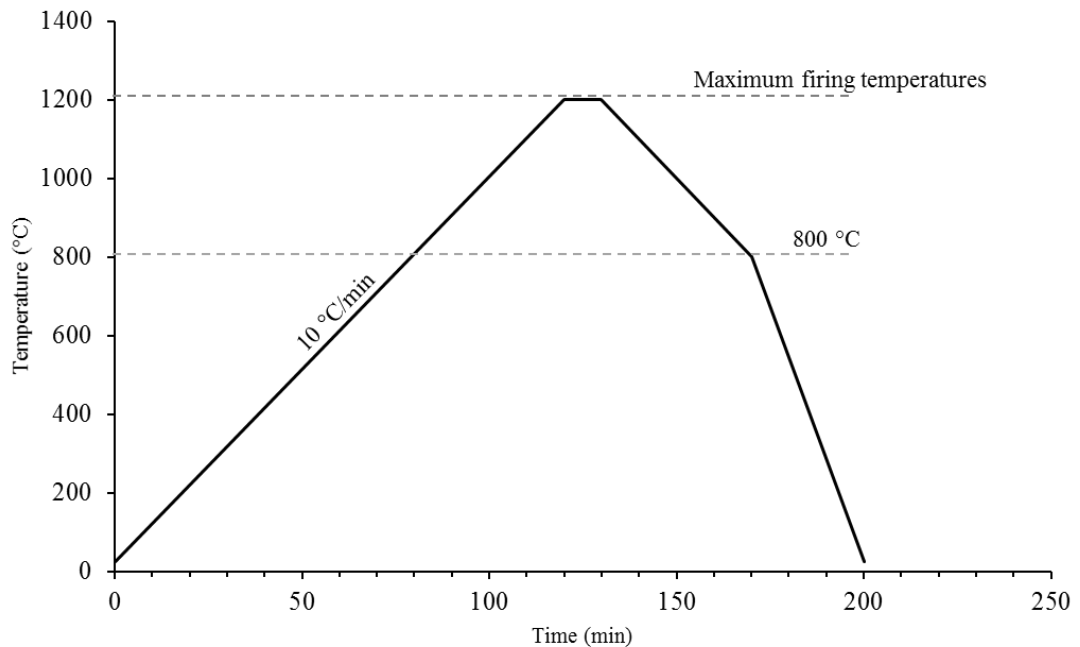


Figure 3.7 Heating regimes applied in muffle furnace during the LWA manufacture.

- Firing temperature

The firing temperature range for each sample of drill cuttings was determined separately. This was because the material characterization data revealed that the three samples of drill cuttings were very different in nature, and therefore would reach pyro-plasticity at different temperature ranges. The minimum temperature at which the material showed sintering was defined as the lower firing limit and the temperature at which melting was initiated was set as the higher firing limit. Both the initial sintering and melting temperatures were determined based on the data obtained from heating microscopy. The first sharp decrease in the cube outline area to 95% of the original area has been associated to the initiation of sintering (Zhang et al., 2011) and therefore, was used in the muffle furnace as the lower firing temperature for LWA manufacturing in this study. The initiation of melting was also determined from heating microscope images, where the liquid phase appeared, and the cube started to lose its structural integrity. The defined

firing temperature range was divided into four segments and the ‘green’ pellets were fired at each interval temperature. Samples that did not exhibit melting over the temperature range used in the heating microscope were fired at four temperatures above the initial sintering point with 10 °C increments to ensure sufficient pyro-plastic viscosity and to maximise energy savings.

- Dwell time

As discussed in Chapter 2, the firing dwell time (the time that pellets were kept at the maximum temperature in the kiln) must be sufficient for bloating to occur and not too long to cause large energy consumption and possibly melting. In the sintering zone of rotary tube kilns (in Figure 2.8) LWA normally resides for 8 – 10 min. In addition, the majority of dwell times used in studies of Table 2.7, range between 5 – 15 min. Therefore, for this study, a mean dwell time of 10 min was used.

### 3.2.3 Physical tests

The applicability of the manufactured LWA for use in concrete products is assessed by measuring three main physical properties including particle density, water absorption and compressive strength, as discussed in Chapter 2. In this study, these properties were determined and compared with those for commercial products that are used in the production of structural concrete products. Furthermore, the effect of LWA pore structure developed during the firing stage on physical properties was investigated. A description of the physical tests used in this study are provided in the followings:

#### 3.2.3.1 Particle density

Particle density on an oven-dried basis was calculated using the Archimedes principle - based on the method described in the British standard (BS EN 1097-6). According to this principle, when an object is immersed in the water, its volume is equal to the mass of displaced water (if density of water is assumed 1.0 g/cm<sup>3</sup>). Since LWA is a porous material with some degree of water absorption, the volume of dried pellets must be determined by excluding the water-accessible pores. Therefore, the volume of the dried pellets is equal to the difference between the mass of water-saturated pellets and its apparent mass (immersed mass in water). Particle density on an over-dried basis ( $\rho_{dr}$ ) for the manufactured LWA was calculated in accordance with the following equation (Cheeseman and Viridi, 2005):

$$\rho_{dr} = (\rho_w \times m_{dr}) / (m_{sat} - m_{imm}) \quad 3.9$$

[Where:  $\rho_w$  is the density of water in g/cm<sup>3</sup>;  $m_{dr}$  is the mass in g of oven-dried test portion;  $m_{sat}$  is the mass of saturated and surface-dried aggregates (24 hours in water and dried in air) in g;  $m_{imm}$  is the apparent mass (immersed mass) in g; and. The measurement was carried out in triplicates using 10 pellets for each test portion.]

#### 3.2.3.2 Water absorption capacity

Water absorption capacity is equal to the increase in weight of dry pellets after immersion in water for 24 hours. Water absorption capacity as a percentage of the dry mass ( $WA_{24}$ ) was calculated in accordance with the following equation:

$$WA_{24} = 100 \times (m_{sat} - m_{dr}) / m_{dr} \quad 3.10$$

### 3.2.3.3 Compressive strength

The majority of the reviewed studies in Table 2.7 obtained the LWA strength data from compressing a single pellet between two rigid surfaces and measured the critical load, which causes the fracture. If the critical load is determined, the compressive strength can be calculated because the porous structure of LWA produces the same stress distribution as in a solid sphere for which a number of equations exist. To calculate the compressive strength of LWA the equation must involve a number of interrelated physical properties – such as the strength of the matrix and geometrical factors such as size and shape (González-Corrochano et al., 2009b). It has been shown that in single pellet crushing tests, porosities <0.82% perform similarly to solid brittle spheres, where fracture failure is due to tensile stress somewhere alongside the axis between two loading points, and most importantly, the strength is increased exponentially with decreasing sample size (Li et al., 2000, Bernhardt et al., 2013). The following equation has been introduced for calculating solid brittle spheres compressive strength and been widely used for LWA (Hiramatsu and Oka, 1966):

$$S = (2.8 \times P_c) / \pi X^2 \quad 3.11$$

[Where:  $P_c$  is the fracture load in N and X is the distance between the loading points in mm.]

In this study, compressive strength (S) was calculated by loading the pellets to fracture between two parallel rigid surfaces and using the above equation. The fracture load was determined using a load ring with 4.55 kN capacity (Wykeham-France) at the loading speed of 0.05 mm/s.

The physical properties of LWA are mainly influenced by the microstructure developed during the firing stage, as discussed in Chapter 2. In addition, the leaching behaviour of LWA is affected by mineralogy of the phases formed during the firing. This research aimed to investigate these relations for various batches of manufactured LWA, as shown in Figure 3.8.

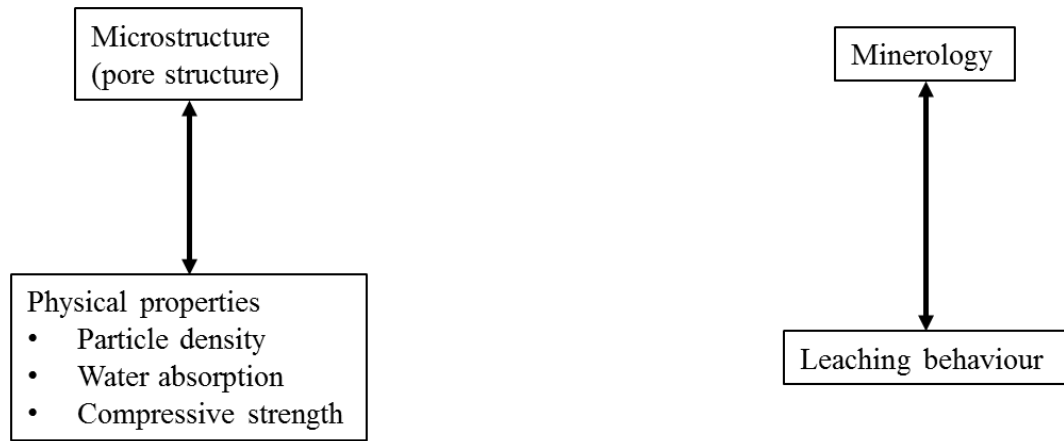


Figure 3.8 Relations investigated between properties of LWA.

## 4 Chapter 4: Characterization of drill cuttings

In this chapter, the research investigated the characteristics of the three samples of SBM drill cuttings; namely SDC, CDC and EDC. The study aimed to determine chemical compositions, mineralogy, particle morphology, thermal behaviour and contaminant leaching. The characterization data was used as a basis to design the manufacturing process in Chapter 5 and explain the LWA physical and leaching characteristics.

### 4.1 Chemical compositions

The chemical compositions of drill cutting samples were determined by XRF analysis. The data was used to: predict the materials capability to bloat, explore the nature and quantity of drilling additives present in cuttings and estimate the total amount of leachable compounds including heavy metals and soluble salts. Table 4.1 shows the results of XRF analysis including major elements reported as oxide weight percentages (wt.%) normalised to 100%, and LOI data. Table 4.2 shows the concentration of minor and trace elements in drill cuttings.

#### 4.1.1 SDC

SDC had 32.89 wt.% SiO<sub>2</sub>, 4.39 wt.% Al<sub>2</sub>O<sub>3</sub> and 30.53 wt.% total flux (Fe<sub>2</sub>O<sub>3</sub> + MgO + CaO + Na<sub>2</sub>O + K<sub>2</sub>O). The viscosity of LWA matrix at the pyro-plastic state is related to SiO<sub>2</sub>/Σ flux ratio and SiO<sub>2</sub>/Al<sub>2</sub>O<sub>3</sub> ratios, as discussed in Chapter 2. The SiO<sub>2</sub>/Σ flux ratio and SiO<sub>2</sub>/Al<sub>2</sub>O<sub>3</sub> ratios were 1.08 and 7.49 respectively indicating an inability of the material to produce a suitable viscosity for bloating. High concentrations of Ba (161,261 mg/kg) and sulphur (42,233 mg/kg) were measured for SDC sample. Comparing these with the values for the molar mass of Ba (137.3 g/mol) and sulphur (32 g/mol), it is likely that BaSO<sub>4</sub> is the main SO<sub>4</sub><sup>2-</sup> bearing phase in SDC sample. As discussed in Chapter 2, BaSO<sub>4</sub> is added to the drilling fluid as a weighting agent (especially for drilling high depths).

#### 4.1.2 CDC

XRF analysis for CDC showed the lowest silica (32.52 wt.%) and the highest calcium oxide content (50.15 wt.%) among the samples. The SiO<sub>2</sub>/Σ flux ratio and SiO<sub>2</sub>/Al<sub>2</sub>O<sub>3</sub> ratio were 0.48 and 4.88 respectively, indicating a lack of bloating. Ba and S were 72,595 mg/kg and 18,369 mg/kg respectively, suggesting again BaSO<sub>4</sub> to be the major sulphur bearing component present.

### 4.1.3 EDC

The analysis of EDC showed the concentrations of SiO<sub>2</sub> and Al<sub>2</sub>O<sub>3</sub> at 41.18 wt.% and 12.75 wt.% respectively. The SiO<sub>2</sub>/Σ flux ratio was 0.91 and the SiO<sub>2</sub>/Al<sub>2</sub>O<sub>3</sub> ratio was 3.22, showing a disproportionate composition for bloating also in EDC sample. Ba and S were 32,019 mg/kg and 39,727 mg/kg respectively. Molar mass calculations revealed the presence of considerable amounts of other sulphur bearing components. Most likely, calcium sulphate and magnesium sulphate may be present in drill cuttings since these are the main minerals formed within salt dome evaporite deposits that are associated with hydrocarbon reservoirs (Warren, 2006).

Table 4.1 Chemical compositions including major oxides and LOI of drill cuttings determined by XRF analysis.

Oxide compositions	SDC (wt.%)	CDC (wt.%)	EDC (wt.%)
SiO <sub>2</sub>	48.59	32.52	41.18
Al <sub>2</sub> O <sub>3</sub>	6.48	6.52	12.75
Fe <sub>2</sub> O <sub>3</sub>	6.07	6.79	3.29
MgO	1.77	2.12	7.34
CaO	35.07	50.15	14.95
Na <sub>2</sub> O	1.46	0.99	17.32
K <sub>2</sub> O	0.74	0.38	2.530
TiO <sub>2</sub>	0.53	0.21	0.447
MnO	0.20	0.20	0.073
P <sub>2</sub> O <sub>5</sub>	0.14	0.12	0.116
Si/ΣF*	1.08	0.48	0.91
Si/Al**	4.50	4.97	3.23
LOI	3.9	8.6	8.2

\* SiO<sub>2</sub>/Σ flux ratio

\*\* SiO<sub>2</sub>/Al<sub>2</sub>O<sub>3</sub> ratio

Table 4.2 Chemical compositions including minor and trace element concentrations of drill cuttings determined by XRF analysis.

Minor and trace elements	(mg/kg)	(mg/kg)	(mg/kg)
Ni	0.8	20.1	36.0
Co	12.0	17.6	13.3
Cr	5.6	29.0	74.3
Sc	4.5	9.5	9.7
Cu	30.7	34.9	23.9
Zn	235.9	108.4	102.4
As	13.4	10.3	11.8
S	42,233	18,369	39,727
F	55	631	352
Cl	8375	17,546	80,911
Br	955.5	2103.5	1128.0
Ga	30.4	12.7	15.3
Pb	140.8	54.5	38.5
Sr	1616	1981	13.20
Rb	40.5	90.0	119.5
Ba	161,261	72,595	32,019
Zr	33.5	97.1	94.7
Nb	2.5	5.5	10.2
Mo	2.2	0.7	1.1

## 4.2 Riley diagram

The measured compositions were plotted in a Riley ( $\text{SiO}_2/\text{Al}_2\text{O}_3/\Sigma \text{ flux}$ ) ternary diagram, that has been frequently used to predict the bloating capabilities of aluminosilicate-based materials (de' Gennaro et al., 2004, Fakhfakh et al., 2007, de Gennaro et al., 2007, González-Corrochano et al., 2009b, González-Corrochano et al., 2009a, Tang et al., 2011, Wei et al., 2011, Chen et al., 2012, Huang and Wang, 2013, González-Corrochano et al., 2014, Quina et al., 2014a, Lu et al., 2015, Zhang et al., 2015, Mueller et al., 2015, González-Corrochano et al., 2016). Figure 4.1 shows that the compositions of all three samples of SBM drill cuttings were located outside of the bloating area established by Riley (1951).

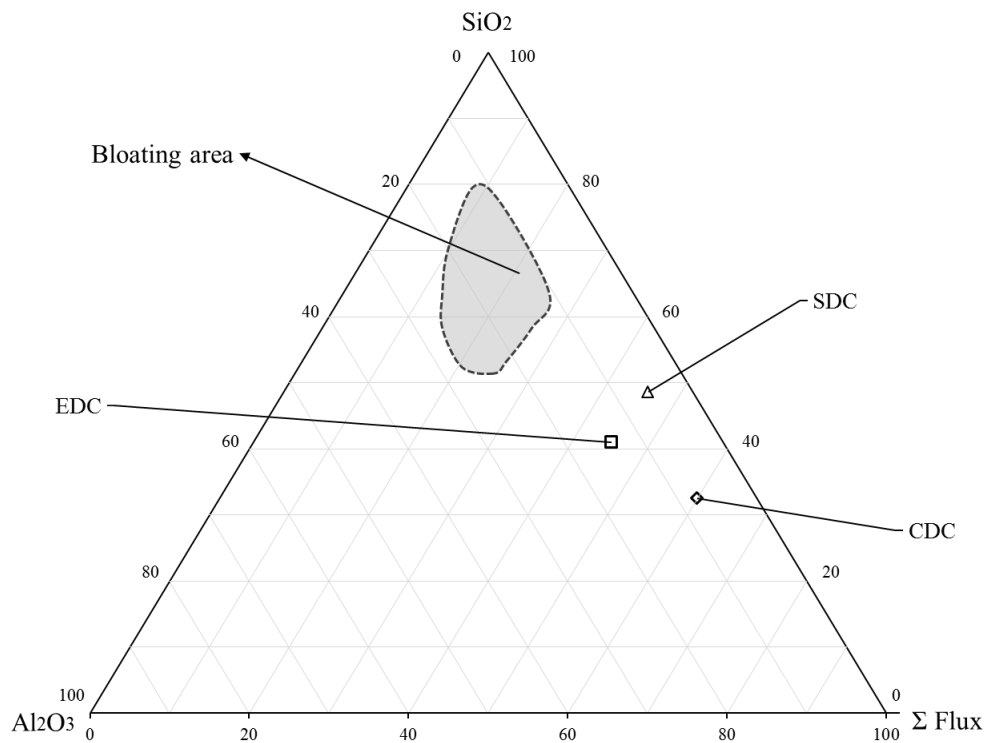


Figure 4.1 The location of bulk chemical composition for samples of drill cuttings in Riley diagram. The shaded area indicates the bloating region established by Riley (1951).

### 4.3 Mineralogy

The mineralogy of drill cuttings was determined using XRD analysis. The information was used to identify the presence of gas-releasing compounds such as carbonates and sulphates necessary for bloating at high temperatures. In addition, XRD analysis revealed the nature and quantity of inorganic salts and drilling additives present in drill cuttings that control the materials' leaching behaviour. XRD patterns for samples of drill cuttings are shown in Figure 4.2. Results of Rietveld quantitative phase analysis are given in Table 4.3. It must be noted that in the Rietveld quantification analysis for major phases, relative errors in the order of 1 – 2% and up to 3 – 4% for minor phases do occur, while the sensitivity of the quantification varies with each mineral phase (De la Torre and Aranda, 2003).

#### 4.3.1 SDC

In SDC,  $\text{CaCO}_3$  (calcite and aragonite),  $\text{BaSO}_4$ ,  $\text{KAlSi}_3\text{O}_8$  (orthoclase),  $\text{NaCl}$  and  $\text{SiO}_2$  (quartz) were identified. Most distinctively, the peaks at  $31.7^\circ 2\theta$  and  $56.5^\circ 2\theta$  are associated to  $\text{NaCl}$  (200) and (222) reflections respectively; the peaks close to  $32.85^\circ 2\theta$  and  $42.9^\circ 2\theta$  were identified as  $\text{BaSO}_4$  (211) and (212) reflections, and the peaks appeared at  $26.2^\circ 2\theta$ ,  $27.25^\circ 2\theta$ ,  $33.15^\circ 2\theta$  and  $52.5^\circ 2\theta$  are associated to aragonite (111), (021), (012) and (113) reflections, according to ICDD reference database. These results were in good agreement with XRF analysis where high concentrations for Cl, Ba and Ca were determined.

In SDC, the quantitative analysis showed that 50.6 wt.% of the total crystalline phase was composed of  $\text{BaSO}_4$ ; 20.2 wt.%  $\text{KAl}_2(\text{Si}_3\text{AlO}_1)(\text{OH})_2$ ; 10.8 wt.%  $\text{NaCl}$ ; 12.1 wt.% carbonate minerals including 4.3 wt.%  $\text{CaCO}_3$  (calcite), 6.4 wt.%  $\text{CaCO}_3$  (aragonite); and 1.4 wt.%  $\text{CaMgCO}_3$  (Table 4.3). From the quantified phases, it could be concluded that the sample is rich in minerals found in shale reservoirs (Clarkson et al., 2013). High quantities of  $\text{BaSO}_4$  in drill cuttings can be due to a poor separation that causes the weighting agent to remain in the drill cuttings waste, as explained in section 2.1.3. This can also indicate the depth at which the material is obtained since more  $\text{BaSO}_4$  is added to the drilling fluid to further increase the density when drilling at higher depths (Dhir et al., 2010). 10.8 wt.%  $\text{NaCl}$  quantified was consistent with XRF analysis of SDC sample. This is mainly originated from the drilled formation rock (Manspeizer, 2015). However, a second source could be from the drilling fluid which may contain high

concentrations of soluble sodium and calcium salts in order to control the fluid loss (dissolution) to the formation (Neff, 2005), as discussed in section 2.1.2. More than half of the 12.1 wt.% of carbonate minerals quantified for SDC sample, was predicted to be aragonite. The quantified concentration of quartz was as low as 2.5 wt.%. The concentrations of calcium sulphates (both  $\text{CaSO}_4$  and  $\text{CaSO}_4 \cdot 2\text{H}_2\text{O}$ ) were also negligible. Three endmembers of feldspar groups -  $\text{NaAlSi}_3\text{O}_8$ ,  $\text{CaAl}_2\text{Si}_2\text{O}_8$  and  $\text{KAlSi}_3\text{O}_8$  - were included as a potential phase during the quantification and the analysis showed 1.7 wt.% of the total crystalline phase to be  $\text{NaAlSi}_3\text{O}_8$  and 2.0 wt.% to be  $\text{CaAl}_2\text{Si}_2\text{O}_8$ .

#### 4.3.2 CDC

In CDC (Figure 4.2),  $\text{SiO}_2$  (quartz),  $\text{CaCO}_3$ ,  $\text{CaSO}_4 \cdot 2\text{H}_2\text{O}$ ,  $\text{CaSO}_4$ ,  $\text{BaSO}_4$  and  $\text{KAlSi}_3\text{O}_8$  could be identified. In this sample, the position of the most intense  $\text{CaCO}_3$  reflection (104) was slightly shifted to a higher angle ( $29.85^\circ 2\theta$ ). This effect has been associated to the substitution of ions such as Mg, Mn and Fe for Ca in the  $\text{CaCO}_3$  crystal structure (Magaritz and Kafri, 1979).  $\text{BaSO}_4$  (121) and (212) reflections appeared at  $28.8^\circ 2\theta$  and  $42.9^\circ 2\theta$ . It was observed that the intensity of NaCl peaks was considerably lower compared to SDC, while the peak intensity of other major mineral phases (most notably quartz) was higher. It is worth mentioning that the heights of the peaks only give an approximate indication of quantity present. Well crystallised minerals like quartz (and to a lesser extent  $\text{CaCO}_3$ ) can give very large peaks when only a relatively small amount is present (Hurst et al., 1997).

In CDC, the quantitative model predicted 63.7 wt.% of the total crystalline phase to be  $\text{CaCO}_3$  (Table 4.3). This is in accordance with approximately 50 wt.% calcium oxide measured by XRF analysis. The second most abundant mineral in this sample was  $\text{BaSO}_4$ , quantified at 18.8 wt.%. Minor concentrations of quartz and  $\text{KAl}_2(\text{Si}_3\text{AlO}_{10})(\text{OH})_2$  were quantified by the model at 5.7 wt.% and 7.8 wt.% respectively.

#### 4.3.3 EDC

Major crystalline phases in EDC (Figure 4.2) were  $\text{CaCO}_3$ ,  $\text{CaMg}(\text{CO}_3)_2$ ,  $\text{SiO}_2$  (quartz),  $\text{KAlSi}_3\text{O}_8$ , NaCl,  $\text{KAl}_2(\text{Si}_3\text{AlO}_{10})(\text{OH})_2$ ,  $\text{BaSO}_4$  and  $\text{CaSO}_4$ . Most of these peaks were clearly visible compared to those identified for the other two drill cuttings samples, at the positions indicated in ICDD reference database. Most distinctive were NaCl (200), (220) and (222) reflections at  $31.7^\circ 2\theta$ ,  $45.45^\circ 2\theta$  and  $56.5^\circ 2\theta$ ;  $\text{CaSO}_4$  (200) at  $25.45^\circ 2\theta$ ; and  $\text{CaMgCO}_3$  (104) and (113) at  $30.1^\circ 2\theta$  and  $41.2^\circ 2\theta$ .

In EDC, carbonate minerals including  $\text{CaCO}_3$  and  $\text{CaMgCO}_3$  were quantified at 7.1 wt.% and 21.8 wt.%. These are the two common carbonates that cement (precipitate) chemically from pore fluid in rock-forming minerals (Ali et al., 2010). They were the most abundant minerals present in the sample and that agreed with the results of XRF analysis where both calcium oxide and magnesium oxide were measured at high concentrations (14.95 wt.% and 7.34 wt.%). The model quantified  $\text{KAl}_2(\text{Si}_3\text{AlO}_{10})(\text{OH})_2$  at 20.5 wt.%.  $\text{KAl}_2(\text{Si}_3\text{AlO}_{10})(\text{OH})_2$  is a dioctahedral mica that belongs to a 2:1 phyllosilicate group of the silicate minerals. Sulphates such as  $\text{CaSO}_4$  and  $\text{BaSO}_4$  were present at the quantities of 11.6 wt.% and 6.0 wt.%, respectively.  $\text{CaSO}_4$  has been documented in drill cuttings obtained from the southern North Sea (Pye and Krinsley, 1986). This showed that the extra  $\text{SO}_4^{2-}$  bearing phase predicted by molar mass calculation in the XRF analysis is mainly comprised of calcium sulphate minerals. Similarly, 10.9 wt.% of NaCl determined by the model, agreed with the high concentrations of  $\text{Cl}^-$  ions observed in XRF results. The quantified mineral phases for EDC strongly indicate that the material is a marine evaporite in nature (Dean, 2013).

Overall, the XRD analysis revealed that gas-releasing compounds, such as carbonates and sulphates in the form of  $\text{CaCO}_3$  and  $\text{CaSO}_4$ , are present in drill cuttings at sufficient quantities required for the bloating mechanism of LWA. These compounds are decomposed at temperatures above 800 °C during the firing stage which provides the gaseous phases necessary for bloating. In addition, the analysis showed more than 10 wt.% of the crystalline phase in SDC and EDC is composed of NaCl; indicating the possibility for high levels of  $\text{Cl}^-$  leaching for these materials. Natural sulphate salts such as  $\text{CaSO}_4$  and drilling additives such as  $\text{BaSO}_4$  were also present in drill cuttings at different concentrations, which can cause high levels of  $\text{SO}_4^{2-}$  leaching.

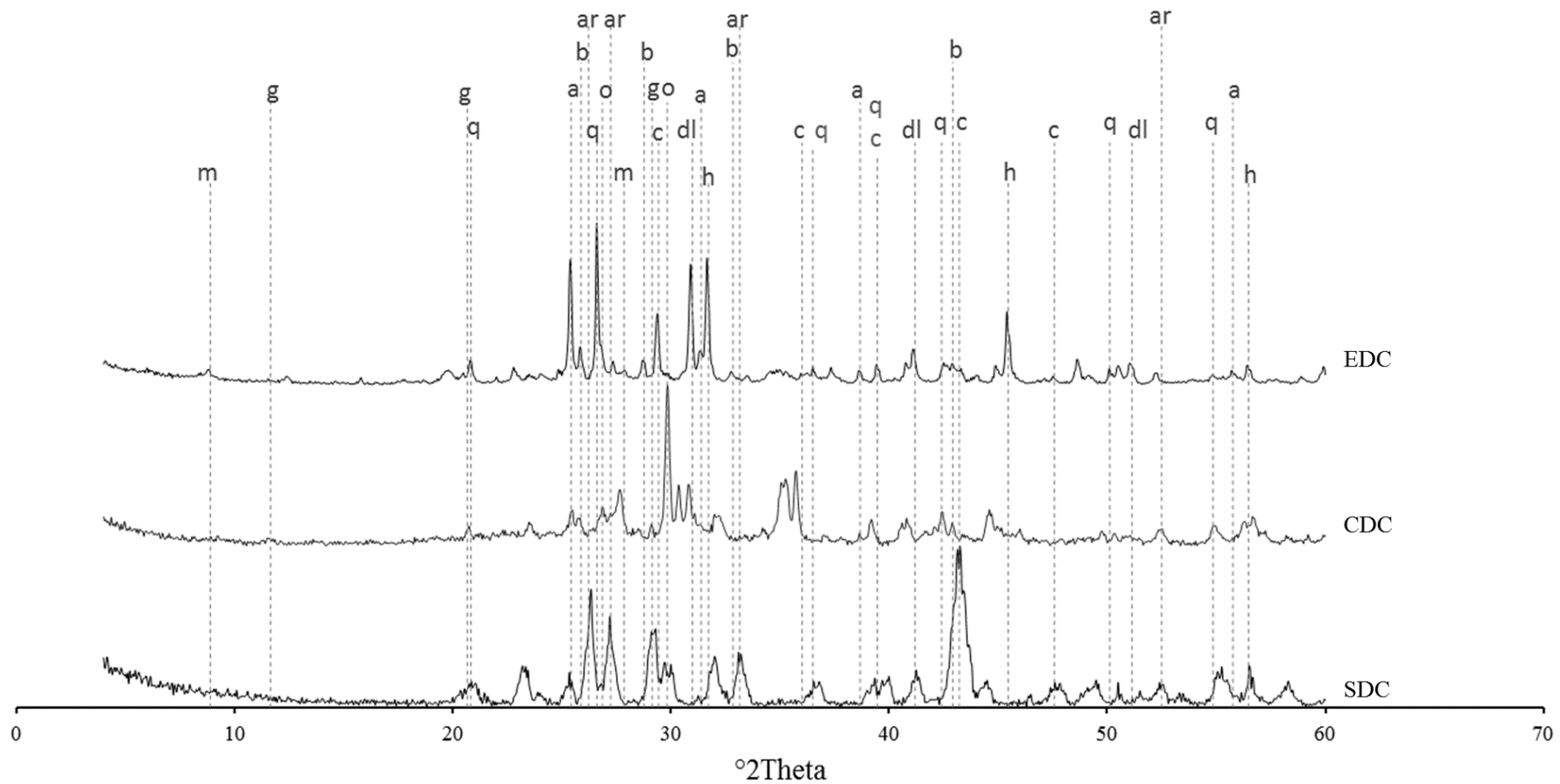


Figure 4.2 X-ray diffraction patterns with some important peak markers for crystalline phase identification in SDC, CDC and EDC samples. Markers include c:  $\text{CaCO}_3$  (calcite), ar:  $\text{CaCO}_3$  (aragonite), dl:  $\text{CaMg}(\text{CO}_3)_2$ , b:  $\text{BaSO}_4$ , h:  $\text{NaCl}$ , q:  $\text{SiO}_2$ , g:  $\text{CaSO}_4 \cdot 2\text{H}_2\text{O}$ , a:  $\text{CaSO}_4$ , o:  $\text{KAlSi}_3\text{O}_8$  and m:  $\text{KAl}_2(\text{Si}_3\text{AlO}_{10})(\text{OH})_2$ .

Table 4.3 Rietveld quantitative analysis of minerals presents in the samples of drill cuttings.

Minerals	Chemical formula	SDC (wt.%)	CDC (wt.%)	EDC (wt.%)
Quartz	SiO <sub>2</sub>	2.5	5.7	7.4
Calcite	CaCO <sub>3</sub>	4.3	63.7	7.1
Aragonite	CaCO <sub>3</sub>	6.4	-*	-
Dolomite	CaMg(CO <sub>3</sub> ) <sub>2</sub>	1.4	2.5	21.8
Halite	NaCl	10.8	0.3	10.9
Barite	BaSO <sub>4</sub>	50.6	18.8	6.0
Muscovite	KAl <sub>2</sub> (Si <sub>3</sub> AlO <sub>10</sub> )(OH) <sub>2</sub>	20.2	7.8	20.5
Gypsum	CaSO <sub>4</sub> ·2H <sub>2</sub> O	0.0	0.1	0.0
Anhydrite	CaSO <sub>4</sub>	0.0	0.0	11.5
Diopside	MgCaSi <sub>2</sub> O <sub>6</sub>	-	-	1.2
Albite	NaAlSi <sub>3</sub> O <sub>8</sub>	1.7	0.0	0.0
Anorthite	CaAl <sub>2</sub> Si <sub>2</sub> O <sub>8</sub>	2.0	0.2	1.8
Orthoclase	KAlSi <sub>3</sub> O <sub>8</sub>	0.0	0.0	0.0
Sanidine	KAlSi <sub>3</sub> O <sub>8</sub>	0.0	0.0	10.9
Kaolinite	Al <sub>2</sub> Si <sub>2</sub> O <sub>5</sub> (OH) <sub>4</sub>	0.5	0.8	0.9

\* Mineral not included in quantification analysis.

#### 4.4 Particle Morphology

In this section, samples of drill cuttings were analysed morphologically by SEM. The analysis provided qualitative information on the effect of ball milling on particle size reduction and particle size distribution of drill cutting particles. In addition, the morphological analysis of raw materials will be used to investigate the transformation of particles at high temperature and the degree of sintering in LWA. Figure 4.3a to Figure 4.3c show the particle morphology of drill cuttings samples. For SDC in Figure 4.3a, a wide particle size distribution with various angular shapes was observed. The particle size distribution of CDC in Figure 4.3b appeared to be coarser than SDC despite using an equal milling time. CDC contained nearly spherical porous rock fragments larger than 100  $\mu\text{m}$  in diameter with a rough outer surface. EDC particles in Figure 4.3c were more irregularly shaped compared to the other two samples. The main reason for this is the presence of various minerals such as carbonates, sulphates and NaCl, each with specific morphological features. For example, distinctive cubic crystals with sizes below 10  $\mu\text{m}$  could be associated with NaCl particles. In addition, it was evident that EDC had a wider size distribution with a lower average particle size compared to the other two drill cuttings samples. Such irregularity in particle shape can be beneficial during pelletization because of the interlocking effect that can reduce the material's flowability (Popov et al., 2003). SEM micrographs of drill cuttings samples obtained at higher magnifications are shown in Appendix I.

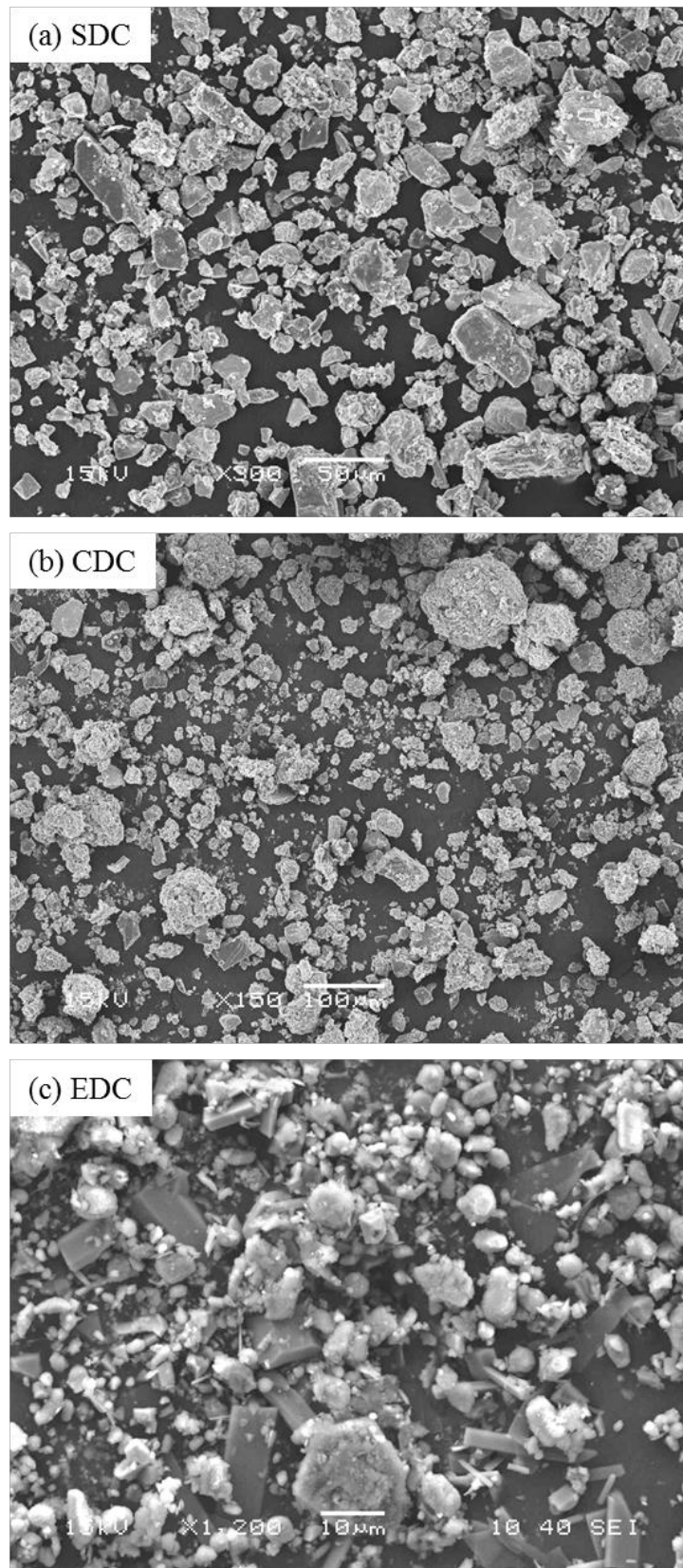


Figure 4.3 SEM micrographs of (a) SDC, (b) CDC and (c) EDC samples showing irregular morphology of drill cutting particles and a wide particle size distribution developed after six hours of ball milling at 300 rpm.

## 4.5 Thermal analysis

Characteristic temperatures such as initial sintering temperature, softening and melting point were determined by thermal analysis for samples of drill cuttings. This involved heating microscopy (HM) and differential thermal analysis (DTA), to define these temperatures and provide accurate data for the optimal design of the firing regime for LWA manufacturing.

### 4.5.1 Heating microscopy

Heating microscopy was conducted to determine the sintering range that would be needed in the muffle furnace. The initiation of sintering was measured as the temperature at which the cube outline area reduced to 95% of its original (Zhang et al., 2011). This temperature was then used as the lower limit of firing in the muffle furnace during LWA manufacturing as described in section 3.2.2. The final sintering temperature (the highest temperature at which the structure of the sample was upheld) was used as the upper limit of firing (Latosińska and Żygadło, 2011).

### 4.5.2 SDC

Figure 4.4a shows the percentage change in the outline of a cubic sample of SDC as a function of temperature together with heating microscope (HM) images. Before 1190 °C, no distinctive dimensional change could be recognized. At 1190 °C the area reduced to 95% of its original and therefore it was considered as the first characteristic temperature associated with the initiation of sintering. It is important to note that the presence of CaCO<sub>3</sub> in this sample did not cause any significant decrease in the cube outline area considering its decomposition which occurs below 850 °C (Stern and Weise, 1969). Above 1190 °C until 1420 °C, a constant drop in the area showed further material shrinkage (with the increase in temperature). This can be attributed to the decomposition of BaSO<sub>4</sub>, which was quantified as the most abundant mineral in this sample. However, determining the initial decomposition temperature for BaSO<sub>4</sub> is difficult since it is not in a pure form. Other studies have reported a BaSO<sub>4</sub> reaction with alumina and silicate at temperatures as low as 1100 °C - to form hexa-BaAl<sub>2</sub>Si<sub>2</sub>O<sub>8</sub>, according to the following reaction (AdabiFiroozjaei et al., 2011, Koshy et al., 2011):



The experiment showed no important bloating behaviour required for the manufacture of LWA. Despite the presence of superfluous gas-releasing compounds which reduced the cube original outline area to more than 60% of its initial size, a lack of plastic phases with appropriate viscosity to capture those gases undermined the materials capability for bloating. This result agreed with the material's position being outside of the bloating region as shown in the Riley diagram (Figure 4.1).

#### 4.5.3 CDC

Figure 4.4b shows the HM images of CDC. Up to 9% increase in the cube outline area was observed from room temperature to 1050 °C. However, this effect was not due to bloating, since the corners of the cube remained at right angles – this again indicates the lack of plastic behaviour. The effect was therefore associated with the material physical expansion upon heating. As determined by XRD quantification, this sample is mainly composed of CaCO<sub>3</sub> for which decomposition is known to increase the porosity of the remaining CaO to more than 50% without causing any significant shrinkage (Stanmore and Gilot, 2005). The 5% decrease in the outline area occurred at around 1200 °C, and thus was selected as the initial sintering temperature. The area remained stable between 1220 °C and 1320 °C, and showed 50% reduction as the temperature reached 1420 °C. This sample also did not show any bloating behaviour over the designated heating range. This result also agreed with the Riley diagram prediction.

#### 4.5.4 EDC

Figure 4.4c shows HM images of EDC. It was observed that at the initial stage of the test (as the temperature increased to approximately 750 °C), the material undergoes a simple expansion of up to 3%. At 750 °C, a minor dimensional change was detected, most likely due to the decomposition of carbonates and the subsequent release of CO<sub>2</sub>. 1175 °C was assigned as the initial sintering temperature. As the sintering process continued, the sample outline remained relatively uniform, but the dimensions continued to reduce until 1190 °C. At 1200 °C, a liquid phase emerged on the surface of the sample. However, the captured image shown at this temperature did not reveal a 'sphere' point, indicating an insufficient surface tension of the liquid phase. Above 1200 °C, the surface tension remained in the control of the sample outline since the majority of the matrix was composed of a melted phase. The sample outline at 1210 °C is known as the 'hemisphere' point (Morin and Lamothe, 1990, Pascual and Pascual, 2001).

The image of 1240 °C shows a complete flattening of the sample, which is also considered as the 'flow' temperature (Pascual and Pascual, 2001). In this experiment, the sample showed minimal bloating effect (images captured at 1180 °C showed little inflation at their outline). It must be noted that the condition in the heating microscope is different from that of the kiln system used for LWA production. This is mainly in terms of heat transfer efficiency and dwell time, both of which can hinder the material true bloating potential (de Gennaro et al., 2005, Quina et al., 2014a).

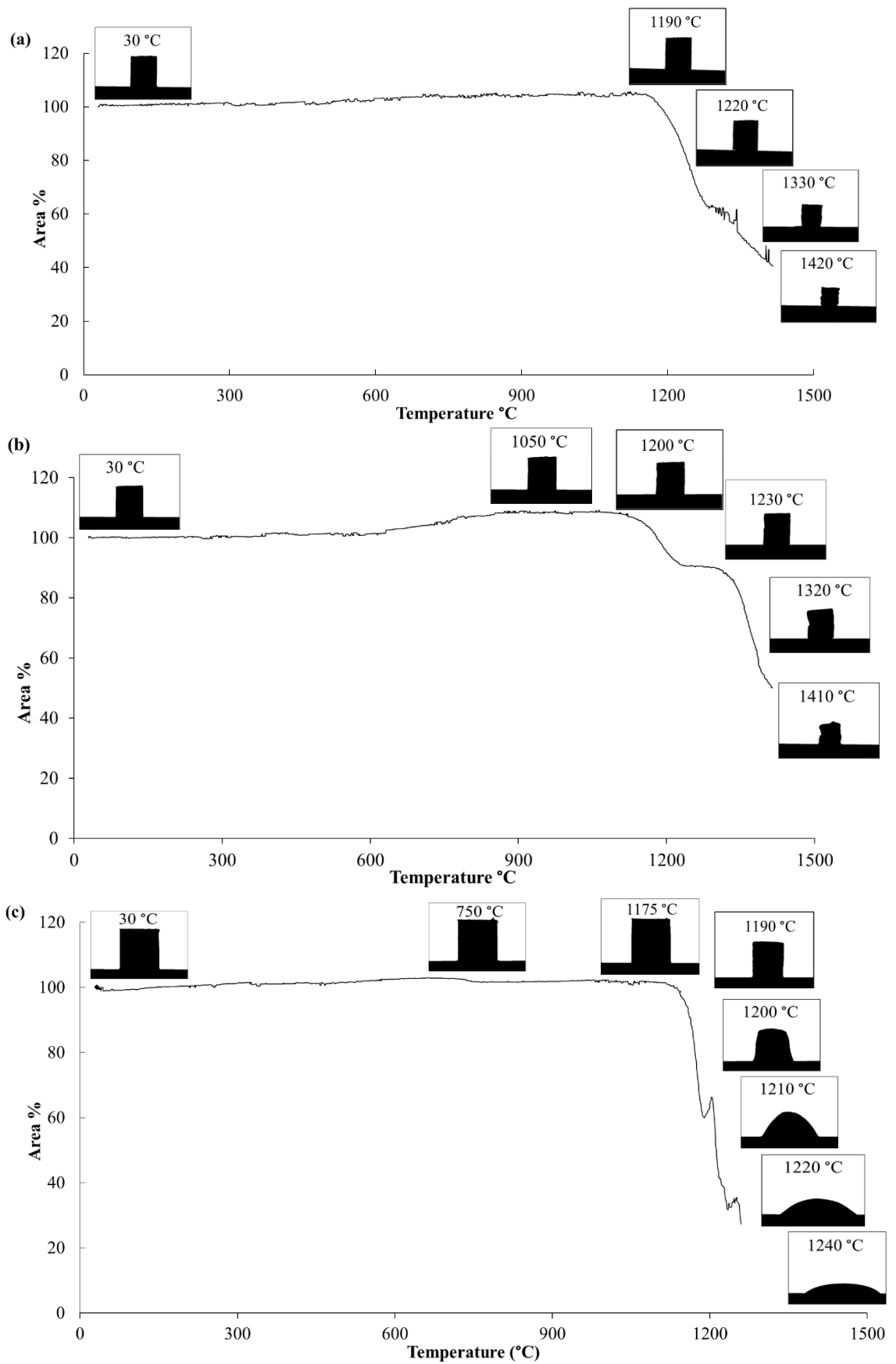


Figure 4.4 Outline area % change as a function of temperature with attached heating microscope images at characteristic temperatures for a cubic sample ( $3 \times 3 \times 3$  mm) of drill cuttings subjected to  $10 \text{ }^\circ\text{C}/\text{min}$  heating rate: (a) SDC, (b) CDC and (c) EDC.

#### 4.5.5 Differential thermal analysis (DTA)

DTA was carried out to determine the nature and temperature range of decomposition reactions, which occurred upon heating. Figure 4.5 shows DTA data, acquired over the range from room temperature to 1100 °C at 10 °C/min. Possible thermal events based on information from the literature were marked on both the heating and cooling curves. All three samples were calcined at 440 °C prior to the analysis to remove the hydrocarbons from the samples.

#### 4.5.6 SDC

DTA data for SDC shown in Figure 4.5a showed a distinctive endothermic peak at approximately 770 °C which can be attributed to the decomposition of carbonate minerals including two polymorphs of CaCO<sub>3</sub> i.e. calcite and aragonite, and dolomite. The endothermic peak at 570 °C is likely due to the transformation of  $\alpha$ -quartz to  $\beta$ -quartz. DTA for this sample showed no other significant thermal events with the applied heating rate. On the cooling curve, DTA showed two exothermic reactions at around 1014 °C and 937 °C, indicating possible crystallization of new phases. The neo-formed mineral phases will be investigated in Chapter 5 XRD analysis.

#### 4.5.7 CDC

Figure 4.5b shows DTA data for CDC. As predicted by the XRD quantification model, this sample is mainly composed of CaCO<sub>3</sub>. Accordingly, the only DTA event observed was a large endothermic reaction starting at approximately 775 °C and ending at 890 °C with a peak at 841 °C. Differential thermal curves of CaCO<sub>3</sub> have been reported in the literature with the same characteristics (Vandevier, 1951).

#### 4.5.8 EDC

Figure 4.5 shows DTA data for EDC. A low temperature endothermic hump between 75 °C to 105 °C was observed which could be due to the evaporation of absorbed water from the environment. Two successive endothermic peaks at 603 °C and 689 °C were detected. The broad characteristics of these peaks could be due to a combination of various thermal events, however both peaks are in the range of calcium carbonates decomposition if the effects of impurities are taken into account (González-Corrochano et al., 2009b). They could also be indicative of peaks associated with CaMgCO<sub>3</sub> decomposition - occurring with MgCO<sub>3</sub> and CaCO<sub>3</sub> reactions at different temperatures (Todor, 1976). Two

exothermic peaks between 750 °C and 780 °C were also seen, which could be attributed to a neo-formation process. The free-lime in the system can react with products of other phase breakdowns, such as  $\text{KAl}_2(\text{Si}_3\text{AlO}_{10})(\text{OH})_2$ , and results in a neo-formed phase (Loutou et al., 2013). On the cooling curve, a sharp exothermic peak was clearly visible at 535 °C, which exactly matches the dihydroxylation of  $\text{KAl}_2(\text{Si}_3\text{AlO}_{10})(\text{OH})_2$  reported to appear on heating curves in work by Chen et al. (2012).

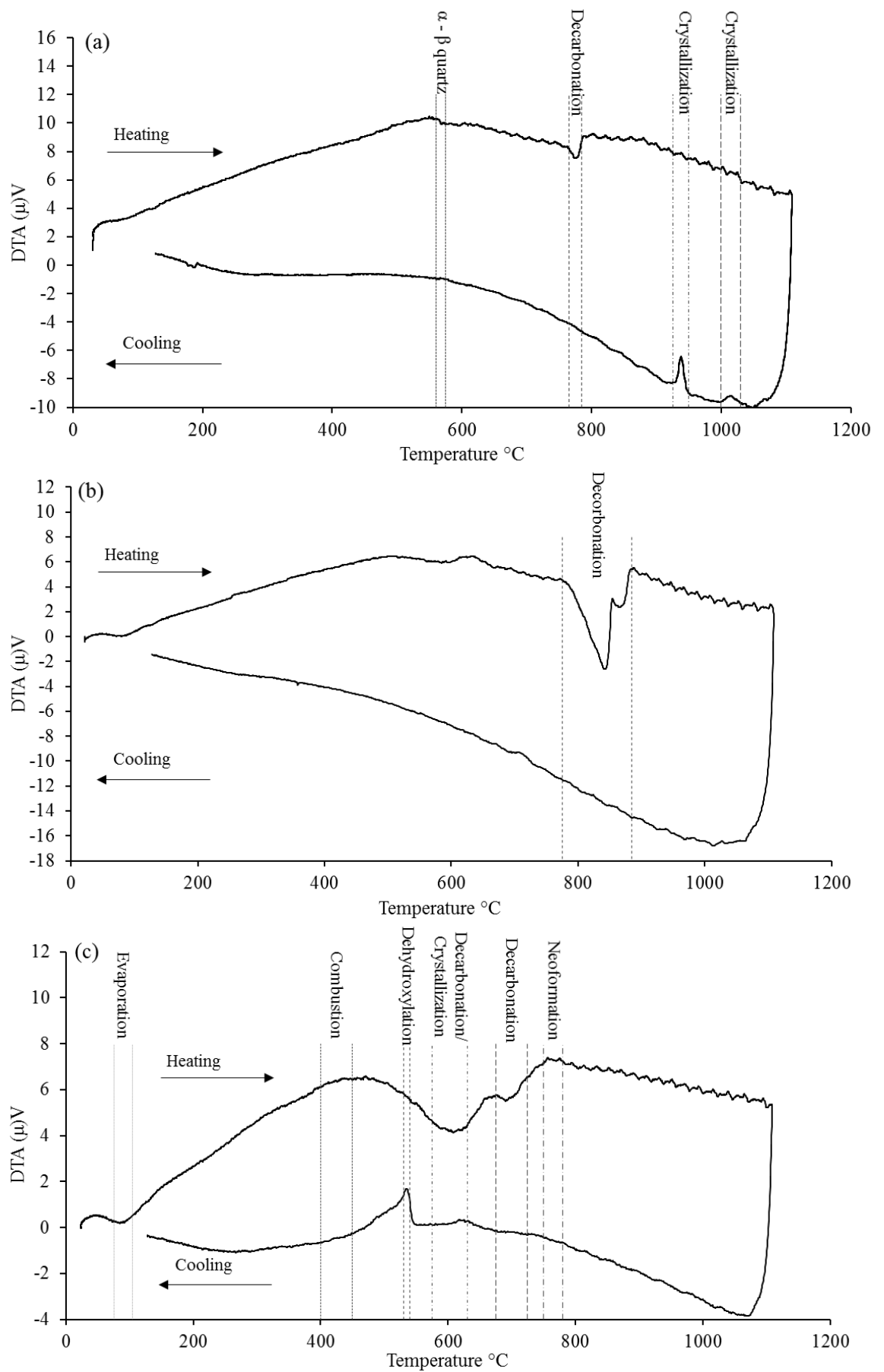


Figure 4.5 DTA data of (a) SDC, (b) CDC and (c) EDC.

#### 4.6 Total Petroleum Hydrocarbon (TPH)

The TPH of drill cuttings was measured as an indication of wt.% of absorbed drilling fluid in the samples. The information was also used to estimate the energy available from combustion of drill cuttings during the firing stage in LWA manufacturing.

Table 4.4 shows the results of TPH measurements. In SDC and CDC, TPH was 123,500 mg/kg (12.3 wt.%) and 143,000 mg/kg (14.3 wt.%). This is above the (HP 5) limit, as determined by the UK Waste Catalogue (WM3, 2015). EDC had a lower TPH content at 56,000 mg/kg (5.6 wt.%), which is above the (HP 10) limit. In addition, most of the TPH of drill cuttings were comprised of hydrocarbons with chain lengths of between 10 and 25 carbon atoms. This indicated the synthetic nature of the absorbed drilling fluid in the samples according to Table 2.1.

Table 4.4 TPH of drill cuttings.

	SDC	CDC	EDC
	(mg/kg)	(mg/kg)	(mg/kg)
TPH > C6* - C10	1558	927	1140
TPH > C10 - C25	121,750	142,000	54,900
TPH > C25 - C40	<454	<155	<236
TPH > C40 - C44	<1191	<406	<617
Total TPH C06 - C44	123,500	143,000	56,000

\* Number of carbon atoms in the polymers chain length.

#### 4.7 Total heavy metal content

Table 4.5 shows the concentrations of metals in drill cuttings measured by acid digestion with Aqua Regia. In the SDC sample, the total content of heavy metals was 1513 mg/kg and mainly associated with levels of Ba (730 mg/kg), Pb (270 mg/kg) and Zn (430 mg/kg). The observed discrepancy between acid soluble Ba and that measured by XRF indicates the stability of BaSO<sub>4</sub> (the main sulphate bearing phase in the SDC sample) in strong acids. The CDC sample had a similar heavy metal content (1510 mg/kg) but was mainly associated with a higher Ba concentration (1240 mg/kg). The EDC sample had the lowest level of heavy metals (451 mg/kg) compare to the other two samples and was mainly associated with Ba (258 mg/kg) and Zn (109 mg/kg) in the digestate.

Table 4.5 Total metal content measured by acid digestion for samples of drill cuttings.

Sample	SDC (mg/kg)	CDC (mg/kg)	EDC (mg/kg)
As	<3.75*	<3.96	<3.92
Ba	730	1240	258
Cd	0.367	<0.215	<0.213
Cr	27.95	32.5	41.3
Cu	30.25	21.7	23.0
Hg	<0.903	84.4	<0.945
Mo	3.3	<2.34	<2.32
Ni	19.05	34.9	41.8
Pb	270	26.7	<0.533
Sb	<4.13	10.5	<4.31
Se	<1.65	<1.74	<1.72
Zn	430.5	61.2	109
Total	1513	1510	451

\* Below ICP-OES quantification limit for the method used.

## 4.8 Leaching analysis

The concentration of water-soluble compounds, including problematic heavy metals and anions were measured by leaching test. Table 4.6 shows the results at L/S ratio of 10 l/kg on SDC, CDC and EDC samples. When the concentration of a given constituent was below the ICP-OES limit of quantification, the calculated values were reported as the highest possible concentration, as described in Chapter 3.

### 4.8.1 Heavy metals

#### 4.8.1.1 SDC

The leaching test results on SDC confirmed that except for Ba, the concentrations of all other analysed metals were below the ICP-OES limit of quantification. The water-soluble concentration of Ba was measured as 3.85 mg/kg which must be because Ba is present in the form of BaSO<sub>4</sub> (as identified by XRD) for which the solubility in water is in the range of 2-3 mg/l. It is worth highlighting that both Pb and Zn which also had a relatively high availability (270 mg/kg and 430 mg/kg in Table 4.5) were both below the quantification limit. This indicates superior chemical fixation of these elements in the material, thus inhibiting their release.

#### 4.8.1.2 CDC

Most of the heavy metals leachable concentration in CDC were also below ICP-OES limit of quantification (Table 4.6). Only concentrations of Ba, Mo and Ni were sufficient to be measured. The Ba concentration was 1.4 mg/kg which was lower than SDC despite its higher acid-soluble concentration (1240 mg/kg in Table 4.5). Ni and Mo were 0.5 mg/kg which were in an acceptable range according to the EoW criteria in Table 3.2.

#### 4.8.1.3 EDC

The leachable concentrations of Ba, Cu and Ni in EDC sample were 0.43 mg/kg, 1.07 mg/kg and 0.42 mg/kg, respectively (Table 4.6). Ba leachable concentration (0.43 mg/kg) was lower compared to the other two samples. It was evident again that other heavy metals with relatively high acid-soluble concentration including Cr (41.3 mg/kg) and Zn (109 mg/kg) were measured below the ICP-OES instrumental limit of quantification. These results showed that all three samples of drill cuttings did not have significant environmental issues in terms of heavy metal leaching and in most cases, suitable chemical

fixation was in play to reduce the release of these potentially problematic constituents in water.

#### 4.8.2 Anions

##### 4.8.2.1 SDC

The concentration of major leachable anions i.e.  $\text{Cl}^-$  and  $\text{SO}_4^{2-}$  from SDC were 7366 mg/kg and 206.7 mg/kg, respectively. The  $\text{F}^-$  concentration for this sample was below the ICP-OES limit of quantification. Comparing these results to XRF data, it was clear that these  $\text{Cl}^-$  had different leaching mechanisms than those observed for heavy metals. The concentration of  $\text{Cl}^-$  ions was in the same range as the total  $\text{Cl}^-$  measured by XRF - showing an availability-controlled leaching. However, the concentration of leachable  $\text{SO}_4^{2-}$  ions (206.7 mg/kg) was considerably below the total concentration of sulphur (42,233 mg/kg from XRF analysis), indicating a strong solubility-controlled leaching mechanism.

##### 4.8.2.2 CDC

The measured concentration of leachable  $\text{Cl}^-$  ions in CDC was 11,946 mg/kg which was nearly twice as high as that in SDC. The concentration of leachable  $\text{SO}_4^{2-}$  ions was 1111 mg/kg. For both CDC and SDC,  $\text{BaSO}_4$  was quantified as the main  $\text{SO}_4^{2-}$ -bearing mineral, which could explain the low release of  $\text{SO}_4^{2-}$  ions in the leachate. Similarly, the leachable concentration of  $\text{F}^-$  ions was below the ICP-OES quantification limit.

##### 4.8.2.3 EDC

The concentration of  $\text{Cl}^-$  ions in the EDC sample was extremely high (85,712 mg/kg). The chlorine content measured by XRF minor element analysis (80,911 mg/kg) and 10.9 wt.% NaCl measured in XRD quantitative analysis, are in accordance with the leaching result. The  $\text{SO}_4^{2-}$  leaching from EDC was also high, with concentrations reaching 45,248 mg/kg (Table 4.6). Unlike  $\text{Cl}^-$ , leaching behaviour of  $\text{SO}_4^{2-}$  ions, especially when they are present in the form of calcium sulphates, is controlled by their solubility in water (Barbudo et al., 2012). However, the high leaching concentration of  $\text{SO}_4^{2-}$  in EDC was due to  $\text{CaSO}_4$  being the major  $\text{SO}_4^{2-}$ -bearing compound. In addition, the release of  $\text{SO}_4^{2-}$  can be affected by the  $\text{Cl}^-$  ions in the solution since their presence will increase the ionic strength of the leach environment and thus, increase the mobility of  $\text{SO}_4^{2-}$  ions (Shirley and Black, 2011). There was evidence that this mechanism was also affecting the release of  $\text{F}^-$  ions. The  $\text{F}^-$  leachable concentration was 31.40 mg/kg; while the total fluorine

content measured by XRF was 352 mg/kg. However, it was observed that the release of  $F^-$  from the CDC sample (with twice as high as total content), was below the ICP-OES quantification limit. This confirms that high contents of soluble  $Cl^-$  in the leachate could increase the release of  $F^-$  ions.

#### 4.8.3 DOC

Dissolved organic carbon (DOC) also showed some levels of variation. SDC contained the highest DOC among the samples (1482 mg/kg). This was again in accordance with highest TPH that was measured for this sample. In the CDC sample, DOC was 696 mg/kg, and EDC had the lowest DOC at 477 mg/kg.

Table 4.6 Results of leaching test (BS EN 12457-2) on SDC, CDC and EDC samples.

	SDC	CDC	EDC
	(mg/kg)	(mg/kg)	(mg/kg)
As	<1.584	<1.582	<1.460
Ba	3.85	1.4	0.43
Cd	<0.071	<0.071	<0.081
Cr	<0.201	<0.201	<0.120
Cu	<0.712	<0.712	1.07
Hg	<1.160	<1.158	<0.353
Mo	<0.152	0.5	<0.152
Ni	<0.325	0.5	0.42
Pb	<2.211	<2.209	<0.235
Sb	<0.860	<0.858	<1.383
Se	<1.010	<1.008	<0.664
Zn	<2.485	<2.483	<3.095
Cl <sup>-</sup>	7366.4	11,946.6	85,712.3
F <sup>-</sup>	<20.5	<20.3	31.4
SO <sub>4</sub> <sup>2-</sup>	206.7	1111	45,248.2
DOC	1482.5	696	477
pH at 20 °C	11.66	9.47	9.9
Conductivity (µS/cm)	2327	3732	22,730

## 4.9 Discussions

Three samples of SBM drill cuttings were characterised for chemical composition, mineralogy, thermal behaviour and contaminant leaching. The information was used to design the manufacturing process and predict the bloating capability of drill cuttings LWA during the firing stage. The analysis showed that the samples contained a complex mixture of minerals with variable amounts of drilling additives and hydrocarbons. Some of these compounds were identified as being able to negatively affect the bloating and cause leaching problems in LWA. In the following, a discussion for each sample of drill cuttings is provided:

XRD analysis of SDC showed that the sample was mainly composed of mica-rich compounds, quartz and different carbonate minerals which resembled the mineralogy of shale materials. The concentration of  $\text{BaSO}_4$  (an additive used for increasing the weight of the drilling mud) in the SDC sample was  $>50$  wt.% of the total crystalline phase present.  $\text{BaSO}_4$  is not capable of solid-state fusion at temperature ranges used in LWA manufacturing, therefore such a large content would negatively affect the properties of LWA, as insufficient sintering would occur. In addition, the proportion of major oxides in SDC indicated a poor pyro-plastic viscosity, which is required for bloating. The thermal analysis results were also in accordance with these findings. The heating microscopy (HM) revealed the initiation of sintering to occur around  $1190$  °C. As the temperature increased the outline of the sample retained its shape and indicated a lack of viscous behaviour needed for the entrapment of the released gases. The decomposition reactions producing these gases were identified as the decarbonation of carbonate minerals by DTA analysis. Overall, despite the presence of clay minerals that are beneficial for low-temperature sintering, the high content of  $\text{BaSO}_4$  can limit the application SDC for use as a raw material for LWA.

CDC was found to contain mainly carbonate-based minerals, with more than 60% of its crystalline phase composed of  $\text{CaCO}_3$ , as determined by XRD analysis. The shape and position of the most significant endothermic peak on the DTA heating curve also strongly corresponded to carbonate-based nature of CDC. As a result, the highest initial sintering temperature was recorded for CDC at  $1200$  °C, where a 5% reduction in the original outline area of the cube was observed. This was because the decomposition of carbonate minerals (despite increasing the porosity) did not cause any significant shrinkage in the cube outline area (Stanmore and Gilot, 2005). Above  $1200$  °C, CDC showed a more

drastic shrinkage, but the cube still retained its shape. This indicated a lack of viscous phase, which was attributed to its very low silica content (32.5 wt.%) as measured by XRF analysis. Overall, CDC was not an ideal composition for LWA raw materials because the majority of the phases present can be decomposed during the firing stage. This would leave high levels of open porosity, negatively affecting the water absorption of LWA.

EDC was mainly composed of clay minerals,  $\text{CaCO}_3$ ,  $\text{CaMgCO}_3$ ,  $\text{CaSO}_4$  and  $\text{NaCl}$ . The mineralogy of EDC strongly resembled that of evaporite rocks found when hydrocarbon seal rocks are drilled. The concentration of  $\text{BaSO}_4$  was lower (6.0 wt.% of total crystalline phase) compared to the other two samples indicating that the material can form a viscous body above its initial sintering temperature (1175 °C). The HM images for EDC also showed a different behaviour as the cube outline started to deform above 1200 °C. The sample reached the ‘hemisphere’ point at 1210 °C and the ‘flow’ point at 1240 °C. EDC did not demonstrate the ‘sphere’ point which is usually observed in clay-bearing minerals HM images (Quina et al., 2014a). This can be attributed to the high total flux content (measured by XRF analysis) decreasing the viscosity and surface tension of the material at the pyro-plastic stage.

Mitigating the release of heavy metals from hazardous mineral waste is one of the most important challenges for various suggested reuse applications (Shirley and Black, 2011, Bogush et al., 2015). However, the total heavy metal content measured by acid digestion showed that the inherent concentrations of heavy metals in all drill cutting samples were in an acceptable range compare to other hazardous mineral wastes such as Energy-from-Waste (EfW) residues (Allegrini et al., 2014). This alleviates the concerns associated with their release if drill cuttings are used as a raw material for LWA. The variation in total heavy metals was mainly caused by Ba in the remaining (absorbed) drilling fluid. Pb, Hg and Zn were also found at different concentrations among the samples. However, it is difficult to pinpoint the origin of these contaminants, due to their low concentrations in the samples.

Water-soluble concentrations of heavy metals measured by the leaching test complied with the EoW criteria. However, IC measurements of the leachates revealed high releases of anions from EDC. Leachable concentrations of  $\text{Cl}^-$  were measured as 85,712 mg/kg. This could make the use of EDC for LWA manufacturing a non-viable option due to the

potential for  $\text{Cl}^-$ -induced corrosion of steel in reinforced concrete structures (Tang et al., 2018).

## 5 Chapter 5 Properties of drill cuttings LWA

In this chapter, the aim was to investigate whether drill cuttings can be pelletised and fired effectively to produce LWA. In doing so, samples of raw material were air-dried, formed into pellets and fired over the sintering range determined by heating microscopy. The investigation focused on how firing temperatures affect the pellets physical properties, mineralogy, microstructure and leaching behaviour.

### 5.1 Structural characteristics of LWA

#### 5.1.1 SDC-LWA

For SDC-LWA in Figure 5.1a, it was observed that the homogeneous nature of the raw materials produced pellets with minimal irregularities and surface defects. However, no distinct bloating mechanism was observed in this series. This was in accordance with the Riley diagram prediction in Chapter 4. It must be noted that the Riley diagram was set up for distinguishing between bloating and non-bloating clay minerals. It has also been used for mineral wastes with substantial non-clay contents, however in these cases, it has been shown to produce a lower accuracy. This is because the diagram does not include some important characteristics of raw materials such as mineralogy and high-temperature viscosity (Dondi et al., 2016). But in the case of SDC, there was a fair agreement between the firing experiment results and the Riley diagram. The high concentration of BaSO<sub>4</sub> (drilling additive) in SDC prevented the formation of phases with suitable pyro-plastic viscosity and thus the material was unable to entrap the released gaseous phases.

#### 5.1.2 CDC-LWA

Figure 5.1b shows the surface and internal structure of CDC-LWA. High degrees of inhomogeneity were obvious in the pellets and increasing the firing temperature had little effect on the appearance. The prevalence of surface defects at all firing temperatures was due to decomposition of both carbonates and hydrocarbons present in the raw materials, generating empty pockets of space between the particles. In addition, over the examined firing temperature range, LWA had a poor structural integrity and despite the presence of large open pores, there was no evidence of a bloating effect. This agreed with the Riley diagram prediction and indicated that the silicate-bearing phases in the material do not exist in sufficient quantities to produce a network at a high temperature.

### 5.1.3 EDC-LWA

Figure 5.1c shows EDC-LWA demonstrating a bloating effect with relatively large bubbles. The bloating of pellets showed similar characteristics over the applied firing temperature range and no remarkable development in the size of large pores could be identified. This suggests that over the applied firing range, there was a sufficient viscous phase capable of forming a three-dimensional closed pore structure. However, this was not in agreement with the prediction of the Riley diagram (Chapter 4). This is because the Riley diagram does not account for high flux contents as favourable for bloating. Conversely, the firing of EDC showed fluxing compounds can produce low-viscosity phases that are capable of holding the generated gases at high temperatures. The reliability of the Riley diagram prediction and the need for a model which takes the pyro-plastic viscosity into account has also been discussed by other researchers (Dondi et al., 2016).

It was observed that a few irregular pores were formed at the contact point with the refractory plate. Other studies have also shown this happening when pellets are fired on the refractory shelves in a muffle furnace (Yang et al., 2015). EDC-LWA was widely heterogeneous in terms of surface smoothness, colour and porosity, despite the relatively narrow firing range used. This was possibly due to the high level of soluble salts measured in the raw material generating a solidified build-up layer on the surface of 'green' pellets during the drying stage. The soluble compounds in EDC can migrate to the surface during the pellet drying stage.

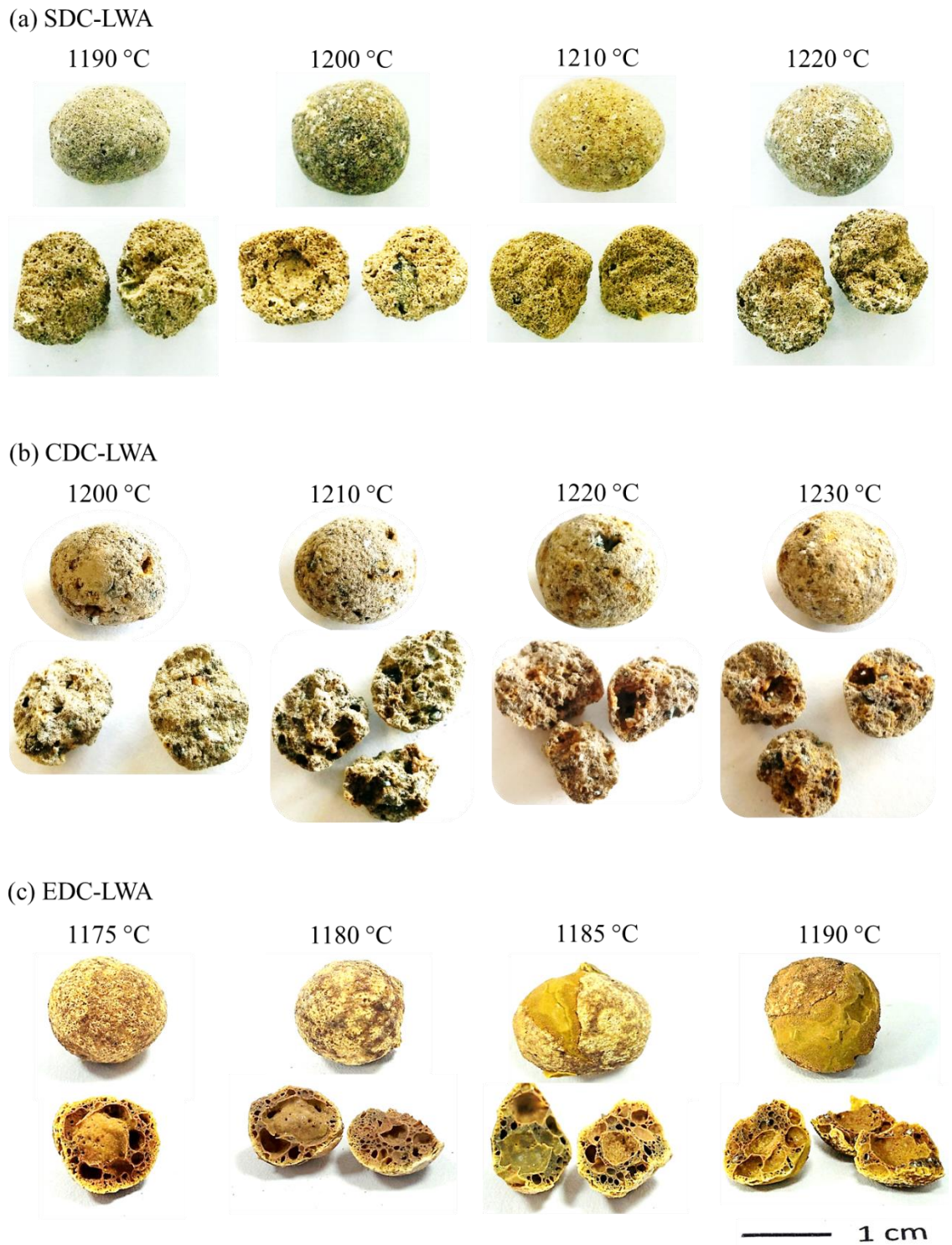


Figure 5.1 Appearance of drill cuttings LWA pellets surface and internal structure. (a) SDC-LWA, (b) CDC-LWA, and (c) EDC-LWA.

## 5.2 Physical properties of LWA

In this section, the effect of firing temperature on physical properties of the fired pellets - including particle density, water absorption and compressive strength - were investigated. Pellets were fired within the temperature range shown in section 5.1. The results were also compared with physical properties of two commercially manufactured LWAs namely: Lytag® and LECA®. Measured physical properties of Lytag and LECA are given in Table 5.1.

Table 5.1 Measured physical properties of Lytag and LECA  $\pm$  one standard deviation.

	Particle density (g/cm <sup>3</sup> )	Water absorption (%)	Compressive strength (MPa)
Lytag®	1.27 $\pm$ 0.02	20.5 $\pm$ 2.3	3.2 $\pm$ 0.6
LECA®	0.77 $\pm$ 0.05	32.7 $\pm$ 3.3	1.7 $\pm$ 0.9

### 5.2.1 SDC-LWA

Figure 5.2a shows the effect of firing temperature on particle densities of SDC-LWA. At 10 °C/min, the average particle density decreased from 1.65 g/cm<sup>3</sup> to its lowest level of 1.56 g/cm<sup>3</sup> when the firing temperature was increased from 1190 °C to 1210 °C. It should be noted that this drop was not due to bloating behaviour and indeed, could be associated to further decomposition reactions increasing the total porosity of pellets. The measured water absorption for this batch was the highest (27.1%) in the series indicating the formation of open porosity. From 1210 °C to 1220 °C, SDC-LWA particle density increased to 1.69 g/cm<sup>3</sup>. The observed densification was likely due to the increase in the degree of sintering. The lowest water absorption was measured at 1220 °C (Figure 5.2b) indicating a reduction in void spaces (total porosity), which is likely due to an increase in the degree of particle fusion. Particle densities of SDC-LWA over the designated firing range were above those measured for both Lytag (1.27 g/cm<sup>3</sup>) and LECA (0.77 g/cm<sup>3</sup>).

Figure 5.2b shows the effect of firing temperature on water absorption of SDC-LWA. The average water absorption varied between 22.7% and 27.1% over the firing range of 1190 °C to 1220 °C. 27.1% was obtained at 1210 °C clearly indicated a lack of sintering

and presence of open porosity. This is because phases such as  $\text{BaSO}_4$  in SDC, have a higher softening point than the designated firing range. In addition, the aluminosilicate network forming phases are not present in sufficient quantities to form a watertight matrix. Despite this, the obtained water absorptions were below those measured for LECA (32.7%) and comparable to those of Lytag (20.5%).

Figure 5.2c shows the effect of firing temperature on the compressive strength of SDC-LWA. The compressive strength for of all batches in the series was below 1.0 MPa, confirming the low degree of sintering. The obtained strengths over the conventional temperature ranges in large-scale LWA manufacturing were inferior to those for Lytag and LECA. This raised the need for the incorporation of an additional material with the ability to enhance matrix formation. In Chapter 7, the addition of secondary materials to promote the degree of sintering is investigated.

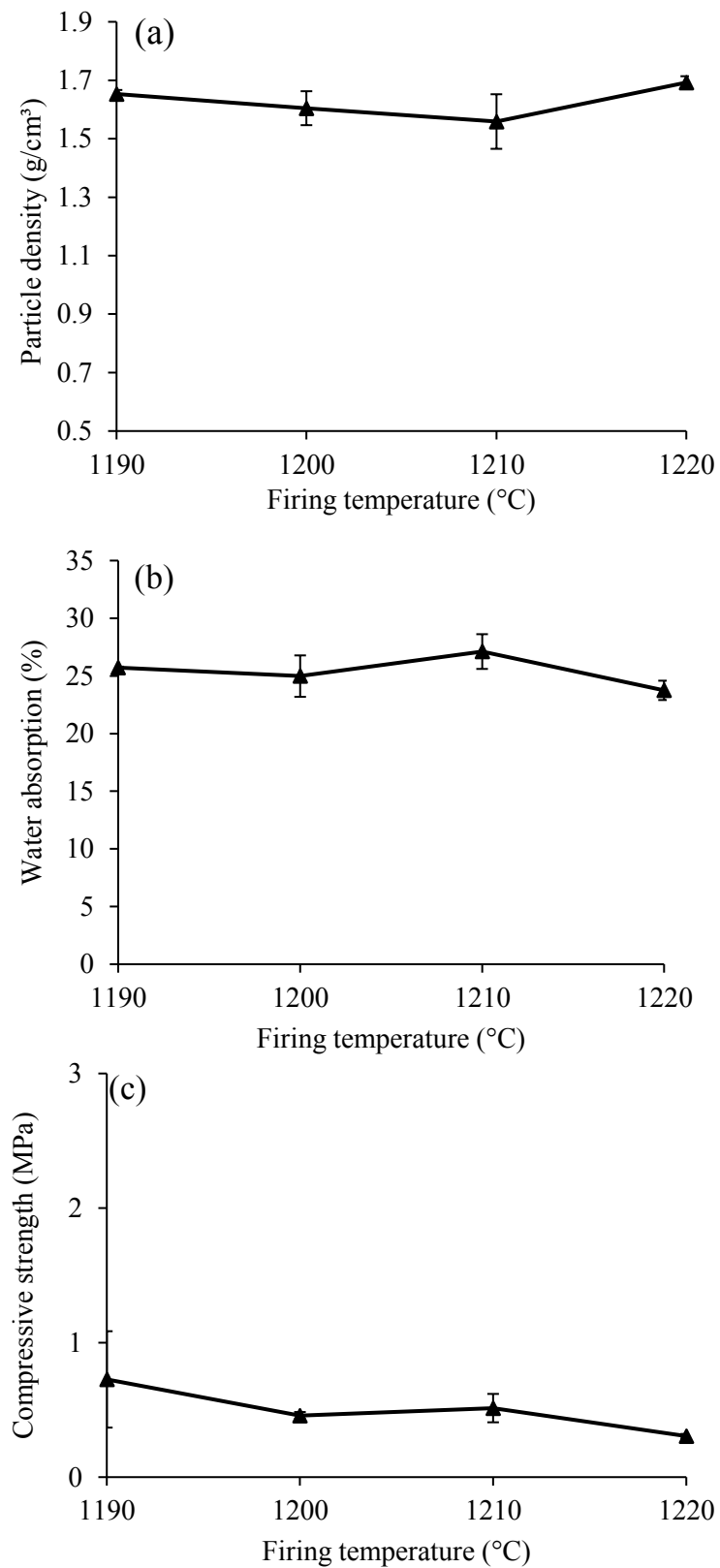


Figure 5.2 Effects of firing temperature on physical properties of SDC-LWA: (a) particle density, (b) water absorption and (c) compressive strength. Error bars are plus and minus one standard deviation.

### 5.2.2 CDC-LWA

Figure 5.3a shows the effect of firing temperature on particle densities of CDC-LWA. The average particle density was 1.21 g/cm<sup>3</sup> at 1200 °C (lowest in the series) and this increased as the firing temperature increased, reaching 1.29 gr/cm<sup>3</sup> at 1230 °C. The obtained particle densities for CDC-LWA were comparable to those measured for Lytag but were still above those for LECA. In addition, CDC-LWA exhibited distinctly lower particle densities than the SDC-LWA although in both cases no bloating mechanism was observed, as shown in Figure 5.1. This could be associated to the high concentration of carbonate minerals, producing pellets with high total porosity.

Figure 5.3b shows the effect of firing temperature on the 24-hour water absorption capacity of CDC-LWA. At 1200 °C, the average water absorption was at its highest, 36.1%. This decreased to 31.4% with the increase in firing temperature of 1230 °C. The drop was possibly due to the effect of sintering on reducing the number of open pores within pellets microstructure. The lowest water absorptions in the CDC-LWA were higher than those obtained for SDC-LWA and Lytag; however, they were comparable to values found for LECA. It is noted that LWA with levels of water absorption comparable to these pellets can be used for agriculture applications where maximum water absorptions are favourable.

Figure 5.3c shows the effect of firing temperature on the compressive strength of CDC-LWA. An increasing trend in compressive strength from 0.35 MPa to 0.76 MPa was observed as the firing temperature was increased from 1200 °C to 1230 °C which again could be associated to the increase in the degree of sintering. However, the overall range of compressive strength was considerably below the requirement for a standard LWA. It was seen that the average compressive strength (even at its maximum), was barely comparable with LECA. It must be noted that in order to achieve higher strengths, increasing the firing temperature is not a sustainable option due to high amounts of energy that would be required to heat up the kiln in large-scale manufacture. To tackle this issue similar approach to those discussed for improving the properties of the SDC-LWA is explored in Chapter 7.

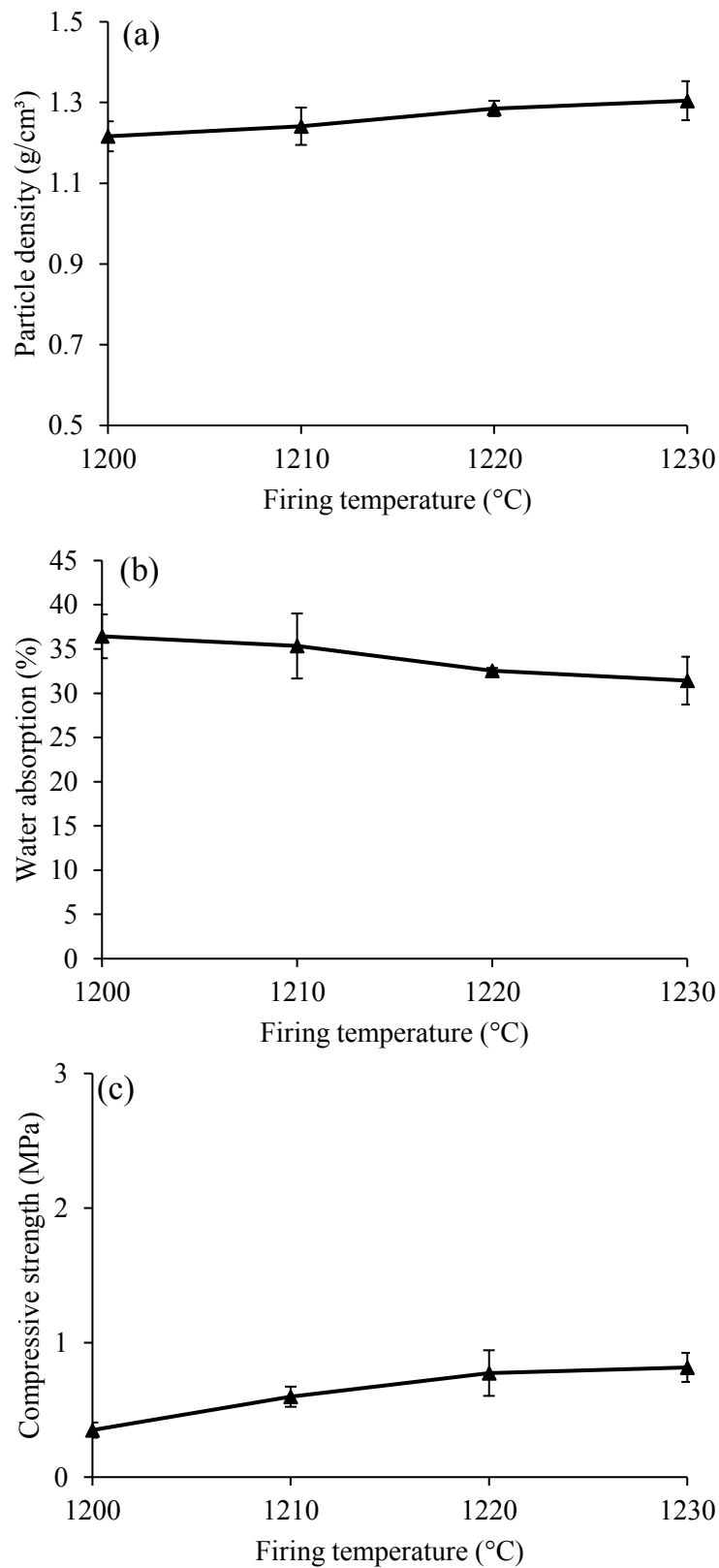


Figure 5.3 Effects of firing temperature on physical properties of CDC-LWA: (a) particle density, (b) water absorption, and (c) compressive strengths. Error bars are plus and minus one standard deviation.

### 5.2.3 EDC-LWA

The effect of firing temperature on the particle density of EDC-LWA is shown in Figure 5.4a. There was a decrease in the average particle density from 1.44 g/cm<sup>3</sup> to 1.25 g/cm<sup>3</sup> as the firing temperature was increased from 1175 °C to 1185 °C. This was due to the bloating effect causing the formation of large bubbles in the pellets matrix as the temperature increased. There was a slight increase in particle density to 1.29 g/cm<sup>3</sup> at 1190 °C. This was likely due to the development of liquid phases causing partial deification of pellets. There was evidence for this in HM images in Chapter 4, as 1190 °C was determined as the final sintering temperature beyond which the material began to flow. Comparing these results to Lytag and LECA, it became clear that the obtained densities were similar to Lytag but were considerably higher than the densities measured for LECA.

Figure 5.4b shows the effect of firing temperature on the water absorption capacity of EDC-LWA. The average water absorption decreased from 9.2% to 7.4% when the firing temperature increased from 1175 °C to 1185 °C showing that the newly formed pores due to bloating were less accessible by water. At 1190 °C, water absorption increased to 9.1% due to the growing sizes of bubbles in the pellets matrix which increased the total porosity of LWA. Furthermore, water absorption values obtained over the firing range were considerably below the values obtained from Lytag and LECA.

Figure 5.4c shows the effect of firing temperature on the compressive strength of EDC-LWA. The average compressive strength remained stable at around 4.0 MPa over the range of 1180 °C to 1190 °C and this can be explained by the narrow sintering range observed for EDC. For this series of samples, increasing the firing temperature did not have an observable effect on pellets' internal structure and therefore compressive strength remained roughly unchanged. EDC-LWA fired at 1175 °C were within the strength range of Lytag.

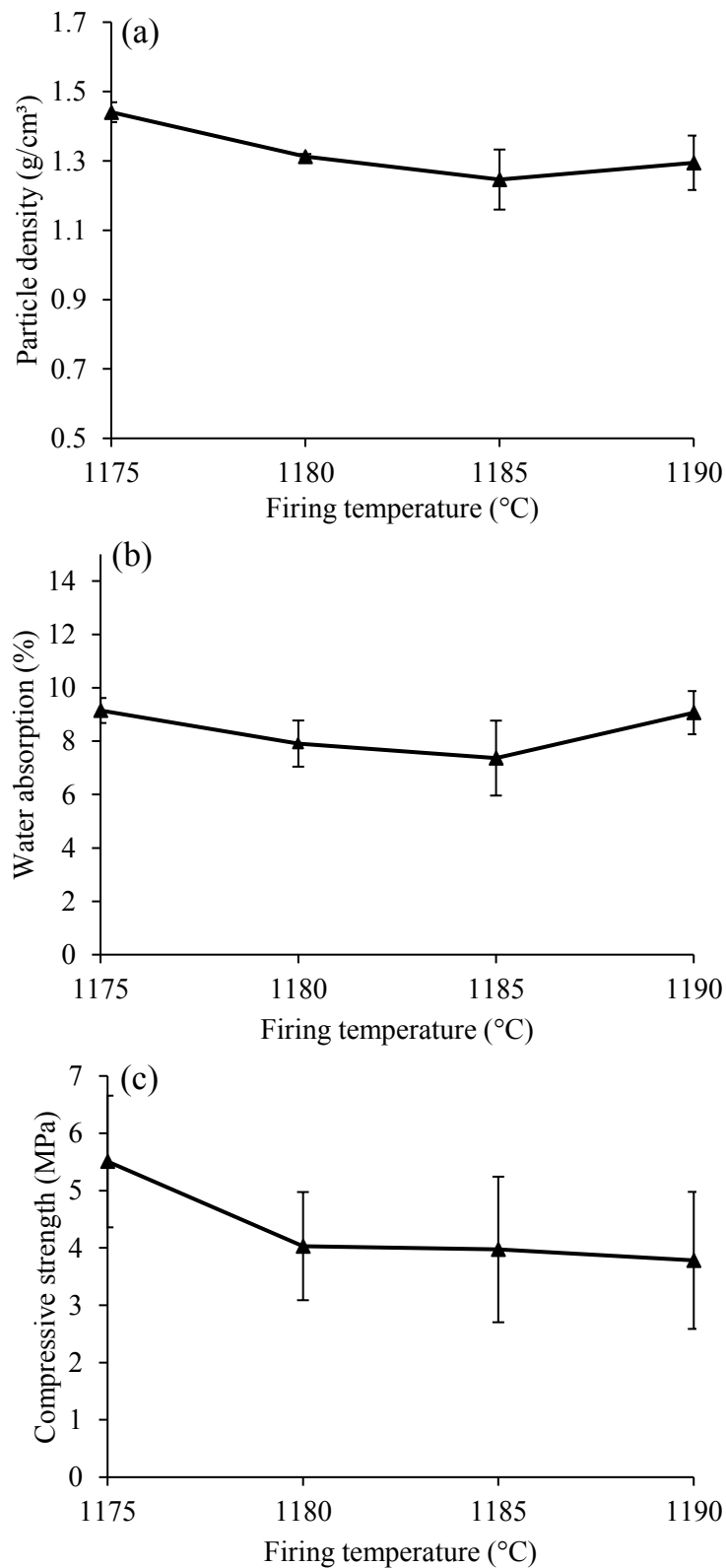


Figure 5.4 Effects of firing temperature on physical properties of EDC-LWA: (a) particle density, (b) water absorption, and (c) compressive strengths. Error bars are plus and minus one standard deviation.

### 5.3 Microstructure of LWA

For microstructural analysis, only EDC-LWA was investigated as the other two samples were not strong enough to withstand the SEM sample preparation and mounting. Figure 5.5 shows SEM micrographs of EDC-LWA fired at 1180 °C and 1190 °C. The SEM micrographs were obtained from the core (fracture surface) and the surface of each sample. The pellets surface had a ragged texture with a large number of open pores and clusters of crystallised materials after being fired at 1180 °C and 1190 °C. For pellets fired at 1180 °C, a crystallised surface (possibly due to efflorescence phenomenon: migration and crystallization of soluble salts on the surface) with large open pores were observed, as illustrated in Figure 5.5a. The surface pores are likely to form as a result of oil burn-off channels created in the early stages of firing. The number of large pores decreased on the surface of pellets fired at 1190 °C possibly due to a higher degree of liquid phase sintering and material flow at the surface. However, as shown in Figure 5.5c the efflorescence effect became more recognisable as the crystalline structure had grown in size with the increase in temperature.

Figure 5.5b shows the fracture surface of the fired pellets at 1180 °C. The presence of a continuous phase composed of solid-sintered drill cutting particles with isolated roughly spherical pores is evident. The observed difference in the crystal size between the core and the surface can be associated both to the transfer of water soluble compounds to the surface during the drying stage and, the oxidative environment inside the furnace. Figure 5.5b highlights semi-spherical pores with approximately 40 µm in diameter generated by bloating. It is seen that pore size distribution is broad, ranging from 10 µm to 500 µm (as shown in the attached overview image taken at a lower magnification). There were also evidence of open porosity in the microstructure (Figure 5.5b). Insufficient sintering causes the fracturing to happen, mainly between the particles. This can be associated to the low compressive strength measured for this series. In addition, hydrocarbons that remain in the core of LWA are burned off when the temperature is increased, leaving open cavity channels. These also keep particles apart from one other, reducing their fusion and thus, the sintering efficiency. This is similar to the negative effect of adding excessive water during pelletisation on bloating of final products, as discussed previously.

Figure 5.5d shows that increasing firing temperature to 1190 °C actually increased the average size of the large pores, with evidence for sizes as large as 3 mm. The temperature rise contribution to bloating could be due to both lowering the viscosity of the matrix and

increasing the pressure of the gases entrapped in the pore system. The increase in pore-size can also affect the physical properties. This effect has been documented by other research works on LWA manufacture (Volland et al., 2014) however, as shown in Figure 5.4 the physical properties pellets remained fairly stable when the firing temperature was increased from 1180 °C to 1190 °C.

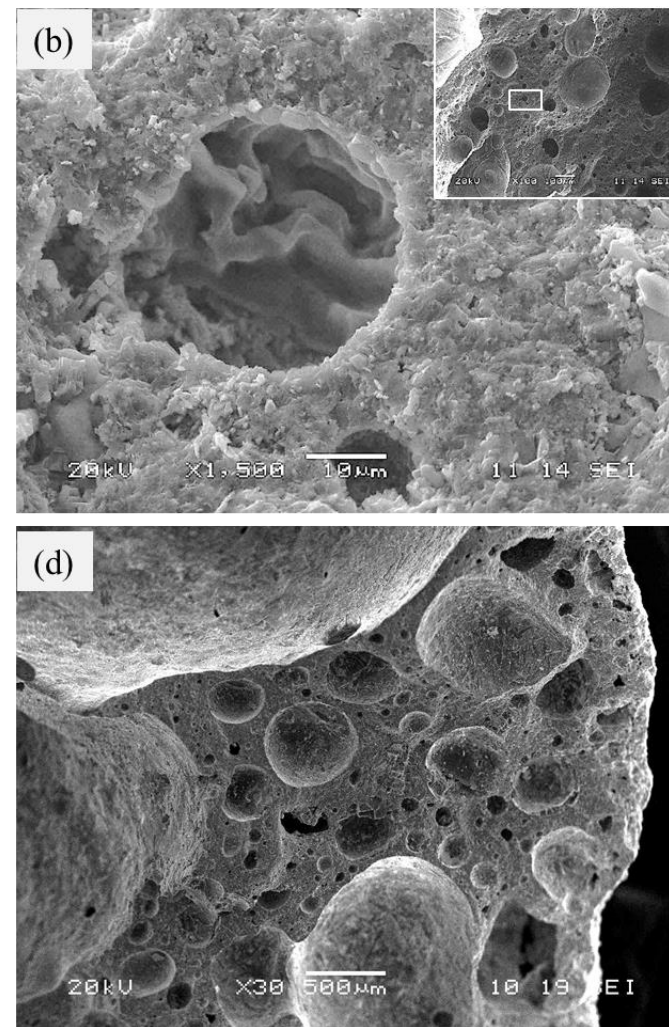
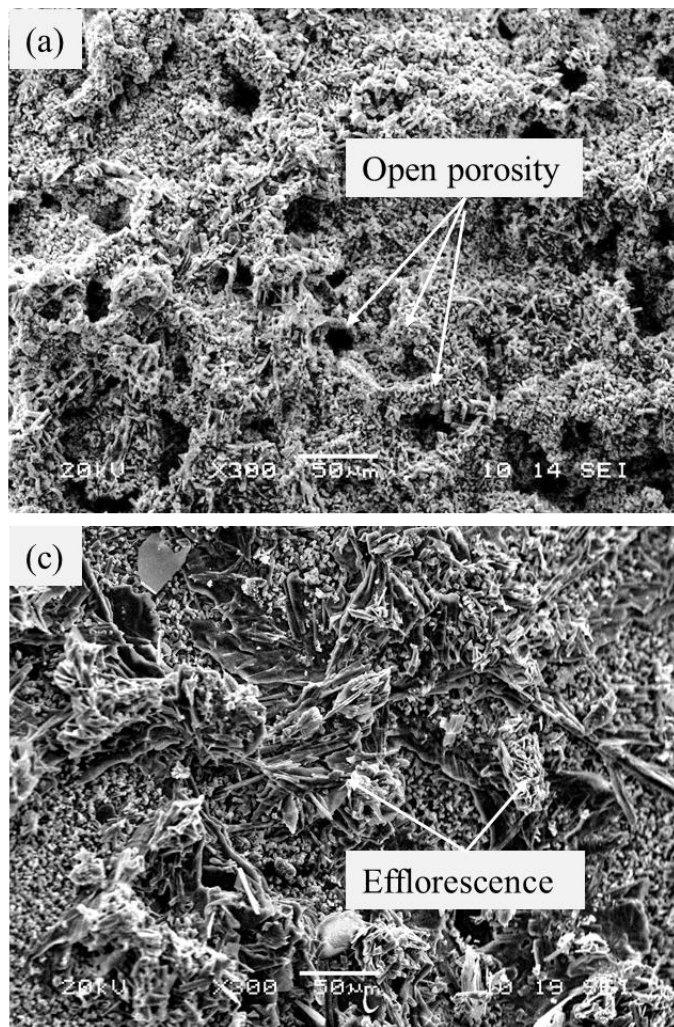


Figure 5.5 SEM micrographs of EDC-LWA: (a) outer surface fired at 1180 °C, (b) core (fracture surface) fired at 1180 °C, (c) outer surface fired at 1190 °C and (d) core (fracture surface) fired at 1190 °C.

## 5.4 Mineralogy of LWA

### 5.4.1 SDC-LWA

Figure 5.6 shows the XRD patterns with markers at major crystalline phases for SDC-LWA fired at 1190 °C (the temperature at which optimal physical properties were achieved). BaSO<sub>4</sub> peaks were present in the fired pellet at slightly higher intensities while the other identified minerals in the raw sample including SiO<sub>2</sub> (quartz), CaCO<sub>3</sub>, CaMgCO<sub>3</sub> and KAl<sub>2</sub>(Si<sub>3</sub>AlO<sub>10</sub>)(OH)<sub>2</sub> were entirely transformed. The major neo-formed phases were diopside (MgCaSi<sub>2</sub>O<sub>6</sub>), CaSO<sub>4</sub>·2(H<sub>2</sub>O) and NaAlSi<sub>3</sub>O<sub>8</sub>. CaSO<sub>4</sub>·2H<sub>2</sub>O (020), (-121) and (-141) reflections were obvious at 11.7 °2θ, 20.7 °2θ and 29.1 °2θ. This was interesting as it indicates the possibility for the highly reactive lime (the product of CaCO<sub>3</sub> decomposition) to react with some of BaSO<sub>4</sub> (as the only sulphate bearing phase in the raw material) to form calcium sulphate.

Table 5.2 shows the results of the Rietveld quantification analysis for SDC-LWA. BaSO<sub>4</sub> was quantified to be 61.3 wt.% of the total crystalline phase. NaAlSi<sub>3</sub>O<sub>8</sub> was quantified as the second most abundant phase at 15.9 wt.%, followed by MgCaSi<sub>2</sub>O<sub>6</sub> and CaSO<sub>4</sub>·2H<sub>2</sub>O, which were predicted at 6.0 wt.% and 5.1 wt.% respectively. The quantification analysis predicted negligible percentages of KAl<sub>2</sub>(Si<sub>3</sub>AlO<sub>10</sub>)(OH)<sub>2</sub> because its decomposition takes place at above 800 °C (Liao et al., 2013). NaCl content was predicted to reduce to 1.6 wt.% in the fired pellets. However, this can still be sufficient to cause Cl<sup>-</sup> leaching problems. Celsian (barium feldspar: BaAl<sub>2</sub>Si<sub>2</sub>O<sub>8</sub>) was added to the analysis as a possible Ba bearing mineral. This would help to understand whether reactive BaO forms at high temperature, as discussed in section 4.5. BaAl<sub>2</sub>Si<sub>2</sub>O<sub>8</sub> was quantified as 1.7 wt.% in the fired pellets and could indicate some degree of reactivity for BaSO<sub>4</sub> phase (Maslennikova et al., 1974). The other quantified phases in the model were quantified at negligible concentrations.

### 5.4.2 CDC-LWA

Figure 5.6 shows the XRD patterns with markers for major crystalline phases for CDC-LWA fired at 1220 °C (optimal temperature in the series). The main phase identified was larnite (also known as belite or C<sub>2</sub>S in Portland cement manufacturing). This was interesting to see that the mineralogy of CDC-LWA was similar to the material in Portland cement. Two high-intensity reflections of dicalcium silicate (larnite - Ca<sub>2</sub>SiO<sub>4</sub>) i.e. (-121) at 32.15 °2θ and (200) at 32.6 °2θ were detected. It should be noted that these

peaks were identified in the region between  $30^{\circ}2\theta$  and  $34^{\circ}2\theta$  where the diffractogram showed considerable overlapping. Traces of  $\text{Ca}_5(\text{SiO}_4)_2\text{SO}_4$  were identified with a distinctive peak at  $31.3^{\circ}2\theta$  associated to its (230) reflection. Other phases identified include  $\text{Ca}_3\text{Fe}_2\text{Si}_3\text{O}_{12}$ ,  $\text{NaAlSi}_3\text{O}_8$  and  $\text{BaSO}_4$ .

Table 5.2 shows the results of the Rietveld quantification analysis for CDC-LWA.  $\text{Ca}_2\text{SiO}_4$  was predicted to form 46.7 wt.% of the total crystalline phase. Other phases normally found in Portland cement chemistry namely tricalcium silicate ( $\text{C}_3\text{S}$ ), tricalcium aluminate ( $\text{C}_3\text{A}$ ), tetracalcium aluminoferrite ( $\text{C}_4\text{AF}$ ) and bredigite ( $\text{Ca}_7\text{Mg}(\text{SiO}_4)_4$ ) were added to the model but as seen in Table 5.2 (except for  $\text{Ca}_7\text{Mg}(\text{SiO}_4)_4$  that was quantified at 4.9 wt.%), the rest of the cement phases were less than 3 – 4 wt.%.  $\text{BaSO}_4$ ,  $\text{Ca}_3\text{Fe}_2\text{Si}_3\text{O}_{12}$ ,  $\text{NaAlSi}_3\text{O}_8$  and  $\text{Ca}_5(\text{SiO}_4)_2\text{SO}_4$  were quantified at 19.1 wt.%, 9.8 wt.%, 4.6 wt.% and 3.0 wt.%, respectively.  $\text{BaSO}_4$  was quantified almost at the same amount predicted in CDC prior to firing.  $\text{BaAl}_2\text{Si}_2\text{O}_8$  was also predicted to be present at a negligible quantity (0.5 wt.%).

#### 5.4.3 EDC-LWA

Major crystalline phases of EDC-LWA are marked in Figure 5.6. XRD patterns were obtained after firing pellets at  $1180^{\circ}\text{C}$  (optimal temperature in the series). The identified phases were  $\text{CaMg}(\text{Si}_2\text{O}_6)$ ,  $\text{KAlSi}_3\text{O}_8$ ,  $\text{CaSO}_4 \cdot 2\text{H}_2\text{O}$ ,  $\text{CaAl}_2\text{Si}_2\text{O}_8$ ,  $\text{CaSO}_4$ ,  $\text{Mg}_2\text{SiO}_4$  and  $\text{BaSO}_4$ .

Table 5.2 shows the results of the Rietveld quantification analysis for EDC-LWA. Among the newly formed mineral phases,  $\text{MgCaSi}_2\text{O}_6$  was quantified as the most abundant phase in the fired samples (47.5 wt.%).  $\text{MgCaSi}_2\text{O}_6$  neo-formation during LWA manufacture has been observed when firing mineral wastes such as washing aggregate sludge with 25 wt.% fly ash at  $1150^{\circ}\text{C}$  (González-Corrochano et al., 2012a) and class-F coal fly ash and 25 wt.% waste glass at  $1050^{\circ}\text{C}$  and  $1250^{\circ}\text{C}$  (Wei et al., 2016).

$\text{CaAl}_2\text{Si}_2\text{O}_8$  and  $\text{NaAlSi}_3\text{O}_8$  were quantified as the calcium and sodium endmembers of the feldspar group at 8.1 wt.% and 8.6 wt.%.  $\text{CaAl}_2\text{Si}_2\text{O}_8$  may have formed by solid-state reactions between  $\text{KAl}_2(\text{Si}_3\text{AlO}_{10})(\text{OH})_2$  and the liberated  $\text{CaO}$  (Bethanis and Cheeseman, 2005). However, it must be noted that the quantitative model showed that  $\text{KAlSi}_3\text{O}_8$  (potassium feldspar) decreased to 0.3 wt.% after firing indicating the possibility for its transformation to other alkali feldspars.

CaSO<sub>4</sub> concentration reduced to 4.5 wt.%. This is mainly because the natural mineral of CaSO<sub>4</sub> is thermodynamically stable up to 1180 °C (Sievert et al., 2005). It is also possible for some of the unreacted CaSO<sub>4</sub> to hydrate as low quantities of neo-formed CaSO<sub>4</sub>·2H<sub>2</sub>O (3.2 wt.%) were predicted by the model.

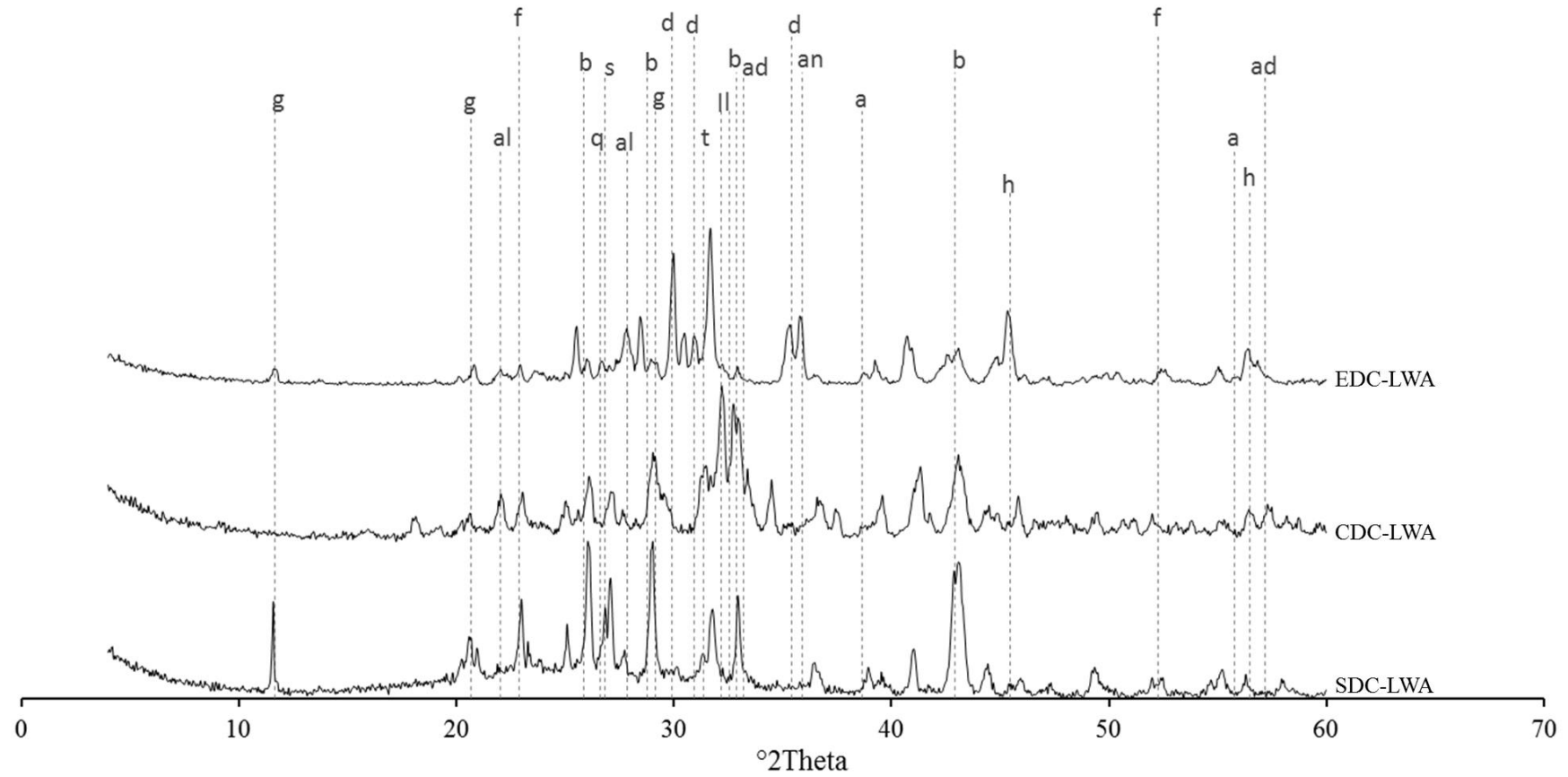


Figure 5.6 X-ray diffraction patterns with some important peak markers for crystalline phase identification in SDC-LWA fired at 1190 °C, CDC-LWA fired at 1230 °C and EDC-LWA fired at 1180 °C. Markers on b: BaSO<sub>4</sub>, h: NaCl, q: SiO<sub>2</sub>, g: CaSO<sub>4</sub>·2H<sub>2</sub>O, a: CaSO<sub>4</sub>, d: MgCaSi<sub>2</sub>O<sub>6</sub>, al: NaAlSi<sub>3</sub>O<sub>8</sub>, s: KAlSi<sub>3</sub>O<sub>8</sub>, an: CaAl<sub>2</sub>Si<sub>2</sub>O<sub>8</sub>, m: KAl<sub>2</sub>(Si<sub>3</sub>AlO<sub>10</sub>)(OH)<sub>2</sub>, f: Mg<sub>2</sub>SiO<sub>4</sub>, l: Ca<sub>2</sub>SiO<sub>4</sub>, t: Ca<sub>5</sub>(SiO<sub>4</sub>)<sub>2</sub>SO<sub>4</sub> and ad: Ca<sub>3</sub>Fe<sub>2</sub>Si<sub>3</sub>O<sub>12</sub>.

Table 5.2 Results of Rietveld quantification analysis for SDC-LWA fired at 1190 °C, CDC-LWA fired at 1230 °C and EDC-LWA fired at 1180 °C.

Minerals	Chemical formula	SDC- LWA (wt.%)	CDC- LWA (wt.%)	EDC- LWA (wt.%)
Quartz	SiO <sub>2</sub>	1.7	-	-
Calcite	CaCO <sub>3</sub>	0.1	-	-
Dolomite	CaMg(CO <sub>3</sub> ) <sub>2</sub>	0.7	-	0.6
Halite	NaCl	1.6	0.0	14.5
Muscovite	KAl <sub>2</sub> (Si <sub>3</sub> AlO <sub>10</sub> )(OH) <sub>2</sub>	2.2	0.0	0.0
Barite	BaSO <sub>4</sub>	61.3	19.1	4.1
Gypsum	CaSO <sub>4</sub> ·2H <sub>2</sub> O	5.1	0.0	3.2
Anhydrite	CaSO <sub>4</sub>	0.4	1.5	4.5
Diopside	MgCaSi <sub>2</sub> O <sub>6</sub>	6.0	-	47.5
Albite	NaAlSi <sub>3</sub> O <sub>8</sub>	15.9	4.6	8.6
Anorthite	CaAl <sub>2</sub> Si <sub>2</sub> O <sub>8</sub>	1.2	-	8.1
Sanidine	KAlSi <sub>3</sub> O <sub>8</sub>	1.2	-	0.6
Celsian	BaAl <sub>2</sub> Si <sub>2</sub> O <sub>8</sub>	1.2	0.5	-
Forsterite	Mg <sub>2</sub> SiO <sub>4</sub>	0.3	-	4.4
Wollastonite	CaSiO <sub>3</sub>	-	-	2.1
Sylvite	KCl	-	-	2.7
Cristoblite	SiO <sub>2</sub>	0.6	-	-
Corundum	Al <sub>2</sub> O <sub>3</sub>	-	-	0.4
Andradite	Ca <sub>3</sub> Fe <sub>2</sub> Si <sub>3</sub> O <sub>12</sub>	-	9.8	-
Potassium sodium sulphate	KNaSO <sub>4</sub>	-	1.2	-
Bredigite	Ca <sub>7</sub> Mg(SiO <sub>4</sub> ) <sub>4</sub>	-	4.9	-
Calcium sulphosilicate	Ca <sub>5</sub> (SiO <sub>4</sub> ) <sub>2</sub> SO <sub>4</sub>	-	3.0	-
Dicalcium silicate	Ca <sub>2</sub> SiO <sub>4</sub>	-	46.7	-
Tricalcium silicate	Ca <sub>3</sub> SiO <sub>5</sub>	-	0.6	-
Tricalcium Aluminate	Ca <sub>3</sub> Al <sub>2</sub> O <sub>6</sub>	-	2.3	-
Tetracalcium aluminoferrite	Ca <sub>4</sub> Al <sub>2</sub> Fe <sub>2</sub> O <sub>10</sub>	-	0.3	-

## 5.5 Leaching analysis of LWA

Table 5.3 shows the results of compliance batch leaching test (BS EN 12457-2) at L/S ratio of 10 l/kg on SDC-LWA, CDC-LWA and EDC-LWA. The firing temperatures for each batch was set as those used for pellets characterised mineralogically i.e. SDC-LWA at 1190 °C; CDC-LWA at 1220 °C; and EDC-LWA at 1180 °C.

### 5.5.1 Heavy metals

The leaching test results of SDC-LWA showed a noticeable increase in the concentration of leachable Ba to 158 mg/kg. Despite the presence of Ba in the form of stable BaSO<sub>4</sub>, there is a possibility for the formation of highly soluble free BaO when BaSO<sub>4</sub> reacts with CaO to form calcium sulphate phases. Except Mo for which the concentration was measured 0.2 mg/kg, the rest of the heavy metals were found to be lower than ICP-OES instrumental limit of quantification. This was also the case for CDC-LWA after firing in which the concentration of Ba, Mo and Ni had reduced to below their associated quantification limits. However, the leachable concentration of Mo in EDC-LWA was increased to 1.2 mg/kg, as highlighted in Table 5.3. It is difficult to determine the exact cause of the increase in Mo leaching in the fired samples. Some authors have suggested that Mo phases formed at high temperatures are unstable under the atmospheric conditions when the material is rapidly cool down (Meima et al., 2002). This effect has also been observed through an increase in the fraction of phases with high Mo availability due to thermal treatments (González-Corrochano et al., 2012a). It is also noted that the changes observed in the concentration of Mo before and after firing could also be due to the inherent variation of Mo in the raw materials.

### 5.5.2 Cl<sup>-</sup>

The concentration of Cl<sup>-</sup> ions was reduced in SDC-LWA. Table 5.3 shows a 72% decrease in Cl<sup>-</sup> (from 7366 mg/kg to 2100 mg/kg). This can happen with the evaporation of Cl<sup>-</sup> at high temperatures. However, some of the Cl<sup>-</sup> ions can be immobilized through a physical encapsulation mechanism in which the migration of ions is limited through decreasing the surface area exposed to the leaching agent and/or isolating the ions from the environment due to impermeable properties of the silicate-based matrix (Chandler et al., 1997).

Cl<sup>-</sup> leaching reduced to below the IC limit of quantification in CDC-LWA, showing a more than 95% reduction. CDC had the lowest silicate concentration necessary for matrix forming and immobilization by encapsulation mechanism compared to the other two samples. This indicates that the majority of Cl<sup>-</sup> were transferred to the gas phase at 1220 °C (firing temperature for CDC-LWA).

The leachable concentrations of Cl<sup>-</sup> in EDC-LWA was 20,365 mg/kg, showing a 77% reduction. This again shows the effectiveness of thermal treatments to reduce the Cl<sup>-</sup> concentration. It is worth mentioning that the neo-formed minerals can also enhance the immobilization of leachable compounds. There are several neo-formed minerals that have been reported to effectively incorporate these ions into their structure. For example, MgCaSi<sub>2</sub>O<sub>6</sub>, which was also present as a neo-formed mineral in EDC-LWA, has applications in waste immobilization purposes due to its superior physical properties and the fact that the material has a strong fixing capacity for a number of leachable compounds (Donatello and Cheeseman, 2013).

### 5.5.3 SO<sub>4</sub><sup>-2</sup>

The concentration of SO<sub>4</sub><sup>-2</sup> ions was below the ICP-OES limit of quantification in SDC-LWA. SO<sub>4</sub><sup>-2</sup> ions had shown a low leachability in SDC as they were present in the form of non-soluble BaSO<sub>4</sub>. It should be noted that the formation of CaSO<sub>4</sub>·2H<sub>2</sub>O in the fired pellets did not affect the release of SO<sub>4</sub><sup>-2</sup>. This could be because at high pH values (as measured for SDC-LWA), CaSO<sub>4</sub>·2H<sub>2</sub>O is not the controlling compound for SO<sub>4</sub><sup>-2</sup> leaching (Quina et al., 2009).

The leaching of SO<sub>4</sub><sup>-2</sup> in CDC-LWA increased to 9186 mg/kg after firing. This may have been due to the formation of soluble SO<sub>4</sub><sup>-2</sup> minerals such as Ca<sub>5</sub>(SiO<sub>4</sub>)<sub>2</sub>SO<sub>4</sub> as predicted by the XRD analysis.

For EDC-LWA, the leachable concentration of SO<sub>4</sub><sup>-2</sup> was reduced to 28,322 mg/kg, around 62% lower than the EDC sample. CaSO<sub>4</sub> was the main solubility controlling mineral for SO<sub>4</sub><sup>-2</sup> ions found after firing. Therefore, the observed reduction is likely due to partial decomposition of CaSO<sub>4</sub> during the firing stage.

#### 5.5.4 F<sup>-</sup>

The leachable concentration F<sup>-</sup> ions increased to 34.1 mg/kg and 64.5 mg/kg in fired SDC-LWA and EDC-LWA, respectively. The most likely source of F<sup>-</sup> in drill cuttings is the KAl<sub>2</sub>(Si<sub>3</sub>AlO<sub>10</sub>)(OH)<sub>2</sub> phase (also quantified at 20.2 wt.% and 20.5 wt.% of crystalline phases in SDC and EDC) (Battaleb-Looie et al., 2012). Therefore, it can be assumed that the F<sup>-</sup> ions were incorporated into compounds with a higher solubility after the decomposition of KAl<sub>2</sub>(Si<sub>3</sub>AlO<sub>10</sub>)(OH)<sub>2</sub> phase during the firing stage.

#### 5.5.5 DOC

DOC in all three samples of drill cuttings was reduced to below the instrumental limit of quantification, as the organic portion was expected to decompose and be completely consumed during the firing stage.

Table 5.3 Results of leaching test (BS EN 12457-2) on SDC-LWA fired at 1190 °C, CDC-LWA fired at 1230 °C and EDC-LWA fired at 1180 °C.

	SDC- LWA	CDC- LWA	EDC- LWA
	(mg/kg)	(mg/kg)	(mg/kg)
As	<1.582	<1.582	<1.582
Ba	158.0	1.0	1.1
Cd	<0.071	<0.071	<0.071
Cr	<0.201	<0.201	0.2
Cu	<0.712	<0.712	<0.712
Hg	<1.158	<1.158	<1.158
Mo	0.2	0.2	1.2
Ni	<0.325	<0.325	<0.325
Pb	<2.209	<2.209	<2.209
Sb	<0.858	<0.858	<0.858
Se	<1.008	<1.008	<1.008
Zn	<2.483	<2.483	<2.483
Cl <sup>-</sup>	2100.1	<51.0	20,365.8
F <sup>-</sup>	34.1	<20.3	64.5
SO <sub>4</sub> <sup>2-</sup>	<37.3	9186.1	28,322.1
DOC	<300.00	<300.00	<300.00
pH	11.93	10.03	9.4
Conductivity (µS/cm)	2262	1405	3732

## 5.6 Discussion

This chapter dealt with firing treatment of drill cuttings pellets to investigate the feasibility of turning the waste into sintered LWA. In so doing, the samples of drill cuttings were pelletised and fired above their initial sintering temperature.

Firing SDC-LWA and CDC-LWA at temperatures above 1200 °C showed that samples of these origins could not effectively be sintered at conventional LWA industry temperature ranges, as discussed in Chapter 2. Insufficient sintering was evident for both samples - as very high water absorptions (25% - 35%) and low compressive strengths (<1.0 MPa) were measured. The main reason for these discrepancies among the samples was large quantities of BaSO<sub>4</sub> and CaCO<sub>3</sub> with high sintering temperatures in the samples, as determined in Chapter 4. Clay minerals in SDC had suitable sintering temperatures, however, their quantity was not sufficient to produce pellets with an acceptable structural integrity. The poor sintering capability of SDC and CDC necessitated the use of additional material to be incorporated in the raw mix. This is discussed in Chapter 7.

EDC-LWA fired at 1180 °C formed sintered pellets with physical properties comparable to commercial products. This was because, in EDC clay minerals were present together with other non-clay minerals such as feldspars and quartz in suitable proportions to enhance the matrix formation capable of entrapping the released gases, causing the pellets to bloat. The physical properties of EDC-LWA were related to the pellets microstructure developed during the firing stage. Bloating was observed in the pellets matrix including very large bubbles with diameters in the millimetres range. This produced pellets with particle densities of 1.25 g/cm<sup>3</sup> to 1.45 g/cm<sup>3</sup>. The presence of highly bloated regions in the microstructure of LWA produced relatively weak pellets in the range of 4.0 MPa due to an uneven distribution of stress during compression testing. In addition, open channels were generated by hydrocarbon burn-off and an efflorescence effect was formed on the surface due to the migration of soluble salts. The release of large amounts of decomposition gas from the pellets extended these channels to the surface and further increased their water absorption capacity to around 10%.

The mineral transformation of drill cuttings during the firing stage was investigated by XRD analysis. Finding similar trends on phase transformation can be used to predict the mineralogy of LWA manufactured from any given sample. The neo-formed minerals influence the properties of LWA and determine the suitability of their use in concrete products. More importantly, the new phases controlled the leaching of problematic

constituents and can be used as an indicator to assess the environmental properties of LWA. The main neo-formed mineral in SDC was sodium feldspar ( $\text{NaAlSi}_3\text{O}_8$ ). In CDC-LWA,  $\text{Ca}_2\text{SiO}_4$  ( $\text{C}_2\text{S}$ ) and other phases that are normally found in Portland cement were neo-formed because of large quantities of calcium carbonates capable of reacting with the present clay minerals at high temperatures. In EDC-LWA, pyroxene phase ( $\text{MgCaSi}_2\text{O}_6$ ) was neo-formed. Some common trends in mineral transformation were found among samples. Most importantly,  $\text{BaSO}_4$  remained generally intact during firing but, there were evidence that some  $\text{BaSO}_4$  was decomposed and the resulting  $\text{BaO}$  could substitute in alkali feldspars to form  $\text{BaAl}_2\text{Si}_2\text{O}_8$ . Furthermore, the released sulphur oxide can react with  $\text{CaO}$  (from decomposition of calcium carbonates) to produce calcium sulphate minerals (Allen and Hayhurst, 1996). The latter phases are less stable in comparison with the original  $\text{BaSO}_4$  and can significantly increase the release of  $\text{SO}_4^{2-}$  ions in water (Bergmans et al., 2016).

In Chapter 4, it was observed that the total heavy metal content in all drill cutting samples was low and those soluble in strong acids had a suitable chemical fixation in the presence of water. However, the firing treatment appeared to be detrimental for Ba speciation as its leaching concentration was increased in SDC-LWA. This was due to the formation of free  $\text{BaO}$  in the material after the firing. However, other heavy metal concentrations in the leachate remained in the range of EoW criteria given in Table 3.2.

Firing treatment produced 72% and 77% reductions in the concentration of leachable  $\text{Cl}^-$  in SDC-LWA and EDC-LWA respectively, and to below IC quantification limits in CDC-LWA. This was both because of the transfer of  $\text{Cl}^-$  to the gas phase due to the high firing temperature used and physical encapsulation of ions in the fired pellets. The effect of firing on  $\text{SO}_4^{2-}$  leaching was complex since both an increasing mechanism (due to the formation of soluble  $\text{SO}_4^{2-}$  phases) and a decreasing mechanism (due to decomposition of calcium sulphates), can occur simultaneously.

Overall, despite the effectiveness of firing in mitigation of leachable compounds, its success can be hindered due to extremely high concentrations soluble salts in the raw materials. This was evident for EDC-LWA, in which high concentrations of  $\text{Cl}^-$  were still present after the firing. Despite the superior physical properties of EDC-LWA the high levels of leaching would undermine its potential use in concrete due to the risk of  $\text{Cl}^-$ -induced corrosion in reinforced bars. To address this, the use of pre-treatments on EDC sample was investigated, as presented in Chapter 6.

## 6 Chapter 6: Effect of washing pre-treatments on properties of LWA

In the previous chapter, the possibility of manufacturing LWA by firing samples of drill cuttings was investigated. It was observed that EDC-LWA were comparable with commercial products in terms of physical properties but had problematic levels of  $\text{Cl}^-$  leaching after firing. To address this issue, the research aimed to find a suitable pre-treatment to be applied to EDC in order to reduce the inherent concentration of  $\text{Cl}^-$  prior to firing. In so doing, the work considered a number of treatments that have already been successfully used in the mitigation of mobile constituents and soluble salts in various hazardous waste materials. Generally, treatments are applied either to transform the leachable constituents to a less mobile compound within the material matrix, as in chemical stabilization and carbonation; or to separate the constituents of concern from the material, as in electro-kinetic and washing treatments. Each treatment is reviewed in the following section and the most appropriate method suited to the characteristics of drill cuttings was then chosen for experimentation in this Chapter.

### 6.1 Potential treatments for mitigation of $\text{Cl}^-$

#### a) Chemical stabilization

In chemical stabilization, reagents such as hydroxides, sulphides, silicates, carbonates and phosphates are used to convert the leachable constituent into less soluble or less mobile forms. At the end of the process, the chemically stabilized constituents remain bounded within the structure of the solid matrix through various mechanisms – including precipitation, absorption and detoxification (Quina et al., 2010). Many studies have investigated the chemical stabilization of mineral wastes (Huang and Lo, 2004, Geysen et al., 2004a, Geysen et al., 2004b, Hu, 2005) with the most common reagents used being soluble phosphates. Treatment with phosphoric acid allows the precipitation of several calcium phosphates such as  $\text{Ca}_3(\text{PO}_4)_2$ , dicalcium phosphate ( $\text{CaHPO}_4 \cdot 2\text{H}_2\text{O}$ ), tricalcium phosphate ( $\text{Ca}_4\text{H}(\text{PO}_4)_3 \cdot 2.5\text{H}_2\text{O}$ ), apatite ( $\text{Ca}_5(\text{PO}_4)_3(\text{OH}, \text{Cl}, \text{F})$ ), copper phosphate hydroxide ( $\text{Cu}_2\text{PO}_4\text{OH}$ ), and other very insoluble minerals containing divalent metals like Pb and Zn (Quina et al., 2010). However, these studies have shown such treatments to be less efficient for stabilizing  $\text{Cl}^-$ , (the problematic ion in evaporite minerals) and therefore was considered disadvantageous for EDC.

#### b) Carbonation/weathering

Carbonation is another treatment that has been developed to reduce the toxicity of hazardous waste materials. The process reduces the environmental impact of waste and can be used as a mean for CO<sub>2</sub> storage. Carbonation treatment has been successfully tested for treating contaminated land and waste produced from industrial thermal processes with high contents of mobile contaminant (Fernández Bertos et al., 2004).

The process involves a reaction between CO<sub>2</sub> and alkali earth hydroxides, oxides and silicates to form stable carbonates containing the mobile contaminant. This is either done under wet conditions where the waste is humidified at moderate temperatures (20 – 25 °C) and pressures (1 – 10 bar) or in dry conditions where reactions are accelerated by applying higher temperature ranges (350 – 400 °C) (Baclocchi et al., 2009). Despite the success of carbonation treatments on mitigating the alkalinity and immobilization of heavy metals, there is a significant uncertainty over its effect on soluble salts, including Cl<sup>-</sup>. Only one study has reported a reduction in leaching of Cl<sup>-</sup> when this process was used for MSWI fly ashes (Li et al., 2007). While the majority of studies reported that Cl<sup>-</sup> remained mobile after carbonation (Wang et al., 2010, Todorovic and Ecke, 2006, Baclocchi et al., 2009). This is problematic for the high content of soluble salts in EDC. In addition, the high temperature range used during the firing stage decompose the carbonated compounds and increase their mobility. Therefore, carbonation was not considered for treating EDC.

#### c) Electro-kinetic processes

Electro-kinetic (electro-remediation) processes involve the application of an electrical field (DC current) across a porous material (soil) to induce the movement of an electrolyte solution and the soluble contaminants towards the electrodes (Yuan and Weng, 2006). Removal of contaminants from porous media is accomplished by the mechanisms of electro-migration (movement/transport of ions toward the electrode of opposite charge), electro-osmosis (the hydraulic flow induced by the electric field), electro-phoresis (transport of charged particles or colloids under the influence of an electric field) and electrolysis of water which produces H<sup>+</sup> and OH<sup>-</sup> in the anode and cathode, respectively (Ferri et al., 2009). The electro-kinetic process set-up is shown in Figure 6.1. Accordingly, highly mobile anions such as Cl<sup>-</sup> are attracted to the anode and cations such as Ni<sup>2+</sup> and Cr<sup>3+</sup> are attracted to the cathode, where they can be collected using methods like

electroplating, precipitation and complexing with ion-exchange resins (Al-Hamdan and Reddy, 2008).

Electro-kinetic methods have been successfully used for contaminated soil (López-Vizcaíno et al., 2014, Skibsted et al., 2018), waste sewage sludge (Ferri et al., 2009) and MSWI fly ash (Traina et al., 2009, Pedersen et al., 2005). Most of these studies have reported an effective reduction in the leaching of  $\text{Cl}^-$  over the range of 80 – 98%. Despite these findings, an electro-kinetic process was not considered to be a suitable treatment in this work because EDC also contained high concentrations of carbonates, which have been reported to negatively affect the process (Virikutyte et al., 2002). In addition, there are still uncertainties around large-scale electro-kinetic treatments due to the use of high-voltages and power consumption, which significantly reduces the efficiency and sustainability of the process.

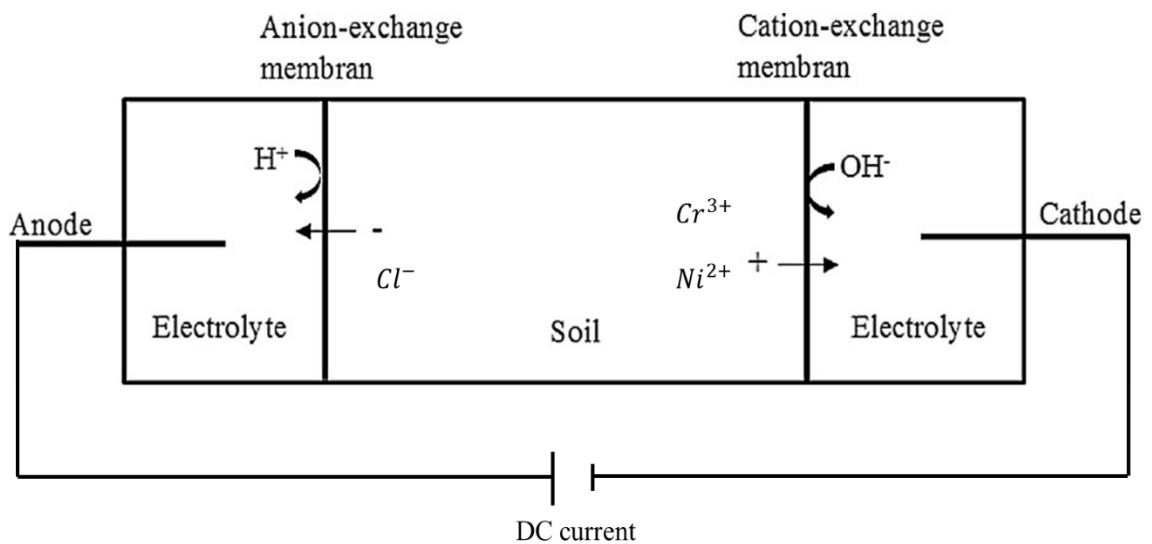


Figure 6.1 Schematic representation of electro-kinetic cell modified from (Skibsted et al., 2018).

#### d) Washing

Washing pre-treatments with water are often employed to remove soluble salts i.e. reduce their total content and thus, the availability for leaching (Sabbas et al., 2003). Washing has been used for several waste materials, such as MSWI fly ash and APCr with extremely high levels of  $\text{Cl}^-$  (Nzihou and Sharrock, 2002, Lundtorp et al., 2003). Some studies attempted to find optimal washing conditions for waste materials with high rates of removing impurities while keeping water consumption and the process costs to a minimum. Derie (1996) reported a general rule for effective washing to reduce the total

content of  $\text{Cl}^-$  that are under the forms of alkaline chlorides: with L/S ratios in the range of 5 – 10 kg/l, a washing duration of one hour would be sufficient to remove most of the soluble alkaline chlorides. Chimenos et al. (2005) found that a two-stage wash followed by a further rinse at L/S ratio of 3 kg/l for one hour would be an ideal condition to wash APCr. Zhu et al. (2010) investigated the behaviour of various  $\text{Cl}^-$  compounds in fly ash from MSWI during washing experiments and concluded that the amount of soluble  $\text{Cl}^-$  including NaCl, KCl and  $\text{CaCl}_2$  decreases rapidly with the increase of L/S ratio or washing frequency.

The main issue with washing treatments is the management of the resulted wastewater. Depending on the nature and quantity of contaminants in the treated waste material, washing can be impractical due to the criticality of managing either extremely polluted or massive quantities of produced wastewater (Abbas et al., 2003). This happens when the contamination is based on heavy metals or corrosive/toxic compounds usually found in hazardous and/or clinical waste. However, the nature of problematic leachable compounds in EDC was NaCl, for which the wastewater can easily be treated or if the environmental permits are available, discharged into the sea. In addition, low quantities of wastewater would be produced in the washing of EDC, due to the high solubility of NaCl in water (359 g/l). Therefore, washing was selected as the most appropriate method for  $\text{Cl}^-$  mitigation and so in this chapter, a novel combination of washing techniques with varying duration/contact time and liquid to solid ratio was designed based on the information obtained from material characterizations.

## 6.2 Designing the washing pre-parameters

It was noted that a standard washing procedure for pre-treatment of wastes does not exist and washing conditions are chosen mainly based on factors such as mineralogy, concentration and solubility of the present ions. The most influential washing parameters including the nature of the washing medium, L/S ratio, duration and washing frequency (the number of steps) were determined for two washing pre-treatments. Deionised water was selected as the washing medium since the problematic  $\text{Cl}^-$  was present in the form of NaCl which has high levels of solubility in water. L/S ratio was kept constant at 10 kg/l to be in the same range as in the leaching test conducted to measure the concentration of

water-soluble constituents. Two washing pre-treatments were designed by varying duration and frequency as given in Table 6.1.

Table 6.1 Washing parameters determined for the pre-treatment of EDC.

	W1	W5
Washing medium	Deionised water	Deionised water
L/S ratio (l/kg)	10	10
Duration (hour)	1	1 (first step) + 5* (second step)
Number of steps	1	2

\* The second step involved agitation in a rotary tumbler.

The washing methods are described as follows:

- a) Single-step washing (W1): deionised water at L/S ratio of 10 l/kg was added to EDC and the mix was stirred at 10 min intervals. After one hour, the water, containing the soluble ions, was removed by decanting and the resulting slurry was vacuum filtered. At the end of the filtration process, the filtrate was rinsed with deionised water to remove any remaining ions. Samples of EDC after W1 pre-treatment were named W1EDC.
- b) Two-step washing (W5): EDC were firstly washed with deionised water at L/S ratio of 10 l/kg for one hour as in W1. In the second stage, deionised water at L/S ratio of 10 l/kg was added to the slurry and the mixture was agitated in a rotary tumbler (shown in Figure 3.4) for five hours, at a rotational speed of 10 rpm. The mix was then vacuum filtered and rinsed as in washing method W1. Samples of EDC after W5 pre-treatment were named W5EDC.

W1EDC and W5EDC were pelletised and fired according to the LWA manufacturing method described in Chapter 3. The fired pellets were named W1EDC-LWA and W5EDC-LWA accordingly. In this chapter, the effect of washing pre-treatment on physical properties, microstructure, mineralogy and leaching behaviour of manufactured LWA were investigated.

### 6.3 Effect of washing on structural characteristics

Figure 6.2 shows images of W1EDC-LWA and W5EDC-LWA. Initially, it was observed that washing had reduced the temperature at which sintering starts to 1160 °C and influenced the quality of the surface. As outlined in Figure 6.2, washing pre-treatments increased the surface homogeneity of LWA, compared to that for pellets made from untreated EDC. This can be attributed to the removal of soluble salts from the raw material that would otherwise form a build-up layer and deteriorate the outer surface of LWA.

W1EDC-LWA exhibited a minor degree of bloating at 1160 °C. Large cellular pores started to develop in the internal structure of pellets fired at 1170 °C. The increased bloating optimised the pore structure developed at 1170 °C. However, at temperatures above 1170 °C, the material suffered from an excessive bloating. At 1190 °C, pellets did not retain their shape and some amount of melted material adhered to the refractory plate. The excessive bloating was problematic because it resulted in inconsistent internal structure and in many cases a non-uniform pore size distribution was obtained. In addition, a prevalent structure for pellets with excessive bloating could be identified; with a densified core in the centre surrounded by a gap incorporating pore bottle-necks connected to a shell. Such a structure is not symmetrical and could cause inconsistency in LWA physical properties.

W5EDC-LWA had a sintered core without any significant bloating at 1160 °C. Some degree of bloating was observed at 1170 °C, but this was not sufficient for an ideal LWA. Bloating increased with firing temperature and reached its maximum at 1190 °C. However, the overall degree of bloating was lower compared to W1EDC-LWA. This may have been due to the removal of gas-releasing compounds, such as calcium sulphate, when a more intense washing pre-treatment was applied (this hypothesis is verified by XRD analysis in section 6.5). No significant build-up layer was found on the LWA surface, however above 1180 °C the development of melted phases caused the W5EDC-LWA to appear smoother. This showed that the removal of soluble compounds had affected the thermal behaviour of the material.

(a) W1EDC-LWA



(b) W5EDC-LWA

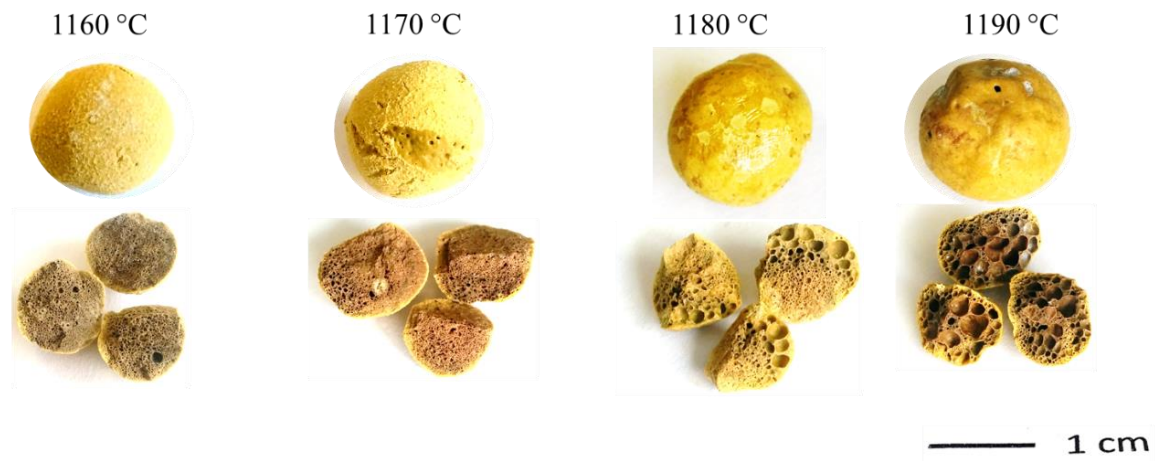


Figure 6.2 Appearance of the surface and internal structure for LWA manufactured from EDC subjected to W1 and W5 pre-treatments.

## 6.4 Effect of washing on physical properties

### 6.4.1 Particle density

Figure 6.3a shows the effect of firing temperature on the particle densities of W1EDC-LWA. The average particle density decreased from 1.88 g/cm<sup>3</sup> to 1.29 g/cm<sup>3</sup> as the firing temperature was increased from 1160 °C to 1180 °C. This was due to the bloating effect, which was intensified with increasing firing temperatures. At 1190 °C, the particle density increased to 1.44 g/cm<sup>3</sup> as the LWA were fired near their melting point which can cause local densification in pellets. It must be noted that a similar trend in the particle density variation over the firing range on EDC-LWA was also observed. The lowest density was obtained for W1EDC-LWA at 1180 °C which was comparable to Lytag (1.27 g/cm<sup>3</sup>) and higher than LECA (0.77 g/cm<sup>3</sup>), as given in Table 5.1.

The obtained particle densities for W5EDC-LWA between 1160 °C and 1180 °C were at a higher range compared to W1EDC-LWA series. The densities at this range were above 2.0 g/cm<sup>3</sup> which did not comply with the British Standard (BS EN 13055-1) for LWA. As discussed previously, W5 (with a longer washing duration) can remove some of the gas-releasing and fluxing compounds and increase the softening point of the material, resulting in LWA with high densities. It was only at 1190 °C when bloating occurred, and the particle density decreased to 1.38 g/cm<sup>3</sup>.

### 6.4.2 Water absorption

Figure 6.3b shows the average water absorption of W1EDC-LWA was 5.3% at 1160 °C. This decreased to its lowest value at 2.7% indicating an increase in the degree of sintering. However, the water absorption increased to 5.7% at 1190 °C as LWA was bloated indicating the formation of pores with a higher degree of connectivity. It was obvious that washing reduced the water absorption and the measured values were remarkably lower than those measured for Lytag (20.5%) and LECA (32.7%). This can be explained by the formation of a non-porous shell over the LWA surface. Washing can inhibit the efflorescence effect (accumulation of soluble ions which migrate to the pellets surface during the drying stage), producing a more homogeneous and impermeable surface during the firing stage (Wei et al., 2008).

A similar trend (decrease with a subsequent increase) on the effect of firing temperature on water absorption of W5EDC-LWA was observed. Initially, the average water absorption decreased from 9.4% to 4.8% as the temperature increased from 1160 °C to

1180 °C indicating a reduction in open porosity. Subsequently, the water absorption increased to 8.9% at 1190 °C due to the formation of water accessible pores produced through LWA bloating.

#### 6.4.3 Compressive strength

Figure 6.3c shows that the average compressive strength of W1EDC-LWA decreased drastically from 21.0 MPa to 2.7 MPa, as the temperature increased from 1160 °C to 1190 °C. The initial strength development in the material confirms the extension of sintering range to lower temperatures after being subjected to W1 pre-treatment. This is because the majority of the soluble salts in drill cuttings are not capable of sintering and thus their removal produces stronger LWA at lower temperatures. However, as the temperature increased to 1180 °C, pellets showed an excessive bloating which resulted in an uneven distribution of stress in pellets causing 80% decrease in compressive strength.

W5EDC-LWA also showed some strength development from 12.4 MPa to 14.6 MPa as the temperature increased from 1160 °C to 1170 °C. This was in accordance with the assumption of an enhanced degree of sintering as a result of washing pre-treatment. Above 1170 °C pellets exhibited a similar decreasing trend in compressive strength which can be associated to the increase in the degree of bloating. The large gas bubbles which were developed during bloating can act as weak points in LWA structure. 6.3 MPa compressive strength measured at 1190 °C was higher than W1EDC-LWA fired at the same temperature and higher than those measured for Lytag (3.2 MPa) and LECA (1.7 MPa). Overall, W5EDC-LWA was recognized as the product with optimal physical properties among the batches tested for the washing experiment, as they showed low density and water absorption, and comparable compressive strength to commercial products.

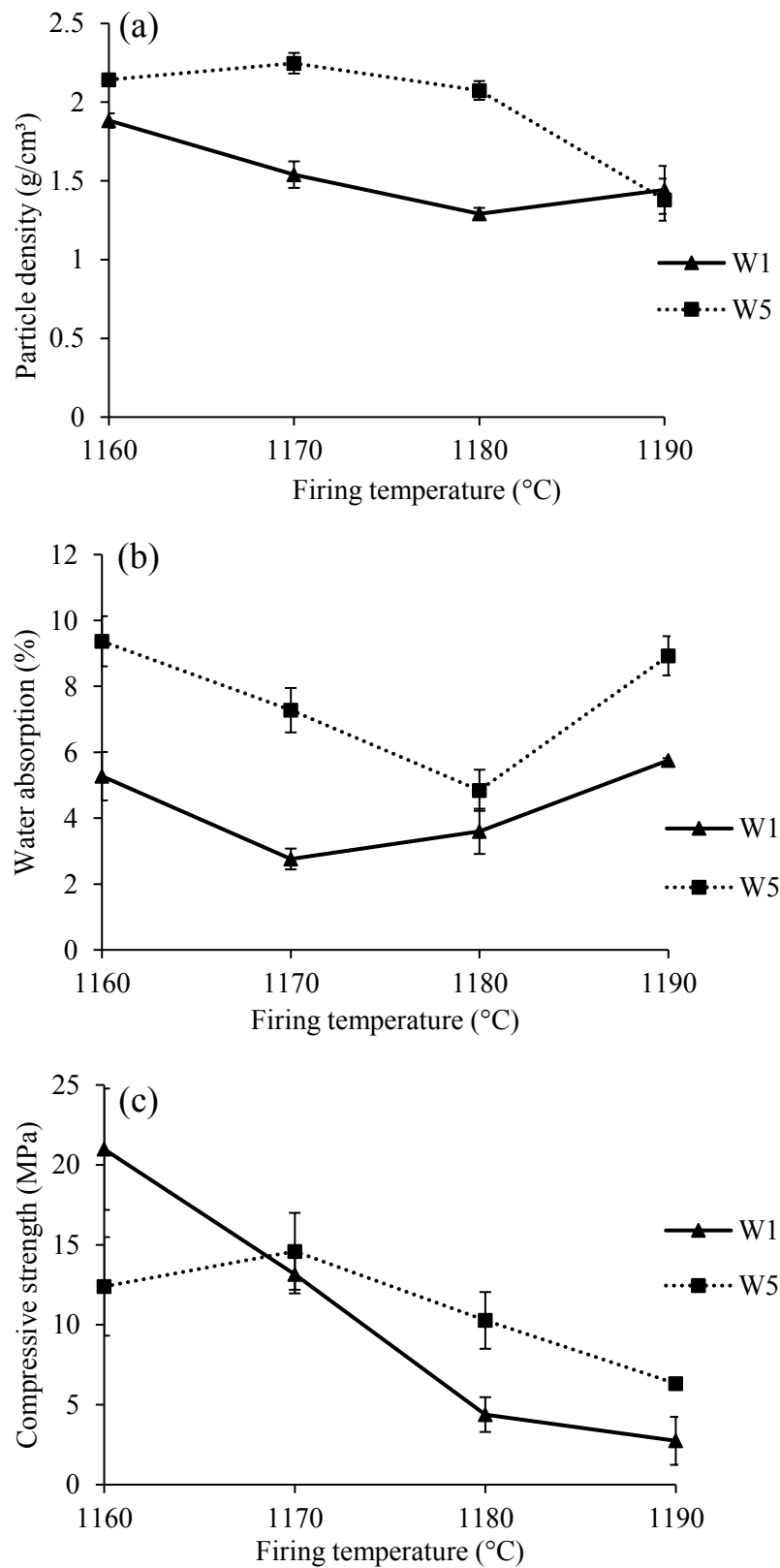


Figure 6.3 Effects of firing temperature on physical properties of W1EDC-LWA and W5EDC-LWA: (a) particle density, (b) water absorption, and (c) compressive strengths. Error bars are plus and minus one standard deviation.

## 6.5 Effect of washing on microstructure

### 6.5.1 W1EDC-LWA

Figure 6.4 shows the SEM micrographs of the fracture surface and the outer surface of W1EDC-LWA. Figure 6.4a shows for pellets fired at 1160 °C a pore structure comprised of uniform closed nearly-spherical pores with sizes decreasing towards the surface. The observed low-temperature bloating effect generated micropores with diameters ranging between 10 µm to 500 µm. This effect did not appear in the untreated sample. It is likely that the removal of soluble salts due to washing has resulted in a continuous matrix necessary for bloating.

Figure 6.4b shows the effect of increasing the temperature to 1190 °C on the core microstructure. A very large bubble formed in the middle of the pellet due to excessive bloating caused by a simultaneous occurrence of the gas release and very low pyro-plastic viscosity of the matrix. This effect that was prevalent in all pellets fired above 1180 °C. However, it is observed that despite the extreme bloating, there was a low degree of connectivity between the central hollow sphere and the shell water-accessible pores. This was also consistent with water absorption capacity measured for this batch (4.3%).

Figure 6.4c to Figure 6.4d show two distinct regions on the outer surface of the pellet fired at 1190 °C. A lower magnification overview image was also attached to both images showing the locations where they were captured. A crystallized surface texture in Figure 6.4c belongs to the efflorescence effect due to the accumulation of remaining soluble compounds on the surface. This layer was incapable of expansion and therefore, showed cracking in order to give way to the bloated core. Figure 6.4d shows a clearly different microstructure, predominantly composed of a melted/densified phase on build-up free regions. It is likely that these phases were pushed toward the surface during the bloating stage and solidified in place. These observations indicated that despite the improvement in the material bloating capability, W1 pre-treatment was not adequate to inhibit the accumulation and crystallization of soluble compound on the surface.

### 6.5.2 W5EDC-LWA

Figure 6.5 shows the SEM micrographs of W5EDC-LWA. The images were captured from the outer surface and core fracture surface of LWA fired at 1160 °C and 1190 °C. It is observed that the solid build-up is almost absent from the surface of both pellets in Figure 6.5a and Figure 6.5b. Some melted phase with open pores is present on the surface

at 1160 °C however, the lack of bloating and pore formation in the core produced LWA with very low water absorption. At 1190 °C, the surface condition was clearly improved in terms of homogeneity compared to that for W1EDC-LWA. Therefore, the increased the washing duration was found to be effective in removing the constituents of the build-up layer.

Figure 6.5c to Figure 6.5d were acquired from the core fracture surface of W5EDC-LWA fired at 1160 °C and 1190 °C, respectively. Figure 6.5c shows very low-viscosity phases producing a cellular open network with minimal bloating. This is consistent with the high particle density measured for LWA fired at 1160 °C. Figure 6.5d shows bloating with the formed bubbles having minimal connectivity as well as thick (up to 100 µm) bottle-necks in W5EDC-LWA core. The result was a strong, but bloated, matrix with relatively low water absorption and explained the optimal physical properties that were achieved for W5EDC-LWA.

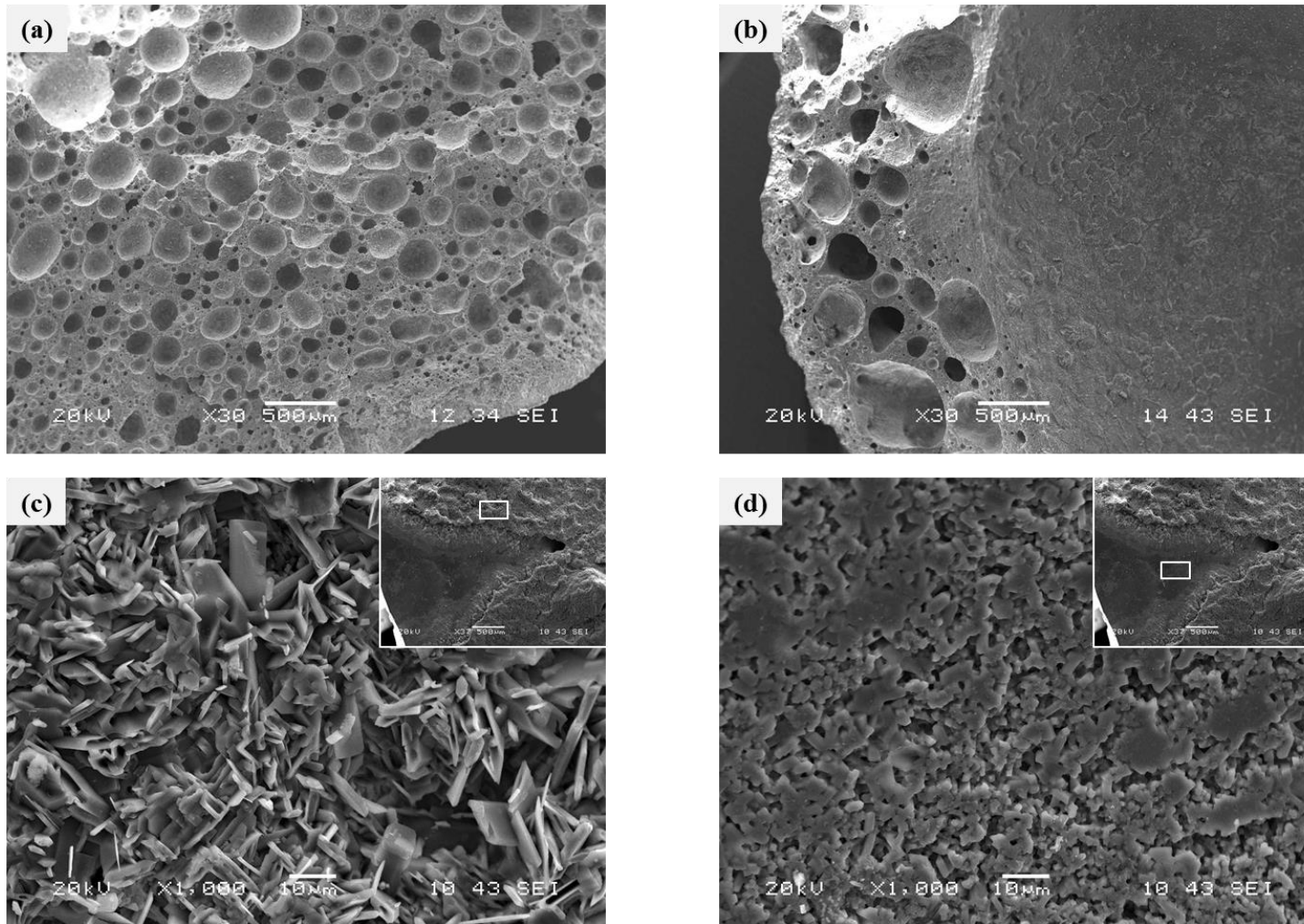


Figure 6.4 SEM micrographs of W1EDC-LWA: (a) core (fracture surface) at 1160 °C, (b) core (fracture surface) at 1190 °C, (c) regions on the outer surface with a build-up layer and (d) regions on the outer surface with solidified phases.

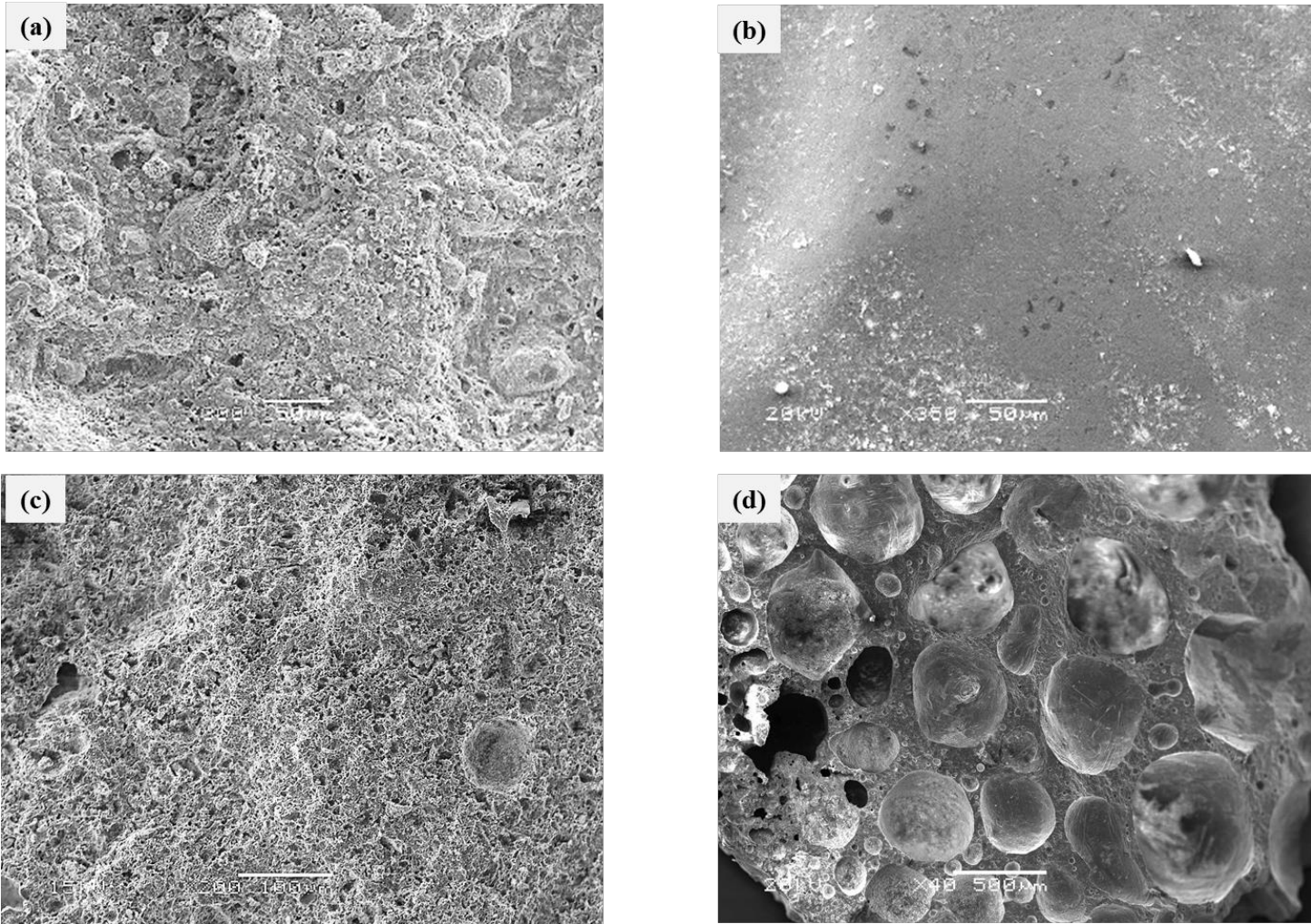


Figure 6.5 SEM micrographs of W5EDC-LWA: (a) outer surface fired at 1160 °C, (b) outer surface at 1190 °C, (c) core (fracture surface) at 1160 °C and (d) core (fracture surface) at 1190 °C.

## 6.6 Effect of washing on mineralogy

Figure 6.6 showed the XRD patterns of W1EDC. The analysis showed the same mineral phases as those found in EDC including SiO<sub>2</sub> (quartz), CaSO<sub>4</sub>, CaSO<sub>4</sub>·2H<sub>2</sub>O, CaCO<sub>3</sub>, CaMg(CO<sub>3</sub>)<sub>2</sub>, BaSO<sub>4</sub> and KAl<sub>3</sub>Si<sub>3</sub>O<sub>10</sub>(OH)<sub>2</sub>. However, the patterns showed that all NaCl peaks were disappeared after only one hour of washing. In Table 6.2, the Rietveld quantification analysis also showed the reduction of NaCl from 10.9 wt.% to almost zero. W5 pre-treatment produced similar results in terms of major phases identified and the absence of the NaCl peak.

CaSO<sub>4</sub>·2H<sub>2</sub>O (020) reflection at 11.7 °2θ became visible after the applying W1 and its intensity increased after W5. The Rietveld analysis showed that minor quantities of CaSO<sub>4</sub>·2H<sub>2</sub>O 3.4 wt.% and 3.9 wt.% were formed after W1 and W5, respectively. It is well understood that CaSO<sub>4</sub> can be hydrated into CaSO<sub>4</sub>·2H<sub>2</sub>O in contact with water (Kirby and Rimstidt, 1994, Sievert et al., 2005) and it may have been the reason that the analysis resulted in higher amounts of CaSO<sub>4</sub>·2H<sub>2</sub>O for W5EDC. After the washing, the contribution of CaSO<sub>4</sub> in the total crystalline phase present did not reduce as 12.1 wt.% and 16.4 wt.% CaSO<sub>4</sub> were quantified in W1EDC and W5EDC, respectively.

Figure 6.7 shows the major neo-formed phase in W1EDC-LWA and W5EDC-LWA fired at 1190 °C was CaMg(Si<sub>2</sub>O<sub>6</sub>). This was quantified as 54.2 wt.% in W1EDC-LWA and as 49.3 wt.% in W5EDC-LWA. These results are consistent with the amount of MgCaSi<sub>2</sub>O<sub>6</sub> found in EDC-LWA. This indicates to a common trend regarding the neo-formation of MgCaSi<sub>2</sub>O<sub>6</sub> which involves the transformation of quartz and KAl<sub>2</sub>(Si<sub>3</sub>AlO<sub>10</sub>)(OH)<sub>2</sub> alongside the decomposition of CaCO<sub>3</sub> and CaMgCO<sub>3</sub> resulting in the formation of MgCaSi<sub>2</sub>O<sub>6</sub> and feldspars. These neo-formed phases can either be crystallized from a silicate melt or formed from a solid-phase reaction between the liberated alkali oxides and aluminosilicates during the firing stage (Vassilev and Vassileva, 1996).

16.4 wt.% and 7.5 wt.% KAlSi<sub>3</sub>O<sub>8</sub> in W1EDC-LWA and W5EDC-LWA were quantified respectively. Some reductions in the share of BaSO<sub>4</sub> from the total crystalline phase in W1EDC-LWA and W5EDC-LWA down to 1.7 wt.% and 1.3 wt.% was determined, respectively. BaSO<sub>4</sub> is non-soluble in water and the observed reductions can be due to the reaction of BaO released from the decomposition of BaSO<sub>4</sub> and the aluminosilicate phases present in EDC. 1.4 wt.% and 2.9 wt.% neo-formed BaAl<sub>2</sub>Si<sub>2</sub>O<sub>8</sub> were present in W1EDC-LWA and W5EDC-LWA confirming the fate of the free BaO.

The intensity of the  $\text{CaSO}_4 \cdot 2\text{H}_2\text{O}$  (020) reflection at  $11.7^\circ 2\theta$  showed an increase compared to the XRD patterns of EDC-LWA. However, in W5EDC-LWA the intensity of the  $\text{CaSO}_4 \cdot 2\text{H}_2\text{O}$  peak was considerably reduced. The results of Rietveld quantification analysis in Table 6.2 showed reductions in calcium sulphate phases in W5EDC-LWA.  $\text{CaSO}_4 \cdot 2\text{H}_2\text{O}$  and  $\text{CaSO}_4$  contribution in the total crystalline phase was estimated at 7.0 wt.% and 3.5 wt.% in W1EDC-LWA respectively, while those in W5EDC-LWA were 0.8 wt.% and 1.5 wt.%. These results indicated to the effectiveness of W5 pre-treatment in the removal of soluble calcium sulphates from W5EDC-LWA. However, the main contributor to this reduction was the decomposition of  $\text{CaSO}_4$  during the firing stage – a mechanism that was also in play for EDC-LWA (discussed in Chapter 5).

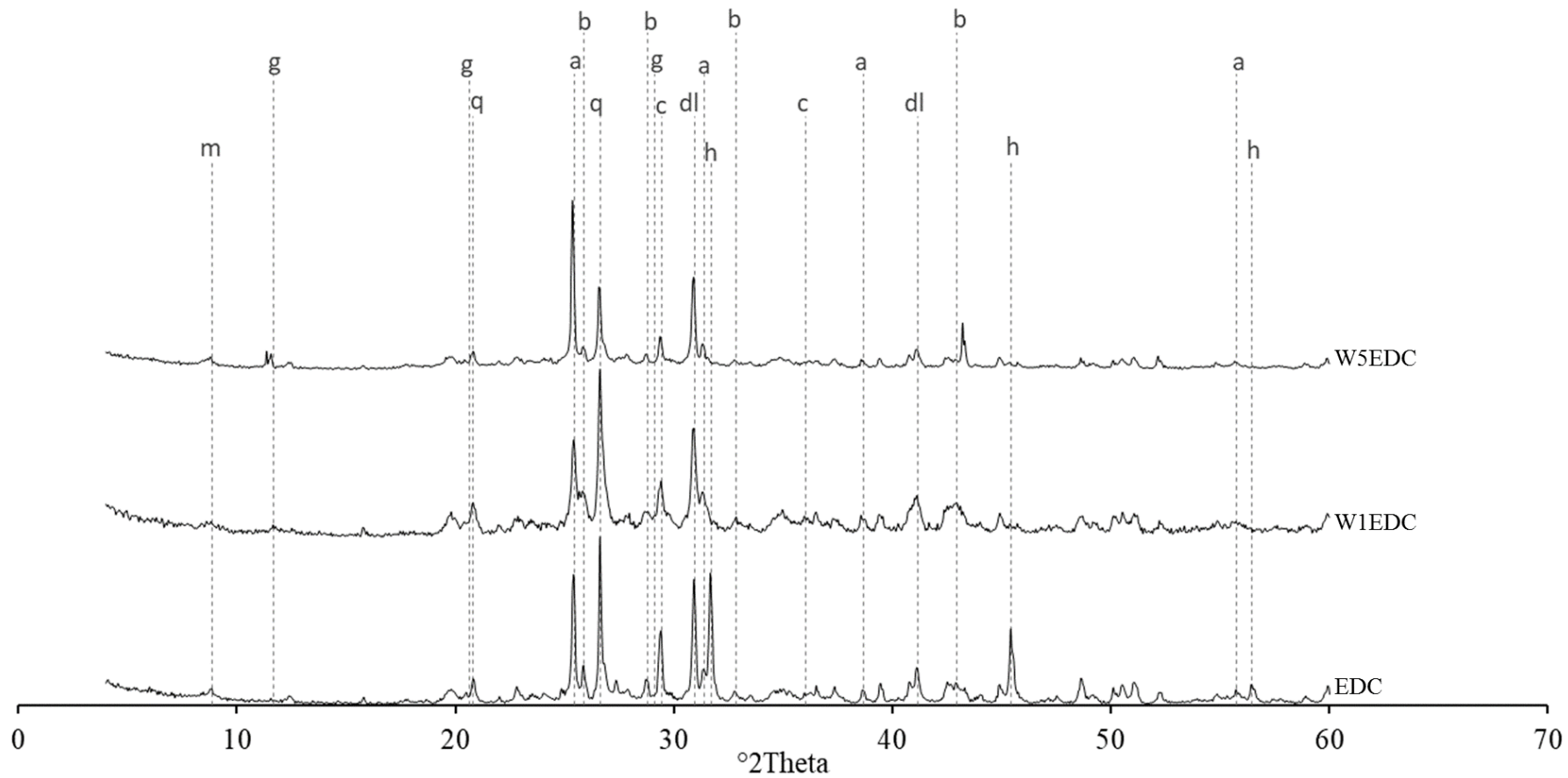


Figure 6.6 X-ray diffraction patterns with some important peak markers for crystalline phase identification in W1EDC and W5EDC. Markers on q:  $\text{SiO}_2$ , a:  $\text{CaSO}_4$ , g:  $\text{CaSO}_4 \cdot 2\text{H}_2\text{O}$ , c:  $\text{CaCO}_3$ , dl:  $\text{CaMg}(\text{CO}_3)_2$ , b:  $\text{BaSO}_4$ , m:  $\text{KAl}_3\text{Si}_3\text{O}_{10}(\text{OH})_2$  and h:  $\text{NaCl}$ .

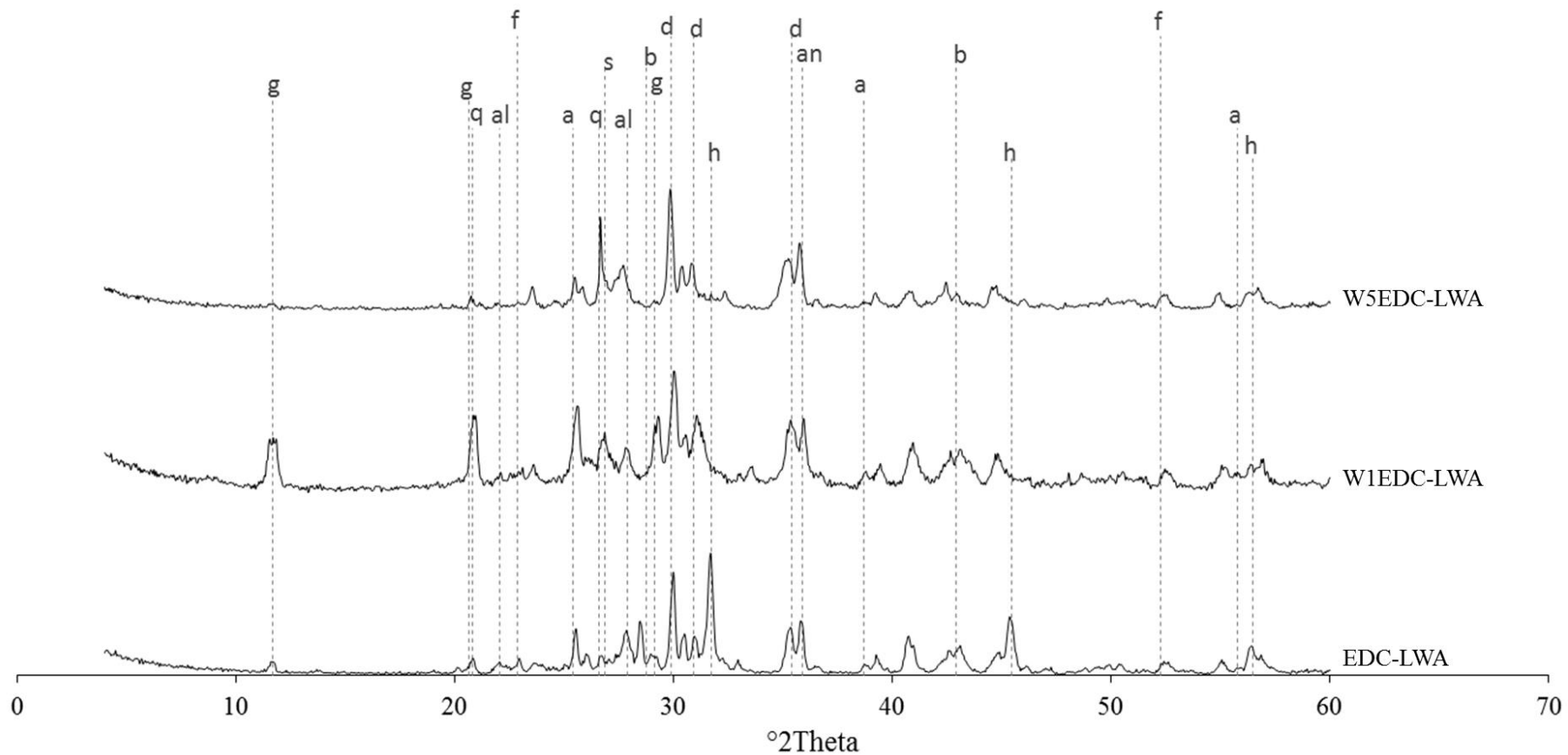


Figure 6.7 X-ray diffraction patterns with some important peak markers for crystalline phase identification in W1EDC-LWA and W5EDC-LWA fired at 1190 °C. Markers on q: SiO<sub>2</sub>, a: CaSO<sub>4</sub>, g: CaSO<sub>4</sub>·2H<sub>2</sub>O, b: BaSO<sub>4</sub>, h: NaCl, d: CaMgSi<sub>2</sub>O<sub>6</sub>, al: NaAlSi<sub>3</sub>O<sub>8</sub>, s: KAlSi<sub>3</sub>O<sub>8</sub>, an: CaAl<sub>2</sub>Si<sub>2</sub>O<sub>8</sub> and f: Mg<sub>2</sub>SiO<sub>4</sub>.

Table 6.2 Results of XRD Rietveld quantification analysis for EDC after washing pre-treatments and LWA fired at 1190 °C.

Minerals	Chemical formula	W1EDC	W5EDC	W1EDC-	W5EDC-
		(wt.%)	(wt.%)	LWA	LWA
Quartz	SiO <sub>2</sub>	7.4	8.3	0.0	0.4
Calcite	CaCO <sub>3</sub>	4.6	5.2	0.0	0.0
Dolomite	CaMg(CO <sub>3</sub> ) <sub>2</sub>	17.1	18.5	0.8	0.9
Halite	NaCl	0.0	0.2	1.3	0.9
Barite	BaSO <sub>4</sub>	5.6	9.2	1.7	1.3
Muscovite	KAl <sub>3</sub> Si <sub>3</sub> O <sub>10</sub> (OH) <sub>2</sub>	25.2	21.5	0.0	0.0
Diopside	MgCaSi <sub>2</sub> O <sub>6</sub>	5.0	3.7	54.2	49.3
Anhydrite	CaSO <sub>4</sub>	12.1	16.4	3.5	1.5
Gypsum	CaSO <sub>4</sub> .2H <sub>2</sub> O	3.4	3.9	7.0	0.8
K-feldspar	K(AlSi <sub>3</sub> O <sub>8</sub> )	12.4	0.0	16.4 <sup>a</sup>	7.5 <sup>b</sup>
Albite	NaAlSi <sub>3</sub> O <sub>8</sub>	0.0	8.1	3.2	0.0
Anorthite	CaAl <sub>2</sub> Si <sub>2</sub> O <sub>8</sub>	5.6	3.8	5.9	28.0
Kaolinite	Al <sub>2</sub> Si <sub>2</sub> O <sub>5</sub> (OH) <sub>4</sub>	0.0	0.0	-	-
Corundum	Al <sub>2</sub> O <sub>3</sub>	1.4	1.2	1.4	0.0
Forsterite	Mg <sub>2</sub> SiO <sub>4</sub>	-	-	2.6	4.0
Celsian	BaAl <sub>2</sub> Si <sub>2</sub> O <sub>8</sub>	-	-	1.4	2.9

<sup>a</sup> as sanidine.

<sup>b</sup> as orthoclase.

## 6.7 Effect of washing on contaminant leaching from LWA

Table 6.3 shows the results of leaching test (BS EN 12457-2) on W1EDC-LWA and W5EDC-LWA fired at 1190 °C.

### 6.7.1 Heavy metals

The concentration of leachable Mo ions was measured 1.5 mg/kg in W1EDC-LWA. Intensifying the washing conditions did not improve this effectively as 1.3 mg/kg leachable Mo was measured for W5EDC-LWA. A similar concentration range was measured for EDC-LWA. However, the acid-soluble concentration of Mo in EDC was below the ICP-OES limit of quantification. Therefore, the appearance of Mo ions in the leachate can again be associated to the formation of unstable Mo-bearing phases at high temperatures, as discussed in Chapter 5. Ba concentration remained at approximately 1.0 mg/kg and below the EoW inert criteria given in Table 3.2.

### 6.7.2 Cl<sup>-</sup>

The concentration of leachable Cl<sup>-</sup> ions in W1EDC-LWA was 1463 mg/kg. This indicates that W1 pre-treatment was effective in mitigating the release of Cl<sup>-</sup>. There was approximately a 93% reduction in leachable Cl<sup>-</sup> ions compared EDC-LWA and 98.3% reduction compared to EDC. This demonstrates the rapid kinetics of Cl<sup>-</sup> release in water during relatively short washing durations. Studies have reported this to occur in only a few seconds (Lampris et al., 2008). Applying W5 pre-treatment resulted in the concentration of Cl<sup>-</sup> ions to further drop to 70.9 mg/kg which is safely below the EoW criteria.

### 6.7.3 SO<sub>4</sub><sup>-2</sup>

The measured concentration of water-soluble SO<sub>4</sub><sup>-2</sup> from W1EDC-LWA was 28,366 mg/kg (Table 6.3), which was similar to that of EDC-LWA (28,322 mg/kg in Table 5.3). In W5EDC-LWA SO<sub>4</sub><sup>-2</sup> concentration was 24,467 mg/kg, 14% lower than that of W1EDC-LWA. It is important to note that for mineral wastes with high SO<sub>4</sub><sup>-2</sup> content, CaSO<sub>4</sub> solubility can explain the SO<sub>4</sub><sup>-2</sup> release when pH values are in the range of 9 to 11 (Eighmy et al., 1995) and below that, CaSO<sub>4</sub>·2H<sub>2</sub>O solubility would become the controlling factor (Astrup et al., 2006, Dijkstra et al., 2006). Both CaSO<sub>4</sub> and CaSO<sub>4</sub>·2H<sub>2</sub>O were present in XRD analysis of W1EDC-LWA and W5EDC-LWA. In addition, the leaching test was conducted at the material own pH which was measured to be 10.58 and

10.29 for W1EDC-LWA and W5EDC-LWA, respectively. This suggests that despite the decomposition of calcium sulphates during the firing stage, the remaining unreacted  $\text{CaSO}_4$  was responsible for the leaching of  $\text{SO}_4^{2-}$  from the manufactured LWA.

#### 6.7.4 $\text{F}^-$

Leaching of  $\text{F}^-$  ions increased to 77.5 mg/kg and 46.6 mg/kg in W1EDC-LWA and W5EDC-LWA, respectively. A similar trend (the increase of  $\text{F}^-$  leachability after firing) was observed for EDC-LWA in section 5.5.4. This was because  $\text{KAl}_2(\text{Si}_3\text{AlO}_{10})(\text{OH})_2$  was the main source of  $\text{F}^-$  in EDC (XRD analysis in Table 4.3) and its decomposition during the firing stage can increase the mobility of the  $\text{F}^-$  ions.

Table 6.3 Results of leaching test (BS EN 12457-2, 2002) on W1EDC-LWA and W5EDC-LWA fired at 1190 °C.

	W1EDC-LWA	W5EDC-LWA
	(mg/kg)	(mg/kg)
As	<1.582	<1.582
Ba	0.8	1.0
Cd	<0.071	<0.071
Cr	<0.201	<0.201
Cu	<0.712	<0.712
Hg	<1.158	<1.158
Mo	1.5	1.3
Ni	<0.325	<0.325
Pb	<2.209	<2.209
Sb	<0.858	<0.858
Se	<1.008	<1.008
Zn	<2.483	<2.483
Cl <sup>-</sup>	1463.5	70.9
F <sup>-</sup>	77.5	46.6
SO <sub>4</sub> <sup>2-</sup>	28,366.5	24,467.0
DOC	<300.00	<300.00
pH at 20 °C	10.58	10.29
Conductivity (µs/cm)	4311	4322

## 6.8 Discussions

This chapter aimed to investigate the effect of washing on properties of LWA made from EDC samples – for which high concentrations of NaCl had been measured in Chapter 4. Single-step (W1) and two-step (W5) washing pre-treatments were designed based on mineralogical information from EDC and applied to the raw materials. Both washing pre-treatments were shown to decrease the initial sintering temperature, which is important for energy saving at large scale LWA manufacture. In addition, washing improved the viscosity of the pyro-plastic phase to such extent that bloating occurred effectively. LWA with optimal physical properties comparable with commercial products were produced over a wide firing range. W5EDC-LWA fired at 1190 °C was identified as the optimal batch with 1.38 g/cm<sup>3</sup> particle density, 8.9% water absorption and 6.3 MPa compressive strength.

SEM microstructural analysis showed that washing could inhibit the formation of the built-up layer, reducing the surface porosity and thus, affecting the water absorption. W5 pre-treatment completely removed the efflorescence effect on the surface of fired pellets observed on EDC-LWA in Chapter 5. SEM images obtained from the fracture surface of the fired pellets confirmed the prevalence of low-viscosity glass phases in the matrix.

XRD analysis showed that the NaCl phase contribution in EDC was reduced to below 1.0 wt.% after W1 pre-treatments. The analysis showed the complete removal of NaCl after W5 pre-treatment and resulted in Cl<sup>-</sup> concentration in the manufactured W5EDC-LWA to reduce below the EoW inert criteria. W5EDC-LWA can be recognised as a successful case for the beneficial reuse of waste drill cuttings with high Cl<sup>-</sup> contents. In addition, CaMgSi<sub>2</sub>O<sub>6</sub> as the major neo-formed phase can enhance the performance of LWA in concrete products. This is because the expansive alkali-silica gel forming reactions between cement and the amorphous silica can be inhibited when LWA mineralogy is rich in CaMgSi<sub>2</sub>O<sub>6</sub> (Rodriguez et al., 2018).

Despite the evidence for calcium sulphates decomposition during the firing stage, the remaining solubility controlling CaSO<sub>4</sub> caused some levels of SO<sub>4</sub><sup>2-</sup> leaching. W5EDC-LWA showed 14% reduction in water-soluble SO<sub>4</sub><sup>2-</sup> content compared to W1EDC-LWA. These results suggested that both washing pre-treatments were not effective to completely remove the sulphate salts in EDC. To address this issue, using a more intense washing pre-treatment by further increasing the L/S ratio in the range of 200 l/kg to 300 l/kg may

be required (Abbas et al., 2003). High levels of  $\text{SO}_4^{2-}$  in aggregates can be detrimental to the durability of concrete products. Although, aggregates produced from construction and demolition waste often contain high levels of  $\text{SO}_4^{2-}$  similar to those measured in W5EDC-LWA. This suggests that attention must be paid to the end-use application of W5EDC-LWA and perhaps incorporated where the presence of  $\text{SO}_4^{2-}$  is tolerated – such as in combination with sulphate resistance Portland cement.

## 7 Chapter 7: Effect of glass addition on properties of LWA

In Chapter 5, it was observed that SDC and CDC samples could not be effectively sintered over the firing temperature ranges that are usually achievable in LWA manufacturing kilns and thus, would jeopardise the technical viability of the process. The aim of this chapter was to address the issue by exploring the use of a secondary material to be incorporated into the SDC-LWA and CDC-LWA (prior to the firing stage). This material needs to be capable of forming a matrix (network) and enhance the sintering of unreacted drill cutting particles. The study also aimed to incorporate an additional material in EDC-LWA as an alternative solution to reduce the observed leaching problem of  $\text{Cl}^-$ , discussed in Chapter 5. Similarly, the suitable material should be capable of matrix forming which can provide physical encapsulation of the leachable constituents within the LWA structure. This approach was successfully tested for mitigation of heavy metals from hazardous mineral waste, such as APCr (Quina et al., 2014b, Roether et al., 2010), however, its effectiveness on the leaching of anions has not been fully investigated. This experiment also allowed for comparisons to be made with results from the washing treatments employed in Chapter 6.

### 7.1 Potential secondary material for incorporation in LWA

Silica and/or aluminosilicate-based materials are known for their effective matrix (network) forming properties (Lin and Chang, 2006) and therefore were deemed fit for the purpose of this experiment. Naturally-available silica and/or aluminosilicate geological materials such as bentonite clay, sand, etc. were suitable for addressing the problem. However, these were not considered for the experiment due to the criticality of using natural resources (as doing so would undermine the sustainable use of materials which was the ultimate goal of this research). In Chapter 2, a number of secondary waste materials that were successfully used for LWA manufacturing were reviewed. In this chapter, the aim was to select a waste material to be incorporated in LWA that can provide technical advantages including matrix forming and bloating capabilities, inertness, large-scale availability and sustainability. In the following sections, information on potential secondary materials are provided and the most advantageous material was then selected for experimentation:

#### a) Pulverised Fuel Ash (PFA)

PFA is the by-product of coal-fired power stations. It has been frequently used as a secondary material for civil engineering applications such as Portland cement replacement in concrete products, soil stabiliser in road construction and as a raw material for manufacturing Lytag (Molineux et al., 2016). Typical chemical composition data for PFA produced in the UK is given in Table 7.1. The material is predominantly comprised of silica (50.1 wt.%), alumina (28.1 wt.%) and iron oxide (11.7); suggesting sufficient capability of the material to form a network and enhance the sintering of drill cuttings particles. In addition, PFA is classified as a non-hazardous waste making it an ideal material for use in LWA manufacturing.

However, the availability of PFA is reducing due to the move away from coal-fired power stations in the UK and EU (Jones et al., 2006). In addition, PFA desirable pozzolanic properties has shifted the attention to alternative reuse applications, as in supplementary cementitious material (SCM) in concrete products (Rayment, 1982, M. D. A. Thomas and Pettifer, 1991, Davies and Kitchener, 1996, Escalante García et al., 2006, Liu, 2010), and this is likely to limit its availability for LWA production (Sarabèr et al., 2012, Molineux et al., 2016). For these reasons, it was considered unsuitable for use in this experiment.

#### b) Municipal Solid Waste Incinerator (MSWI) bottom ash

MSWI bottom ash is the residue of combustion in energy from waste (EfW) plants. It can be a candidate for incorporation in drill cuttings LWA because it has advantageous sintering properties, which can react with drill cutting particles to form an aluminosilicate-based matrix. MSWI bottom ash usually has lower sintering temperature ranges compared to PFA and that is due to high total flux contents in the material, as shown in Table 7.1 (Bourtsalas et al., 2015).

MSWI bottom ash production in the UK is estimated to be in the range of 3.7 million tonnes per annum indicating the vast availability of this secondary material (Dou et al., 2017). MSWI bottom ash has been used in LWA manufacturing (Cheeseman et al., 2005) however, a number of studies on characterization of MSWI bottom ash have noted a large amount of variability in the waste (Bethanis et al., 2002). The variability arises from the material ferrous and non-ferrous metals (including heavy metals), ceramics, glass, other non-combustibles and residual organic matter. The extreme heterogeneity of MSWI bottom ash, together with the presence of heavy metals, is the main issue regarding its

inertness. The characterization of drill cuttings showed negligible heavy metal contents in Chapter 4 and the incorporation of MSWI bottom ash will adversely affect the leaching properties of drill cuttings LWA. Therefore, MSWI bottom ash was also considered unsuitable for use in this chapter.

#### c) Incineration Sewage Sludge Ash (ISSA)

Sewage sludge is a by-product of water treatment which is normally incinerated to reduce the waste by approximately 70% by mass and 90% by volume, leaving behind ISSA (Lynn et al., 2015). ISSA is aluminosilicate-based waste material with compositions favourable for the formation of a liquid phase during sintering and thus a potential candidate for incorporation in LWA. As reported in the literature, ISSA is a polyphasic material comprised of ~60% crystalline and ~40% amorphous phase. The chemical composition reported in Table 7.1 shows that ISSA is mainly composed of Si, Ca, P and Al. These are usually found in the forms of SiO<sub>2</sub> (quartz) and whitlockite (Ca<sub>3</sub>(PO<sub>4</sub>)<sub>2</sub>), while Al is typically present in feldspar and amorphous glassy phases (Cyr et al., 2007). As shown in Table 7.1, the amount of CaO and P<sub>2</sub>O<sub>5</sub> are high (~26%) compared to the other secondary materials reviewed while SiO<sub>2</sub> and Al<sub>2</sub>O<sub>3</sub> are present less than 50%.

ISSA is currently landfilled in the UK, however, due to its superior pozzolanic and sintering properties, a number of reuse applications including its use in LWA have been investigated (Donatello and Cheeseman, 2013). LWA was produced by firing ISSA and clay at a temperature range of between 1050 °C and 1070 °C (Cheeseman and Viridi, 2005). However, the main issue for the use of ISSA in LWA is the low Si/Al ratio of the material as shown in Table 7.1. This was addressed by Tsai et al. (2006) showing ISSA derived LWA require additional matrix forming components such as a glass cullet for improving physical properties. The Si/Al ratio in drill cuttings shown in Table 4.1 was also measured at similar ranges to ISSA. This indicated that ISSA itself would not solve the inherent lack of aluminosilicate content in drill cuttings samples and therefore, was again not a suitable candidate for incorporation in LWA for this experiment.

#### d) Excavated clay

Clay is another aluminosilicate-based candidate for incorporation in drill cuttings LWA. The possibility of using waste clay in the manufacture of LWA was reviewed in Chapter 2. It was discussed that the use of waste clay generated by major infrastructure development projects to make LWA has a positive environmental impact and contributes

towards a more circular economy. For example, construction of the Crossrail 1 underground tunnel in London UK, resulted in more than 4 million tonnes of waste London clay which was primarily used in land reclamation (Boarder et al., 2016). The composition of a typical London clay is given in Table 7.1. However, the main issue with the use of waste clay as a matrix forming material is the inherent compositional variation based on the location and depth of excavation. This adds to the variability observed in drill cuttings and produces LWA with inconsistent properties.

e) Waste glass

Glass is a silica-based secondary material with excellent matrix forming capability, inertness and compositional consistency. In materials science, the term ‘glass’ refers to solids with amorphous crystalline structures lacking any ordered molecular arrangement. The most common glasses are based on a SiO<sub>2</sub> network in which various metal oxides are incorporated to reduce the mix melting point. For example, soda (Na<sub>2</sub>O: 10 – 16%), lime (CaO: 5 – 14%) and minor amounts of magnesia (MgO) and alumina (Al<sub>2</sub>O<sub>3</sub>) are added to reduce the melting point of pure silica (1723 °C) to below 1100 °C and produce soda-lime glass (Haldimann et al., 2008, Khatib, 2016).

Glass represents a sustainable resource in construction and packaging applications - as it can be easily reprocessed/recycled to make materials with similar properties to the original (Chiellini, 2008). According to the European Container Glass Federation (FEVE) the average glass recycling rate in the UK reached 67% in 2014 with the remaining 23% being sent to landfill. The remaining fraction of total produced glass is often referred to as ‘waste glass’ and so alternative recycling options have received a great deal of interest, particularly in the construction materials sector.

Table 7.1 shows typical compositions of waste glass. Studies have examined the use of waste glass as concrete aggregate and reported promising results (Degirmenci et al., 2011, Sikora et al., 2015). However, a major concern over this application has been the expansive nature of alkali–silica reactions between cement and the amorphous silica, which comprises up to 70% of the aggregate (Ducman et al., 2002). Foamed materials with superior engineering properties have been produced from waste glass (Arulrajah et al., 2015, Blengini et al., 2012, Gong et al., 2016). The fluxing properties of glass should reduce the temperature range at which the materials soften and bind non-reactive particles together (Velis et al., 2014). Milled waste glass has also been used as an admixture in the manufacture of LWA from industrial by-products, such as coal fly-ash (Ilic et al., 2003,

Wei et al., 2016); waste silica sludge, waste clay and granite polishing residue (Ducman and Mirtič, 2009); harbour sediments (Wei et al., 2011); sewage sludge (Tuan et al., 2013); and MSWI fly ash (Lu et al., 2015). In these studies, the glass addition has been reported to serve mainly as a fluxing agent during the sintering process, it also improved physical properties of LWA – in particular, their water absorption capacities. Based on all these benefits waste glass seemed to be the best fit material for inclusion into the samples and was therefore selected as the suitable candidate for incorporation in LWA for this study.

Table 7.1 Typical oxide compositions of matrix forming secondary materials reviewed for incorporation in LWA.

Oxide compositions	PFA (Ilic et al., 2003)	MSWI bottom ash (del Valle-Zermeño et al., 2013)	ISSA (Cyr et al., 2007)	London clay (Zhou et al., 2017)	Waste glass (Tuan et al., 2013)
	(wt.%)	(wt.%)	(wt.%)	(wt.%)	(wt.%)
SiO <sub>2</sub>	50.1	47.8	34.2	45.8	74.0
Al <sub>2</sub> O <sub>3</sub>	28.1	12.2	12.6	12.8	6.0
Fe <sub>2</sub> O <sub>3</sub>	11.7	7.8	4.7	7.7	0.3
CaO	1.6	15.6	20.6	1.1	9.7
MgO	1.5	2.02	1.9	1.8	0.0
Na <sub>2</sub> O	0.3	6.5	1.0	0.9	8.2
K <sub>2</sub> O	0.6	1.3	1.7	3.7	0.8
SO <sub>3</sub>	-	0.4	2.8	1.3	0.2
P <sub>2</sub> O <sub>3</sub>	-	-	14.8	0.1	0.1

## 7.2 Incorporation of glass in LWA

For the experiment, a sample of 20 kg crushed amber glass was supplied by Waste Care Group Limited. Amber glass was selected from other types of waste glass because it has the lowest recycling rate in the UK - British Glass Manufacturers Confederation reported that only 25% of the produced amber glass is being recycled (British Glass, 2008). The crushed glass was ball milled and sieved through a 250  $\mu\text{m}$  mesh. The SEM images of waste glass powder were shown in Appendix I. The prepared glass powder was then added to the milled drill cuttings prior to the pelletisation. 40 wt.% glass addition was used based on the work of Kourti and Cheeseman (2010). These authors tested a series of LWA with different glass levels and suggested 40 wt.% substitution level for achieving the optimum physical properties. Half of this quantity, 20 wt.%, was also selected for the substitution level to further investigate the effect of glass addition on physical properties and microstructure of LWA.

Initially, to evaluate the effectiveness of glass addition on the sintering behaviour of the material, a similar experimental approach to the previous chapters was applied. A sample of waste glass was characterised for chemical composition by XRF and the results were shown in Table 7.2. The new compositional locations of drill cuttings/glass mixes were plotted in a Riley diagram (Figure 7.1). It can be seen that the compositions are moving toward the 'bloating area' and thus an improved bloating behaviour can be expected.

Table 7.2 Oxide compositions measured by XRF analysis for waste glass sample used for incorporation in LWA.

Oxide compositions	(wt.%)
SiO <sub>2</sub>	71.45
Al <sub>2</sub> O <sub>3</sub>	2.16
Fe <sub>2</sub> O <sub>3</sub>	0.53
MgO	2.51
CaO	10.11
Na <sub>2</sub> O	11.79
K <sub>2</sub> O	0.91
TiO <sub>2</sub>	0.09
MnO	0.02
SO <sub>3</sub>	0.05
P <sub>2</sub> O <sub>5</sub>	0.02

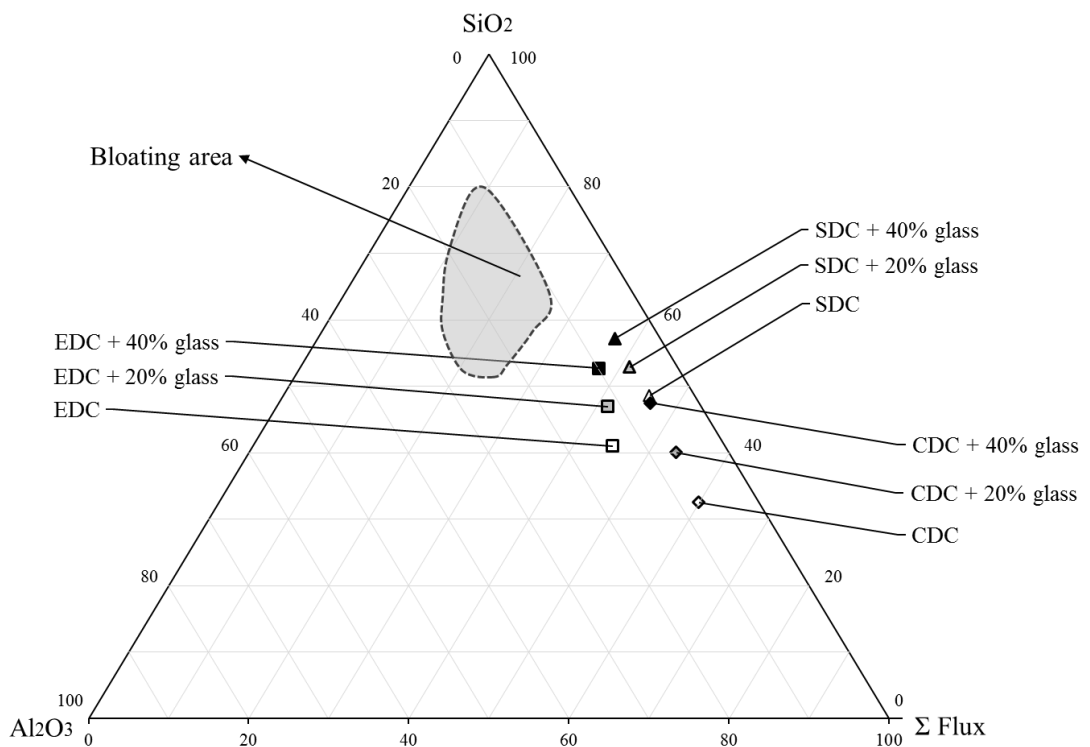


Figure 7.1 Compositional location of drill cuttings after addition of glass in Riley diagram.

### 7.3 Effect of glass addition on structural characteristics

The addition of milled glass to SDC and CDC significantly reduced the initial sintering temperature to 1110 °C (compared to 1190 °C and 1200 °C measured respectively in Chapter 4) and increased the structural integrity of pellets after firing. This showed glass was an effective matrix forming material for incorporation in drill cuttings LWA.

#### 7.3.1 SDC-LWA

Figure 7.2a shows images of the outer surface and fracture surface of SDC-LWA with 40 wt.% added glass and fired between 1110 °C and 1170 °C. Fired pellets were brighter and had a smoother surface where the waste glass was added. Bloating appeared at 1110 °C and reached a suitable degree at 1150 °C. Firing at 1170 °C was detrimental as pellets lost their structural integrity and became agglomerated.

#### 7.3.2 CDC-LWA

Figure 7.2b shows CDC-LWA with 40 wt.% added glass fired, between 1110 °C and 1170 °C. The empty pockets of space due to decomposition of carbonate minerals observed in CDC-LWA were sealed with glass, improving both structural integrity and surface quality of the pellets. However, some defects were still present on the surface at lower firing temperatures. The LWA also exhibited the ability to bloat, indicating sufficient quantities of silica-based phases to retain the decomposition reaction gases, but bloating behaviour did not noticeably vary over the applied firing temperature range.

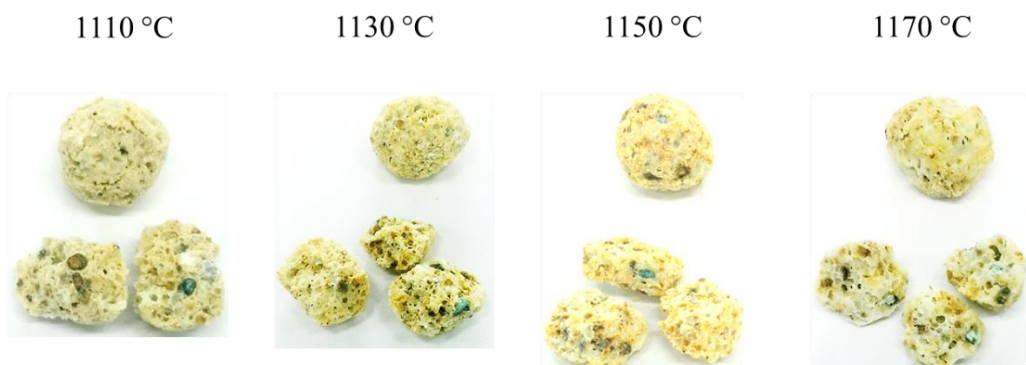
#### 7.3.3 EDC-LWA

Figure 7.2c shows the EDC-LWA with 40 wt.% added glass. No significant reduction in the initial sintering temperature was observed and pellets with an acceptable structural integrity were formed above 1160 °C. Some degree of bloating appeared over the applied firing range up until 1190 °C. However, the bloating was poor despite the compositional location ( $\text{SiO}_2/\text{Al}_2\text{O}_3/\Sigma$  flux ratio) being shifted closer to the bloating area (Figure 7.1).

(a) SDC-LWA + 40% glass



(b) CDC-LWA + 40% glass



(c) EDC-LWA + 40% glass



— 1 cm

Figure 7.2 Appearance of the surface and internal structure of (a) SDC-LWA, (b) CDC-LWA and (c) EDC-LWA with 40 wt.% added glass.

## 7.4 Effect of glass addition on physical properties

### 7.4.1 Particle density

Figure 7.3a shows the effect of firing temperature on particle densities of SDC-LWA with 20 wt.% and 40 wt.% glass. The average particle density of SDC-LWA with 20 wt.% glass showed a slight increase over the firing range, from 1.83 g/cm<sup>3</sup> at 1110 °C to 1.99 g/cm<sup>3</sup> at 1170 °C. These particle densities were above those obtained for SDC-LWA (between 1.56 g/cm<sup>3</sup> and 1.69 g/cm<sup>3</sup>) at a higher firing range (above 1200 °C). Conversely, the average particle density of SDC-LWA with 40 wt.% glass showed a moderate decrease with the increase in temperature, 1.94 g/cm<sup>3</sup> at 1110 °C to 1.76 g/cm<sup>3</sup> at 1150 °C. This was attributed to the bloating effect observed in the internal structure of the pellets. In this series, the particle density and other physical properties of pellets fired at 1170 could not be measured - as this temperature caused melting and agglomeration (as shown in Figure 7.2a). Particle densities at both glass concentrations were higher than those measured for Lytag (1.29 g/cm<sup>3</sup>) and LECA (0.77 g/cm<sup>3</sup>), as given in Table 5.1.

Figure 7.3b shows the effect of firing temperature on particle densities of CDC-LWA with 20 wt.% and 40 wt.% glass. Both series show gradually increasing trends over the firing range. This was likely because the pores generated by the decomposition of carbonates were filled with the glass viscous flow. The average particle density after a 20 wt.% glass addition was 1.08 g/cm<sup>3</sup> at 1110 °C and this increased to 1.27 g/cm<sup>3</sup> at 1170 °C. This was higher after 40 wt.% addition, 1.28 g/cm<sup>3</sup> at 1110 °C and a further increase to 1.71 g/cm<sup>3</sup> at 1170 °C were measured. It is worth pointing out that with 20 wt.% the material particle densities at the lower firing range were comparable to those measured for Lytag.

Figure 7.3c shows the effect of firing temperature on particle densities of EDC-LWA with 20 wt.% and 40 wt.% added glass. For the 20 wt.% series, the average particle density increased from 1.35 g/cm<sup>3</sup> to 1.86 g/cm<sup>3</sup> when the firing temperature was increased from 1160 °C to 1190 °C. This was a small increase compared to those measured for EDC-LWA at the equivalent firing temperatures. The increase was more evident when the glass content was doubled. For the 40 wt.% series the average particle density was 1.9 g/cm<sup>3</sup> and reached its maximum of 2.1 g/cm<sup>3</sup> at 1180 °C. This increase was because glass had a negative effect on bloating capability of EDC, which was investigated by SEM microstructural analysis in section 7.5.3. Overall particle densities were higher than those measured for Lytag and LECA in both series.

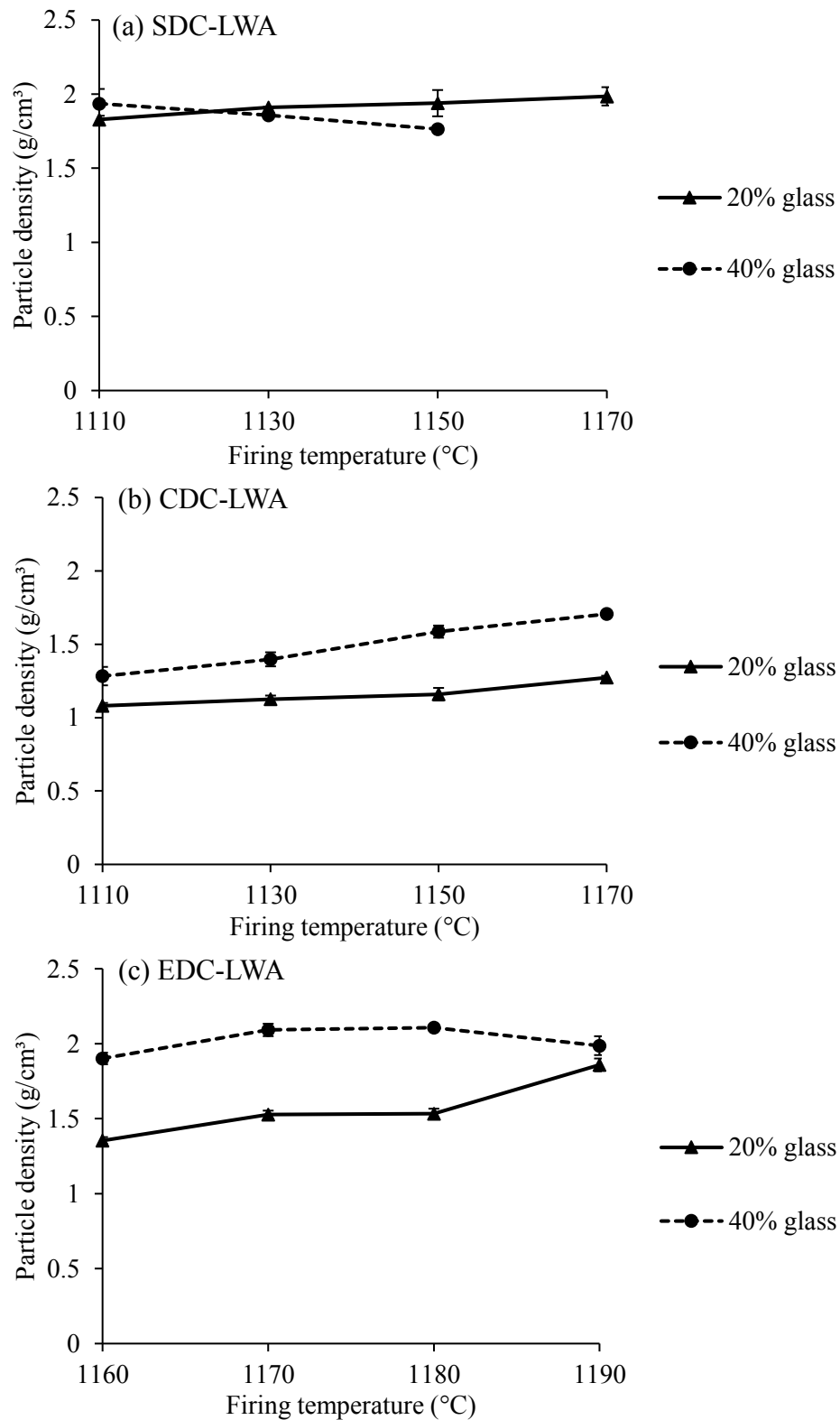


Figure 7.3 Effects of firing temperature on particle density of (a) SDC-LWA, (b) CDC-LWA and (c) EDC-LWA with 20 wt.% and 40 wt.% glass. Error bars are ± one standard deviation.

#### 7.4.2 Water absorption

Figure 7.4a shows the effect of firing temperature on 24-hour water absorption of SDC-LWA with 20 wt.% and 40 wt.% glass. For 20 wt.% series, the average water absorption decreased from 10.7% to 3.8% when the firing temperature was increased from 1110 °C to 1170 °C. This indicated an increase in sintering efficiency and thus reductions in open porosity of pellets. The water absorptions of SDC-LWA were in the range of 22.8% to 27.1% (Figure 5.2b). The effect of glass was more pronounced for pellets with 40 wt.% substitution where the water absorption remained stable between 2.5% and 2.8% over the applied firing temperature range. Obviously, water absorptions at both glass concentrations were lower than those measured for Lytag (20.5%) and LECA (32.7%).

Figure 7.4b shows water absorption of CDC-LWA with 20 wt.% and 40 wt.% glass. Two similar decreasing trends with an increase in firing temperature was observed in both series. The average water absorption for the series with 20 wt.% added glass was highest (39.3%) at 1110 °C and this decreased to 27.3% at 1170 °C. The 40 wt.% series, gave 20.5% at 1110 °C and this decreased to 5.3% at 1170 °C. These trends clearly showed the effect of glass on formation of a water-tight matrix and the fact that the degree of sintering increased with temperature. This experiment showed that for CDC-LWA adding 40 wt.% glass together with firing temperatures above 1130 °C were necessary to produce LWA with water absorption lower than Lytag.

Figure 7.4c shows a substantial reduction in the average water absorption of EDC-LWA with 20 wt.% glass from 30.4% at 1160 °C to 8.1% at 1190 °C. This indicates incomplete sintering at 1160 °C despite the presence of 20 wt.% of waste glass in the mix. This is possibly because the chemical composition of EDC produced a higher softening point and 20 wt.% glass was insufficient to reach the eutectic point (Kim, 2011). Only when 40 wt.% glass was added, it served as an effective sintering promoter reducing the average water absorption to 8.7% at 1160 °C and 0.4% at 1190 °C. Positively, 0.4% water absorption was the lowest achieved in the experiment on all the samples.

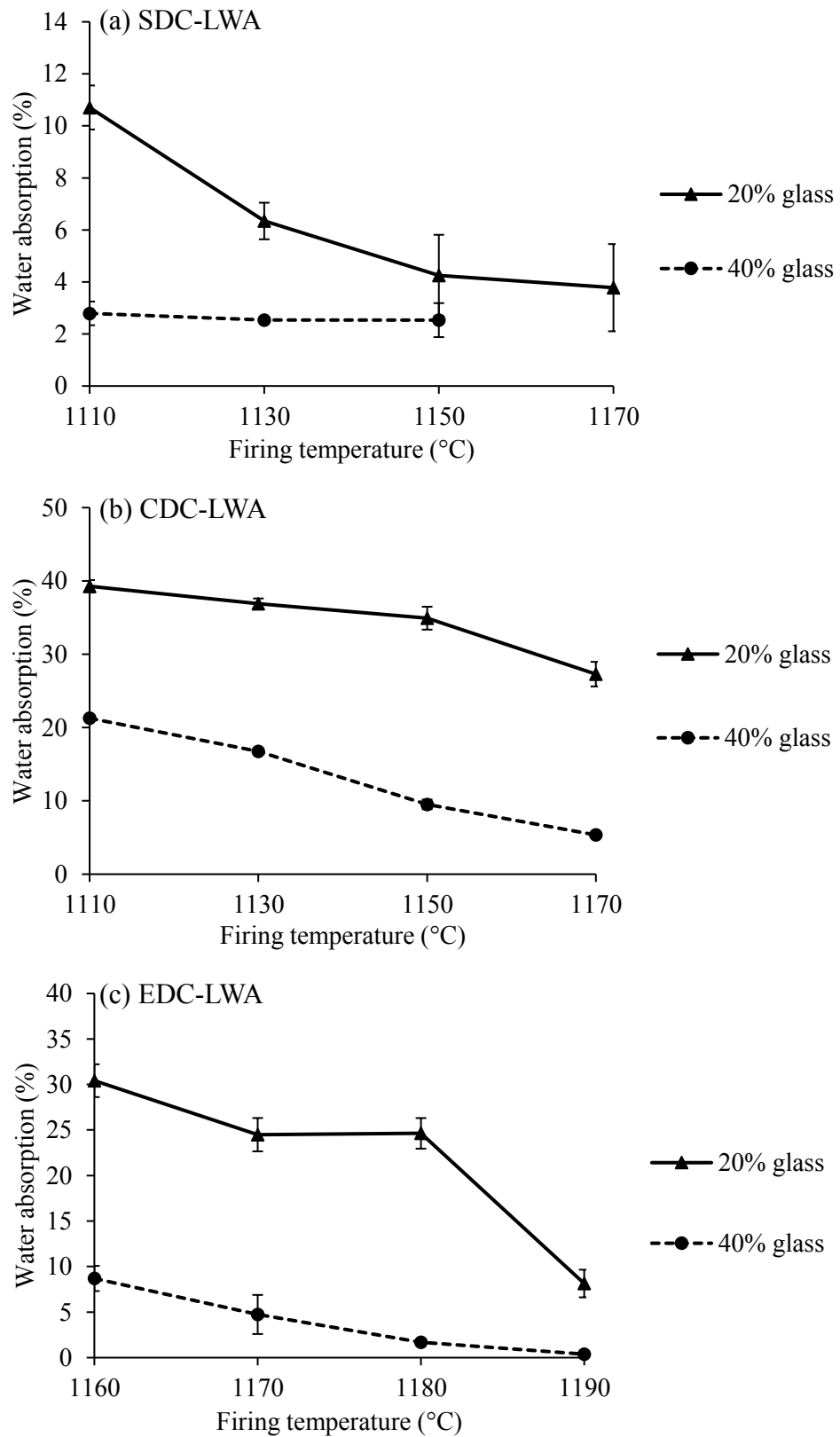


Figure 7.4 Effects of firing temperature on water absorption of (a) SDC-LWA, (b) CDC-LWA and (c) EDC-LWA with 20 wt.% and 40 wt.% glass. Error bars are  $\pm$  one standard deviation.

### 7.4.3 Compressive strength

Figure 7.5a shows the effect of firing temperature on the compressive strength of SDC-LWA containing 20 wt.% and 40 wt.% glass. For 20 wt.% series, the average compressive strength was 5.8 MPa at 1110 °C. It increased to 8.4 MPa with a 20 °C temperature rise and then decreased back to 5.8 MPa at 1170 °C. Despite the observed fluctuation, these compressive strengths were above those obtained for SDC-LWA where values below 1.0 MPa at higher firing temperatures had been obtained. This confirms the effective role of glass as a matrix forming material for use in drill cuttings LWA. For SDC-LWA containing 40 wt.% glass a compressive strength of 10.4 MPa at 1110 °C was measured and increasing the temperature reduced the strength to 7.9 MPa at 1130 °C and 8.7 MPa at 1150 °C due to the bloating effect. However, the measured particle density and water absorption of SDC-LWA after the glass addition revealed that a 40 wt.% substitution level was necessary for manufacturing LWA with comparable properties to those of commercial products (which is in agreement with the Kourti and Cheeseman (2010)). The compressive strength values after adding glass increased above the Lytag (3.2 MPa) and LECA (1.7 MPa).

Figure 7.5b shows the compressive strength of CDC-LWA with 20 wt.% and 40 wt.% glass. The average compressive strength for both series increased with temperature. At 1170 °C, it was measured 3.7 MPa for 20 wt.% series and 10.7 MPa for 40 wt.% series. The obtained compressive strengths show clearly that the added glass can improve pellet strength and produce superior LWA at lower temperature ranges. Compressive strength increased to values above those measured for Lytag after a 40 wt.% glass addition.

Figure 7.5c shows the compressive strength of EDC-LWA with 20 wt.% and 40 wt.% glass. The average compressive strength increased both as a function of temperature and the amount of glass added. The highest compressive strength, with 20 wt.% glass, was obtained at 1190 °C (5.75 MPa) which was also higher than those for EDC-LWA fired at the same temperature (3.78 MPa in Figure 5.4c). After a 40 wt.% addition, the average compressive strength reached 25.2 MPa at 1190 °C (which was the highest achieved in all fired batches in this study). This can be explained through the effect of liquid phase sintering as a result of a sufficient amount of flux and temperature - bringing the mixture above its eutectic point.

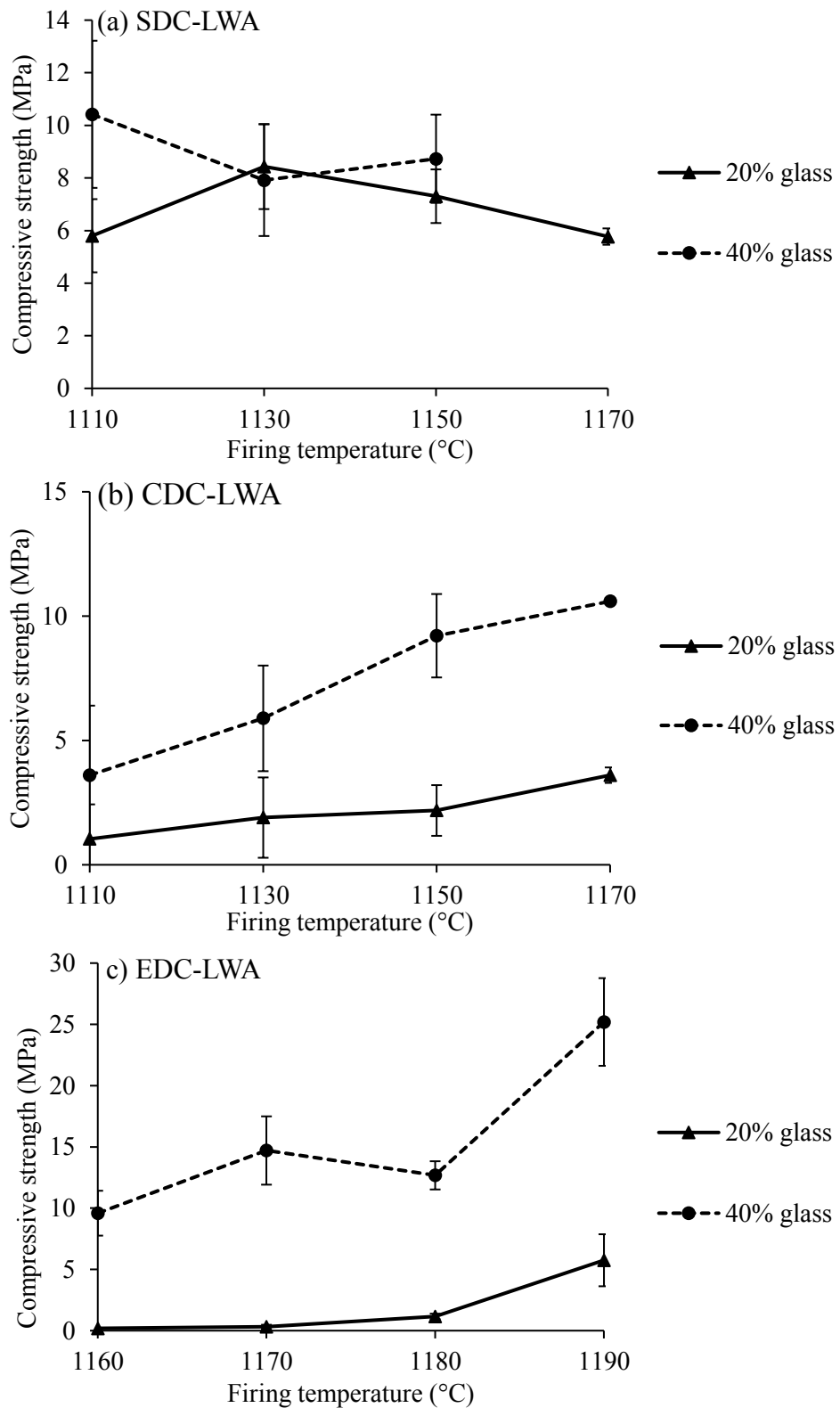


Figure 7.5 Effects of firing temperature on the compressive strength of (a) SDC-LWA, (b) CDC-LWA and (c) EDC-LWA with 20 wt.% and 40 wt.% glass. Error bars are  $\pm$  one standard deviation.

## 7.5 Effect of glass addition on microstructure

### 7.5.1 SDC-LWA

Figure 7.6 shows the SEM micrographs of SDC-LWA with 20 wt.% and 40 wt.% glass. For this analysis, the firing temperature was kept constant at 1150 °C (also optimum temperature for physical properties) to focus on the effect of different amounts of added glass on microstructure. Images were obtained from the core fracture surface and the outer surface of LWA.

The microstructure of fracture surface for SDC-LWA with 20 wt.% glass at 2000x magnification (shown in Figure 7.6a) appeared to be mainly composed of a continuous glass network holding the drill cutting particles together. No distinct pore formation with diameters in the range of 10 – 100 µm occurred however, the presence of spherical micropores in the continuous phase indicates some sort of local bubbling mechanism, as marked in the image. This is because the remaining space between relatively large particles of drill cuttings can produce a pathway for gases to escape, making the material incapable of bloating.

Figure 7.6b shows the outer surface of this sample. Some of the glass phase had migrated to the surface but not enough to close all the surface pores. Figure 7.6c shows the fracture surface after a 40 wt.% glass addition, where a well-formed dense matrix was effective in entrapping the gases and produced bubbles with >300 µm in diameter. It appears that most of the unreacted particles were transformed and re-crystallized/devitrified within the glass phase.

The outer surface of this pellet is shown in Figure 7.6d. It was observed that at a 40 wt.% glass addition, most of the surface pores were sealed by the continuous glass phase. This effect can be associated with the negligible water absorption capacity of this series (~ 2.5%) as previously measured (Figure 7.5a).

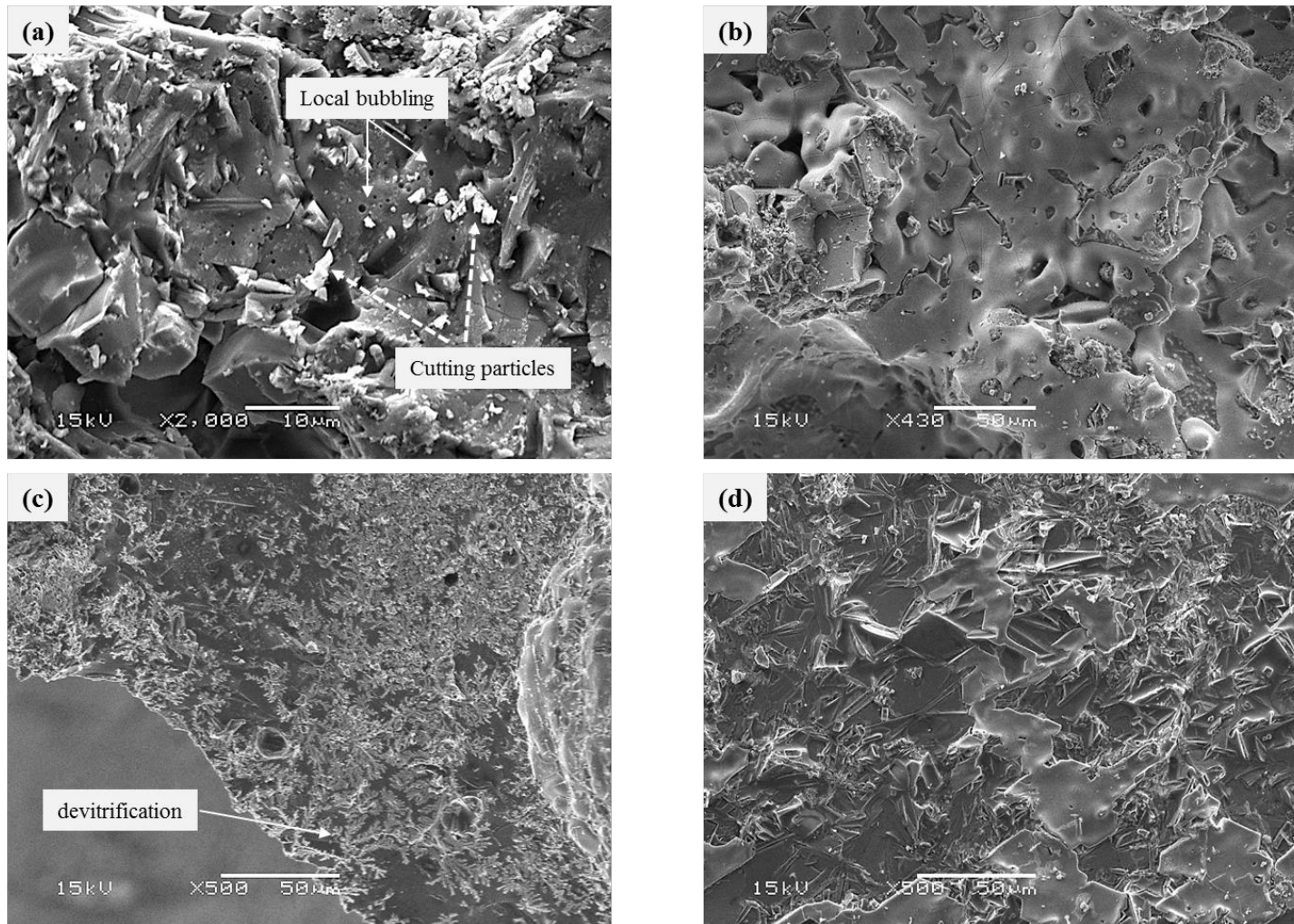


Figure 7.6 SEM micrographs of SDC-LWA fired at 1150 °C with: a) 20 wt.% glass (core fracture surface), b) 20 wt.% glass (outer surface), c) 40 wt.% glass (core fracture surface) and d) 40 wt.% glass (outer surface).

### 7.5.2 CDC-LWA

Figure 7.7 shows SEM micrographs of CDC-LWA with 20 wt.% and 40 wt.% glass. Pellets were chosen from the batch fired at 1150 °C (optimum temperature for physical properties). The SEM image of the fracture surface (Figure 7.7a) shows that 20 wt.% glass was effective in forming a matrix. Disconnected spherical pores with 10 – 30 µm in diameter were also present showing some degree of bloating. However, similar to SDC-LWA with 20 wt.% added glass, unreacted drill cutting particles are visible - hindering the material's potential for capturing the gas and provide water accessible routes to the matrix (water absorption up to 35% was measured for this batch). The outer surface of pellets (shown in Figure 7.7b) revealed an insufficient degree of particle fusion and large irregular macro-pores.

Figure 7.7c and show that the addition of 40 wt.% glass had a significant effect on both the closure of cavities and dissipation of drill cutting particles into the glass phase. A distinctive bloating with bubbles in the 10 – 100 µm range appeared in the matrix (the overview image of Figure 7.7c) however this did not cause a substantial decrease in the particle density since it was offset by a densifying (pore-filling) effect caused by the liquid flow of the glass phase. An important feature observed Figure 7.7d was the presence of hollow pointed pores on the pellets' outer surface. These were most likely the unreacted drill cutting particles that had a weak bond to the glass matrix and possibly detached during sample preparation.

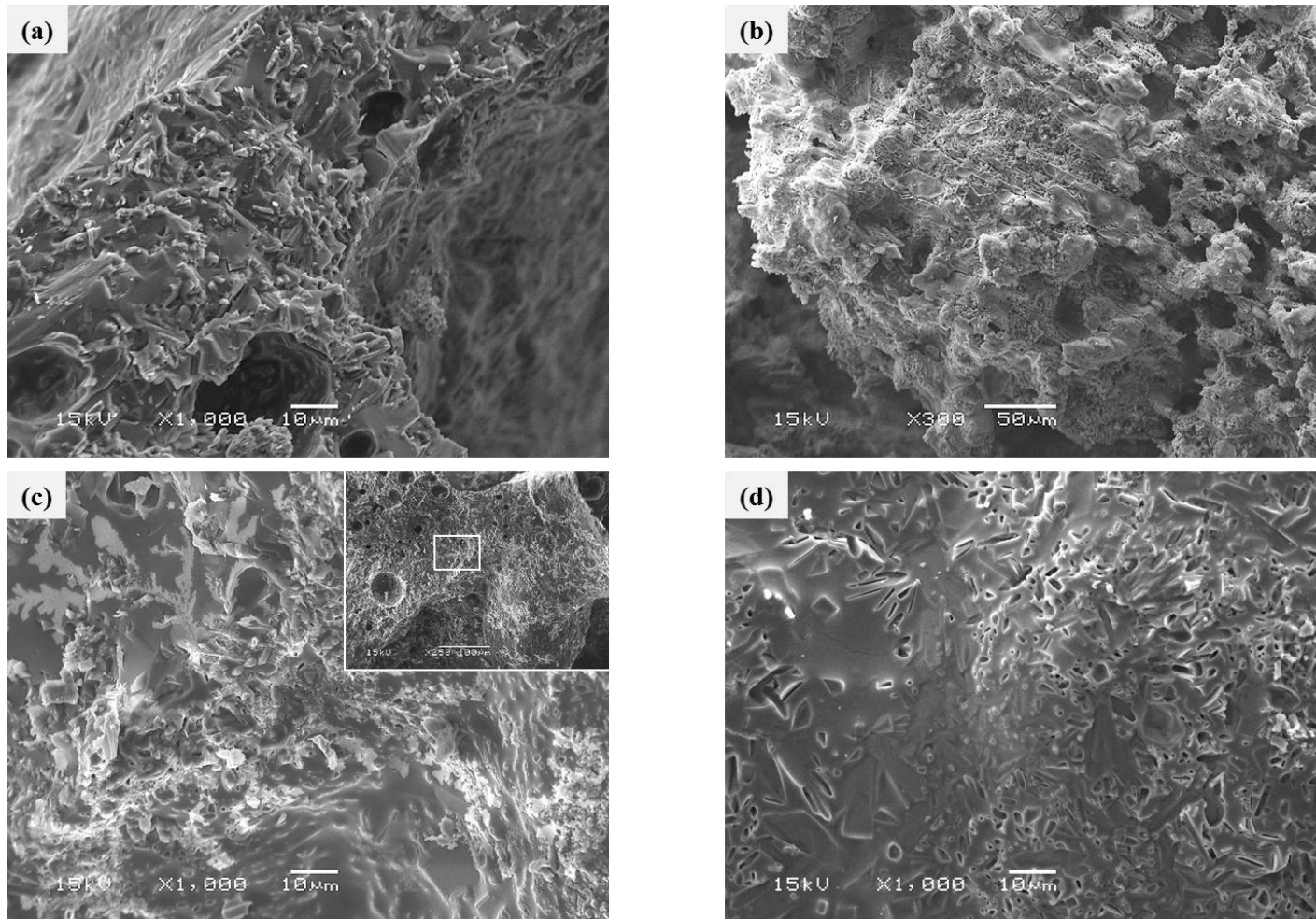


Figure 7.7 SEM micrographs of CDC-LWA fired at 1150 °C with: a) 20 wt.% glass (core fracture surface), b) 20 wt.% glass (outer surface), c) 40 wt.% glass (core fracture surface) and d) 40 wt.% glass (outer surface).

### 7.5.3 EDC-LWA

Figure 7.8 shows the SEM micrographs of EDC-LWA with 20 wt.% and 40 wt.% glass. Pellets were chosen from the batch fired at 1180 °C (optimum temperature for physical properties). SEM images revealed a different microstructure compare to the other two samples. The fracture surface of pellets with 20 wt.% glass (Figure 7.8a) shows an open pore network with cavities smaller than 10 µm in diameter, which can significantly increase the materials capillary water absorption (Mueller et al., 2015).

The image of pellets outer surface (Figure 7.8b) outlines the prevalence of the same microstructural features on the surface. The effect of increasing the added glass is obvious, as seen in Figure 7.8c, which shows that the majority of the cavities were filled as a result of the glass flow at high temperatures. This effect was also observed in SDC-LWA and CDC-LWA with the increase in the glass substitution level, and as discussed previously, would allow for the densification of the matrix (highlighted by an increase of particle density from 1.53 g/cm<sup>3</sup> to 2.11 g/cm<sup>3</sup>) and thus, enhance the compressive strength of the pellets (1.16 MPa to 12.68 MPa). Figure 7.8c also highlights the formation of bubbles, showing some degree of bloating in the matrix. This resulted in spherical pores (associated with bloating effect) seen at two different size ranges: those with average 10 µm in diameter and located in the vicinity of drill cutting particles (the presence which could provide the necessary gas phase for bloating), and those with an average diameter below 1 µm – that were isolated within the glass phase with limited gas to capture. However, the observed bloating effect was minimal and failed to reduce the density of EDC-LWA to below 2 g/cm<sup>3</sup>.

The latter pores could also be found in the continuous glass phase for other series. The effect of increasing the added glass from 20 wt.% to 40 wt.% can be visibly seen on the outer surface of the pellets (Figure 7.8d). The glass phase had covered most of the pellets' surface providing one of the lowest water absorption capacity measured in this study (1.7%).

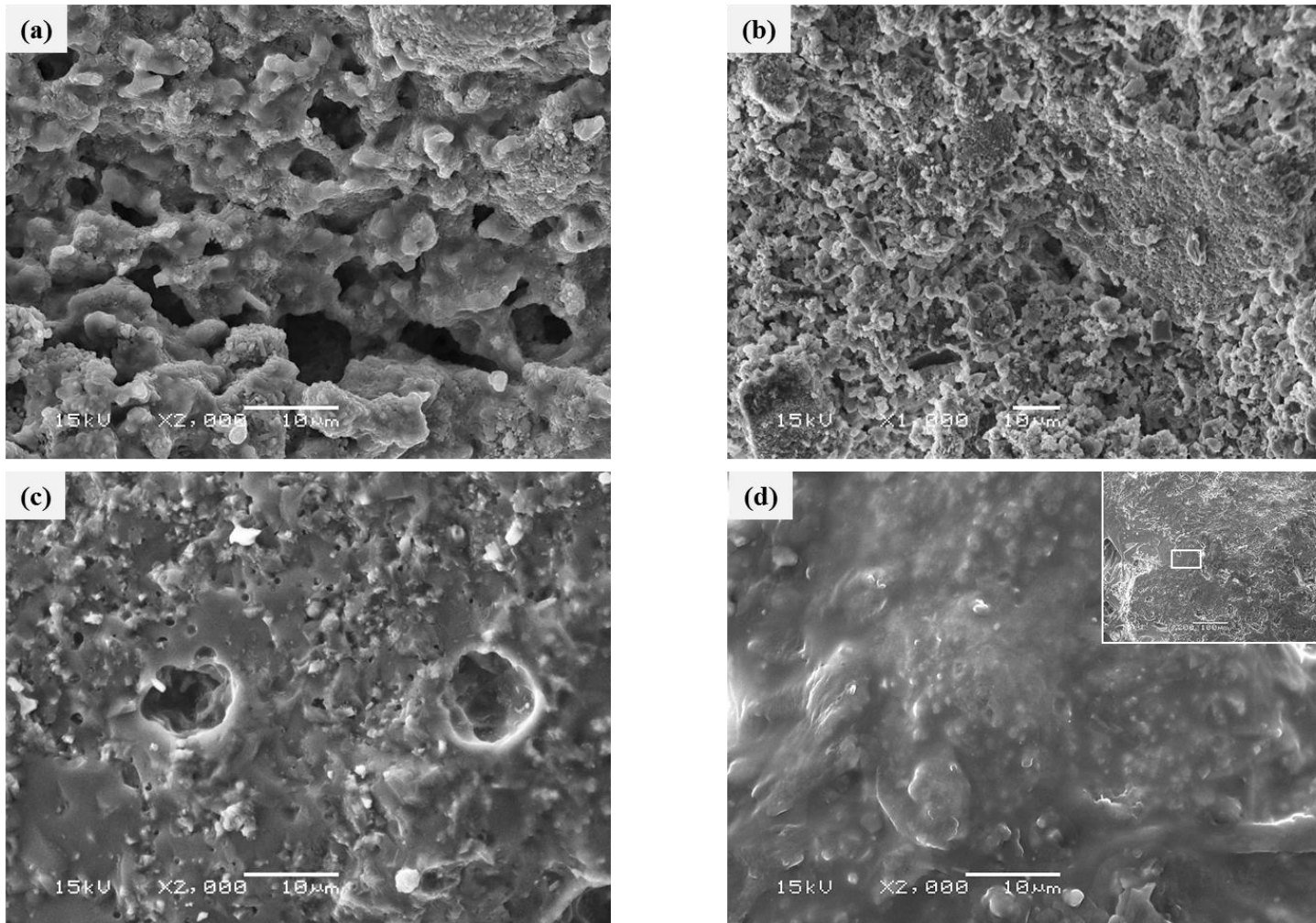


Figure 7.8 SEM micrographs of EDC-LWA fired at 1180 °C with: a) 20 wt.% glass (core fracture surface), b) 20 wt.% glass (outer surface), c) 40 wt.% glass (core fracture surface) and d) 40 wt.% glass (outer surface).

## 7.6 Effect of glass addition on mineralogy

### 7.6.1 SDC-LWA

For XRD analyses, a 40 wt.% glass addition was chosen to ensure the detection of phases neo-formed from the reaction of drill cuttings and waste glass. Figure 7.9 shows XRD patterns with markers at major crystalline phases for SDC-LWA containing 40 wt.% glass and fired at 1150 °C (the temperature at which optimal physical properties were achieved). The strongest BaSO<sub>4</sub> (211) reflection at 32.8 °2θ reduced indicating the possibility for incorporation of Ba into the amorphous phase. The quantification analysis (Table 7.3) also showed the contribution of BaSO<sub>4</sub> in the total crystalline phase to drop from 61.3% to 8.8%. The major neo-formed phases after the addition of glass were wollastonite (CaSiO<sub>3</sub>) and gehlenite (Ca<sub>2</sub>Al(SiAl)O<sub>7</sub>). These phases contributed to 38.6 wt.% and 16.8 wt.% of the crystalline phase respectively. They are formed due to the reaction of CaO from decomposition of calcium carbonate minerals with the present silica (from the added glass) and aluminosilicate compounds from dihydroxylation and/or decomposition of clay minerals (KAl<sub>2</sub>(Si<sub>3</sub>AlO<sub>10</sub>)(OH)<sub>2</sub> in the case of SDC (Poletini et al., 2004, Erol et al., 2008). The formation of CaSiO<sub>3</sub> phase has been associated to the enhancement of sintering behaviour (due to its relatively lower melting point), as well as improvement of immobilization capacity for leachable compounds (Wei et al., 2016). Dicalcium silicate (Ca<sub>2</sub>SiO<sub>4</sub>), and bredigite (Ca<sub>7</sub>Mg(SiO<sub>4</sub>)<sub>4</sub>) were also predicted to be present at 6.6 wt.% and 8.5 wt.%, respectively. High-temperature polymorphs of SiO<sub>2</sub> including cristobalite and tridymite were formed during the firing stage and quantified at 5.9 wt.% and 3.0 wt.%, respectively.

### 7.6.2 CDC-LWA

Figure 7.9 shows the XRD patterns for CDC-LWA with 40 wt.% added glass and fired at 1150 °C (the temperature of optimal physical properties). The main neo-formed phases identified were CaSiO<sub>3</sub>, Ca<sub>2</sub>Al(SiAl)O<sub>7</sub> and Ca<sub>2</sub>SiO<sub>4</sub>. Results of the quantification model shown in Table 7.3 predicted the contribution of these minerals to the total crystalline phase to be at 38.9 wt.%, 12.3 wt.% and 16.7 wt.%, respectively. Similar mechanisms for the formation of CaSiO<sub>3</sub> and Ca<sub>2</sub>Al(SiAl)O<sub>7</sub> to those observed for SDC-LWA with added glass can be recognised. However, the abundance of CaO in CDC-LWA at high temperatures has evidently favoured the formation of Ca<sub>2</sub>SiO<sub>4</sub> (16.7 wt.%). Minor amounts of hedenbergite (CaFeSi<sub>2</sub>O<sub>6</sub>: 4.0 wt.%) were predicted by the quantification

analysis; this could be explained due to the high concentration of iron oxide in CDC which could have been incorporated into the glass matrix to produce hedenbergite as a devitrification product (Müller and Rübner, 2006). High-temperature polymorphs of SiO<sub>2</sub> i.e. cristobalite and tridymite were also formed in this batch and their quantities were predicted to be 1.6 wt.% and 8.5 wt.%, respectively.

### 7.6.3 EDC-LWA

Figure 7.9 also shows the XRD patterns with markers for major crystalline phases for EDC-LWA with 40 wt.% added glass and fired at 1180 °C (the temperature at which optimal physical properties were achieved). The main neo-formed phases identified were MgCaSi<sub>2</sub>O<sub>6</sub> and sulpho-silicate hauyne (Na<sub>3</sub>Ca(Si<sub>3</sub>Al<sub>3</sub>)O<sub>12</sub>(SO<sub>4</sub>)). MgCaSi<sub>2</sub>O<sub>6</sub> was quantified at 71.2 wt.% of the total crystalline phase; as was the dominant neo-formed pyroxene in EDC-LWA found throughout the study. This was because the type of minerals from the solid solution series of the pyroxene group was dependent on elements such as Ca, Mg, Fe, etc. made available for reaction by decomposition of those phases present in the drill cutting samples (Polettini et al., 2004). For samples of EDC, high concentrations of CaMgCO<sub>3</sub> favour the Mg/Ca/Fe ratio and thus, promote the formation of MgCaSi<sub>2</sub>O<sub>6</sub>. Na<sub>3</sub>Ca(Si<sub>3</sub>Al<sub>3</sub>)O<sub>12</sub>(SO<sub>4</sub>) was quantified at 8.8 wt.% indicating the incorporation of SO<sub>4</sub><sup>-2</sup> into the aluminosilicate matrix.

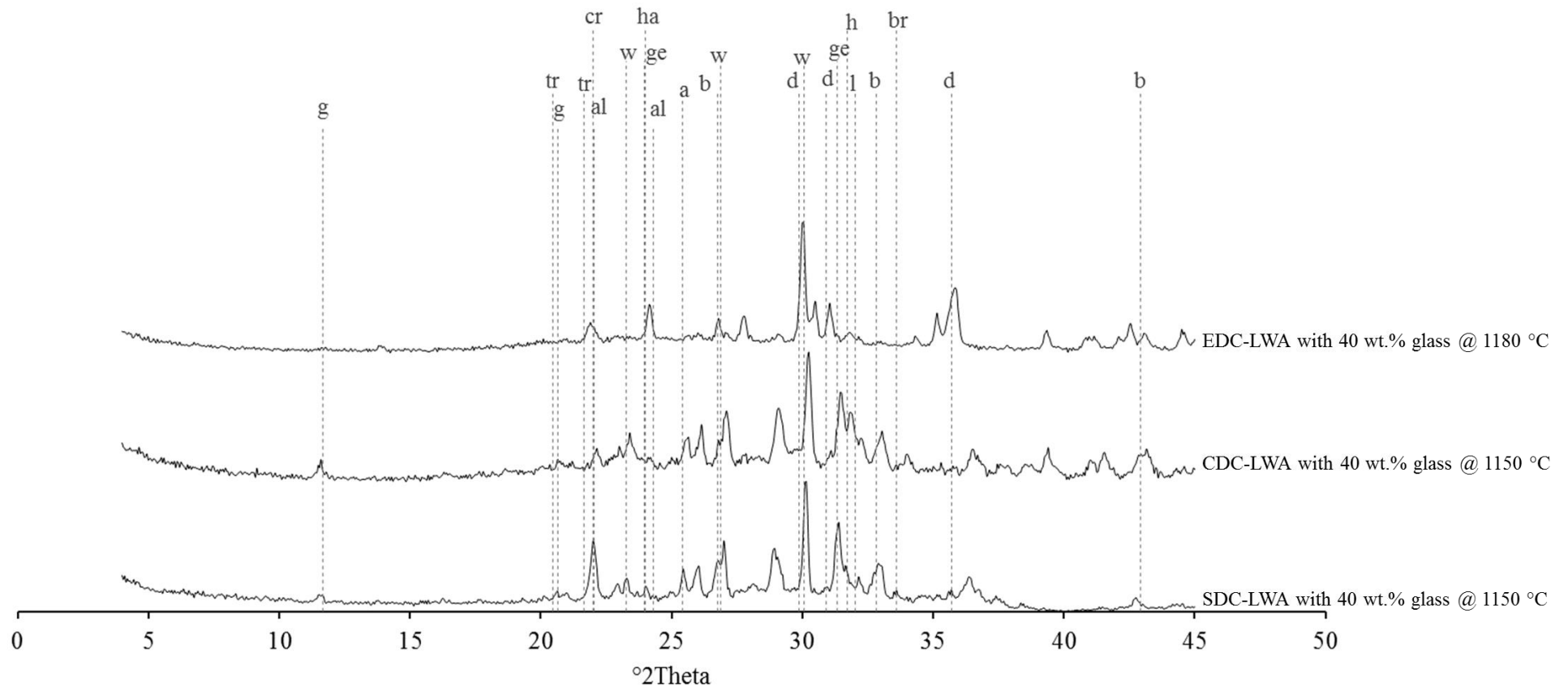


Figure 7.9 X-ray diffraction patterns with some important peak markers for crystalline phase identification in SDC-LWA, CDC-LWA and EDC-LWA with 40 wt.% glass. Markers on b: BaSO<sub>4</sub>, h: NaCl, g: CaSO<sub>4</sub>·2H<sub>2</sub>O, (d: MgCaSi<sub>2</sub>O<sub>6</sub>), al: NaAlSi<sub>3</sub>O<sub>8</sub>, l: Ca<sub>2</sub>SiO<sub>4</sub>, w: CaSiO<sub>3</sub>, ge: Ca<sub>2</sub>Al(SiAl)O<sub>7</sub>, tr: SiO<sub>2</sub> (tridymite), br: Ca<sub>7</sub>Mg(SiO<sub>4</sub>)<sub>4</sub> and cr: SiO<sub>2</sub> (cristobalite).

Table 7.3 Results of Rietveld quantification analysis for SDC-LWA, CDC-LWA and EDC-LWA with 40 wt.% glass.

Mineral	Chemical formula	SDC-LWA	CDC-LWA	EDC-LWA
Wollastonite	CaSiO <sub>3</sub>	38.6	38.9	5.7
Dicalcium silicate (C <sub>2</sub> S)	Ca <sub>2</sub> SiO <sub>4</sub>	6.6	16.7	-
Gehlenite	Ca <sub>2</sub> Al(SiAl)O <sub>7</sub>	16.8	12.3	-
Bredigite	Ca <sub>7</sub> Mg(SiO <sub>4</sub> ) <sub>4</sub>	8.5	-	-
Barite	BaSO <sub>4</sub>	8.8	11.0	3.8
Tridymite	SiO <sub>2</sub>	3.0	8.5	6.2
Halite	NaCl	0.7	1.6	0.6
Hedenbergite	CaFeSi <sub>2</sub> O <sub>6</sub>	-	4.0	-
Albite	NaAlSi <sub>3</sub> O <sub>8</sub>	1.7	1.5	1.2
K-feldspar	KAlSi <sub>3</sub> O <sub>8</sub>	0.0	0.9	-
Quartz	SiO <sub>2</sub>	3.4	1.9	0.8
Enstatite	MgSiO <sub>3</sub>	4.6	-	-
Cristobalite	SiO <sub>2</sub>	5.9	1.6	-
Diopside	MgCaSi <sub>2</sub> O <sub>6</sub>	1.0	-	71.2
Hauyne	Na <sub>3</sub> Ca(Si <sub>3</sub> Al <sub>3</sub> )O <sub>12</sub> (SO <sub>4</sub> )	-	-	8.0

## 7.7 Effect of glass addition on leaching characteristics

Table 7.4 shows the results of the batch leaching test (BS EN 12457-2) on SDC-LWA, CDC-LWA and EDC-LWA with 40 wt.% glass. The manufacturing conditions used for this experiment were those of XRD analyses (also the conditions at which optimal physical properties had been measured). Therefore, the firing temperature used for SDC-LWA and CDC-LWA was 1150 °C, and 1180 °C for EDC-LWA.

### 7.7.1 Heavy metals

The leaching test results showed 0.6 mg/kg of Ba, 0.4 mg/kg of Cr and 0.7 mg/kg of Mo in SDC-LWA with 40 wt.% glass (Table 7.4). The release of other heavy metals measured remained below the ICP-OES quantification limit. This suggested that the addition of glass did not interfere with the speciation of heavy metals in SDC as their release remained unchanged. Similar effects were observed for CDC-LWA and EDC-LWA where the concentrations of Cr and Mo were measured as 4.9 mg/kg and 1.4 mg/kg, and 0.5 mg/kg and 0.4 mg/kg, respectively. As discussed previously, the minor increase in solubility of these metals was due to the heat treatment and therefore was independent of the glass addition.

### 7.7.2 Cl<sup>-</sup>

Table 7.4 shows that adding 40 wt.% glass to SDC-LWA reduced the concentration of leachable Cl<sup>-</sup> from 7366 mg/kg in SDC and 2100 mg/kg in SDC-LWA without glass addition, down to 996.7 mg/kg. These results highlighted the dilution effect that glass addition had on Cl<sup>-</sup> and indicate that 40 wt.% replacement was sufficient to meet the EoW criteria.

For CDC-LWA pellets with 40 wt.% glass (Table 7.4), the concentration of leachable Cl<sup>-</sup> was measured as 3890 mg/kg. This was a significant reduction from Cl<sup>-</sup> measured as 11,946 mg/kg in CDC but more than that measured in CDC-LWA without glass addition, which was found to be below the ICP-OES detection limit (Table 4.6 and Table 5.3). As previously discussed in Chapter 5, the complete removal (evaporation) of Cl<sup>-</sup> in CDC-LWA was due to the higher temperature (1220 °C) used during the firing stage. However, in this chapter, Cl<sup>-</sup> was expected to remain in the material during the firing stage because at temperatures around 1150 °C, Cl<sup>-</sup> can only partially evaporate based on previous results

in earlier chapters. Therefore, the observed reduction was mainly associated to the dilution effect caused by the incorporation of glass.

Table 7.4 shows that the addition of 40 wt.% glass to EDC-LWA further reduced the leachable  $\text{Cl}^-$  from a previously reported 72% reduction (observed for EDC-LWA without glass incorporation in Table 5.3) to more than 92% as the leachable  $\text{Cl}^-$  concentration was reduced to 6593 mg/kg (from 85,712 mg/kg measured for EDC). These results again indicate the lack of physical encapsulation as a result of adding glass and the observed reduction in  $\text{Cl}^-$  was due to the dilution effect.

### 7.7.3 $\text{SO}_4^{-2}$

The concentration of leachable  $\text{SO}_4^{-2}$  in SDC-LWA with 40 wt.% glass increased to 17,263 mg/kg, as given in Table 7.4.  $\text{SO}_4^{-2}$  concentration of SDC and SDC-LWA without glass addition were 206.7 mg/kg and below the ICP-OES quantification limit, despite the presence of  $\text{BaSO}_4$  at high quantities (Table 4.6 and Table 5.3). Therefore, this indicates the formation of  $\text{SO}_4^{-2}$  phases with high solubility from a possible reaction between the added glass and  $\text{BaSO}_4$  at high temperatures. As shown in Figure 7.9, the appearance of a peak around  $11.7^\circ 2\theta$  associated to calcium sulphate dihydrate ( $\text{CaSO}_4 \cdot 2\text{H}_2\text{O}$ ) can support this hypothesis. In addition, a number of other  $\text{SO}_4^{-2}$ -bearing phases can also be formed, each with a concentration below the Rietveld quantification analysis limit of quantification. It must also be noted that the use of a lower firing temperature,  $1150^\circ\text{C}$ , would reduce the decomposition rate of any soluble  $\text{SO}_4^{-2}$  bearing phases that may have had neo-formed in the material.

Table 7.4 shows that for CDC-LWA with 40 wt.% glass, the concentration of leachable  $\text{SO}_4^{-2}$  increased to 23,741.8 mg/kg compared to CDC and CDC-LWA without glass addition in which  $\text{SO}_4^{-2}$  were measured as 1111 mg/kg and 9186 mg/kg. This again confirmed the possibility for formation of soluble  $\text{SO}_4^{-2}$  bearing compounds due to the reaction of glass with other  $\text{SO}_4^{-2}$  bearing phases present during the firing stage.

The concentration of leachable  $\text{SO}_4^{-2}$  in EDC-LWA with 40 wt.% was 11,068 mg/kg, as shown in Table 7.4. Comparing the measured concentration to those of EDC and EDC-LWA without added glass (45,248 mg/kg and 28,322 mg/kg, respectively), a significant reduction in  $\text{SO}_4^{-2}$  was evident. The formation of soluble  $\text{SO}_4^{-2}$  bearing phases during the firing stage was negligible due to the low concentration of  $\text{BaSO}_4$  compared to SDC and CDC. Consequently, the observed reduction in  $\text{SO}_4^{-2}$  points to the added glass having a

diluting effect but also the partial decomposition of  $\text{CaSO}_4$  (the major  $\text{SO}_4^{2-}$  bearing phase in EDC) should not be ruled out.

#### 7.7.4 $\text{F}^-$

The concentration of leachable  $\text{F}^-$  ions remained below the ICP-OES limit of quantification in samples of SDC-LWA with 40 wt.% added glass (Table 7.4). For CDC-LWA and EDC-LWA with 40 wt.% glass, this was 67.4 mg/kg and 34.5 mg/kg, respectively. These results showed that the addition of glass did not affect the leaching of  $\text{F}^-$ .

Table 7.4 Results of batch leaching test (BS EN 12457-2) on SDC-LWA, CDC-LWA and EDC-LWA with 40 wt.% added glass.

	SDC-LWA with 40 wt.% glass (mg/kg)	CDC-LWA with 40 wt.% glass (mg/kg)	EDC-LWA with 40 wt.% glass (mg/kg)
As	<1.582	<1.582	<1.584
Ba	0.6	0.5	0.4
Cd	<0.071	<0.071	<0.071
Cr	0.4	4.9	0.5
Cu	<0.712	<0.712	<0.712
Hg	<0.353	<1.158	<1.158
Mo	0.7	1.4	0.4
Ni	<0.325	<0.325	<0.325
Pb	<2.209	<2.209	<2.209
Sb	<0.858	<0.858	<0.858
Se	<1.008	<1.008	<1.008
Zn	<2.483	<2.483	<2.483
Cl <sup>-</sup>	996.7	3890.2	6593.3
F <sup>-</sup>	<20.3	67.4	34.5
SO <sub>4</sub> <sup>-2</sup>	17,263.7	23,741.8	11,068.3
DOC	<300.00	<300.00	<300.00
pH	10.19	11.78	9.98
Conductivity (μS/cm)	5684	4898	3732

## 7.8 Discussions

In this chapter, milled waste glass was initially identified as a suitable matrix forming material for incorporation in drill cuttings in order to improve structural/physical and leaching properties of the manufactured LWA. It was observed that the glass addition provided an extended sintering range and more importantly (in case of SDC-LWA and CDC-LWA) produced LWA with structural integrity at significantly reduced optimum firing temperature ranges (between 1110 °C to 1150 °C). This was up to 100 °C lower compared to LWA manufactured without glass addition and thus showed an important technological improvement for LWA manufacturing, both in terms of energy savings and control over the sintering process. This effect was less pronounced in EDC-LWA as the effective sintering range was extended to between 1160 °C and 1190 °C which was 15 °C lower than that measured in Chapter 4.

Similar trends on how glass affected the physical properties of all three drill cutting samples were observed. Particle density increased as more glass was incorporated into LWA; mainly due to pore-filling effects that would occur due to the glass viscous flow. Furthermore, glass also formed a matrix capable of bloating. This reduced the particle density of SDC-LWA with 40 wt.% glass, however, the effect of bloating on density was generally less dominant compared to the pore-filling mechanism. The particle densities of EDC-LWA obtained after 40 wt.% glass addition increased to between 1.9 g/cm<sup>3</sup> and 2.1 g/cm<sup>3</sup>, which were in the range of normal weight aggregates.

The addition of glass also had a positive effect on water absorption due to a similar mechanism. This was evident in CDC-LWA where the open porosity produced by the decomposition of carbonates were filled with the glass flow, reducing water absorption from 36% to 5% (after 40 wt.% glass addition). The very low water absorptions of drill cuttings derived LWA is beneficial to the concrete mix. This is because properties of hardened concrete are highly sensitive to variations in water-to-cement (w/c) ratios that are caused by LWA with high water absorbency (Nadesan and Dinakar, 2017).

The greatest influence of glass addition was arguably on the LWA compressive strength. An increasing effect on compressive strength with the amount glass and temperature was observed in most cases - but especially in case of SDC-LWA and CDC-LWA, the addition of glass was found to be essential at shifting the strength from below 1 MPa to ideal values in the range of 8 – 10 MPa.

Batches with optimal physical properties were identified for SDC-LWA and CDC-LWA (densities of EDC-LWA were not in the range of the British Standard (BS EN 13055-1) for LWA). These batches include:

1. SDC-LWA with 40 wt.% glass fired at 1150 °C – produced sintered pellets with 1.70 g/cm<sup>3</sup> particle density, 2.5% water absorption and 8.7 MPa compressive strength.
2. CDC-LWA with 40 wt.% glass fired at 1150 °C – produced sintered pellets with 1.58 g/cm<sup>3</sup> particle density, 9.5% water absorption and 9.2 MPa compressive strength.

The effect of glass addition on physical properties could be observed in LWA microstructure. A continuous glassy phase appeared both on the core fracture surface and the outer surface of LWA, which held unreacted drill cutting particles together, reduced the porosity generated due to decomposition reactions, and in case of EDC, filled the oil burn-off open channels. Another prevalent microstructural feature was the appearance of devitrification products in the continuous phase indicating neo-formed phases from the reaction of glass and drill cuttings. These all contributed to the improvement of physical properties.

Similar neo-formation mechanisms were seen in LWA following the reaction of the added glass with certain minerals in drill cuttings, yet the nature of these neo-formed phases was greatly influenced by the concentration of other major metal oxides in the mix. Since all three samples of drill cuttings were rich in carbonate minerals, glass could react with highly-reactive CaO at high temperatures to form minerals belonging to the inosilicate group (including pyroxene and pyroxenoid). The neo-formed phases were affected by the proportions of Ca/Mg/Fe. SDC and CDC (rich in CaCO<sub>3</sub>) reactions with glass produced CaSiO<sub>3</sub>. The presence of Fe<sub>2</sub>O<sub>3</sub> promoted the formation of CaFeSi<sub>2</sub>O<sub>6</sub> in CDC-LWA. EDC (rich in CaMgCO<sub>3</sub>) reaction with glass produced MgCaSi<sub>2</sub>O<sub>6</sub> as the most abundant neo-formed pyroxene phase.

The addition of glass did not affect the concentration of leachable heavy metals in the manufactured LWA and most of the measured concentrations remained below the EoW criteria or ICP-OEC limit of quantification. Glass had a diluting effect on the concentration of leachable Cl<sup>-</sup>, since the amount of Cl<sup>-</sup> leached per mass of drill cuttings was almost equal after the addition of waste glass to the mix (Leonard and Stegemann, 2010). This was effective to reduce the Cl<sup>-</sup> to below the EoW criteria in SDC-LWA after

40 wt.% glass addition. However, it was evident that glass despite its excellent matrix forming capabilities did not provide any effective physical encapsulation mechanism and the  $\text{Cl}^-$  concentration remained significant in EDC-LWA after 40 wt.% of waste glass was added. This shows that for samples of drill cuttings with high initial  $\text{Cl}^-$  content (such as in EDC: >85,000 mg/kg), employing a washing treatment would be a better option for mitigation, as shown in Chapter 6. The effect of glass on the release of  $\text{SO}_4^{2-}$  was variable (inconclusive). The formation of soluble  $\text{SO}_4^{2-}$  bearing compounds during firing increased and both dilution and decomposition decreased the concentration of leachable  $\text{SO}_4^{2-}$ .

## 8 Chapter 8 Estimation of energy and CO<sub>2</sub> emissions for production of drill cuttings LWA

The CO<sub>2</sub> emissions for the production LWA come mainly from excavation, transportation of the raw materials and the manufacturing process. These need to be taken into account for a comprehensive and accurate estimation of the CO<sub>2</sub> emissions (Syngros et al., 2017). However, the use of mineral wastes such as drill cuttings in LWA can be associated with significant CO<sub>2</sub> saving. This is because the CO<sub>2</sub> associated with excavation of raw material can be eliminated, as the waste is normally available from industrial processes such as drilling operations for oil and gas extraction. Ideally, the CO<sub>2</sub> emissions from the production of a typical LWA can be estimated from an accurate Life Cycle Assessment (LCA) in which the transportation of raw materials to a LWA manufacturing plant will be highly site-specific (Napolano et al., 2016). This produces a significant variability in the estimated CO<sub>2</sub> emissions in different scenarios based on the distance between the plant and the waste stream.

The focus of this chapter was to calculate LWA CO<sub>2</sub> emissions during the manufacturing process of LWA, for which limited information is currently available. This was based on a new approach involving the construction of an energy balance to compare the energy produced within the system from the combustion of the drill cuttings oil fraction and the burner fuel and, the energy consumed during the drying and firing stage. For each type of drill cuttings sample under the study, the batch with optimal properties was selected for the calculation. These included SDC-LWA and CDC-LWA with 40 wt.% glass fired at 1150 °C and W5EDC-LWA fired at 1190 °C, as identified in the previous chapters. The results were compared to an estimation of CO<sub>2</sub> emissions conducted for LWA manufactured from PFA using sinter strand technology and that for a management scenario involving microwave-assisted thermal desorption.

### 8.1 Energy and CO<sub>2</sub> emissions

For LWA manufacturing, the main energy consuming stages are pellet drying and kiln firing, together with the energy lost from the system. The energy consumed during the mineral transformation and solid-phase sintering was assumed to be negligible compared to other sources and was therefore excluded from the calculations. Energy is generated in the system through combustion of hydrocarbons i.e. drilling fluids and burner fuels.

To reach a balanced energy flow in the system:

$$Q_d + Q_k + Q_l = Q_{c1} + Q_{c2} \quad 8.1$$

$Q_d$ : Energy for pellet drying;

$Q_k$ : Kilning energy;

$Q_l$ : Energy loss;

$Q_{c1}$ : Energy provided by burner;

$Q_{c2}$ : Combustion of drilling fluids;

Therefore, for each drill cuttings sample with specific oil content, the amount of energy available in the system can be calculated and compared to that required for the manufacturing process. For a system with optimal performance, these energies should be in the same range. If extra energy is provided from combustion, CO<sub>2</sub> emissions increase unnecessarily and, if there is a lack of combustion energy in the system, extra energy should be supplied by the burner to increase the kiln contents temperature for sintering to occur.

Pellets leaving the dryer were assumed to undergo 20 wt.% moisture reduction. It is estimated that industrial convection dryers typically consume 3.6 MJ/kg of water removed (Robinson et al., 2009). This way, the amount of removed water and the required energy for drying ( $Q_d$ ) was estimated.

The energy required in the kiln was calculated as:

$$Q_k = m_m C_{p,m} \Delta T \quad 8.2$$

$$C_{p,m} = \sum_{i=1}^{N_i} X_i C_{p,i} \quad 8.3$$

[Where,  $Q_k$  is the kilning energy for the temperature rise of both solids and gases in J.  $m_m$  is the mass of kiln contents in kg,  $C_{p,m}$  is the mix specific heat capacity (SHC) in kJ/kg.°C,  $X_i$  is the weight fraction of each component (solids and gases), and  $\Delta T$  is the kiln content temperature rise.]

SHC of dried pellets was calculated using the weight fractions of dry cuttings, drilling fluid and added glass. The values for materials SHC are shown in Table 8.1. SHC

estimated for clay was used for cuttings (Martin et al., 2003). From TPH analysis in Chapter 3, the majority of absorbed hydrocarbons in drill cuttings was determined to be poly-alpha-olefins with a chain length between C<sub>10</sub> to C<sub>25</sub>. For simplification, eicosane (C<sub>20</sub>H<sub>42</sub>: 282.556 g/mol and 47.01 MJ/kg heating value) was assumed as the synthetic-based drilling fluid (Bureau et al., 2002, Takai et al., 2005, Zamora et al., 2013).

The heat loss from the kiln was calculated based on the modelling of heat transfer through a pilot-scale rotary kiln (Martin et al., 2003). The kiln was assumed to be 1.5 m in length and 0.5 m in diameter with 90 mm alumina fibre insulation and stainless-steel cladding at 80 °C.

Table 8.1 Specific heat capacities used for mass and energy balance.

Specific heat capacity	Materials	(J/kg °C)	Reference
C <sub>p,c</sub> (J/kg °C)	Cuttings	880	(Martin et al., 2003)
C <sub>p,w</sub> (J/kg °C)	Water	4180	-
C <sub>p,h</sub> (J/kg °C)	Eicosane	2128	(Prosen and Rossini, 1954)
C <sub>p,g</sub> (J/kg °C)	Glass	840	(Kandare et al., 2011)
C <sub>p,air</sub> (J/kg °C)	Air	1005	-

Q<sub>c1</sub> and Q<sub>c2</sub> for the burner fuel and drilling fluid combustion are calculated as:

$$Q_c = Q_{c1} + Q_{c2} = m_1 H_{v,p1} + m_2 H_{v,p2} \quad 8.4$$

[Where, H<sub>v,p</sub>, is the heating value (enthalpy of combustion) of hydrocarbons in J/kg and m is the mass of the fuel combusted in kg.]

To calculate Q<sub>c1</sub>, the amount of burner fuel that can provide a temperature rise of kiln contents until the flash point of drilling fluids, was calculated using 8.2 and 8.4. The flash point temperature (FPT) of drilling fluids is the minimum temperature at which sufficient vapour is produced to form a mixture capable of combustion after being ignited with the burner (Albahri, 2003). As the source of ignition is provided by the burner, the combustion can be assumed to be self-sustaining when the kiln contents are above FTP. In addition, the energy released from the combustion of drilling fluids can be used to elevate the kiln contents to the desired sintering temperature.

The initial temperature-rise for kiln contents (supplied by the burner) was assumed to be from 20 °C to 150 °C (FPT of eicosane). Burner fuel was assumed propane with 50.4 MJ/kg heating value with following combustion reaction:



The energy generated from combustion of drilling fluid ( $Q_{c2}$ ) was used for the temperature-rise of kiln contents from 150 °C to 1150 °C (for W5EDC-LWA a temperature-rise to 1190 °C was used). The amount of air required for combustion was calculated based on the required oxygen to complete the drilling fluid combustion. For the calculations, air/oxygen ratio of 4.32 and 30% excess dry air for combustion were used.

To simplify the calculation of the energy required for kiln gases temperature rise, it is assumed that the kiln environment is filled with air, water and CO<sub>2</sub> generated from the burner (equation 8.5) and combustion of drilling fluid (equation 8.6):



The propane and drilling fluid (eicosane) combustion reactions (8.5 and 8.6, respectively) were used for the calculation of CO<sub>2</sub> emissions from combustion.

## 8.2 Results and discussions

Table 8.2 shows the results of energy and CO<sub>2</sub> emissions for 1.0 tonne of LWA produced from each type of drill cuttings. For SDC-LWA with 40 wt% added glass, it was calculated that 4770 MJ energy is generated from the combustion of drilling fluid and burner fuel. This is more than 2808 MJ required for the pellets drying, kiln content temperature rise and energy loss. This provides 1962 MJ extra energy in the system that should be removed from the system to avoid melting. For CDC-LWA with 40 wt.% glass, the excess energy from combustion was calculated to be higher at 2909 MJ due to the high drilling fluid content in CDC. The difference was calculated as the lowest amount (921.7 MJ) for W5EDC-LWA highlighting a system operating closer to the balanced point; where the energy available from combustion is sufficient to be used for pellet drying and kiln firing.

To compare these results with CO<sub>2</sub> emissions data of PFA-LWA, a transportation scenario with 150 km distance (used by Sarabèr et al. (2012)) between the waste stream and production plant was assumed. Total CO<sub>2</sub> emissions for the three optimal batches of drill cuttings were given in Table 8.2. The CO<sub>2</sub> emissions for 1.0 tonne of SDC-LWA with 40 wt.% glass were calculated as 336.7 kg while the lowest emissions were for production of W5EDC-LWA as 236.0 kg. The CO<sub>2</sub> emissions for W5EDC-LWA was also comparable with that of PFA-LWA. For this reason, W5EDC-LWA was identified as the optimal product manufactured in this study in terms of both CO<sub>2</sub> emissions and, physical and environmental properties discussed in the previous chapters.

These results show the importance of the remaining fraction of drilling fluids on cuttings as the main contributor to the release of CO<sub>2</sub>. High drilling fluid contents (despite being beneficial in providing the kilning energy) can be disadvantageous for LWA CO<sub>2</sub> emissions and thus, should be avoided if possible. The reduction of oil content can be achieved through common separation techniques such as shale shaker, hydro-cyclones and centrifuge decanting, as discussed in section 2.1.3, however, the estimated results suggest that the addition of waste glass to the mix, to dilute the total hydrocarbon content, could also be considered as a viable option.

An estimation of CO<sub>2</sub> emissions for microwave-assisted thermal desorption of 1.0 tonne of waste drill cuttings, including the transport and solid waste final disposal, was also given in Table 8.2. The case study calculation used a multi-criteria LCA for drill cuttings produced in the offshore Brazilian pre-salt area (de Almeida et al., 2017). The estimation

showed approximately 1566 MJ energy consumption for a management scenario involving microwave treatment. As discussed in Chapter 2, thermal desorption techniques require high amounts of energy to elevate the temperature of drill cuttings to approximately 600 °C. CO<sub>2</sub> emissions were accordingly high for this management scenario (409 kg CO<sub>2</sub> per 1.0 tonne of drill cuttings) due to the additional CO<sub>2</sub> associated with transport and disposal of the treated solid waste at the end of the process. This shows that the CO<sub>2</sub> emissions calculated for drill cuttings LWA compare favourably to that of a management scenario involving microwave assisted thermal desorption.

Table 8.2 Estimation of energy required and total CO<sub>2</sub> for the manufacture of 1.0 tonne drill cuttings LWA.

Cuttings type	SDC- LWA	CDC- LWA	W5EDC- LWA	PFA-LWA (Sarabèr et al., 2012)	Microwave and disposal (de Almeida et al., 2017)
Glass (wt.%)	40	40	-		
TPH (wt.%)	12.3	14.3	5.6		
H <sub>2</sub> O <sup>1</sup> (wt.%)	10.2	8.1	6.2		
T <sup>2</sup> (°C)	1150	1150	1190		
Q <sub>d</sub> (MJ)	245.3	190.4	237.9		
Q <sub>k</sub> (MJ)	2549.4	2823.8	2088.4		
Q <sub>l</sub> (MJ)	13.5	13.5	13.5		
Total (MJ)	2808.2	3027.7	2339.8		
Q <sub>c1</sub> <sup>3</sup> (MJ)	366.6	407.4	288.7		
Q <sub>c2</sub> (MJ)	4404.2	5529.6	2972.8		
	4770.8	5937.0	3261.5		
CO <sub>2</sub> production (kg)	314.2	364.3	214.5		
CO <sub>2</sub> transportation <sup>4</sup> (kg)	22.5	22.5	22.5		
Total energy (MJ)				2.214.0	1566.0
Total CO <sub>2</sub> (kg)	336.7	386.8	236.0	221.0	409.0

<sup>1</sup> Moisture content calculated by a gravimetric method after extracting the TPH content and drying at 105 °C for 24 hours.

<sup>2</sup> T: Firing temperature.

<sup>3</sup> Minimum burner energy required to elevate the kiln content to 150 °C with propane as fuel and efficiency of 95%.

<sup>4</sup> CO<sub>2</sub> per tonne per 150 km for road transportation (Eurostat).

## 9 Chapter 9 Conclusions and future works

### 9.1 Conclusions

This research has investigated the use of waste drill cuttings from the oil and gas extraction operations in the North Sea, as a raw material for the manufacture of LWA. Samples of drill cuttings were characterised for chemical compositions, mineralogy, thermal behaviour, particle morphology and contaminant leaching. Properties of LWA manufactured by pelletising and firing drill cuttings were evaluated. The effect of washing on mitigating the release of soluble compounds was investigated. The addition of milled waste glass to the raw materials was explored and the effects on sintering properties, mineralogy, microstructure and leaching behaviour were determined. The carbon dioxide emissions for production of 1.0 tonne of LWA was estimated to determine the economic and environmental viability of the proposed reuse application for waste drill cuttings.

The main conclusions that can be drawn from this research are:

- 1) Different types of rock associated with petroleum geology, such as shale (source rock), carbonate (reservoir rock) and evaporite (seal or cap rock) were present in drill cutting samples. In addition, different offshore separation techniques for drilling fluids produce further compositional variabilities especially in the remaining additives such as weighting agent for drilling deep wells and the absorbed hydrocarbons on drill cuttings which act as major sources of contamination.
- 2) In shale-based (SDC) and carbonate-based (CDC) drill cuttings large quantities of  $\text{BaSO}_4$  and  $\text{CaCO}_3$  negatively affected the materials sintering efficiency and matrix formation during the firing stage and produced LWA with poor physical properties. Therefore, the incorporation of additional silica or aluminosilicate-based phases was essential to produce viable LWA. The research identified waste glass as a suitable matrix-forming material with an inert nature, large-scale availability and minimal compositional variability.
- 3) A 40 wt.% glass addition to SDC-LWA and CDC-LWA produced pellets with physical properties comparable to commercial products at 1150 °C: SDC-LWA had a particle density of 1.76 g/cm<sup>3</sup>, water absorption of 2.5% and compressive

strength of 8.7 MPa; CDC-LWA had a particle density of 1.58 g/cm<sup>3</sup>, water absorption of 9.5% and compressive strength of 9.2 MPa. Microstructures of LWA were also improved, as the glass viscous flow filled the pores generated from decomposition reactions, forming a matrix capable of bloating with gas bubbles in the size range of 10 µm to 500 µm. This effect produced low-density but high strength LWA. The migration of the glass phase to the pellets surface produced pore-free regions and reduced the water absorption. The low water absorptions obtained after the addition of glass made the manufactured LWA suitable for applications in concrete products.

- 4) The water-soluble concentrations of heavy metals in LWA were negligible. This was a long-term environmental advantage over other waste-derived LWA. However, in the case of evaporite-based drill cuttings (EDC), 85,812 mg/kg concentration of water-soluble Cl<sup>-</sup> caused a substantial leaching problem. Firing reduced this by 77% through volatilization of Cl<sup>-</sup>. Although some of the Cl<sup>-</sup> release was reduced due to the impermeable properties of the LWA matrix formed at high temperatures. Nevertheless, the effectiveness of firing in mitigation of Cl<sup>-</sup> was only partially successful as the manufactured LWA were still non-viable for concrete applications due to the criticality of the Cl<sup>-</sup>- induced corrosion of steel in reinforced concrete structures. Using a single-step washing pre-treatment (W1) at L/S ratio of 10 l/kg and duration of one hour for EDC, provided a 98% reduction in water-soluble Cl<sup>-</sup> in the fired samples. A two-step washing (W5) with a higher contact time further decreased the concentrations of Cl<sup>-</sup> in LWA to comply with the EoW criteria. W5EDC-LWA with an ideal pore structure and optimal properties i.e. particle densities of 1.38 g/cm<sup>3</sup>, water absorption of 8.9% and compressive strength of 6.3 MPa was successfully manufactured at 1190 °C.
- 5) Firing led to the formation of pyroxenes (mainly MgCaSi<sub>2</sub>O<sub>6</sub>) and feldspars (mainly NaAlSi<sub>3</sub>O<sub>8</sub> and CaAl<sub>2</sub>Si<sub>2</sub>O<sub>8</sub>). The type of pyroxene neo-formed was affected by the proportions of Ca/Mg/Fe in drill cuttings. CaSiO<sub>3</sub> was the most abundant mineral in SDC-LWA and CDC-LWA due to high concentrations of carbonates whilst MgCaSi<sub>2</sub>O<sub>6</sub> was quantified up to 71 wt.% of the crystalline phase in EDC-LWA, with high concentrations of Mg-bearing CaMgCO<sub>3</sub>. The formation of MgCaSi<sub>2</sub>O<sub>6</sub> was another advantage for the performance of LWA in

concrete products as it inhibits the expansive nature of alkali-silica reaction between cement and aggregate.

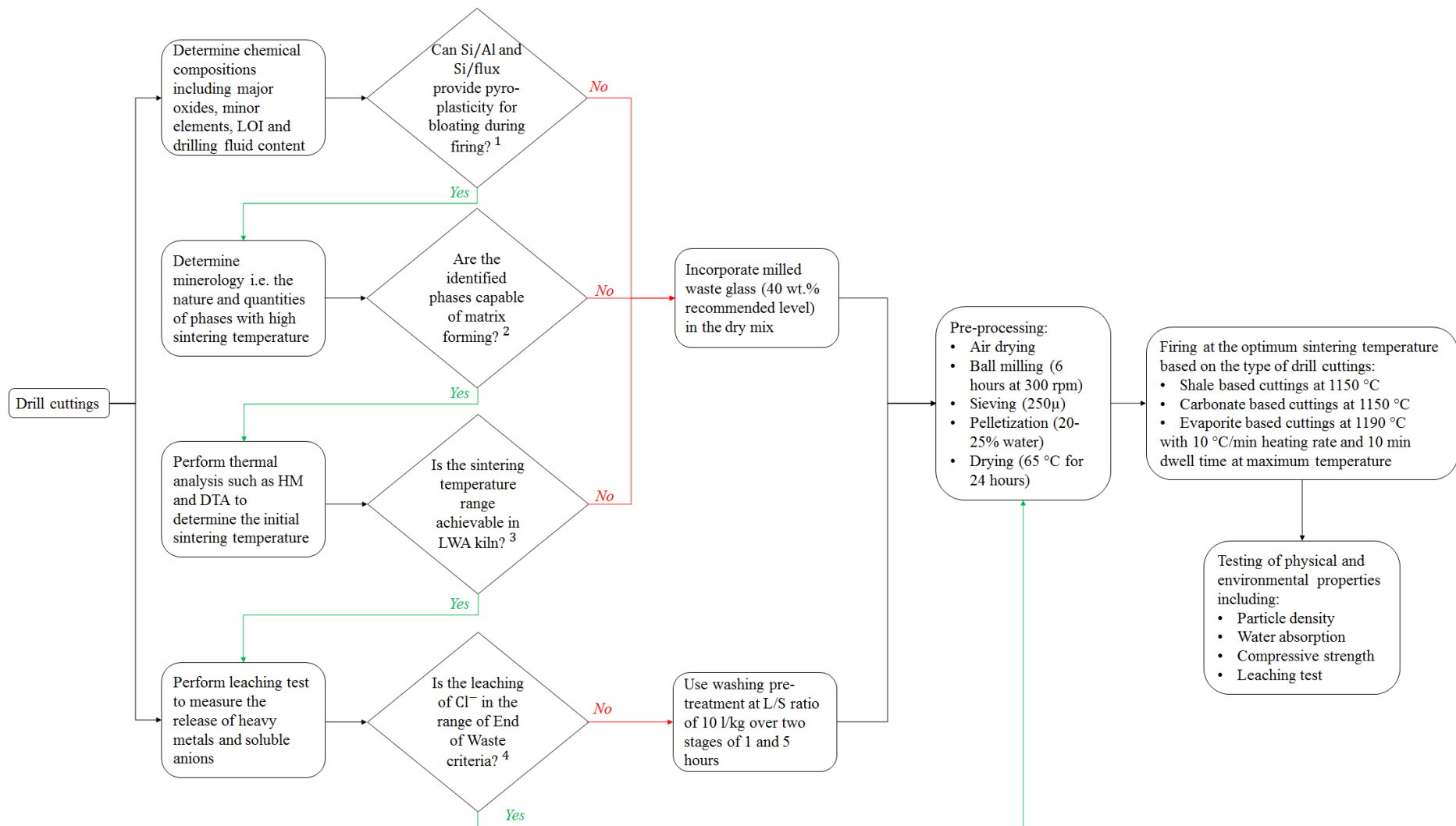
- 6) Firing drill cuttings with high drilling fluid contents (as in SDC and CDC) was problematic for  $\text{SO}_4^{-2}$  leaching because  $\text{BaSO}_4$  became reactive at high temperatures.  $\text{BaSO}_4$  also reacted with glass and increased the leaching of  $\text{SO}_4^{-2}$  however in drill cuttings with low drilling fluid contents (EDC) glass had a dilution effect and reduced the release of  $\text{SO}_4^{-2}$ . The mitigation of  $\text{SO}_4^{-2}$  remained a challenge and therefore must be considered for end-use applications where the presence of  $\text{SO}_4^{-2}$  can be tolerated.
  
- 7) The amount of  $\text{CO}_2$  emissions for production of drill cuttings LWA was also comparable to commercial products.  $\text{CO}_2$  emissions were calculated as 236.0 kg for production of 1.0 tonne of W5EDC-LWA and compared favourably to current management scenario for waste drill cuttings such as microwave assisted thermal desorption. The major source of  $\text{CO}_2$  emissions was the absorbed drilling fluid in the raw material. It was concluded that high concentrations of absorbed drill fluid (despite being beneficial in supplying the kilning energy) should be avoided. The optimization of this oil content can be achieved through separation techniques or with the addition of waste glass which results in a dilution effect of the oil content – reducing the release of  $\text{CO}_2$  emissions to ranges acceptable for the sustainability of manufacturing building materials.

## 9.2 Contribution to knowledge

- 1) A novel reuse application for problematic waste drill cuttings in the manufacture of LWA has been developed. This involved the expansion of knowledge on the chemical composition, mineralogy and environmental characteristics of waste drill cuttings. A production process framework for manufacturing LWA with optimal physical and environmental properties from various types of waste drill cuttings was constructed as shown in Figure 9.1.
- 2) To produce LWA with comparable properties to commercial products, pre-treatments, such as washing, and incorporation of secondary materials, such as waste glass, were investigated.
- 3) The study of crystalline phase transformations at high temperature, including the interaction of drill cuttings particles and those sintered with added glass, provided insight on the mechanism through which the neo-formed phases affect the leaching characteristics of LWA.
- 4) The research provided an improved understanding of the microstructure of LWA surface and internal porosity and their relation to physical properties of LWA – including particle density, water absorption and compressive strength.
- 5) A new approach for estimation of carbon dioxide emissions during production of LWA was presented. The research demonstrated that carbon dioxide emissions of drill cutting LWA, comparable to other waste-derived LWA, is achievable.

### 9.3 Production process framework

Figure 9.1 shows the production process framework for manufacturing LWA with optimal physical and environmental properties from various types of waste drill cuttings. The framework necessitates an initial comprehensive material characterization stage to determine the subsequent production method. If the presence of sufficient quantities of aluminosilicate phases, capable of forming a matrix and producing suitable pyro-plastic viscosity for bloating is confirmed (verified with methods such as x-ray fluorescence and x-ray diffraction analysis), drill cuttings can be used for LWA manufacturing. The sintering range for kiln firing can be determined through heating microscopy. The lack of matrix forming phases and high sintering ranges can be addressed by incorporating waste milled glass into the mix prior to firing. If drill cuttings contain high chloride contents, the framework suggests the use of a washing pre-treatment with deionised water. The pre-processing includes drying, milling and pelletisation. Optimum firing temperature should be based on the type of drilling cuttings available, as shown in Figure 9.1. The last stage is the analysis of the LWA physical and environmental properties, which must be determined and compared with technical and regulatory requirements.



1. Ranges suggested by Dondi et al., (2016): 4-5.6 for Si/Al and 4-7.6 for Si/flux should be used.
2. Barite (drilling additive) and carbonate minerals are problematic and must be quantified through XRD analysis.
3. The sintering range should be between 1050 °C and 1250 °C.
4. Waste acceptance criteria for inert landfill should be used.

Figure 9.1 Production process framework for manufacturing drill cuttings LWA.

#### 9.4 Recommendations for future work

This research has successfully manufactured LWA from SBM drill cuttings waste on a laboratory-scale. The feasibility for industrial/commercial scale-up is therefore vital since currently, no viable recycling option for drilling waste exists. Considering the state of oil and gas industry, it is clear that increased quantities of drilling waste will be produced and with no existing reuse technology being available, more waste is destined to landfills for the foreseeable future.

Manufacturing on a pilot scale using a gas-fired rotary kiln is strongly recommended. The discrepancies in properties of LWA manufactured on a laboratory-scale and pilot-scale due to pelletization methods, kiln entry temperature and, heating and cooling rates must be recognized. In addition, the assessment of technical viability for the manufacture of large quantities of LWA should involve the measurement of  $\text{Cl}^-$  and volatile metals emissions during the firing stage. Furthermore, to evaluate the commercial aspects LWA manufacture, feasibility studies looking at the logistics of building a production plant near onshore reception points/landfills would be valuable.

The removal of sulphates from drill cuttings with high initial concentration of anhydrite and gypsum via pre-treatments is a promising research topic. In addition, methods for transforming highly leachable  $\text{SO}_4^{2-}$  (produced at high temperatures) to non-soluble compounds should be investigated.

Other available standard leaching tests capable of simulating LWA end-use application scenarios such as backfilling, landscaping, and gardening should be explored. Column leaching test over a varying range of L/S ratios (0.1 l/kg to 10 l/kg) and pH-dependence leaching tests are recommended to simulate more extreme conditions.

The performance of LWA in concrete should also be studied and compared with commercial LWA such Lytag and LECA. Preliminary tests on the influence of drill cuttings LWA on the properties of concrete has been positive. In-depth studies on lightweight concrete mix-design for drill cuttings LWA and concrete durability should be examined with attention to the long-term release of sulphates.

## References

- 1999/31/EC (1999) 'Directive 1999/31/EC on the landfill of waste', *Off J Eur Union L*, 182, pp. 1-19.
- 2003/33/EC (2003) 'Council Decision 2003/33/EC of 19 December 2002 establishing criteria and procedures for the acceptance of waste at landfills pursuant to Article 16 of and Annex II to Directive 1999/31/EC', *Official Journal of the European Communities*, 16(2003), pp. L11.
- 2008/98/EC (2008) Directive 2008/98/EC of the European Parliament and of the Council of 19 November 2008 on waste: *The Official Journal of the European Union*, L, 312(13), pp.22-11.
- Abbas, Z., Moghaddam, A. P. and Steenari, B.-M. (2003) 'Release of salts from municipal solid waste combustion residues', *Waste management*, 23(4), pp. 291-305.
- Abbe, O., Grimes, S., Fowler, G. and Boccaccini, A. (2009) 'Novel sintered glass-ceramics from vitrified oil well drill cuttings', *Journal of materials science*, 44(16), pp. 4296-4302.
- Aboutabikh, M., Soliman, A. M. and El Naggar, M. H. (2016) 'Properties of cementitious material incorporating treated oil sands drill cuttings waste', *Construction and Building Materials*, 111, pp. 751-757.
- Adabi Firoozjaei, E., Koshy, P. and Rastkerdar, E. (2011) 'Effects of Different Barium Compounds on the Corrosion Resistance of Andalusite-Based Low-Cement Castables in Contact with Molten Al-Alloy', *Metallurgical and Materials Transactions B*, 42(4), pp. 901-913.
- Al-Ansary, M. S. and Al-Tabbaa, A. 'Stabilisation/solidification of synthetic North Sea drill cuttings containing oil and chloride'. Proceedings of the International RILEM Conference on Use of Recycled Materials in Building and Structures, 833-842.
- Al-Hamdan, A. Z. and Reddy, K. R. (2008) 'Electrokinetic remediation modeling incorporating geochemical effects', *Journal of geotechnical and geoenvironmental engineering*, 134(1), pp. 91-105.
- Albahri, T. A. (2003) 'Flammability characteristics of pure hydrocarbons', *Chemical Engineering Science*, 58(16), pp. 3629-3641.

- Ali, S. A., Clark, W. J., Moore, W. R. and Dribus, J. R. (2010) 'Diagenesis and reservoir quality', *Oilfield Review*, 22(2), pp. 14-27.
- Allegrini, E., Maresca, A., Olsson, M. E., Holtze, M. S., Boldrin, A. and Astrup, T. F. (2014) 'Quantification of the resource recovery potential of municipal solid waste incineration bottom ashes', *Waste Management*, 34(9), pp. 1627-1636.
- Allen, D. and Hayhurst, A. N. (1996) 'Reaction between gaseous sulfur dioxide and solid calcium oxide mechanism and kinetics', *Journal of the Chemical Society, Faraday Transactions*, 92(7), pp. 1227-1238.
- Alves, M. and Omotoso, O. (2009) 'Improving Rietveld-based clay mineralogic quantification of Oxisols using Siroquant', *Soil Science Society of America Journal*, 73(6), pp. 2191-2197.
- Anagnostopoulos, I. M. and Stivanakis, V. E. (2009) 'Utilization of lignite power generation residues for the production of lightweight aggregates', *Journal of Hazardous Materials*, 163(1), pp. 329-336.
- Arulrajah, A., Disfani, M. M., Maghoolpilehrood, F., Horpibulsuk, S., Udonchai, A., Imteaz, M. and Du, Y.-J. (2015) 'Engineering and environmental properties of foamed recycled glass as a lightweight engineering material', *Journal of Cleaner Production*, 94, pp. 369-375.
- Astrup, T., Dijkstra, J. J., Comans, R. N., van der Sloot, H. A. and Christensen, T. H. (2006) 'Geochemical modeling of leaching from MSWI air-pollution-control residues', *Environmental science & technology*, 40(11), pp. 3551-3557.
- Ayati, B., Ferrándiz-Mas, V., Newport, D. and Cheeseman, C. R. (2018) 'Use of clay in the manufacture of lightweight aggregate', *Construction and Building Materials*, 162, pp. 124-131.
- Bacocchi, R., Costa, G., Poletini, A., Pomi, R. and Prigiobbe, V. (2009) 'Comparison of different reaction routes for carbonation of APC residues', *Energy Procedia*, 1(1), pp. 4851-4858.
- Bai, Y., Ibrahim, R. and Basheer, P. M. 'Properties of lightweight concrete manufactured with fly ash, furnace bottom ash, and Lytag', *International workshop on sustainable development and concrete technology*, Beijing, 77-88.

- Bakke, T., Klungsøyr, J. and Sanni, S. (2013) 'Environmental impacts of produced water and drilling waste discharges from the Norwegian offshore petroleum industry', *Marine environmental research*, 92, pp. 154-169.
- Ball, A. S., Stewart, R. J. and Schliephake, K. (2012) 'A review of the current options for the treatment and safe disposal of drill cuttings', *Waste Management & Research*, 30(5), pp. 457-473.
- Barbudo, A., Galvín, A. P., Agrela, F., Ayuso, J. and Jiménez, J. R. (2012) 'Correlation analysis between sulphate content and leaching of sulphates in recycled aggregates from construction and demolition wastes', *Waste Management*, 32(6), pp. 1229-1235.
- Battaleb-Looie, S., Moore, F., Jacks, G. and Ketabdari, M. R. (2012) 'Geological sources of fluoride and acceptable intake of fluoride in an endemic fluorosis area, southern Iran', *Environmental geochemistry and health*, 34(5), pp. 641-650.
- Baykal, G. and Döven, A. G. (2000) 'Utilization of fly ash by pelletization process; theory, application areas and research results', *Resources, Conservation and Recycling*, 30(1), pp. 59-77.
- Beckhoff, B., Kanngießler, B., Langhoff, N., Wedell, R. and Wolff, H. (2007) *Handbook of practical X-ray fluorescence analysis*. Springer Science & Business Media.
- Bergmans, J., Nielsen, P., Snellings, R. and Broos, K. (2016) 'Recycling of autoclaved aerated concrete in floor screeds: Sulfate leaching reduction by ettringite formation', *Construction and Building Materials*, 111, pp. 9-14.
- Bernhardt, M., Justnes, H., Tellesbø, H. and Wiik, K. (2014a) 'The effect of additives on the properties of lightweight aggregates produced from clay', *Cement and Concrete Composites*, 53, pp. 233-238.
- Bernhardt, M., Tellesbø, H., Justnes, H. and Wiik, K. (2013) 'Mechanical properties of lightweight aggregates', *Journal of the European Ceramic Society*, 33(13–14), pp. 2731-2743.
- Bernhardt, M., Tellesbø, H., Justnes, H. and Wiik, K. (2014b) 'Fibre reinforced lightweight aggregates', *Journal of the European Ceramic Society*, 34(5), pp. 1341-1351.

- Bethanis, S., Cheeseman, C. and Sollars, C. (2002) 'Properties and microstructure of sintered incinerator bottom ash', *Ceramics International*, 28(8), pp. 881-886.
- Bethanis, S. and Cheeseman, C. R. 'Manufacture of Lightweight Aggregate from Incinerator Bottom Ash and Pulverised Fuel Ash'. Proceedings of the Heleco Conference, 2005: Citeseer.
- Bish, D. L. and Howard, S. (1988) 'Quantitative phase analysis using the Rietveld method', *Journal of Applied Crystallography*, 21(2), pp. 86-91.
- Bjørlykke, K. (1992) Clay minerals in North Sea sandstones. Available at: [archives.datapages.com](http://archives.datapages.com) (Accessed on 12/02/2018).
- Bjørlykke, K. (2015) ' Introduction to Petroleum Geology. In: Bjørlykke K. (eds) Petroleum Geoscience.', *Petroleum Geoscience*: Springer, Berlin, Heidelberg, pp. 1-29.
- Blengini, G. A., Busto, M., Fantoni, M. and Fino, D. (2012) 'Eco-efficient waste glass recycling: Integrated waste management and green product development through LCA', *Waste Management*, 32(5), pp. 1000-1008.
- Bloys, B., Davis, N., Smolen, B., Bailey, L., Houwen, O., Reid, P., Sherwood, J., Fraser, L., Hodder, M. and Montrouge, F. (1994) 'Designing and managing drilling fluid', *Oilfield Review*, 6(2), pp. 33-43.
- Boarder, R. F. W., Owens, P. L. and Khatib, J. M. (2016) 'The sustainability of lightweight aggregates manufactured from clay wastes for reducing the carbon footprint of structural and foundation concrete', *Sustainability of Construction Materials (Second Edition)*: Woodhead Publishing, , pp. 209-244.
- Bogush, A., Stegemann, J. A., Wood, I. and Roy, A. (2015) 'Element composition and mineralogical characterisation of air pollution control residue from UK energy-from-waste facilities', *Waste Management*, 36, pp. 119-129.
- Bollen, W. M. (1954) 'Thermal decomposition of calcium sulfate'.
- Bourtsalas, A., Vandeperre, L. J., Grimes, S. M., Themelis, N. and Cheeseman, C. R. (2015) 'Production of pyroxene ceramics from the fine fraction of incinerator bottom ash', *Waste Management*, 45, pp. 217-225.

- Bremner, T., Ries, J. and Wolfe, W. 'Environmentally Friendly Uses of Lightweight Aggregates'. Invited Paper Published in Proceedings of the International Symposium on Sustainable Development of Cement, Concrete Structures, VM Malhorta and K. Sakai, Oct, 5-7.
- Breuer, E., Shimmield, G. and Peppe, O. (2008) 'Assessment of metal concentrations found within a North Sea drill cuttings pile', *Marine Pollution Bulletin*, 56(7), pp. 1310-1322.
- Breuer, E., Stevenson, A. G., Howe, J. A., Carroll, J. and Shimmield, G. B. (2004) 'Drill cutting accumulations in the Northern and Central North Sea: a review of environmental interactions and chemical fate', *Marine Pollution Bulletin*, 48(1-2), pp. 12-25.
- British Geological Survey (2001) North Sea Geology: BGS. Available at: [https://www.gov.uk/government/uploads/system/uploads/attachment\\_data/file/197333/TR\\_SEA2\\_Geology.pdf](https://www.gov.uk/government/uploads/system/uploads/attachment_data/file/197333/TR_SEA2_Geology.pdf) (Accessed: 29/06/2016).
- British Glass (2008) Recycled Content Fact Sheet: British Glass Manufacturers Confederation. Available at: <http://www.britglass.org.uk/publications/recycled-content-fact-sheet> (Accessed: 02/06/2017).
- Brouwer, P. (2006) *Theory of XRF*. Almelo, Netherlands: PANalytical BV.
- BS EN 1097-6 (2013) Tests for mechanical and physical properties of aggregates. Determination of particle density and water absorption.
- BS EN 1484 (1997) Water analysis. Guidelines for the determination of total organic carbon (TOC) and dissolved organic carbon (DOC).
- BS EN 6068-2.46 (1995) Water quality. Determination of dissolved anions by liquid chromatography of ions. Determination of fluoride, chloride, nitrite, orthophosphate, bromide, nitrate and sulfate ions. Method for water with low contamination.
- BS EN 12457-2 (2002) Characterisation of Waste-Leaching-Compliance Test for Leaching of Granular Waste Materials and Sludges: Part 2. One Stage Batch Test at a Liquid to Solid Ratio of 10 L/kg for Materials with Particle Size below 4 mm (without or with Size Reduction).

- BS EN 12879 (2000) Characterization of sludges. Determination of the loss of ignition of dry mass.
- BS EN 13055-1 (2002) Lightweight aggregates. Part 1: Lightweight aggregates for concrete, mortar and grout.
- BS EN 14429 (2005) Characterization of waste. Leaching behaviour test. Influence of pH on leaching with initial acid/base addition.
- BS EN ISO 11885 (2009) Water quality. Determination of selected elements by inductively coupled plasma optical emission spectrometry (ICP-OES).
- BS EN ISO 16703 (2011) Soil quality. Determination of content of hydrocarbon in the range C10 to C40 by gas chromatography.
- Bureau, N., De Hemptinne, J., Audibert, A. and Herzhaft, B. 'Interactions Between Drilling Fluid and Reservoir Fluid'. SPE Annual Technical Conference and Exhibition: Society of Petroleum Engineers.
- Candler, J. E., Rushing, J. H. and Leuterman, A. J. J. 'Synthetic-based mud systems offer environmental benefits over traditional mud systems'. SPE/EPA Exploration and Production Environmental Conference: Society of Petroleum Engineers.
- CAPP (2001) CAPP (Canadian Association of Petroleum Producers). Technical Report: Offshore Drilling Waste Management Review, Canada.
- Chandler, A. J., Eighmy, T. T., Hjelm, O., Kosson, D. S., Sawell, S. E., Vehlow, J., van der Sloot, H. A. and Hartlén, J. (1997) *Municipal Solid Waste Incinerator Residues*. Elsevier Science.
- Chang, F.-C., Lo, S.-L., Lee, M.-Y., Ko, C.-H., Lin, J.-D., Huang, S.-C. and Wang, C.-F. (2007) 'Leachability of metals from sludge-based artificial lightweight aggregate', *Journal of Hazardous Materials*, 146(1–2), pp. 98-105.
- Cheeseman, C. R., Makinde, A. and Bethanis, S. (2005) 'Properties of lightweight aggregate produced by rapid sintering of incinerator bottom ash', *Resources, Conservation and Recycling*, 43(2), pp. 147-162.

- Cheeseman, C. R. and Viridi, G. S. (2005) 'Properties and microstructure of lightweight aggregate produced from sintered sewage sludge ash', *Resources, Conservation and Recycling*, 45(1), pp. 18-30.
- Chen, H.-J., Wang, S.-Y. and Tang, C.-W. (2010) 'Reuse of incineration fly ashes and reaction ashes for manufacturing lightweight aggregate', *Construction and Building Materials*, 24(1), pp. 46-55.
- Chen, H.-J., Yang, M.-D., Tang, C.-W. and Wang, S.-Y. (2012) 'Producing synthetic lightweight aggregates from reservoir sediments', *Construction and Building Materials*, 28(1), pp. 387-394.
- Chen, Z., Chen, Z., Yin, F., Wang, G., Chen, H., He, C. and Xu, Y. (2017) 'Supercritical water oxidation of oil-based drill cuttings', *Journal of Hazardous Materials*, 332, pp. 205-213.
- Chénard, P. G. 'Composition of oil-based drilling muds'. Report of the Workshop on Environmental Considerations in the Offshore Use of Oil-Based Drilling Muds, 23-4.
- Chiellini, E. (2008) *Environmentally Compatible Food Packaging*. Elsevier Science.
- Chimenos, J. M., Fernández, A. I., Cervantes, A., Miralles, L., Fernández, M. A. and Espiell, F. (2005) 'Optimizing the APC residue washing process to minimize the release of chloride and heavy metals', *Waste Management*, 25(7), pp. 686-693.
- Chindaprasirt, P., Jaturapitakkul, C. and Rattanasak, U. (2009) 'Influence of fineness of rice husk ash and additives on the properties of lightweight aggregate', *Fuel*, 88(1), pp. 158-162.
- Chiou, I.-J., Wang, K.-S., Chen, C.-H. and Lin, Y.-T. (2006) 'Lightweight aggregate made from sewage sludge and incinerated ash', *Waste Management*, 26(12), pp. 1453-1461.
- Clarkson, C. R., Solano, N., Bustin, R. M., Bustin, A. M. M., Chalmers, G. R. L., He, L., Melnichenko, Y. B., Radliński, A. P. and Blach, T. P. (2013) 'Pore structure characterization of North American shale gas reservoirs using USANS/SANS, gas adsorption, and mercury intrusion', *Fuel*, 103, pp. 606-616.

- Commission, O. (2004) OSPAR List of Substances/Preparations Used and Discharged Offshore which Are Considered to Pose Little or No Risk to the Environment (PLONAR). Available at: [https://www.cefas.co.uk/media/1384/13-06e\\_plonor.pdf](https://www.cefas.co.uk/media/1384/13-06e_plonor.pdf) (Accessed: 13/02/2018).
- Conklin, P., Drysdale, D., Doughtie, D., Rao, K., Kakareka, J., Gilbert, T. and Shokes, R. (1983) 'Comparative toxicity of drilling muds: role of chromium and petroleum hydrocarbons', *Marine environmental research*, 10(2), pp. 105-125.
- Coungny, G. (1990) 'Specifications for clayey raw materials used to produce expanded light-weight aggregates', *Bulletin of the International Association of Engineering Geology*, 41(1), pp. 47-55.
- Cresswell, D. (2007) Industrial sector study on the utilisation of alternative materials in the manufacture of manufactured aggregates. DEFRA Project Code WRT\_177 / WRO115. Mineral Industry Research Organisation (MIRO), Birmingham, UK., Birmingham, UK: Mineral Industry Research Organisation (MIRO).
- Cyr, M., Coutand, M. and Clastres, P. (2007) 'Technological and environmental behavior of sewage sludge ash (SSA) in cement-based materials', *Cement and Concrete Research*, 37(8), pp. 1278-1289.
- Davies, D. R. and Kitchener, J. N. (1996) 'Massive use of pulverised fuel ash in concrete for the construction of a U.K. power station', *Waste Management*, 16(1), pp. 169-180.
- Davies, J. M., Addy, J. M., Blackman, R. A., Blanchard, J. R., Ferbrache, J. E., Moore, D. C., Somerville, H. J., Whitehead, A. and Wilkinson, T. (1984) 'Environmental effects of the use of oil-based drilling muds in the North Sea', *Marine Pollution Bulletin*, 15(10), pp. 363-370.
- de' Gennaro, R., Cappelletti, P., Cerri, G., de' Gennaro, M., Dondi, M. and Langella, A. (2004) 'Zeolitic tuffs as raw materials for lightweight aggregates', *Applied Clay Science*, 25(1-2), pp. 71-81.
- de Almeida, P. C., Araújo, O. d. Q. F. and de Medeiros, J. L. (2017) 'Managing offshore drill cuttings waste for improved sustainability', *Journal of Cleaner Production*, 165, pp. 143-156.

- de Gennaro, R., Cappelletti, P., Cerri, G., de' Gennaro, M., Dondi, M., Graziano, S. F. and Langella, A. (2007) 'Campanian Ignimbrite as raw material for lightweight aggregates', *Applied Clay Science*, 37(1–2), pp. 115-126.
- de Gennaro, R., Cappelletti, P., Cerri, G., de'Gennaro, M., Dondi, M. and Langella, A. (2005) 'Neapolitan Yellow Tuff as raw material for lightweight aggregates in lightweight structural concrete production', *Applied Clay Science*, 28(1–4), pp. 309-319.
- De la Torre, A. G. and Aranda, M. A. G. (2003) 'Accuracy in Rietveld quantitative phase analysis of Portland cements', *Journal of Applied Crystallography*, 36(5), pp. 1169-1176.
- Dean, W. E. (2013) 'Marine Evaporites', in Harff, J., Meschede, M., Petersen, S. & Thiede, J. (eds.) *Encyclopedia of Marine Geosciences*. Dordrecht: Springer Netherlands, pp. 1-10.
- Deer, W. A., Howie, R. A. and Zussman, J. 'Rock-forming Minerals: Feldspars, Volume 4A'. Geological Society of London.
- DEFRA (2010) Department of Environment, Food and Rural Affairs. A Strategy for Hazardous Waste Management in England. Available at: <http://www.alpheus.co.uk/sites/default/files/inline-files/policy%5B1%5D.pdf> (Accessed: 13/02/2018).
- Defra (2011) Guidance on applying the waste hierarchy to hazardous waste Available at: [https://www.gov.uk/government/uploads/system/uploads/attachment\\_data/file/69457/pb13687-hazardous-waste-hierarchy-111202.pdf](https://www.gov.uk/government/uploads/system/uploads/attachment_data/file/69457/pb13687-hazardous-waste-hierarchy-111202.pdf) (Accessed: 03/05/2017).
- Degirmenci, N., Yilmaz, A. and Cakir, O. A. (2011) 'Utilization of waste glass as sand replacement in cement mortar', *Indian Journal of Engineering and Materials Sciences (IJEMS)*, 18(4), pp. 303-308.
- del Valle-Zermeño, R., Formosa, J., Chimenos, J. M., Martínez, M. and Fernández, A. I. (2013) 'Aggregate material formulated with MSWI bottom ash and APC fly ash for use as secondary building material', *Waste Management*, 33(3), pp. 621-627.
- Derie, R. (1996) 'A new way to stabilize fly ash from municipal incinerators', *Waste Management*, 16(8), pp. 711-716.

- Dhir, R., Csetenyi, L., Dyer, T. and Smith, G. (2010) 'Cleaned oil-drill cuttings for use as filler in bituminous mixtures', *Construction and Building Materials*, 24(3), pp. 322-325.
- Dijkstra, J. J., van der Sloot, H. A. and Comans, R. N. J. (2006) 'The leaching of major and trace elements from MSWI bottom ash as a function of pH and time', *Applied Geochemistry*, 21(2), pp. 335-351.
- Donatello, S. and Cheeseman, C. R. (2013) 'Recycling and recovery routes for incinerated sewage sludge ash (ISSA): A review', *Waste Management*, 33(11), pp. 2328-2340.
- Dondi, M., Cappelletti, P., D'Amore, M., de Gennaro, R., Graziano, S. F., Langella, A., Raimondo, M. and Zanelli, C. (2016) 'Lightweight aggregates from waste materials: Reappraisal of expansion behavior and prediction schemes for bloating', *Construction and Building Materials*, 127, pp. 394-409.
- Dou, X., Ren, F., Nguyen, M. Q., Ahamed, A., Yin, K., Chan, W. P. and Chang, V. W.-C. (2017) 'Review of MSWI bottom ash utilization from perspectives of collective characterization, treatment and existing application', *Renewable and Sustainable Energy Reviews*, 79, pp. 24-38.
- Ducman, V. and Mirtič, B. (2009) 'The applicability of different waste materials for the production of lightweight aggregates', *Waste Management*, 29(8), pp. 2361-2368.
- Ducman, V., Mladenović, A. and Šuput, J. S. (2002) 'Lightweight aggregate based on waste glass and its alkali-silica reactivity', *Cement and Concrete Research*, 32(2), pp. 223-226.
- Ducrotoy, J.-P., Elliott, M. and de Jonge, V. N. (2000) 'The North Sea', *Marine Pollution Bulletin*, 41(1-6), pp. 5-23.
- Eighmy, T. T., Eusden, J. D., Krzanowski, J. E., Domingo, D. S., Staempfli, D., Martin, J. R. and Erickson, P. M. (1995) 'Comprehensive approach toward understanding element speciation and leaching behavior in municipal solid waste incineration electrostatic precipitator ash', *Environmental science & technology*, 29(3), pp. 629-646.
- Environment Agency (2006) *The Determination of Metals in Solid Environmental Samples: Methods for the Examination of Waters and Associated Materials.*

Available at: <https://www.gov.uk/government/publications/standing-committee-of-analysts-sca-blue-books> (Accessed: 03/03/2016).

Environment Agency (2012) Treating waste by thermal desorption – Addendum to S5.06.

Available at: <http://webarchive.nationalarchives.gov.uk/20140328084622/http://www.environment-agency.gov.uk/business/sectors/39737.aspx> (Accessed: 13/01/2017).

Environment Agency (2013) Aggregates from inert waste - End of waste criteria for the production of aggregates from inert waste. Available at: [https://assets.publishing.service.gov.uk/government/uploads/system/uploads/attachment\\_data/file/296499/LIT\\_8709\\_c60600.pdf](https://assets.publishing.service.gov.uk/government/uploads/system/uploads/attachment_data/file/296499/LIT_8709_c60600.pdf) (Accessed: 05/10/2016).

Erol, M., Küçükbayrak, S. and Ersoy-Meriçboyu, A. (2008) 'Characterization of sintered coal fly ashes', *Fuel*, 87(7), pp. 1334-1340.

Escalante García, J. I., Campos-Venegas, K., Gorokhovskiy, A. and Fernández, A. (2006) 'Cementitious composites of pulverised fuel ash and blast furnace slag activated by sodium silicate: effect of Na<sub>2</sub>O concentration and modulus', *Advances in Applied Ceramics*, 105(4), pp. 201-208.

European Commission (2015) Sustainable development in the European Union, 2015 monitoring report of the EU Sustainable Development Strategy. Available at: <http://ec.europa.eu/eurostat/documents/3217494/6975281/KS-GT-15-001-EN-N.pdf> (Accessed: 13/02/2018).

Eurostat 'Environmental Data Centre on Waste, Waste statistics. [Online] Available from <http://ec.europa.eu/eurostat/>. Accessed on 04/01/2017.'

Eurostat ' Specific CO<sub>2</sub> emissions per tonne-km and per mode of transport in Europe. [Online] Available from <http://ec.europa.eu/eurostat/>. Accessed 07/09/2018.'

Fakhfakh, E., Hajjaji, W., Medhioub, M., Rocha, F., López-Galindo, A., Setti, M., Kooli, F., Zargouni, F. and Jamoussi, F. (2007) 'Effects of sand addition on production of lightweight aggregates from Tunisian smectite-rich clayey rocks', *Applied Clay Science*, 35(3), pp. 228-237.

Fens, T. W. (2000) *Petrophysical properties from small rock samples using image analysis techniques*. TU Delft, Delft University of Technology.

- Fernández Bertos, M., Simons, S. J. R., Hills, C. D. and Carey, P. J. (2004) 'A review of accelerated carbonation technology in the treatment of cement-based materials and sequestration of CO<sub>2</sub>', *Journal of Hazardous Materials*, 112(3), pp. 193-205.
- Ferri, V., Ferro, S., Martínez-Huitle, C. A. and De Battisti, A. (2009) 'Electrokinetic extraction of surfactants and heavy metals from sewage sludge', *Electrochimica Acta*, 54(7), pp. 2108-2118.
- Fisher, W. L. and Garner, L. E. (1967) *Bloating Characteristics of East Texas Clays*. University of Texas, Bureau of Economic Geology, .
- Fragoulis, D., Stamatakis, M. G., Chaniotakis, E. and Columbus, G. (2004) 'Characterization of lightweight aggregates produced with clayey diatomite rocks originating from Greece', *Materials Characterization*, 53(2-4), pp. 307-316.
- Friedheim, J. E. and Conn, H. L. 'Second generation synthetic fluids in the north sea: are they better?'. SPE/IADC Drilling Conference: Society of Petroleum Engineers.
- Gerrard, S., Grant, A., Marsh, R. and London, C. (1999) Drill cuttings piles in the North Sea: management options during platform decommissioning: Centre for Environmental Risk Research Report. Available at: <http://www.offshorecenter.dk/log/bibliotek/cuttings.pdf> (Accessed: 13/02/2018).
- Geysen, D., Imbrechts, K., Vandecasteele, C., Jaspers, M. and Wauters, G. (2004a) 'Immobilization of lead and zinc in scrubber residues from MSW combustion using soluble phosphates', *Waste Management*, 24(5), pp. 471-481.
- Geysen, D., Vandecasteele, C., Jaspers, M. and Wauters, G. (2004b) 'Comparison of immobilisation of air pollution control residues with cement and with silica', *Journal of Hazardous Materials*, 107(3), pp. 131-143.
- Gong, Y., Dongol, R., Yatongchai, C., Wren, A. W., Sundaram, S. K. and Mellott, N. P. (2016) 'Recycling of waste amber glass and porcine bone into fast sintered and high strength glass foams', *Journal of Cleaner Production*, 112, pp. 4534-4539.
- González-Corrochano, B., Alonso-Azcárate, J. and Rodas, M. (2009a) 'Characterization of lightweight aggregates manufactured from washing aggregate sludge and fly ash', *Resources, Conservation and Recycling*, 53(10), pp. 571-581.

- González-Corrochano, B., Alonso-Azcárate, J. and Rodas, M. (2009b) 'Production of lightweight aggregates from mining and industrial wastes', *Journal of Environmental Management*, 90(8), pp. 2801-2812.
- González-Corrochano, B., Alonso-Azcárate, J. and Rodas, M. (2012a) 'Chemical partitioning in lightweight aggregates manufactured from washing aggregate sludge, fly ash and used motor oil', *Journal of Environmental Management*, 109, pp. 43-53.
- González-Corrochano, B., Alonso-Azcárate, J. and Rodas, M. (2012b) 'Effect of thermal treatment on the retention of chemical elements in the structure of lightweight aggregates manufactured from contaminated mine soil and fly ash', *Construction and Building Materials*, 35, pp. 497-507.
- González-Corrochano, B., Alonso-Azcárate, J. and Rodas, M. (2014) 'Effect of pre-firing and firing dwell times on the properties of artificial lightweight aggregates', *Construction and Building Materials*, 53, pp. 91-101.
- González-Corrochano, B., Alonso-Azcárate, J., Rodríguez, L., Lorenzo, A. P., Torío, M. F., Ramos, J. J. T., Corvinos, M. D. and Muro, C. (2016) 'Valorization of washing aggregate sludge and sewage sludge for lightweight aggregates production', *Construction and Building Materials*, 116, pp. 252-262.
- Goodarznia, I. and Esmaeilzadeh, F. (2006) 'Treatment of oil-contaminated drill cuttings of South Pars gas field in Iran using supercritical carbon dioxide', *Iranian Journal of Science and Technology, Transaction B: Engineering*, 30, pp. 607-611.
- Guo, J., Baker, A. L., Guo, H., Lanagan, M. and Randall, C. A. (2017) 'Cold sintering process: A new era for ceramic packaging and microwave device development', *Journal of the American Ceramic Society*, 100(2), pp. 669-677.
- Haddad, P. R. and Jackson, P. E. (1990) *Ion chromatography*. Netherlands: Elsevier.
- Haldimann, M., Luible, A., Overend, M. and Ibrahim, R. (2008) *Structural Use of Glass*. UK: International Association for Bridge and Structural Engineering.
- Halliburton, A. D. (2001) *Basic Petroleum Geology and Log Analysis*. USA: Halliburton Company.

- Harikrishnan, K. I. and Ramamurthy, K. (2006) 'Influence of pelletization process on the properties of fly ash aggregates', *Waste Management*, 26(8), pp. 846-852.
- Hester, R. E. and Harrison, R. M. (2001) *Assessment and reclamation of contaminated land*. London: Thomas Telford.
- Hillier, S. (2000) 'Accurate quantitative analysis of clay and other minerals in sandstones by XRD: comparison of a Rietveld and a reference intensity ratio (RIR) method and the importance of sample preparation', *Clay Minerals*, 35(1), pp. 291-302.
- Hiramatsu, Y. and Oka, Y. (1966) 'Determination of the tensile strength of rock by a compression test of an irregular test piece', *International Journal of Rock Mechanics and Mining Sciences & Geomechanics Abstracts*, 3(2), pp. 89-90.
- Holdway, D. A. (2002) 'The acute and chronic effects of wastes associated with offshore oil and gas production on temperate and tropical marine ecological processes', *Marine Pollution Bulletin*, 44(3), pp. 185-203.
- Hu, S.-H. (2005) 'Stabilization of heavy metals in municipal solid waste incineration ash using mixed ferrous/ferric sulfate solution', *Journal of Hazardous Materials*, 123(1), pp. 158-164.
- Huang, C.-H. and Wang, S.-Y. (2013) 'Application of water treatment sludge in the manufacturing of lightweight aggregate', *Construction and Building Materials*, 43, pp. 174-183.
- Huang, S.-C., Chang, F.-C., Lo, S.-L., Lee, M.-Y., Wang, C.-F. and Lin, J.-D. (2007) 'Production of lightweight aggregates from mining residues, heavy metal sludge, and incinerator fly ash', *Journal of Hazardous Materials*, 144(1-2), pp. 52-58.
- Huang, W.-J. and Lo, J.-S. (2004) 'Synthesis and efficiency of a new chemical fixation agent for stabilizing MSWI fly ash', *Journal of Hazardous Materials*, 112(1), pp. 79-86.
- Hudgins, C. M. (1991) Chemical usage in North Sea oil and gas production and exploration operations, Stavanger, Norway: The Norwegian Oil Industry Association, Environment Committee.

- Hurst, V. J., Schroeder, P. A. and Styron, R. W. (1997) 'Accurate quantification of quartz and other phases by powder X-ray diffractometry', *Analytica Chimica Acta*, 337(3), pp. 233-252.
- Husein, M. M., Patruyo, L., Pereira-Almao, P. and Nassar, N. N. (2010) 'Scavenging H<sub>2</sub>S (g) from oil phases by means of ultradispersed sorbents', *Journal of colloid and interface science*, 342(2), pp. 253-260.
- Hwang, C.-L., Bui, L. A.-T., Lin, K.-L. and Lo, C.-T. (2012) 'Manufacture and performance of lightweight aggregate from municipal solid waste incinerator fly ash and reservoir sediment for self-consolidating lightweight concrete', *Cement and Concrete Composites*, 34(10), pp. 1159-1166.
- Ikonnikova, S., Gülen, G., Browning, J. and Tinker, S. W. (2015) 'Profitability of shale gas drilling: A case study of the Fayetteville shale play', *Energy*, 81, pp. 382-393.
- Ilic, M., Cheeseman, C., Sollars, C. and Knight, J. (2003) 'Mineralogy and microstructure of sintered lignite coal fly ash☆', *Fuel*, 82(3), pp. 331-336.
- IOGP (2016) IOGP (The International Association of Oil & Gas Producers). Drilling waste management technology review. Report 557. First release.
- Islam, M. and Khan, M. (2013) *The Petroleum Engineering Handbook: Sustainable Operations*. Elsevier.
- Johnson, H., Leslie, A. B., Wilson, C. K., Andrews, I. and Cooper, R. M. (2005) *Middle Jurassic, Upper Jurassic and Lower Cretaceous of the UK Central and Northern North Sea*. British Geological Survey.
- Jones, D. A., Lelyveld, T., Mavrofidis, S., Kingman, S. and Miles, N. (2002) 'Microwave heating applications in environmental engineering—a review', *Resources, conservation and recycling*, 34(2), pp. 75-90.
- Jones, M. R., Sear, L. K., McCarthy, M. J. and Dhir, R. K. 'Changes in coal fired power station fly ash: recent experiences and use in concrete'. Proc. Ash Technology Conference, UK Quality Ash Association.
- Jorissen, F., Bicchi, E., Duchemin, G., Durrieu, J., Galgani, F., Cazes, L., Gaultier, M. and Camps, R. (2009) 'Impact of oil-based drill mud disposal on benthic

- foraminiferal assemblages on the continental margin off Angola', *Deep Sea Research Part II: Topical Studies in Oceanography*, 56(23), pp. 2270-2291.
- Kandare, E., Kandola, B. K., McCarthy, E. D., Myler, P., Edwards, G., Jifeng, Y. and Wang, Y. C. (2011) 'Fiber-reinforced epoxy composites exposed to high temperature environments. Part II: modeling mechanical property degradation', *Journal of Composite Materials*, 45(14), pp. 1511-1521.
- Khatib, J. (2016) *Sustainability of Construction Materials*. Elsevier Science.
- Khodja, M., Canselier, J. P., Dali, C., Hafid, S. and Ouahab, R. (2007) 'A diagnostic of the treatment of oil well drilling waste in Algerian fields', *Recens Progress en Genie des Procedes*, 94, pp. 1-11.
- Kim, K.-D. (2011) 'Sintering-viscosity relation for mixed-alkali glass powder compacts', *Journal of Materials Research*, 10(7), pp. 1846-1849.
- Kirby, C. S. and Rimstidt, J. D. (1994) 'Interaction of municipal solid waste ash with water', *Environmental science & technology*, 28(3), pp. 443-451.
- Kogbara, R. B., Ayotamuno, J. M., Onuomah, I., Ehio, V. and Damka, T. D. (2016) 'Stabilisation/solidification and bioaugmentation treatment of petroleum drill cuttings', *Applied Geochemistry*, 71, pp. 1-8.
- Korat, L., Ducman, V., Legat, A. and Mirtič, B. (2013) 'Characterisation of the pore-forming process in lightweight aggregate based on silica sludge by means of X-ray micro-tomography (micro-CT) and mercury intrusion porosimetry (MIP)', *Ceramics International*, 39(6), pp. 6997-7005.
- Koshy, P., Gupta, S., Edwards, P. and Sahajwalla, V. (2011) 'Effect of BaSO<sub>4</sub> on the interfacial phenomena of high-alumina refractories with Al-alloy', *Journal of Materials Science*, 46(2), pp. 468-478.
- Kosson, D. S., van der Sloot, H. A. and Eighmy, T. T. (1996) 'An approach for estimation of contaminant release during utilization and disposal of municipal waste combustion residues', *Journal of Hazardous Materials*, 47(1-3), pp. 43-75.
- Kotake, N., Kuboki, M., Kiya, S. and Kanda, Y. (2011) 'Influence of dry and wet grinding conditions on fineness and shape of particle size distribution of product in a ball mill', *Advanced Powder Technology*, 22(1), pp. 86-92.

- Kourti, I. and Cheeseman, C. R. (2010) 'Properties and microstructure of lightweight aggregate produced from lignite coal fly ash and recycled glass', *Resources, Conservation and Recycling*, 54(11), pp. 769-775.
- Lampris, C. (2013) Solidification/Stabilisation of Air Pollution Control Residues from Municipal Solid Waste Incineration. Doctoral dissertation, Imperial College London.
- Lampris, C., Stegemann, J. A. and Cheeseman, C. R. (2008) 'Chloride leaching from air pollution control residues solidified using ground granulated blast furnace slag', *Chemosphere*, 73(9), pp. 1544-1549.
- Lampris, C., Stegemann, J. A., Pellizon-Birelli, M., Fowler, G. D. and Cheeseman, C. R. (2011) 'Metal leaching from monolithic stabilised/solidified air pollution control residues', *Journal of Hazardous Materials*, 185(2-3), pp. 1115-1123.
- Latosińska, J. and Żygadło, M. (2009) 'Effect of sewage sludge addition on porosity of lightweight expanded clay aggregate (LECA) and level of heavy metals leaching from ceramic matrix', *Environment Protection Engineering*, 35(2), pp. 189-196.
- Latosińska, J. and Żygadło, M. (2011) 'The application of sewage sludge as an expanding agent in the production of lightweight expanded clay aggregate mass', *Environmental Technology*, 32(13), pp. 1471-1478.
- Laursen, K., White, T. J., Cresswell, D. J. F., Wainwright, P. J. and Barton, J. R. (2006) 'Recycling of an industrial sludge and marine clay as light-weight aggregates', *Journal of Environmental Management*, 80(3), pp. 208-213.
- Leonard, S. A. and Stegemann, J. A. (2010) 'Stabilization/solidification of petroleum drill cuttings: Leaching studies', *Journal of Hazardous Materials*, 174(1-3), pp. 484-491.
- Li, X., Bertos, M. F., Hills, C. D., Carey, P. J. and Simon, S. (2007) 'Accelerated carbonation of municipal solid waste incineration fly ashes', *Waste Management*, 27(9), pp. 1200-1206.
- Li, Y., Wu, D., Zhang, J., Chang, L., Wu, D., Fang, Z. and Shi, Y. (2000) 'Measurement and statistics of single pellet mechanical strength of differently shaped catalysts', *Powder Technology*, 113(1-2), pp. 176-184.

- Liao, Y.-C. and Huang, C.-Y. (2011) 'Effects of heat treatment on the physical properties of lightweight aggregate from water reservoir sediment', *Ceramics International*, 37(8), pp. 3723-3730.
- Liao, Y.-C., Huang, C.-Y. and Chen, Y.-M. (2013) 'Lightweight aggregates from water reservoir sediment with added sodium hydroxide', *Construction and Building Materials*, 46, pp. 79-85.
- Lichte, F., Golightly, D. and Lamothe, P. (1987) 'Inductively coupled plasma-atomic emission spectrometry', *Methods for Geochemical Analysis*, pp. B1-B10.
- Lin, K. (2006) 'Mineralogy and microstructures of sintered sewage sludge ash as lightweight aggregates', *Journal of Industrial and Engineering Chemistry*, 12(3), pp. 425.
- Lin, K. L. and Chang, C. T. (2006) 'Leaching characteristics of slag from the melting treatment of municipal solid waste incinerator ash', *Journal of Hazardous Materials*, 135(1-3), pp. 296-302.
- Liu, M. (2010) 'Self-compacting concrete with different levels of pulverized fuel ash', *Construction and Building Materials*, 24(7), pp. 1245-1252.
- Liu, M., Xu, G. and Li, G. (2017) 'Effect of the ratio of components on the characteristics of lightweight aggregate made from sewage sludge and river sediment', *Process Safety and Environmental Protection*, 105, pp. 109-116.
- Lo, T. Y., Cui, H., Memon, S. A. and Noguchi, T. (2015) 'Manufacturing of sintered lightweight aggregate using high-carbon fly ash and its effect on the mechanical properties and microstructure of concrete', *Journal of Cleaner Production*, 112, pp. 753-762.
- López-Vizcaíno, R., Alonso, J., Cañizares, P., León, M. J., Navarro, V., Rodrigo, M. A. and Sáez, C. (2014) 'Electroremediation of a natural soil polluted with phenanthrene in a pilot plant', *Journal of Hazardous Materials*, 265, pp. 142-150.
- Loutou, M., Hajjaji, M., Mansori, M., Favotto, C. and Hakkou, R. (2013) 'Phosphate sludge: Thermal transformation and use as lightweight aggregate material', *Journal of Environmental Management*, 130, pp. 354-360.

- Lu, C.-H., Chen, J.-C., Chuang, K.-H. and Wey, M.-Y. (2015) 'The different properties of lightweight aggregates with the fly ashes of fluidized-bed and mechanical incinerators', *Construction and Building Materials*, 101, Part 1, pp. 380-388.
- Lundtorp, K., Jensen, D. L., Sørensen, M. A., Mosbæk, H. and Christensen, T. H. (2003) 'On-site treatment and landfilling of MSWI air pollution control residues', *Journal of Hazardous Materials*, 97(1-3), pp. 59-70.
- Lynn, C. J., Dhir, R. K., Ghataora, G. S. and West, R. P. (2015) 'Sewage sludge ash characteristics and potential for use in concrete', *Construction and Building Materials*, 98, pp. 767-779.
- M. D. A. Thomas, P. J. N. and Pettifer, K. (1991) 'Effect of Pulverised-Fuel Ash With a High Total Alkali Content on Alkali Silica Reaction in Concrete Containing Natural UK Aggregate', *Special Publication*, 126.
- Magaritz, M. and Kafri, U. (1979) 'Concentration of magnesium in carbonate nodules of soils: An indication of fresh groundwater contamination by intruding seawater', *Chemical Geology*, 27(1-2), pp. 143-155.
- Manning, T. J. and Grow, W. R. (1997) 'Inductively Coupled Plasma - Atomic Emission Spectrometry', *The Chemical Educator*, 2(1), pp. 1-19.
- Manspeizer, W. (2015) *Triassic-Jurassic rifting: continental breakup and the origin of the Atlantic Ocean and passive margins*. Elsevier.
- Marsh, R. (2003) 'A database of archived drilling records of the drill cuttings piles at the North West Hutton oil platform', *Marine Pollution Bulletin*, 46(5), pp. 587-593.
- Martin, J. K., Matela, R. J. and Sherwen, R. G. (2003) 'Modelling heat transfer through a novel design of rotary kiln', *International journal of computer applications in technology*, 17(4), pp. 233-243.
- Maslennikova, G. N., Fomina, N. P., Kharitonov, F. and Naidenova, G. A. (1974) 'The use of barium sulfate in the synthesis of celsian ceramic', *Glass and Ceramics*, 31(12), pp. 872-875.
- McCusker, L., Von Dreele, R., Cox, D., Louër, D. and Scardi, P. (1999) 'Rietveld refinement guidelines', *Journal of Applied Crystallography*, 32(1), pp. 36-50.

- Meima, J. A., van der Weijden, R. D., Eighmy, T. T. and Comans, R. N. J. (2002) 'Carbonation processes in municipal solid waste incinerator bottom ash and their effect on the leaching of copper and molybdenum', *Applied Geochemistry*, 17(12), pp. 1503-1513.
- Melton, H. R., Smith, J. P., Mairs, H. L., Bernier, R. F., Garland, E., Glickman, A. H., Jones, F. V., Ray, J. P., Thomas, D. and Campbell, J. A. 'Environmental aspects of the use and disposal of non aqueous drilling fluids associated with offshore oil & gas operations'. SPE International Conference on Health, Safety, and Environment in Oil and Gas Exploration and Production: Society of Petroleum Engineers.
- Mohamed, G. E. T. (2012) Physical and Chemical Composition of Particulate Pollutants in an Urban Area of Cardiff, Wales. Cardiff Metropolitan University.
- Molineux, C. J., Newport, D. J., Ayati, B., Wang, C., Connop, S. P. and Green, J. E. (2016) 'Bauxite residue (red mud) as a pulverised fuel ash substitute in the manufacture of lightweight aggregate', *Journal of Cleaner Production*, 112, Part 1, pp. 401-408.
- Montanari, F., Miselli, P., Leonelli, C., Boschetti, C., Henderson, J. and Baraldi, P. (2014) 'Calibration and Use of the Heating Microscope for Indirect Evaluation of the Viscosity and Meltability of Archeological Glasses', *International Journal of Applied Glass Science*, 5(2), pp. 161-177.
- Moore, D. M. and Reynolds, R. C. (1989) *X-ray Diffraction and the Identification and Analysis of Clay Minerals*. Oxford university press Oxford.
- Morillon, A., Vidalie, J.-F., Hamzah, U. S., Suripno, S. and Hadinoto, E. K. 'Drilling and waste management'. SPE International Conference on Health, Safety and Environment in Oil and Gas Exploration and Production: Society of Petroleum Engineers.
- Morin, L. and Lamothe, J.-M. (1990) 'Testing on Perlite and Vermiculite Samples from British Columbia', *Geological Field Work*, pp. 265-268.
- Mostavi, E., Asadi, S. and Ugochukwu, E. (2015) 'Feasibility Study of the Potential Use of Drill Cuttings in Concrete', *Procedia Engineering*, 118, pp. 1015-1023.

- Mu, Y., Saffarzadeh, A. and Shimaoka, T. (2017) 'Influence of ignition process on mineral phase transformation in municipal solid waste incineration (MSWI) fly ash: Implications for estimating loss-on-ignition (LOI)', *Waste Management*, 59, pp. 222-228.
- Mueller, A., Schnell, A. and Ruebner, K. (2015) 'The manufacture of lightweight aggregates from recycled masonry rubble', *Construction and Building Materials*, 98, pp. 376-387.
- Mueller, A., Sokolova, S. N. and Vereshagin, V. I. (2008) 'Characteristics of lightweight aggregates from primary and recycled raw materials', *Construction and Building Materials*, 22(4), pp. 703-712.
- Müller, U. and Rübner, K. (2006) 'The microstructure of concrete made with municipal waste incinerator bottom ash as an aggregate component', *Cement and Concrete Research*, 36(8), pp. 1434-1443.
- Mun, K. J. (2007) 'Development and tests of lightweight aggregate using sewage sludge for nonstructural concrete', *Construction and Building Materials*, 21(7), pp. 1583-1588.
- Nadesan, M. S. and Dinakar, P. (2017) 'Mix design and properties of fly ash waste lightweight aggregates in structural lightweight concrete', *Case Studies in Construction Materials*, 7, pp. 336-347.
- Napolano, L., Menna, C., Graziano, S. F., Asprone, D., D'Amore, M., de Gennaro, R. and Dondi, M. (2016) 'Environmental life cycle assessment of lightweight concrete to support recycled materials selection for sustainable design', *Construction and Building Materials*, 119, pp. 370-384.
- Neff, J. M. (2005) *Composition, environmental fates, and biological effect of water based drilling muds and cuttings discharged to the marine environment: A synthesis and annotated bibliography*, Washington, DC.
- Neff, J. M. (2008) 'Estimation of bioavailability of metals from drilling mud barite', *Integrated Environmental Assessment and Management*, 4(2), pp. 184-193.
- Neff, J. M., McKelvie, S. and Ayers, R. C. (2000) *Environmental impacts of synthetic based drilling fluids*: US Department of the Interior, Minerals Management

- Service, Gulf of Mexico OCS Region. Available at: <https://www.boem.gov/ESPIS/3/3175.pdf> (Accessed: 13/02/2018).
- NEN, N. (1995) Leaching characteristics of solid earthy and stony building and waste materials. Leaching tests. Delft: Nederlands Normalisatie-instituut.
- Neville, A. M. (1995) *Properties of concrete*. Longman London.
- Nzihou, A. and Sharrock, P. (2002) 'Calcium phosphate stabilization of fly ash with chloride extraction', *Waste Management*, 22(2), pp. 235-239.
- Oil and Gas Authority (2016) UK Continental Shelf Unsanctioned Discoveries Information Pack Available at: <https://www.ogauthority.co.uk/media/2960/420297-small-pools-22.pdf> (Accessed: 17/01/2018).
- Oil and Gas UK (2016a) Economic Report 2016 Available at: <https://oilandgasuk.co.uk/wp-content/uploads/2016/09/Economic-Report-2016-Oil-Gas-UK.pdf> (Accessed: 13/02/2018).
- Oil and Gas UK (2016b) Environment Report 2016 Available at: <https://oilandgasuk.co.uk/wp-content/uploads/2016/11/Environment-Report-2016-Oil-Gas-UK.pdf> (Accessed: 13/02/2018).
- Oil and Gas UK (2017) Environment Report 2017 Available at: <https://oilandgasuk.co.uk/wp-content/uploads/2017/12/Environment-Report-2017.pdf> (Accessed: 17/01/2018).
- Olsgard, F. and Gray, J. S. (1995) 'A comprehensive analysis of the effects of offshore oil and gas exploration and production on the benthic communities of the Norwegian continental shelf', *Marine Ecology Progress Series*, 122, pp. 277-306.
- Oppelt, E. T. (1987) 'Incineration Of Hazardous Waste', *JAPCA*, 37(5), pp. 558-586.
- Pascual, M. J. and Pascual, L. (2001) 'Determination of the viscosity–temperature curve for glasses on the basis of fixed viscosity points determined by hot stage microscopy', *Physics and chemistry of Glasses*, 42(1), pp. 61-66.

- Pedersen, A. J., Ottosen, L. M. and Villumsen, A. (2005) 'Electrodialytic removal of heavy metals from municipal solid waste incineration fly ash using ammonium citrate as assisting agent', *Journal of Hazardous Materials*, 122(1), pp. 103-109.
- Pereira, I. S. M. (2013) Microwave processing of oil contaminated drill cuttings. University of Nottingham.
- Pereira, M. S., Panisset, C. M. d. Á., Martins, A. L., Sá, C. H. M. d., Barrozo, M. A. d. S. and Ataíde, C. H. (2014) 'Microwave treatment of drilled cuttings contaminated by synthetic drilling fluid', *Separation and Purification Technology*, 124, pp. 68-73.
- Pessanha, S., Fonseca, C., Santos, J., Carvalho, M. and Dias, A. (2018) 'Comparison of standard-based and standardless methods of quantification used in X-ray fluorescence analysis: Application to the exoskeleton of clams', *X-Ray Spectrometry*, 47(2), pp. 108-115.
- Petri Junior, I., Pereira, M. S., dos Santos, J. M., Duarte, C. R., Ataíde, C. H. and Panisset, C. M. d. Á. (2015) 'Microwave remediation of oil well drill cuttings', *Journal of Petroleum Science and Engineering*, 134, pp. 23-29.
- Piszczyńska-Karaś, K., Łuczak, J. and Hupka, J. (2016) 'Release of selected chemical elements from shale drill cuttings to aqueous solutions of different pH', *Applied Geochemistry*, 72, pp. 136-145.
- Polettini, A., Pomi, R., Trinci, L., Muntoni, A. and Lo Mastro, S. (2004) 'Engineering and environmental properties of thermally treated mixtures containing MSWI fly ash and low-cost additives', *Chemosphere*, 56(10), pp. 901-910.
- Popov, K. I., Pavlović, M. G., Pavlović, L. J., Ivanović, E. R., Krstić, S. B. and Obradović, M. Č. (2003) 'The effect of the particle shape and structure on the flow ability of electrolytic copper powder II: The experimental verification of the model of the representative powder particle', *Journal of the Serbian Chemical Society*, 68(10), pp. 779-783.
- Prosen, E. J. and Rossini, F. D. (1954) 'Heats of combustion and formation of the paraffin hydrocarbons at 25 C', *J. Res. NBS*, 34, pp. 263-267.

- Pye, K. and Krinsley, D. H. (1986) 'Diagenetic carbonate and evaporite minerals in Rotliegend aeolian sandstones of the southern North Sea: their nature and relationship to secondary porosity development', *Clay Minerals*, 21(4), pp. 443-457.
- Quina, M. J., Almeida, M. A., Santos, R., Bordado, J. M. and Quinta-Ferreira, R. M. (2014a) 'Compatibility analysis of municipal solid waste incineration residues and clay for producing lightweight aggregates', *Applied Clay Science*, 102, pp. 71-80.
- Quina, M. J., Bordado, J. C. and Quinta-Ferreira, R. M. (2008) 'Treatment and use of air pollution control residues from MSW incineration: An overview', *Waste Management*, 28(11), pp. 2097-2121.
- Quina, M. J., Bordado, J. C. M. and Quinta-Ferreira, R. M. (2009) 'The influence of pH on the leaching behaviour of inorganic components from municipal solid waste APC residues', *Waste Management*, 29(9), pp. 2483-2493.
- Quina, M. J., Bordado, J. C. M. and Quinta-Ferreira, R. M. (2010) 'Chemical stabilization of air pollution control residues from municipal solid waste incineration', *Journal of Hazardous Materials*, 179(1), pp. 382-392.
- Quina, M. J., Bordado, J. M. and Quinta-Ferreira, R. M. (2014b) 'Recycling of air pollution control residues from municipal solid waste incineration into lightweight aggregates', *Waste Management*, 34(2), pp. 430-438.
- Raask, E. (1979) 'Sintering characteristics of coal ashes by simultaneous dilatometry-electrical conductance measurements', *Journal of Thermal Analysis and Calorimetry*, 16(1), pp. 91-102.
- Rachwal, J. D. (2010) X-ray diffraction applications in thin films and (100) silicon substrate stress analysis. Doctoral dissertation, University of South Florida.
- Rahaman, M. N. (2007) *Sintering of Ceramics*. Boca Raton, Florida: CRC Press.
- Rayment, P. L. (1982) 'The effect of pulverised-fuel ash on the c/s molar ratio and alkali content of calcium silicate hydrates in cement', *Cement and Concrete Research*, 12(2), pp. 133-140.
- Reed, S. J. B. (2005) *Electron microprobe analysis and scanning electron microscopy in geology*. Cambridge University Press.

- Richards, P. C. (1993) *Jurassic of the central and northern North Sea*. British Geological Survey.
- Riley, C. M. (1951) 'Relation of Chemical Properties to the Bloating of Clays', *Journal of the American Ceramic Society*, 34(4), pp. 121-128.
- Robinson, J. P., Kingman, S. W. and Onobrakpeya, O. (2008) 'Microwave-assisted stripping of oil contaminated drill cuttings', *Journal of Environmental Management*, 88(2), pp. 211-218.
- Robinson, J. P., Kingman, S. W., Snape, C. E., Barranco, R., Shang, H., Bradley, M. S. A. and Bradshaw, S. M. (2009) 'Remediation of oil-contaminated drill cuttings using continuous microwave heating', *Chemical Engineering Journal*, 152(2-3), pp. 458-463.
- Rodriguez, E. T., Anovitz, L. M., Clement, C. D., Rondinone, A. J. and Cheshire, M. C. (2018) 'Facile emulsion mediated synthesis of phase-pure diopside nanoparticles', *Scientific reports*, 8(1), pp. 3099.
- Roether, J. A., Daniel, D. J., Amutha Rani, D., Deegan, D. E., Cheeseman, C. R. and Boccaccini, A. R. (2010) 'Properties of sintered glass-ceramics prepared from plasma vitrified air pollution control residues', *Journal of Hazardous Materials*, 173(1-3), pp. 563-569.
- Rushing, J., Churan, M. and Jones, F. 'Bioaccumulation from mineral oil-wet and synthetic liquid-wet cuttings in an estuarine fish, *Fundulus grandis*'. SPE Health, Safety and Environment in Oil and Gas Exploration and Production Conference: Society of Petroleum Engineers.
- Sabbas, T., Poletini, A., Pomi, R., Astrup, T., Hjelmar, O., Mostbauer, P., Cappai, G., Magel, G., Salhofer, S., Speiser, C., Heuss-Assbichler, S., Klein, R. and Lechner, P. (2003) 'Management of municipal solid waste incineration residues', *Waste Management*, 23(1), pp. 61-88.
- Sarabèr, A., Overhof, R., Green, T. and Pels, J. (2012) 'Artificial lightweight aggregates as utilization for future ashes – A case study', *Waste Management*, 32(1), pp. 144-152.

- Saveyn, H., Eder, P., Garbarino, E., Muchova, L., Hjelmar, O., Van der Sloot, H., Comans, R., Van Zomeren, A., Hyks, J. and Oberender, A. (2014) Study on methodological aspects regarding limit values for pollutants in aggregates in the context of the possible development of end-of-waste criteria under the EU Waste Framework Directive: Institute for Prospective Technological Studies. Available at:  
<http://susproc.jrc.ec.europa.eu/activities/waste/documents/Aggregates%20leaching%20Main.pdf> (Accessed: 14/02/2018).
- Seaton, S., Morris, R., Blonquist, J. and Hogan, B. 'Analysis of Drilling Fluid Base Oil Recovered from Drilling Waste by Thermal Desorption'. International Petroleum Environmental Conference.
- Shirley, R. and Black, L. (2011) 'Alkali activated solidification/stabilisation of air pollution control residues and co-fired pulverised fuel ash', *Journal of Hazardous Materials*, 194, pp. 232-242.
- Sievert, T., Wolter, A. and Singh, N. B. (2005) 'Hydration of anhydrite of gypsum (CaSO<sub>4</sub>.II) in a ball mill', *Cement and Concrete Research*, 35(4), pp. 623-630.
- Sikora, P., Horszczaruk, E. and Rucinska, T. (2015) 'The Effect of Nanosilica and Titanium Dioxide on the Mechanical and Self-Cleaning Properties of Waste-Glass Cement Mortar', *Procedia Engineering*, 108, pp. 146-153.
- Skibsted, G., Ottosen, L. M., Elektorowicz, M. and Jensen, P. E. (2018) 'Effect of long-term electrolytic soil remediation on Pb removal and soil weathering', *Journal of Hazardous Materials*.
- Soltan, A. M. M., Kahl, W.-A., Abd El-Raouf, F., Abdel-Hamid El-Kaliouby, B., Abdel-Kader Serry, M. and Abdel-Kader, N. A. (2016) 'Lightweight aggregates from mixtures of granite wastes with clay', *Journal of Cleaner Production*, 117, pp. 139-149.
- Środoń, J., Drits, V. A., McCarty, D. K., Hsieh, J. C. and Eberl, D. D. (2001) 'Quantitative X-ray diffraction analysis of clay-bearing rocks from random preparations', *Clays and Clay Minerals*, 49(6), pp. 514-528.

- Stanmore, B. R. and Gilot, P. (2005) 'Review - calcination and carbonation of limestone during thermal cycling for CO<sub>2</sub> sequestration', *Fuel Processing Technology*, 86(16), pp. 1707-1743.
- Stern, K. H. and Weise, E. L. (1969) High Temperature Properties and Decomposition of Inorganic Salts. Part 2. Carbonates: National standard reference data system. Available at: <http://nvlpubs.nist.gov/nistpubs/Legacy/NSRDS/nbsnsrds30.pdf> (Accessed: 13/02/2018).
- Stinton, G. W. (2006) Structural studies into AM (2) O (7) framework materials and parametric Rietveld refinement. Durham University.
- Strachan, M. F. (2010) Studies on the impact of a water-based drilling mud weighting agent (Barite) on some Benthic invertebrates. Doctoral dissertation, Heriot-Watt University.
- Street, C. G. and Guigard, S. E. (2009) 'Treatment of oil-based drilling waste using supercritical carbon dioxide', *Journal of Canadian Petroleum Technology*, 48(06), pp. 26-29.
- Syngros, G., Balaras, C. A. and Koubogiannis, D. G. (2017) 'Embodied CO<sub>2</sub> emissions in building construction materials of Hellenic dwellings', *Procedia Environmental Sciences*, 38, pp. 500-508.
- Takai, K., Moyer, C. L., Miyazaki, M., Nogi, Y., Hirayama, H., Nealson, K. H. and Horikoshi, K. (2005) 'Marinobacter alkaliphilus sp. nov., a novel alkaliphilic bacterium isolated from subseafloor alkaline serpentine mud from Ocean Drilling Program Site 1200 at South Chamorro Seamount, Mariana Forearc', *Extremophiles*, 9(1), pp. 17-27.
- Tang, C.-W., Chen, H.-J., Wang, S.-Y. and Spaulding, J. (2011) 'Production of synthetic lightweight aggregate using reservoir sediments for concrete and masonry', *Cement and Concrete Composites*, 33(2), pp. 292-300.
- Tang, J., Cheng, H., Zhang, Q., Chen, W. and Li, Q. (2018) 'Development of properties and microstructure of concrete with coral reef sand under sulphate attack and drying-wetting cycles', *Construction and Building Materials*, 165, pp. 647-654.
- Todor, D. N. (1976) *Thermal analysis of minerals*. Abacus press.

- Todorovic, J. and Ecke, H. (2006) 'Demobilisation of critical contaminants in four typical waste-to-energy ashes by carbonation', *Waste Management*, 26(4), pp. 430-441.
- Traina, G., Ferro, S. and De Battisti, A. (2009) 'Electrokinetic stabilization as a reclamation tool for waste materials polluted by both salts and heavy metals', *Chemosphere*, 75(6), pp. 819-824.
- Tsai, C.-C., Wang, K.-S. and Chiou, I.-J. (2006) 'Effect of SiO<sub>2</sub>-Al<sub>2</sub>O<sub>3</sub>-flux ratio change on the bloating characteristics of lightweight aggregate material produced from recycled sewage sludge', *Journal of Hazardous Materials*, 134(1-3), pp. 87-93.
- Tuan, B. L. A., Hwang, C.-L., Lin, K.-L., Chen, Y.-Y. and Young, M.-P. (2013) 'Development of lightweight aggregate from sewage sludge and waste glass powder for concrete', *Construction and Building Materials*, 47, pp. 334-339.
- Turner, K. P. (2002) Bioremediation of drill cuttings from oil based muds. University of Nottingham.
- van der Sloot, H. A., Comans, R. N. J. and Hjelmar, O. (1996) 'Similarities in the leaching behaviour of trace contaminants from waste, stabilized waste, construction materials and soils', *Science of The Total Environment*, 178(1-3), pp. 111-126.
- Vandever, P. L. (1951) Differential Thermal Analysis of some Carbonate Minerals, California. Available at: [http://www.minsocam.org/ammin/AM32/AM32\\_111.pdf](http://www.minsocam.org/ammin/AM32/AM32_111.pdf) (Accessed: 13/02/2018).
- Vassilev, S. V. and Vassileva, C. G. (1996) 'Mineralogy of combustion wastes from coal-fired power stations', *Fuel Processing Technology*, 47(3), pp. 261-280.
- Velis, C. A., Franco-Salinas, C., O'sullivan, C., Najorka, J., Boccaccini, A. R. and Cheeseman, C. R. (2014) 'Up-cycling waste glass to minimal water adsorption/absorption lightweight aggregate by rapid low temperature sintering: optimization by dual process-mixture response surface methodology', *Environmental science & technology*, 48(13), pp. 7527-7535.
- Velzeboer, I. and Zomeren, A. v. (2017) End of Waste criteria for inert aggregates in Member States. Available at:

<https://www.ecn.nl/publicaties/PdfFetch.aspx?nr=ECN-E--17-010> (Accessed: 17/07/18).

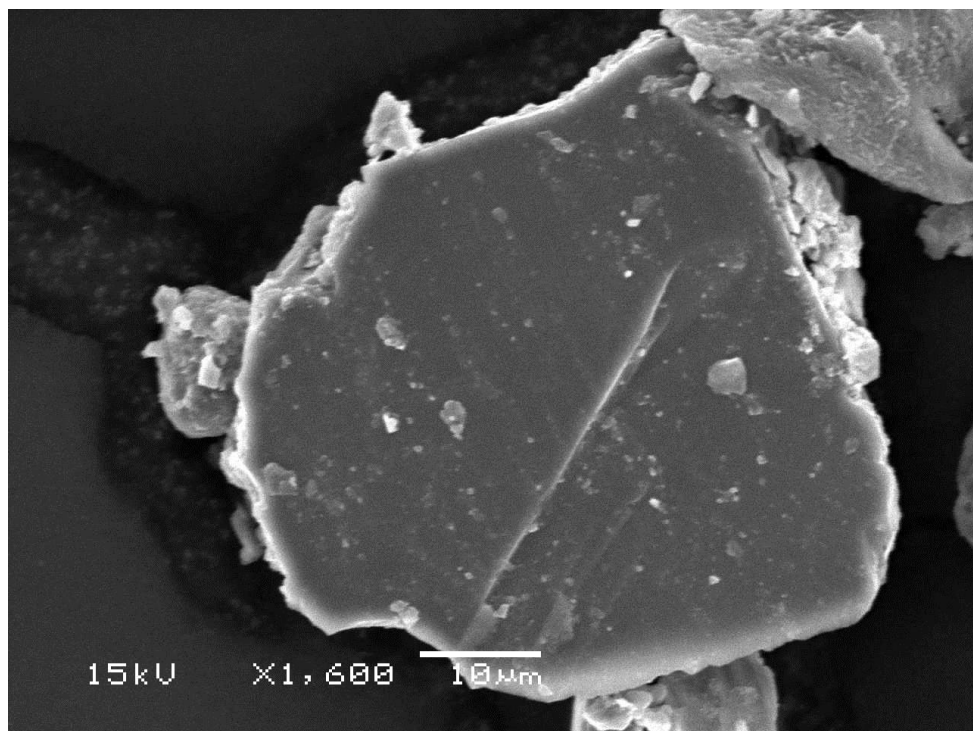
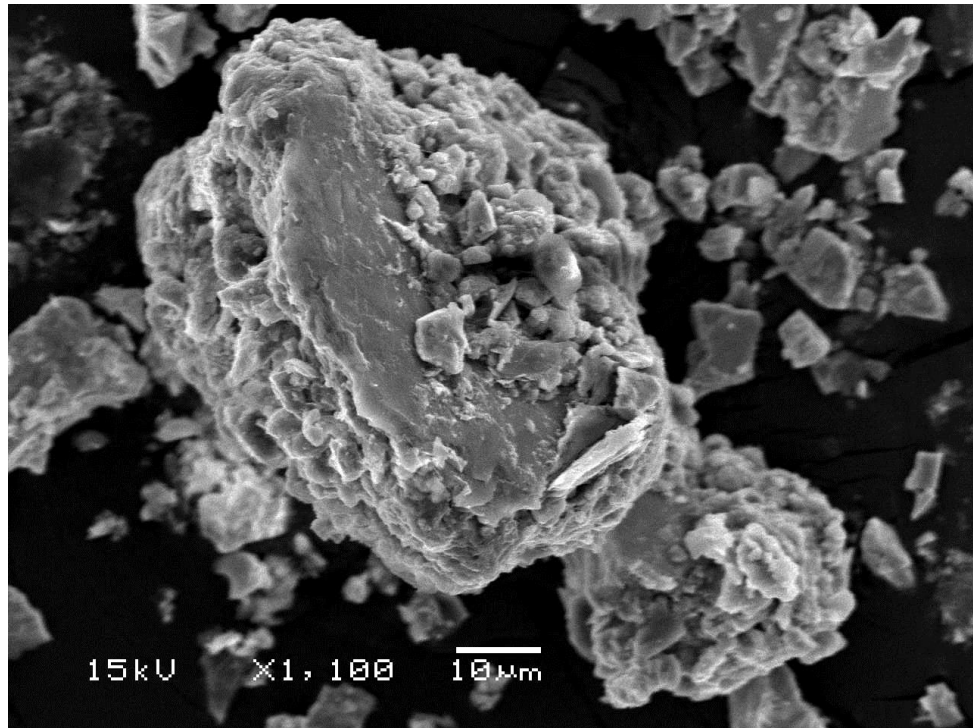
- Vidali, M. (2001) 'Bioremediation. an overview', *Pure and Applied Chemistry*, 73(7), pp. 1163-1172.
- Virkutyte, J., Sillanpää, M. and Latostenmaa, P. (2002) 'Electrokinetic soil remediation — critical overview', *Science of The Total Environment*, 289(1), pp. 97-121.
- Vold, M. J. (1949) 'Differential thermal analysis', *Analytical chemistry*, 21(6), pp. 683-688.
- Volland, S. and Brötz, J. (2015) 'Lightweight aggregates produced from sand sludge and zeolitic rocks', *Construction and Building Materials*, 85, pp. 22-29.
- Volland, S., Kazmina, O., Vereshchagin, V. and Dushkina, M. (2014) 'Recycling of sand sludge as a resource for lightweight aggregates', *Construction and Building Materials*, 52, pp. 361-365.
- Wainwright, P. J. and Cresswell, D. J. F. (2001) 'Synthetic aggregates from combustion ashes using an innovative rotary kiln', *Waste Management*, 21(3), pp. 241-246.
- Wait, S. T. and Thomas, D. 'The Characterisation of Base Oil Recovered From the Low Temperature Thermal Desorption of Drill Cuttings', *SPE/EPA/DOE Exploration and Production Environmental Conference*, 2003. SPE: Society of Petroleum Engineers.
- Wang, L., Jin, Y. and Nie, Y. (2010) 'Investigation of accelerated and natural carbonation of MSWI fly ash with a high content of Ca', *Journal of Hazardous Materials*, 174(1), pp. 334-343.
- Wang, W. (2010) Inorganic and organic speciation of atmospheric aerosols by ion chromatography and aerosol chemical mass closure. Doctoral Dissertation, Department of Analytical Chemistry, Ghent University.
- Ward, C. R. and French, D. 'Relation between coal and fly ash mineralogy, based on quantitative X-ray diffraction methods'. *World Coal Ash (WOCA)*, 11-15.
- Warren, J. K. (2006) *Evaporites: Sediments, Resources and Hydrocarbons*. Springer Berlin Heidelberg.

- Wei, Y.-L., Cheng, S.-H. and Ko, G.-W. (2016) 'Effect of waste glass addition on lightweight aggregates prepared from F-class coal fly ash', *Construction and Building Materials*, 112, pp. 773-782.
- Wei, Y.-L., Lin, C.-Y., Ko, K.-W. and Wang, H. P. (2011) 'Preparation of low water-sorption lightweight aggregates from harbor sediment added with waste glass', *Marine Pollution Bulletin*, 63(5–12), pp. 135-140.
- Wei, Y.-L., Yang, J.-C., Lin, Y.-Y., Chuang, S.-Y. and Wang, H. P. (2008) 'Recycling of harbor sediment as lightweight aggregate', *Marine Pollution Bulletin*, 57(6–12), pp. 867-872.
- Weiss, J. (2016) *Handbook of Ion Chromatography 3 Volume Set*. John Wiley & Sons.
- Wheaton, S. R. and Manu, T. 'Jubilee Field Development, Ghana - In-Country Activities and Their Impact', *Offshore Technology Conference*, Houston, 2012. OTC.
- WM3 (2015) 'Technical Guidance WM3, Guidance on the classification and assessment of waste (1st edition). UK Environment Agency (Bristol), Scottish Environment Protection Agency (Stirling), Northern Ireland Environment Agency (Belfast) & Natural Resources Wales (Cardiff). Available at [https://www.gov.uk/government/uploads/system/uploads/attachment\\_data/file/427077/LIT\\_10121.pdf](https://www.gov.uk/government/uploads/system/uploads/attachment_data/file/427077/LIT_10121.pdf) (accessed March 2017).'
- Xu, G., Liu, M. and Li, G. (2013) 'Stabilization of heavy metals in lightweight aggregate made from sewage sludge and river sediment', *Journal of Hazardous Materials*, 260, pp. 74-81.
- Yang, C., Cui, C. and Qin, J. (2015) 'Recycling of low-silicon iron tailings in the production of lightweight aggregates', *Ceramics International*, 41(1, Part B), pp. 1213-1221.
- Ye, Y., Li, J., Zhang, Q., Feng, J., Zhu, J. and Yin, D. (2017) 'Nanoemulsion for oil-contaminated oil-based drill cuttings removal in lab', *International Journal of Hydrogen Energy*, 42(29), pp. 18734-18740.
- Yuan, C. and Weng, C.-H. (2006) 'Electrokinetic enhancement removal of heavy metals from industrial wastewater sludge', *Chemosphere*, 65(1), pp. 88-96.

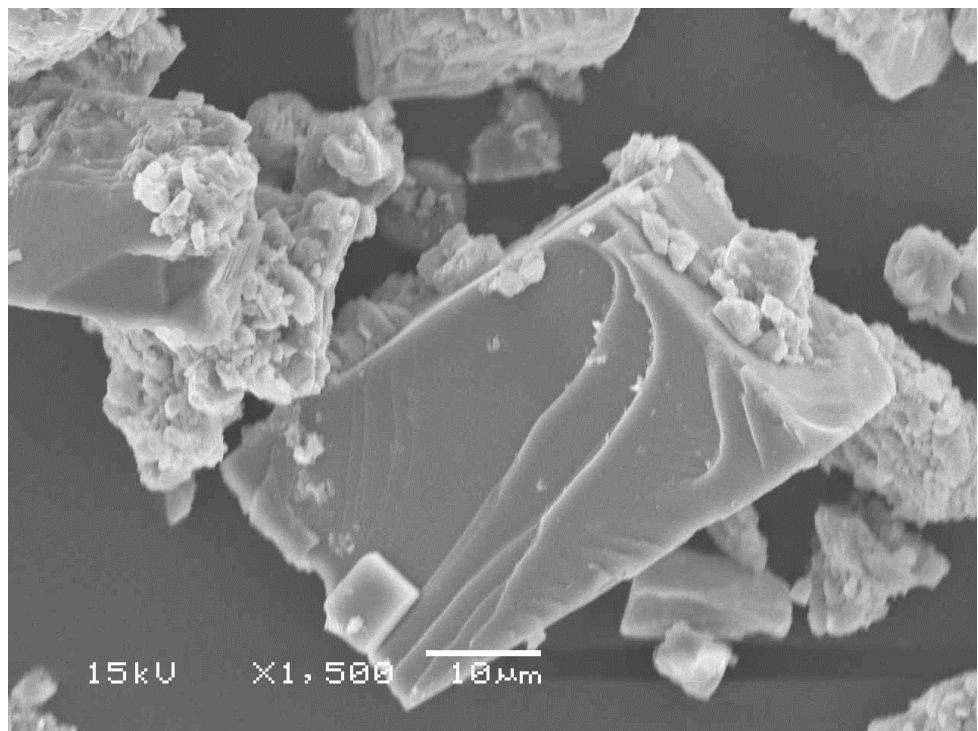
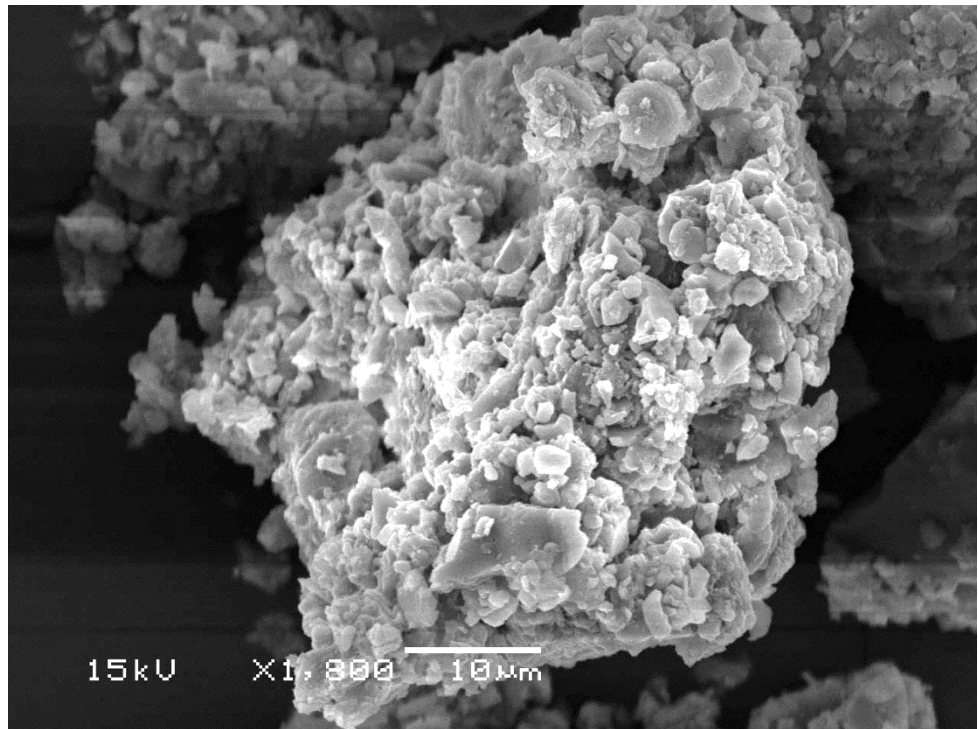
- Zamora, M., Roy, S., Slater, K. S. and Troncoso, J. C. (2013) 'Study on the Volumetric Behavior of Base Oils, Brines, and Drilling Fluids Under Extreme Temperatures and Pressures'.
- Zhang, S., Liu, L., Tan, K., Zhang, L. and Tang, K. (2015) 'Influence of burning temperature and cooling methods on strength of high carbon ferrochrome slag lightweight aggregate', *Construction and Building Materials*, 93, pp. 1180-1187.
- Zhang, Z., Wu, X., Zhou, T., Chen, Y., Hou, N., Piao, G., Kobayashi, N., Itaya, Y. and Mori, S. (2011) 'The effect of iron-bearing mineral melting behavior on ash deposition during coal combustion', *Proceedings of the Combustion Institute*, 33(2), pp. 2853-2861.
- Zhou, D., Wang, R., Tyrer, M., Wong, H. and Cheeseman, C. (2017) 'Sustainable infrastructure development through use of calcined excavated waste clay as a supplementary cementitious material', *Journal of Cleaner Production*, 168, pp. 1180-1192.
- Zhu, F., Takaoka, M., Oshita, K., Kitajima, Y., Inada, Y., Morisawa, S. and Tsuno, H. (2010) 'Chlorides behavior in raw fly ash washing experiments', *Journal of Hazardous Materials*, 178(1-3), pp. 547-552.

Appendix I (SEM images of drill cuttings samples)

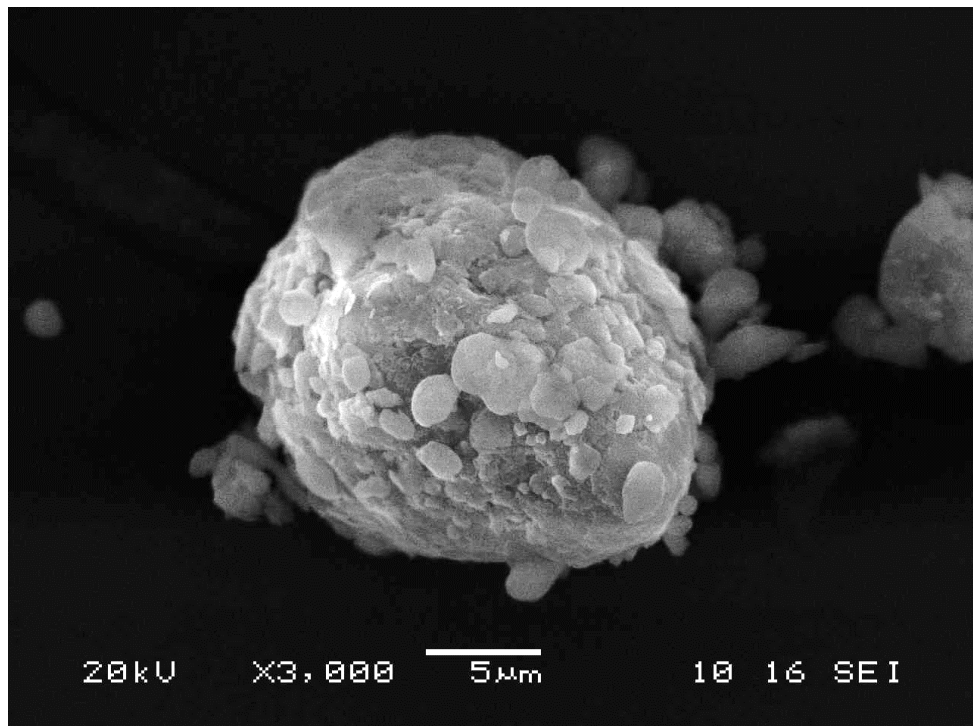
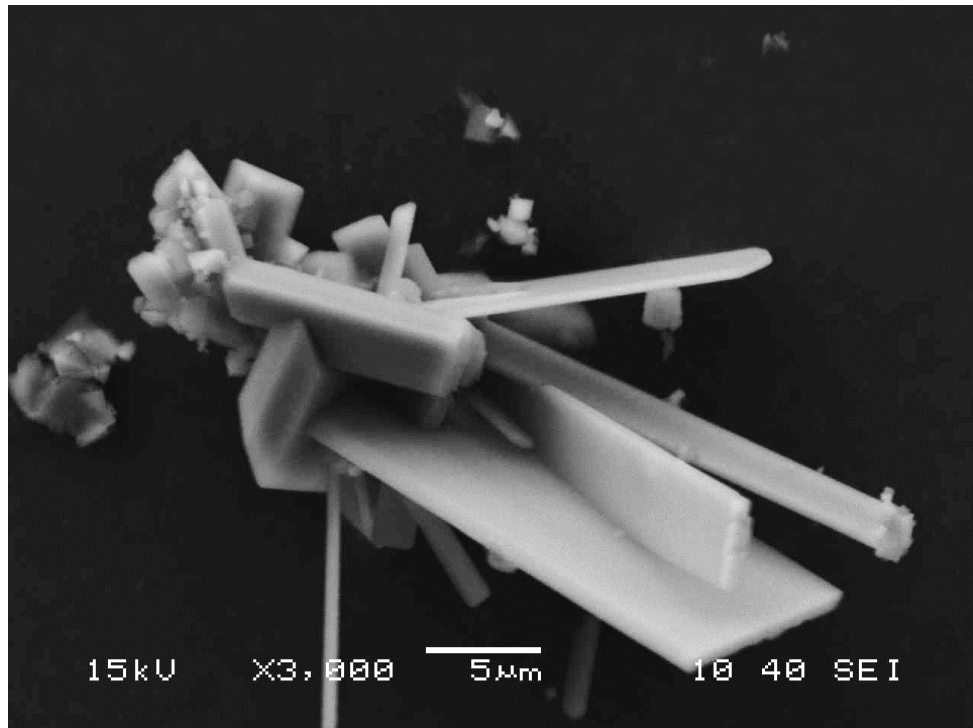
(a) SDC



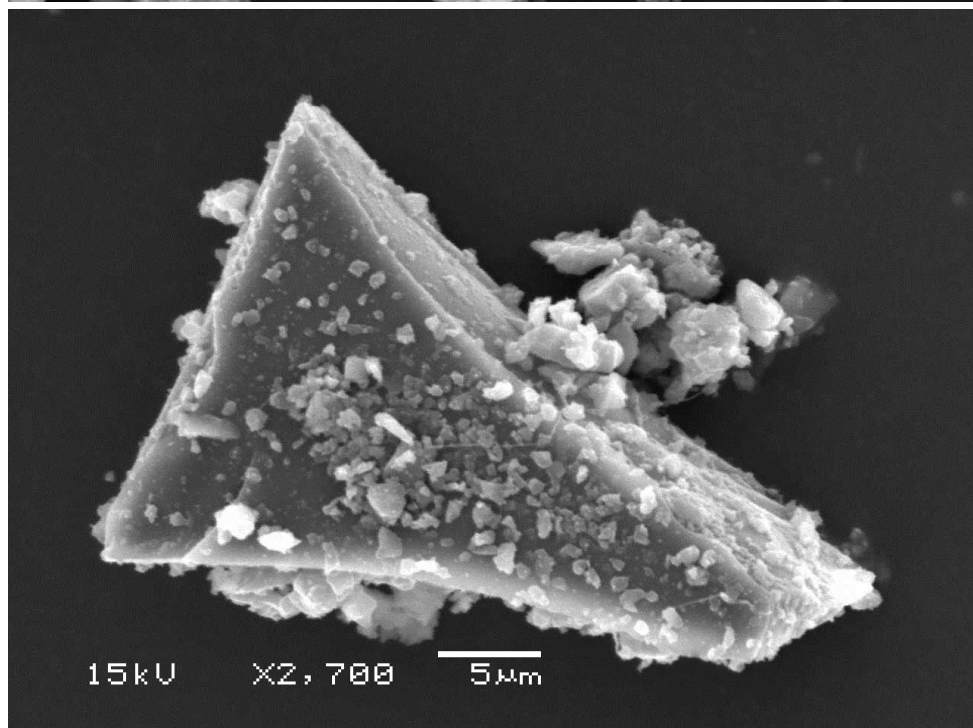
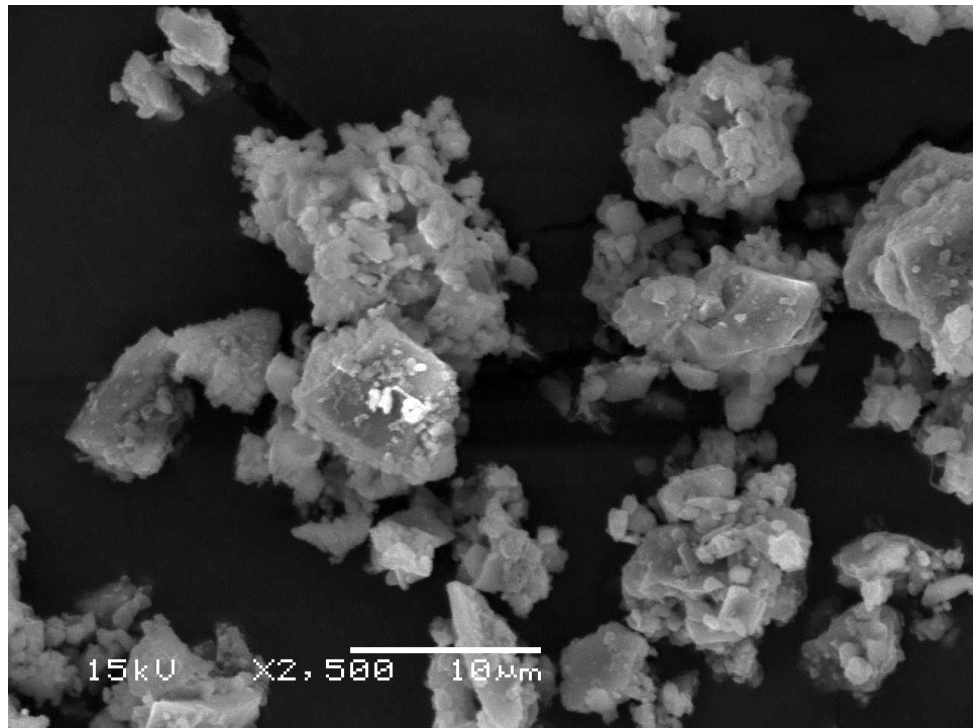
(b) CDC



(c) EDC



(d) Waste glass



## Appendix II

Rietveld quantification analysis results for EDC (Yellow is the original trace; red is the best fit modelled trace; blue is the weighted profile R-factor).

